TECHNICAL MEMORANDUM

ANL-CT-83-7
PART 2

FREE-PISTON STIRLING ENGINE EXPERIMENTAL PROGRAM: PART 2 — AN EVALUATION OF LOSS MECHANISMS

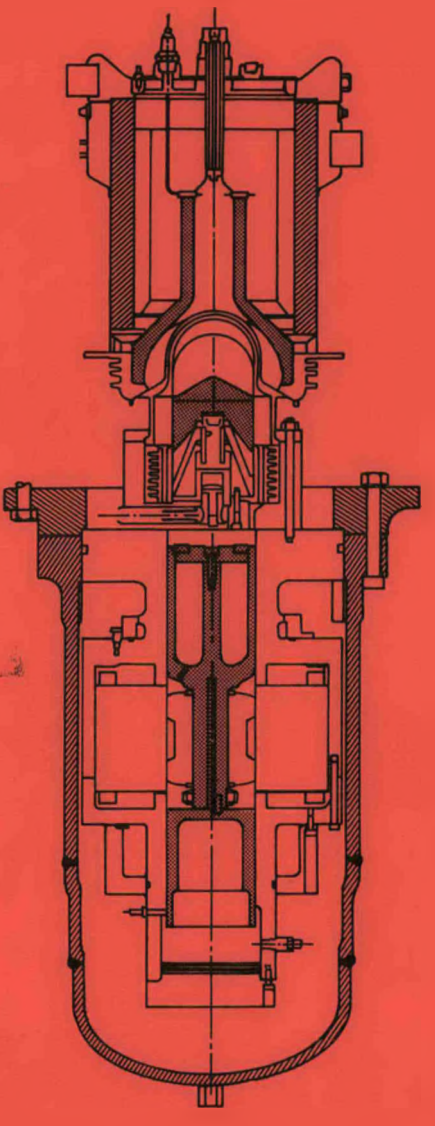

Components Technology Division

ARGONNE NATIONAL LABORATORY, ARGONNE, ILLINOIS

Operated by THE UNIVERSITY OF CHICAGO
for the U. S. DEPARTMENT OF ENERGY
under Contract W-31-109-Eng-38

DISCLAIMER

Printed in the United States of America
Available from
National Technical Information Service
U. S. Department of Commerce
5285 Port Royal Road
Springfield, VA 22161

NTIS price codes
Printed copy: A09
Microfiche copy: A01

Distribution Category:
Energy Conversion
(UC-93)

ANL-CT--83-7-Pt.2

DE84 003658

ANL-CT-83-7
Part 2

FREE-PISTON STIRLING ENGINE EXPERIMENTAL PROGRAM: PART 2 - AN EVALUATION OF LOSS MECHANISMS

by

T. Moynihan, R. Berggren, and G. Dochat

Mechanical Technology Incorporated
Latham, New York

Prepared for Argonne National Laboratory
under Subcontract No. 31-109-38-6420

Project Manager

James G. Daley

Components Technology Division
ARGONNE NATIONAL LABORATORY
9700 South Cass Avenue
Argonne, Illinois 60439

June 1983

Cover

The Technology Demonstrator Engine (TDE) represented on the cover is a Free-Piston Stirling Engine linear alternator power conversion system developed at Mechanical Technology, Incorporated, Latham, New York, under federal government sponsorship. The original program objective in 1976 was development of a 2-kWe radioisotope heat source, space power conversion system for readiness in 1985. This objective was changed and presently the TDE is used in validations and development of analytical codes, technology improvement and engine component development under an ongoing DOE/ECUT program.

PREFACE

The Energy Conversion and Utilization Technology (ECUT) Division, Office of Energy Systems Research, of the Department of Energy is concerned with improving the technology base for development of Stirling engines through release of computer analysis codes, carrying out experiments that improve understanding of the thermodynamics of Stirling engines, and exploratory development of advanced component designs.

Free-piston Stirling engines are a potentially important variant of Stirling-cycle machines that are hermetically sealed, thus avoiding the difficult sealing problem experienced with kinematic (mechanical drive) Stirling engines. Useful work is obtained either by attaching magnets to the power piston to generate electricity as the magnets reciprocate past electric windings, or using the movement of the power piston to pump a fluid. This latter embodiment could serve as the compressor of residential heat pumps operating on natural gas, thereby improving utilization of this resource.

Free piston Stirling engine technology is not as mature as that of kinematic engines and, although the two types of engines have the same theoretical performance, the demonstrated performance of free-piston Stirling engines has not achieved comparable levels.

The experimental and analytical effort described in this report was supported by ECUT in an attempt to improve understanding of thermodynamics and heat transfer of Stirling engines in general and to raise the performance of free piston Stirling engines by identifying sources of efficiency and power loss. A test matrix was designed to isolate and experimentally determine the relative effect of each of several potential loss mechanisms in an existing DOE engine. Analytical predictions of test results were formed prior to the experiments to assess existing analytical modeling capabilities.

TABLE OF CONTENTS

Page

LIST OF FIGURES.....viii

LIST OF TABLES.....xvi

ABSTRACT.....xvii

1. SUMMARY.....1-1

1.1 APPROACH.....1-1

1.2 LOSS MECHANISM RESULTS/CONCLUSIONS.....1-1

1.2.1 Baseline Testing.....1-1
1.2.2 Compression-Space Hysteresis Loss Test.....1-1
1.2.3 Regenerator Matrix Test.....1-3
1.2.4 Displacer Appendix Gap Test.....1-5
1.2.5 Displacer Seal Clearance Test.....1-5

1.3 CONCLUSIONS.....1-12

2. INTRODUCTION.....2-1

3. HARDWARE.....3-1

3.1 CRITICAL COMPONENTS AND CLEARANCES.....3-1

3.1.1 Expansion-Space Clearance Volume.....3-1
3.1.2 Appendix Gap.....3-1
3.1.3 Regenerator.....3-4
3.1.4 Displacer Seal Gap.....3-4
3.1.5 Cold Connecting Duct.....3-4
3.1.6 Displacer Drive Support.....3-4
3.1.7 Compression Space.....3-4

3.2 TDE BUILD HISTORY.....3-4

4. BASELINE ENGINE TESTS.....4-1

4.1 TEST OBJECTIVES.....4-1

4.2 TEST METHODS.....4-1

4.2.1 Test Series 1.....4-1
4.2.2 Test Series 2.....4-2
4.2.3 Test Series 3.....4-2

4.3 TEST RESULTS.....4-3

TABLE OF CONTENTS

Page

4.3.1 Performance Mapping....4-3
4.3.2 System Repeatability....4-3

4.4 ANALYTICAL COMPARISON....4-14

4.4.1 Power Drop-Off and Efficiency Loss Mechanisms....4-16

4.5 CONCLUSIONS AND RECOMMENDATIONS....4-22

5. COMPRESSION-SPACE HYSTERESIS LOSS TESTS....5-1

5.1 TEST OBJECTIVES....5-1

5.2 TEST METHODS....5-1

5.3 EXPERIMENTAL RESULTS....5-3

5.3.1 Indicated Power Trends with Pressure and Stroke....5-7
5.3.2 Finned Plug versus Unfinned Plug Power Trends....5-8
5.3.3 Indicated Efficiency Trends....5-23

5.4 ANALYTICAL COMPARISON....5-25

5.4.1 Power Correlation....5-25

5.5 CONCLUSIONS AND RECOMMENDATIONS....5-32

5.5.1 Conclusions....5-32
5.5.2 Recommendations....5-37

6. REGENERATOR MATRIX TEST....6-1

6.1 TEST OBJECTIVE....6-1

6.2 TEST METHODS....6-1

6.3 EXPERIMENTAL RESULTS....6-8

6.3.1 Indicated Power Results....6-8
6.3.2 Indicated Efficiency Test Results....6-21

6.4 ANALYTICAL COMPARISON....6-32

6.5 CONCLUSIONS AND RECOMMENDATIONS....6-38

6.5.1 Conclusions....6-38
6.5.2 Recommendations....6-38

TABLE OF CONTENTS

Page

7. DISPLACER APPENDIX GAP TEST....7-1

7.1 TEST OBJECTIVE....7-1

7.2 METHOD OF EXECUTION....7-1

7.3 EXPERIMENTAL RESULTS....7-1

7.3.1 Indicated Power and Efficiency Trends....7-1

7.4 ANALYTICAL COMPRESSION....7-11

7.5 CONCLUSIONS AND RECOMMENDATIONS....7-21

7.5.1 Conclusions....7-21
7.5.2 Recommendations....7-21

8. DISPLACER CLEARANCE SEAL TEST....8-1

8.1 OBJECTIVES....8-1

8.2 METHOD OF EXECUTION....8-1

8.3 EXPERIMENTAL RESULTS....8-3

8.3.1 Displacer Clearance Seal Tests....8-3
8.3.2 Piston Ring Tests....8-3

8.4 ANALYTICAL COMPARISON....8-28

8.5 CONCLUSIONS AND RECOMMENDATIONS....8-28

8.5.1 Conclusions....8-28
8.5.2 Recommendations....8-28

REFERENCES R-1

LIST OF FIGURES

No.	Title	Page
1-1	Comparison between Measured and Predicted Indicated Power and Efficiency for Baseline Engine Test Data	1-2
1-2	Hysteresis Test: Ratio of Measured to Predicted Indicated Efficiency	1-3
1-3	Regenerator Porosity Test: Comparison between Measured and Predicted Indicated Power and Efficiency	1-4
1-4	Displacer Appendix Gap Test: Comparison between Experimental and Predicted Indicated Power	1-6
1-5	Displacer Appendix Gap Test: Comparison between Experimental and Predicted Indicated Efficiency	1-7
1-6	Displacer Clearance Test: Indicated Power Measurements with Various Clearances	1-8
1-7	Displacer Clearance Test: Indicated Efficiency Measurements with Various Clearances	1-9
1-8	Displacer Clearance Test: Indicated Power Measurements at Various Clearances with and without Piston Rings	1-10
1-9	Displacer Clearance Test: Indicated Efficiency Measurements at Various Clearances with and without Piston Rings	1-11
3-1	TDE Layout	3-2
3-2	TDE Gas Passages	3-3
3-3	TDE Compression-space Geometry	3-3
4-1	Power Range for Test Series 1	4-4
4-2	Efficiency Range for Test Series 1	4-4
4-3	Temperature Range for Test Series 1	4-5
4-4	Displacer Stroke Ratio Range for Test Series 1	4-5
4-5	Displacer Phase Angle Range for Test Series 1	4-6
4-6	Engine Frequency Range for Test Series 1	4-6
4-7	Power Range for Test Series 2	4-7
4-8	Efficiency Range for Test Series 2	4-7
4-9	Heater Temperature Range for Test Series 2	4-8
4-10	Displacer Stroke Ratio Range for Test Series 2	4-8
4-11	Displacer Phase Angle Range for Test Series 2	4-9
4-12	Engine Frequency Range for Test Series 2	4-9

LIST OF FIGURES

No.	Title	Page
4-13	Operating Envelope for Test Series 3	4-10
4-14	Power Dependence on Piston Stroke, Builds 21-1 and 21-4	4-12
4-15	Efficiency Dependence on Piston Stroke, Builds 21-1 and 21-4	4-12
4-16	Power Dependence on Temperature, Builds 21-4 and 21-8	4-13
4-17	Efficiency Dependence on Temperature, Builds 21-4 and 21-8	4-13
4-18	Comparison of Indicated Power and Efficiency Predictions (VCR closed) for Baseline Engine Test	4-15
4-19	Error between Measured and Predicted Heat Input for Baseline Test	4-16
4-20	Comparison of Indicated Power and Efficiency Predictions with Revised Engine Model for Baseline Test	4-17
4-21	Comparison of Indicated Efficiency Predictions After Adjustment for "Power Drop-Off" for Baseline Test	4-17
4-22	Error between Measured and Predicted Heat Input for Baseline Test	4-18
4-23	A Comparison between Measured and Predicted Pressure Amplitude and Phase Angle	4-19
4-24	TDE Compression-Space Geometry	4-20
4-25	Typical TDE Displacer Seal and Appendix Gap Geometry	4-21
5-1	Hysteresis Test: Area Mean Temperature	5-4
5-2	Hysteresis Test: Effect of Pressure on Displacer Stroke Ratio	5-5
5-3	Hysteresis Test: Effect of Pressure on Displacer Phase Angle	5-6
5-4	TDE Power Flow	5-7
5-5	Hysteresis Test: Effect of Pressure on Indicated Power	5-9
5-6	Hysteresis Test: Engine Frequency Variation with Pressurization	5-10
5-7	Hysteresis Test: Engine Pressure Amplitude Variation with Pressurization	5-11
5-8	Hysteresis Test: Engine Pressure Angle Variation with Pressurization	5-12
5-9	Hysteresis Test: Indicated Power Measurements at 30 Bar	5-13
5-10	Hysteresis Test: Indicated Power Measurements at 35 Bar	5-14
5-11	Hysteresis Test: Indicated Power Measurements at 40 Bar	5-15

LIST OF FIGURES

No.	Title	Page
5-12	Hysteresis Test: Indicated Power Variation with Pressure at Fixed Piston Stroke	5-16
5-13	Hysteresis Test: Engine Frequency Measurements	5-17
5-14	Hysteresis Test: Compression Space Pressure Amplitude Measurements	5-18
5-15	Hysteresis Test: Compression Space Phase Angle Measurements	5-19
5-16	Hysteresis Test: Displacer Power Measurements	5-20
5-17	Hysteresis Test: Engine P-V Power Measurements	5-21
5-18	Hysteresis Test: Cold-Space Temperature Measurements	5-22
5-19	Hysteresis Test: Insensitivity of Power to Hysteresis Effects	5-24
5-20	Hysteresis Test: Indicated Efficiency Measurement Summary	5-26
5-21	Hysteresis Test: Effect of Pressurization on Engine Heat Rejection	5-27
5-22	Hysteresis Test: Comparison between Measured and Predicted Power, Finned Plug	5-28
5-23	Hysteresis Test: Comparison between Measured and Predicted Power, Unfinned Plug	5-29
5-24	Hysteresis Test: Comparison between Measured and Predicted Pressure Amplitude, Finned Plug	5-30
5-25	Hysteresis Test: Comparison between Measured and Predicted Compression Space Phase Angle	5-31
5-26	Hysteresis Test: Comparison between Measured and Predicted Heat Exchanger Pressure Drop Amplitude	5-33
5-27	Hysteresis Test: Correlation between Measured and Predicted Power	5-34
5-28	Hysteresis Test: Comparison between Measured and Predicted Indicated Efficiency, Finned Plug	5-35
5-29	Hysteresis Test: Comparison between Measured and Predicted Indicated Efficiency, Unfinned Plug	5-36
5-30	Hysteresis Test: Correlation between Measured and Predicted Indicated Efficiency	5-37
6-1	Regenerator Test: Mean Head Temperature Measurements, Tcontrol=500°C	6-2
6-2	Regenerator Test: Engine Stroke Ratio Measurements, Tcontrol=500°C	6-3

LIST OF FIGURES

No.	Title	Page
6-3	Regenerator Test: Engine Phase Angle Measurements, Tcontrol=500°C	6-4
6-4	Regenerator Test: Mean Head Temperature Measurements, Tcontrol=400°C	6-5
6-5	Regenerator Test: Engine Stroke Ratio Measurements, Tcontrol=400°C	6-6
6-6	Regenerator Test: Engine Phase Angle Measurements, Tcontrol=400°C	6-7
6-7	Regenerator Test: Indicated Power Measurements, Tcontrol=400°C	6-9
6-8	Regenerator Test: Indicated Power Measurements, Tcontrol=500°C	6-10
6-9	Regenerator Test: Indicated Power and Efficiency Measurements at Constant Piston Stroke	6-11
6-10	Regenerator Test: Displacer Gas Spring Power Measurements, Tcontrol=400°C	6-12
6-11	Regenerator Test: Displacer Gas Spring Power Measurements, Tcontrol=500°C	6-12
6-12	Regenerator Test: Engine P-V Power Measurements, Tcontrol=400°C	6-13
6-13	Regenerator Test: Engine P-V Power Measurements, Tcontrol=500°C	6-14
6-14	Regenerator Test: Engine Pressure Amplitude Measurements, Tcontrol=400°C	6-15
6-15	Regenerator Test: Engine Pressure Amplitude Measurements, Tcontrol=500°C	6-16
6-16	Regenerator Test: Engine Frequency Measurements, Tcontrol=400°C	6-17
6-17	Regenerator Test: Engine Frequency Measurements, Tcontrol=500°C	6-18
6-18	Regenerator Test: Engine Pressure Angle Measurements, Tcontrol=400°C	6-19
6-19	Regenerator Test: Engine Pressure Angle Measurements, Tcontrol=500°C	6-20
6-20	Regenerator Test: Cold Temperature Measurements, Tcontrol=400°C	6-22
6-21	Regenerator Test: Cold Temperature Measurements, Tcontrol=500°C	6-23

LIST OF FIGURES

No.	Title	Page
6-22	Regenerator Test: Dome Temperature Measurements, Tcontrol=400°C	6-24
6-23	Regenerator Test: Heater Dome Temperature Measurements, Tcontrol=500°C	6-25
6-24	Regenerator Test: Displacer Pumping Power Measurements, Tcontrol=400°C	6-26
6-25	Regenerator Test: Displacer Pumping Power Measurements, Tcontrol=500°C	6-26
6-26	Regenerator Test: Heater Head Temperature Distribution, Tcontrol=400°C	6-27
6-27	Regenerator Test: Heater Head Temperature Distribution, Tcontrol=500°C	6-28
6-28	Regenerator Test: Temperature Measurements at Cold Side of Regenerator, Tcontrol=500°C	6-29
6-29	Regenerator Test: Temperature Measurements at Cold Side of Regenerator, Tcontrol=400°C	6-30
6-30	Regenerator Test: Indicated Efficiency Measurements, Tcontrol-400°C	6-31
6-31	Regenerator Test: Indicated Efficiency Measurements, Tcontrol=500°C	6-33
6-32	Regenerator Test: Heat Rejection Measurements, Tcontrol=400°C	6-34
6-33	Regenerator Test: Heat Rejection Measurements, Tcontrol=500°C	6-35
6-34	Regenerator Test: Summary of Regenerator Porosity Effect on Power and Efficiency	6-36
6-35	Regenerator Test: Heat Exchanger Pressure Drop Measurements	6-37
7-1	Displacer Appendix Gap Test: Mean Head Temperature Measurements	7-2
7-2	Displacer Appendix Gap Test: Stroke Ratio Measurements	7-3
7-3	Displacer Appendix Gap Test: Phase Angle Measurements	7-4
7-4	Displacer Appendix Gap Test: Indicated Power Measurements	7-5
7-5	Displacer Appendix Gap Test: P-V Power Factor (Equation 5.1) Measurements	7-6
7-6	Displacer Appendix Gap Test: AC Power Measurements	7-7

LIST OF FIGURES

No.	Title	Page
7-7	Displacer Appendix Gap Test: Engine Pressure Amplitude Measurements	7-8
7-8	Displacer Appendix Gap Test: Engine Pressure Angle Measurements	7-9
7-9	Displacer Appendix Gap Test: Engine Frequency Measurements	7-10
7-10	Displacer Appendix Gap Test: Average Dome Temperature Measurements and Calculated Expansion Space Gas Temperatures	7-12
7-11	Displacer Appendix Gap Test: Compression-Space Temperature Measurements	7-13
7-12	Displacer Appendix Gap Test: Displacer Pumping Power/ δP Phase Angle/Heat Exchanger δP	7-14
7-13	Displacer Appendix Gap Test: Indicated Efficiency Measurements	7-15
7-14	Displacer Appendix Gap Test: Shuttle Loss Mechanism and Control Volume	7-16
7-15	Displacer Appendix Gap Test: Calculated Appendix Gap Losses	7-17
7-16	Displacer Appendix Gap Test: Comparison between Measured and Calculated Indicated Power	7-18
7-17	Displacer Appendix Gap Test: Comparison between Measured and Calculated Compression Space Pressure Amplitude and Phase Angle	7-19
7-18	Displacer Appendix Gap Test: Comparison between Measured and Calculated Indicated Efficiency	7-20
8-1	Displacer Clearance Test: Average Head Temperature/Phase Angle/Stroke Ratio Measurements	8-2
8-2	Displacer Clearance Test: Mean Head Temperature/ Phase Angle/Stroke Ratio Measurements at .0015-in. Clearance with and without Piston Ring	8-4
8-3	Displacer Clearance Test: Mean Head Temperature/Phase Angle/Stroke Ratio Measurements at .0031-in. Clearance with and without Piston Ring	8-5
8-4	Displacer Clearance Test: Mean Head Temperature/Phase Angle/Stroke Ratio Measurements at .0050-in. Clearance with and without Piston Ring	8-6
8-5	Displacer Clearance Test: Mean Head Temperature/Phase Angle/Stroke Ratio Measurements at .0050-in. Clearance Using Piston Ring with O-Ring Backing	8-7

LIST OF FIGURES

No.	Title	Page
8-6	Displacer Clearance Test: Indicated Power Measurements with Various Clearances	8-8
8-7	Displacer Clearance Test: Engine Pressure Amplitude Measurements at Various Clearances	8-9
8-8	Displacer Clearance Test: Engine Pressure Angle Measurements at Various Clearances	8-10
8-9	Displacer Clearance Test: Engine Heat Rejection Measurements at Various Clearances	8-11
8-10	Displacer Clearance Test: Compression Space Temperature Ratio Measurements	8-12
8-11	Displacer Clearance Test: Water-In Temperature Measurements	8-13
8-12	Displacer Clearance Test: Indicated Efficiency Measurements at Various Clearances	8-14
8-13	Displacer Clearance Test: Indicated Power Measurements at 0.002-in. Clearance	8-15
8-14	Displacer Clearance Test: Indicated Efficiency Measurements at 0.002-in. Clearance	8-16
8-15	Displacer Clearance Test: Indicated Power Measurements at Various Clearances with and without Piston Rings	8-17
8-16	Displacer Clearance Test: Indicated Power Measurements with Piston Ring at .0050-in. Clearance with and without O-Ring Backing	8-19
8-17	Displacer Clearance Test: P-V Power Factor (Equation 5.1) for Various Clearances with Piston Ring	8-20
8-18	Displacer Clearance Test: P-V Power Factor (Equation 5.1) at .0015-in. Clearance with and without Piston Ring	8-21
8-19	Displacer Clearance Test: P-V Power Factor (Equation 5.1) at .0031-in. Clearance with and without Piston Ring	8-22
8-20	Displacer Clearance Test: P-V Power Factor (Equation 5.1) at .0050-in. Clearance with and without Piston Ring	8-23
8-21	Displacer Clearance Test: Indicated Efficiency Measurements at Various Clearances with and without Piston Ring	8-24
8-22	Displacer Clearance Test: Indicated Efficiency Measurements with Piston Ring at .0050-in. Clearance with and without O-Ring Backing	8-25
8-23	Displacer Clearance Test: Heat Exchanger ΔP Amplitude at Various Clearances with and without Piston Ring	8-26
8-24	Displacer Clearance Test: Heat Exchanger ΔP Phase Angle at Various Clearances with and without Piston Ring	8-26

LIST OF FIGURES

No.	Title	Page
8-25	Displacer Pumping Damping vs. Displacer Stroke	8-27
8-26	Dispacer Clearance Test: Comparison between Measured and Calculated Indicated Power and Efficiency for Various Clearances	8-27

LIST OF TABLES

No.	Title	Page
3-1	TDE Build History	3-6
3-2	TDE/ECUT Component Hardware Description	3-8
4-1	Test Conditions for Generating Thermodynamic Map of Indicated Power vs. Efficiency	4-11
5-1	Pretest Analysis of Hysteresis Losses	5-2
6-1	Effect of Porosity on Compression-Space Pressure Amplitude and Phase	6-38
7-1	Effect of Dead Volume on Compression-Space Pressure and Phase	7-21

FREE-PISTON STIRLING ENGINE EXPERIMENTAL PROGRAM: PART 2 - AN EVALUATION OF LOSS MECHANISMS

by

T. Moynihan, R. Berggren, and G. Dochat
Mechanical Technology Incorporated, Latham, New York

ABSTRACT

A series of experiments is described in which measurements were taken on a free-piston Stirling engine to isolate effects believed to degrade engine performance. The effects examined were: compression-space hysteresis, regenerator losses, displacer seal clearance loss, and displacer appendix gap loss. The experimental data from these experiments are given and represent a valuable resource for validation of Stirling engine analysis methods. The most significant of the above effects was found to be the clearance between the displacer and cylinder wall. Best performance was attained by a close clearance seal of 2 mils. Greater clearances or use of a piston ring degraded performance. Overall efficiency of the engine was raised several points due to this finding. The base-line performance of the engine and its operating envelope are summarized here from Part 1 of this report which was prepared separately.

1. SUMMARY

The objective of this analytical/experimental study was to improve the understanding of free-piston engine technology by evaluating specific loss mechanisms within the engine. The specific loss mechanisms evaluated include:

- Compression-space hysteresis,
- Regenerator losses,
- Displacer seal clearance loss, and
- Displacer appendix gap loss.

1.1 APPROACH

The experimental approach involved back-to-back engine performance comparison before and after modifications that would affect the loss level in each area. The magnitude of each loss was assessed indirectly from measured and predicted changes in engine performance.

The Technology Demonstrator Engine (TDE) was used as the experimental free-piston Stirling engine (FPSE) test bed. The TDE is a 1-kW FPSE coupled with a linear alternator that incorporates close-clearance, non-contacting seals where the moving components are supported on gas bearings. The TDE has the necessary, sufficient instrumentation and range of operating paramters to be utilized in free-piston loss mechanism evaluation.

1.2 LOSS MECHANISM RESULTS/CONCLUSIONS

Loss mechanism results include both analytical predictions using MTI's proprietary computer code and experimental test data. The following sections (presented in chronological order of evaluation) are major results and conclusions of the study.

1.2.1 Baseline Testing

Baseline testing of the test-bed TDE, prior to evaluation of the specific loss mechanisms, indicated unexpected losses compared with analytical predictions; the losses resulted in a power drop-off at high strokes, and reduced efficiency at all piston strokes (shown in Fig. 1-1). The power drop-off was tentatively related to additional cold-connecting-duct pumping losses and enhanced appendix gap losses. Reduced efficiency was thought initially, and later confirmed by test, to be related to displacer seal clearance losses.

1.2.2 Compression-Space Hysteresis Loss Test

Compression-space hysteresis loss is attributed to irreversible thermal transfers that occur in the boundary layers on the various surfaces within the working space. Compression-space hysteresis loss test evaluations were performed with back-to-back testing using 0.16-m^2 and 0.22-m^2 wetted areas in the compression space. Both predicted and experimental results indicated little change in hysteresis loss with wetted areas (see Fig. 1-2).

The major conclusions drawn from this testing are:

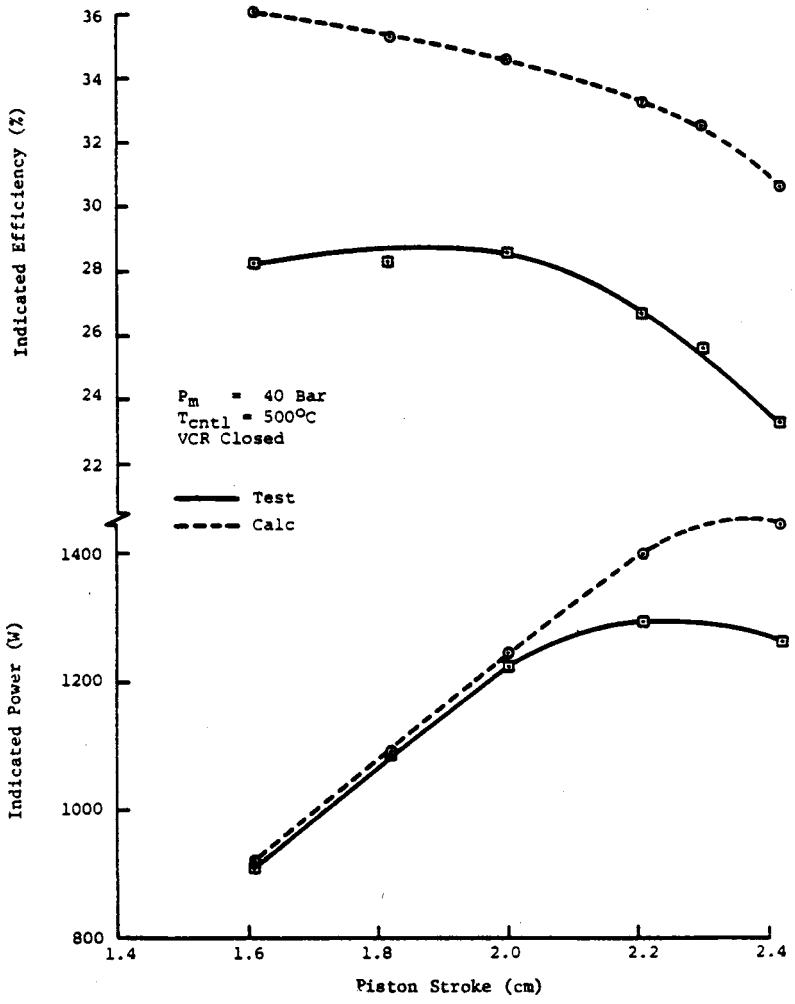

Fig. 1-1. Comparison between Measured and Predicted Indicated Power and Efficiency for Baseline Engine Test Data

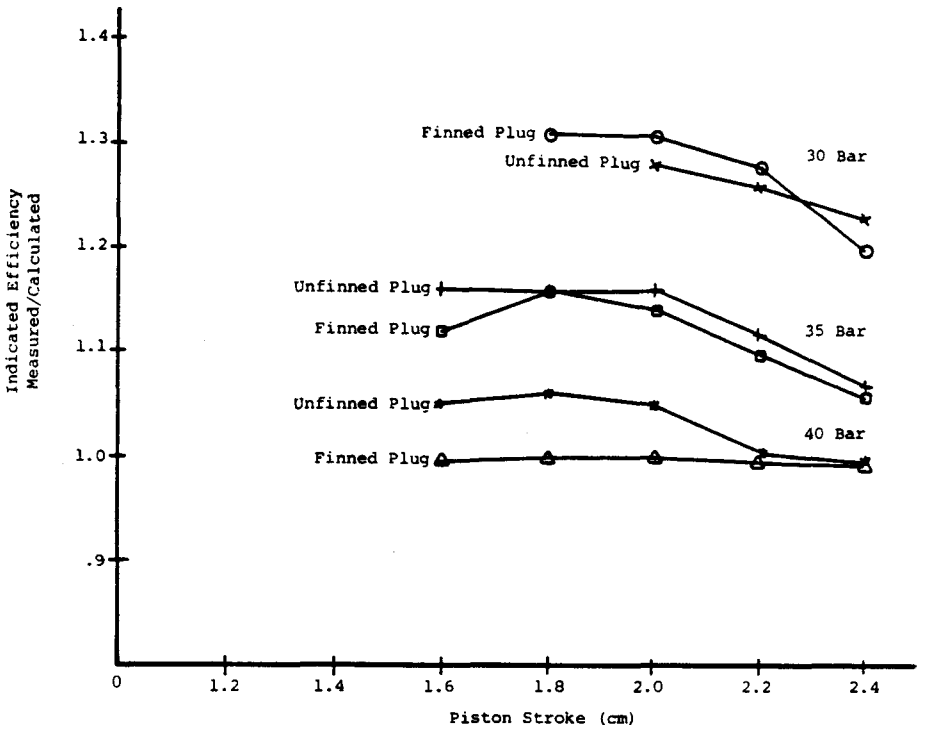

Fig. 1-2. Hysteresis Test: Ratio of Measured to Predicted Indicated Efficiency

- Hysteresis losses are not underestimated by the analytical code, the present hysteresis analysis is adequate, and
- The analytical code does not track engine power trends as a function of pressure, and underpredicts the power at lower pressures due to underprediction of the compression-space pressure wave.

1.2.3 Regenerator Matrix Test

The regenerator used in the TDE is composed of 91%-porosity, 1-mil, 100 x 100 mesh wire screen. Two series of tests were conducted to evaluate 2.5- and 3.5-mil woven-wire regenerators with porosities of 70, 75, 80, and 85%. Test results of the 3.5-mil woven-wire regenerator are presented in Figure 1-3. The regenerator loss analytical model diverges from the measured loss as porosity is increased, but does a reasonable job of predicting performance at low porosities (~70%). This thermodynamic effect is not completely understood.

Pressure drop and heat-transfer characteristics used for code calculations were derived from empirical correlations from a single-flow regenerator test rig using 6-mil woven-wire. Major conclusions were:

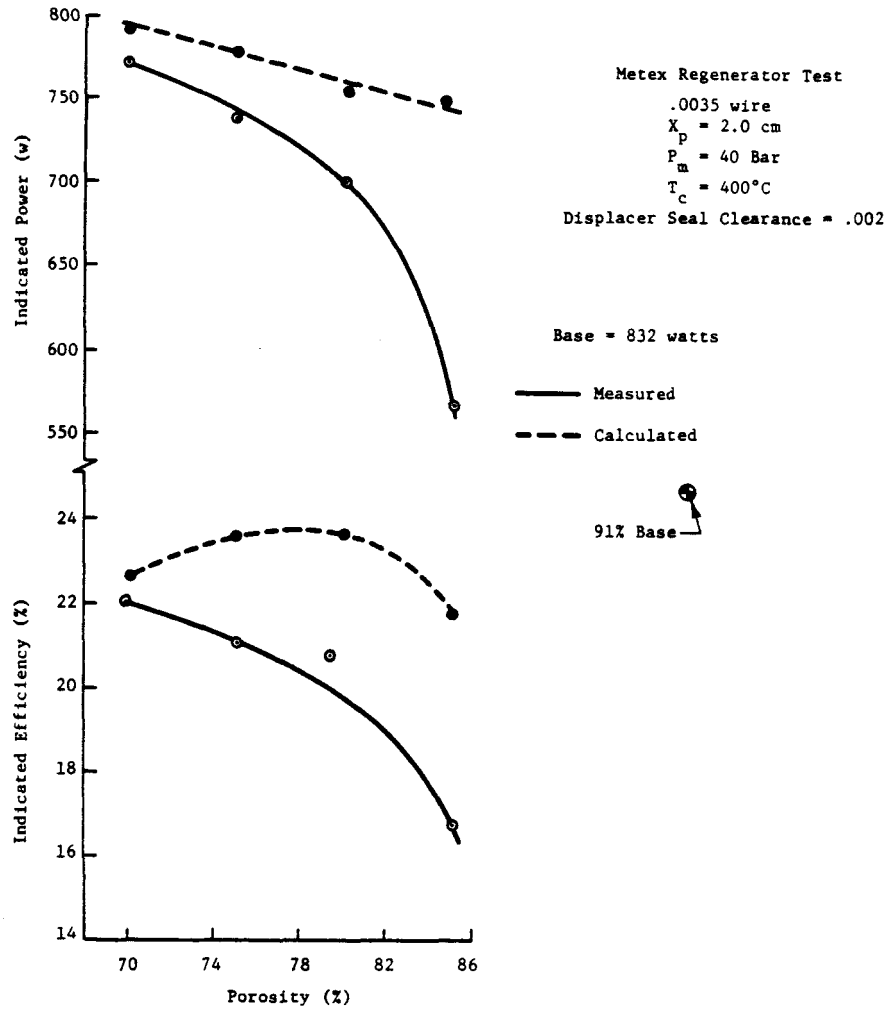

Fig. 1-3. Regenerator Porosity Test: Comparison between Measured and Predicted Indicated Power and Efficiency

- Reducing woven-wire regenerator porosities results in improved performance.
- Performance of the woven-wire regenerators did not exceed the performance of the wire screen; in fact, efficiency was degraded by 2 to 3 efficiency points.
- Additional work is required to obtain a better understanding of pressure drop and heat-transfer characteristics under periodic flow, and the effects of flow maldistribution, and to evaluate alternative regenerator material.

1.2.4 Displacer Appendix Gap Test

The displacer appendix gap is the annulus between the displacer cylinder and displacer cylinder wall located above the close-clearance displacer seal. Losses are associated with heat and mass transport in this region as the displacer reciprocates. Tests were run with three different displacers that varied the mean appendix gap from 0.5 to 2.3 mil. Test results, as compared with analytical projections, are shown in Figure 1-4 for power, and in Figure 1-5 for efficiency. The main conclusions drawn from the displacer appendix gap tests are:

- Analytical code evaluation effectively matches engine performance for reasonably small appendix gaps (as most engines are designed), but overpredicts power at large gaps (calculated efficiency is reasonable at small gaps, but is underpredicted at large gaps, indicating that parasitic loss at large gaps is too high),
- Engine power is significantly reduced at large gaps, and
- Engines must be designed with as small an appendix gap as practical.

1.2.5 Displacer Seal Clearance Test

The displacer seal clearance provides separation of the hot expansion and cold compression spaces; flow through this seal results in pumping losses and thermal energy transfer. Tests were performed with various clearance seal gaps [0.0048 (during baseline tests), 0.0029, and 0.002 in.], and with piston rings. Test results for power and efficiency with various clearances are presented in Figures 1-6 and 1-7, respectively, and test results for power and efficiency with piston rings compared to clearance seals are presented in Figures 1-8 and 1-9, respectively. Some major conclusions that can be drawn from Figures 1-6 through 1-9 are:

- Power and efficiency increase as displacer seal clearance decreases.
- Efficiency improves significantly (by as much as 7.5 percentage points) as displacer seal clearance is reduced (from ~0.005 to 0.002 in.).
- At small displacer seal clearances (~0.002 in.), performance is degraded with the installation of a displacer piston ring (probably because of the increase in displacer friction power caused by the rubbing piston ring).
- At larger displacer seal clearances, performance is improved with the installation of a displacer piston ring.
- Power and efficiency measurements with displacer piston rings are not sensitive to the clearance gap.

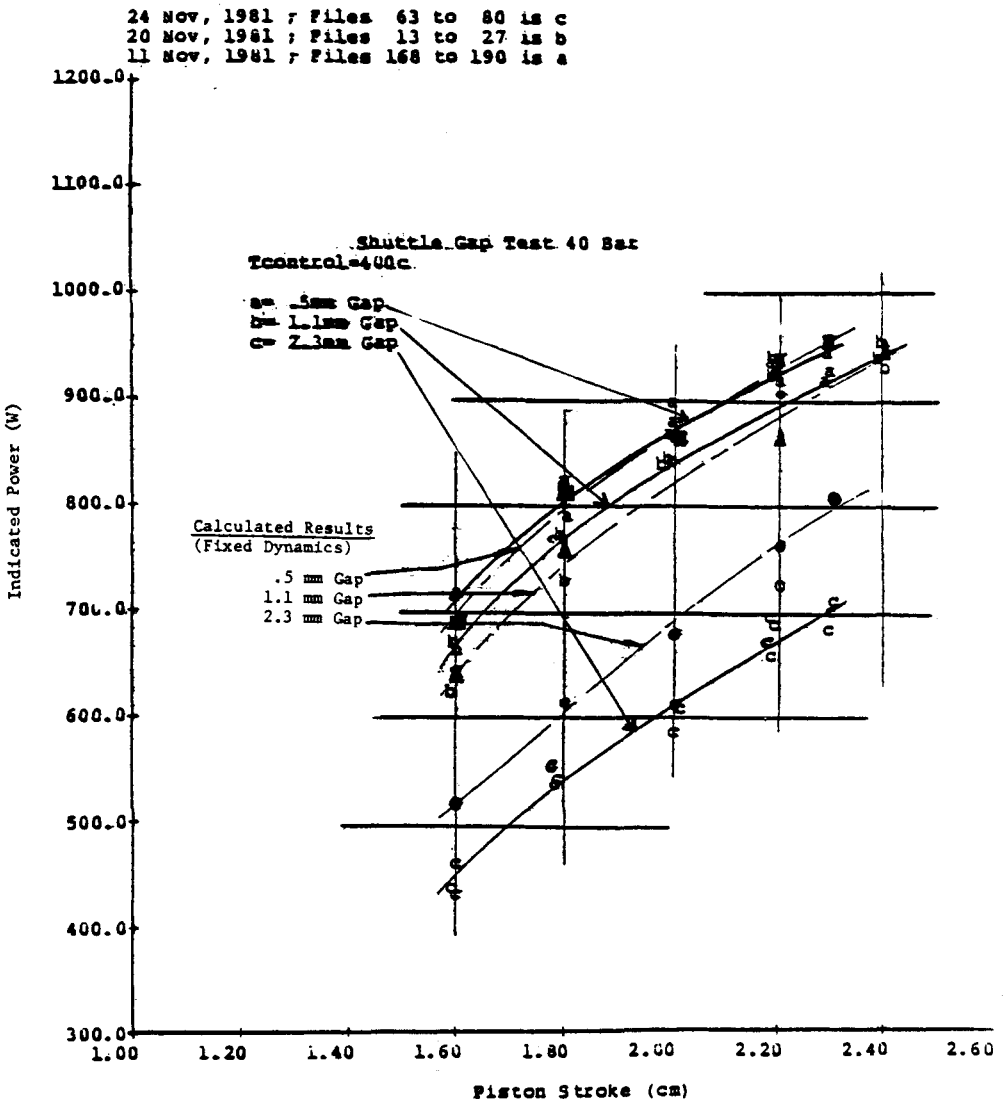

Fig. 1-4. Displacer Appendix Gap Test: Comparison between Experimental and Predicted Indicated Power

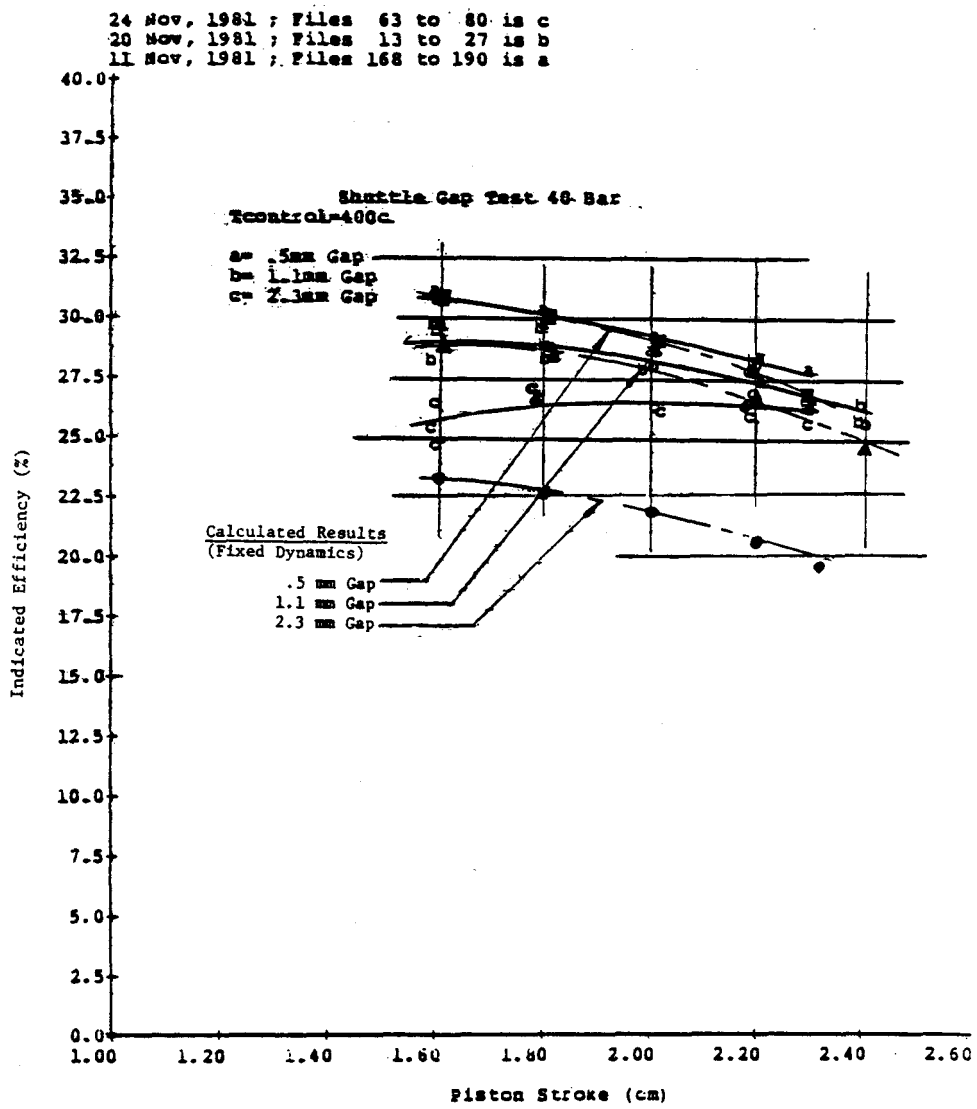

Fig. 1-5. Displacer Appendix Gap Test: Comparison between Experimental and Predicted Indicated Efficiency

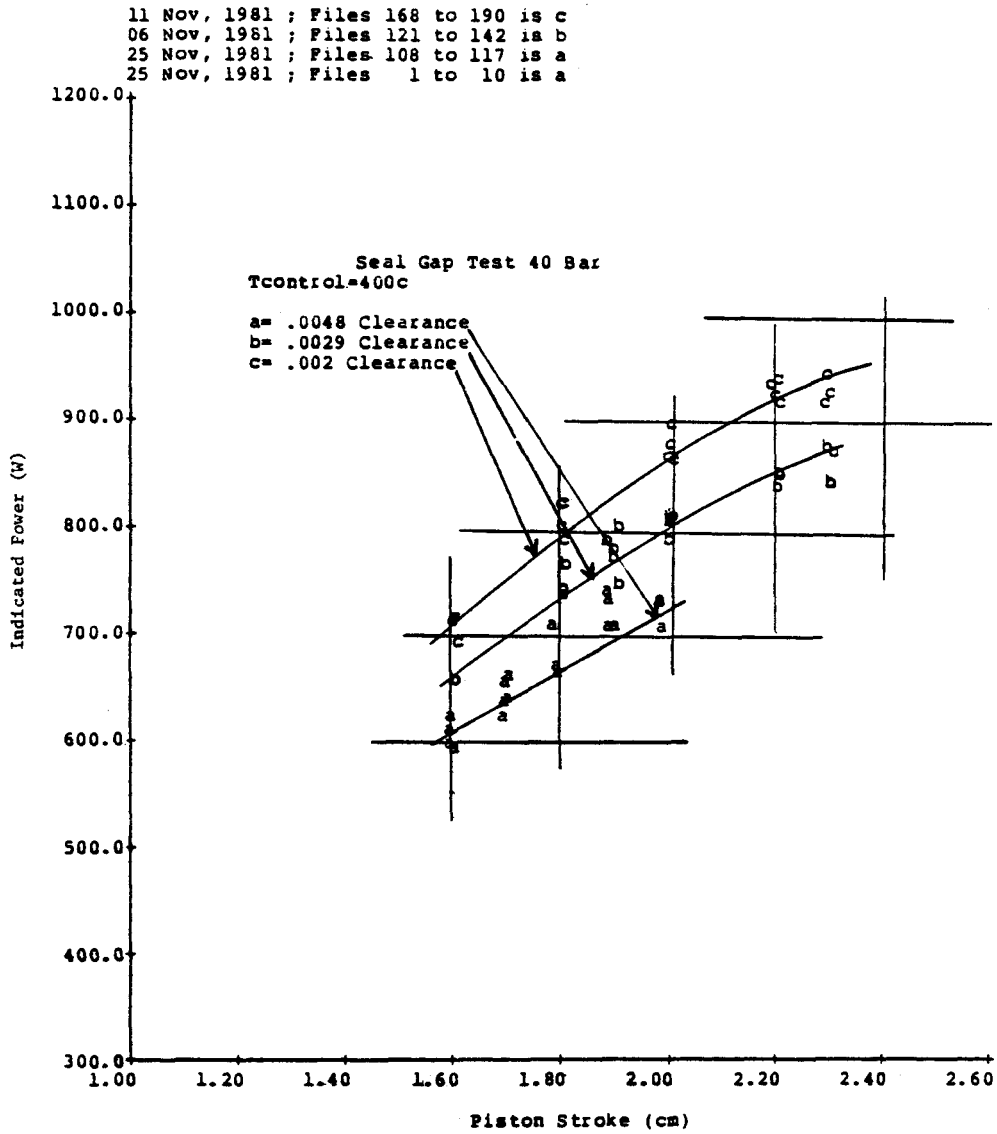

Fig. 1-6. Displacer Clearance Test: Indicated Power Measurements with Various Clearances

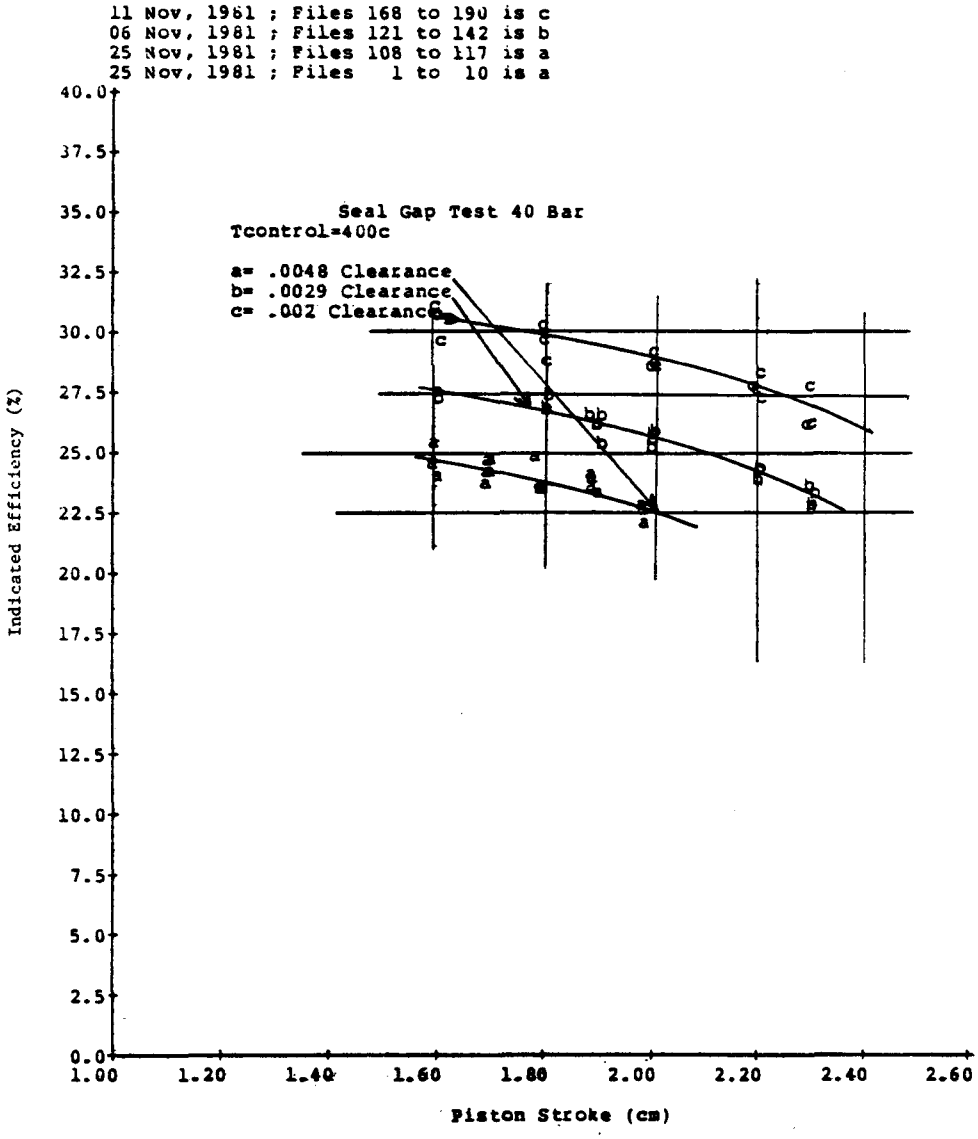

Fig. 1-7. Displacer Clearance Test: Indicated Efficiency Measurements with Various Clearances

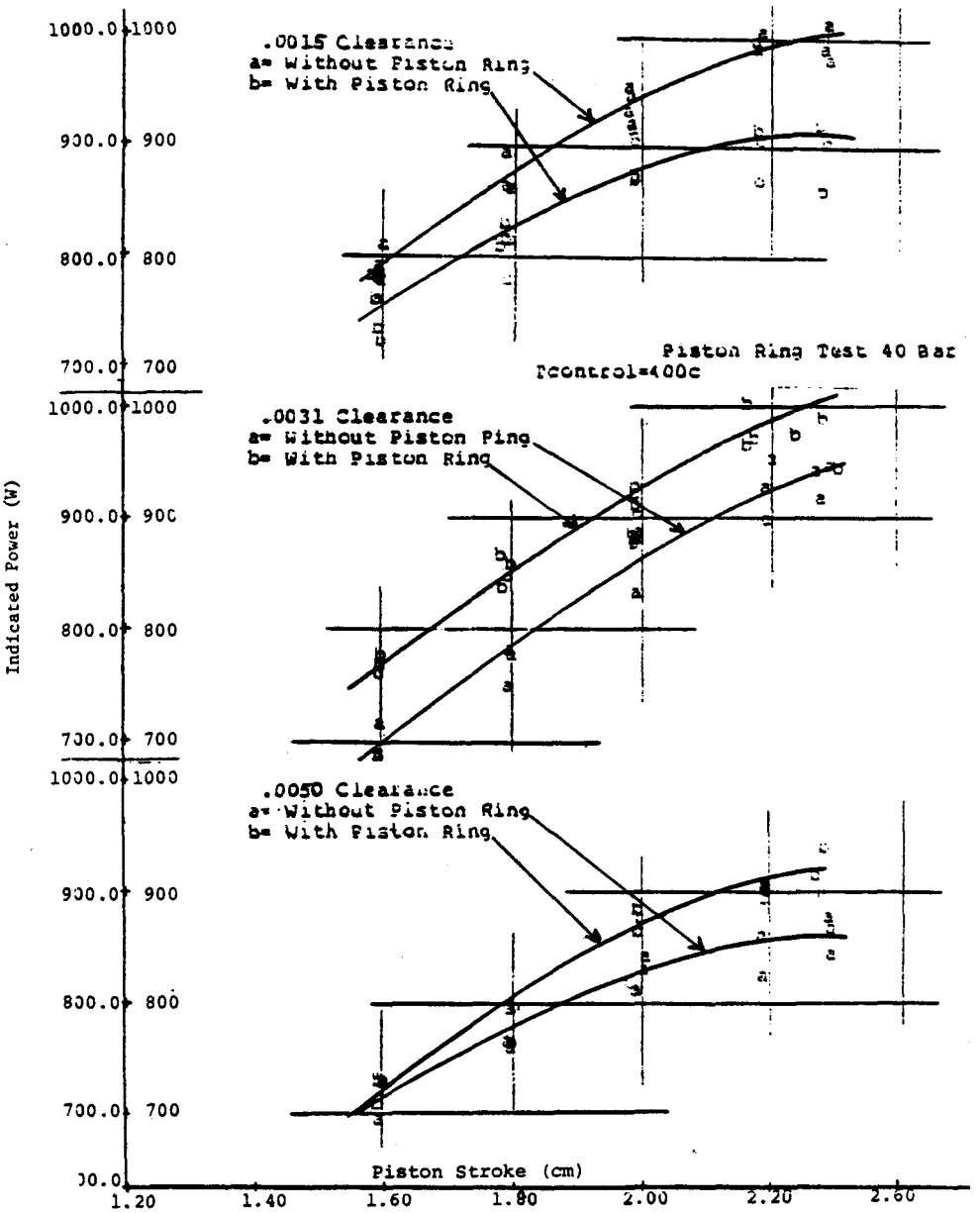

Fig. 1-8. Displacer Clearance Test: Indicated Power Measurements at Various Clearances with and without Piston Rings

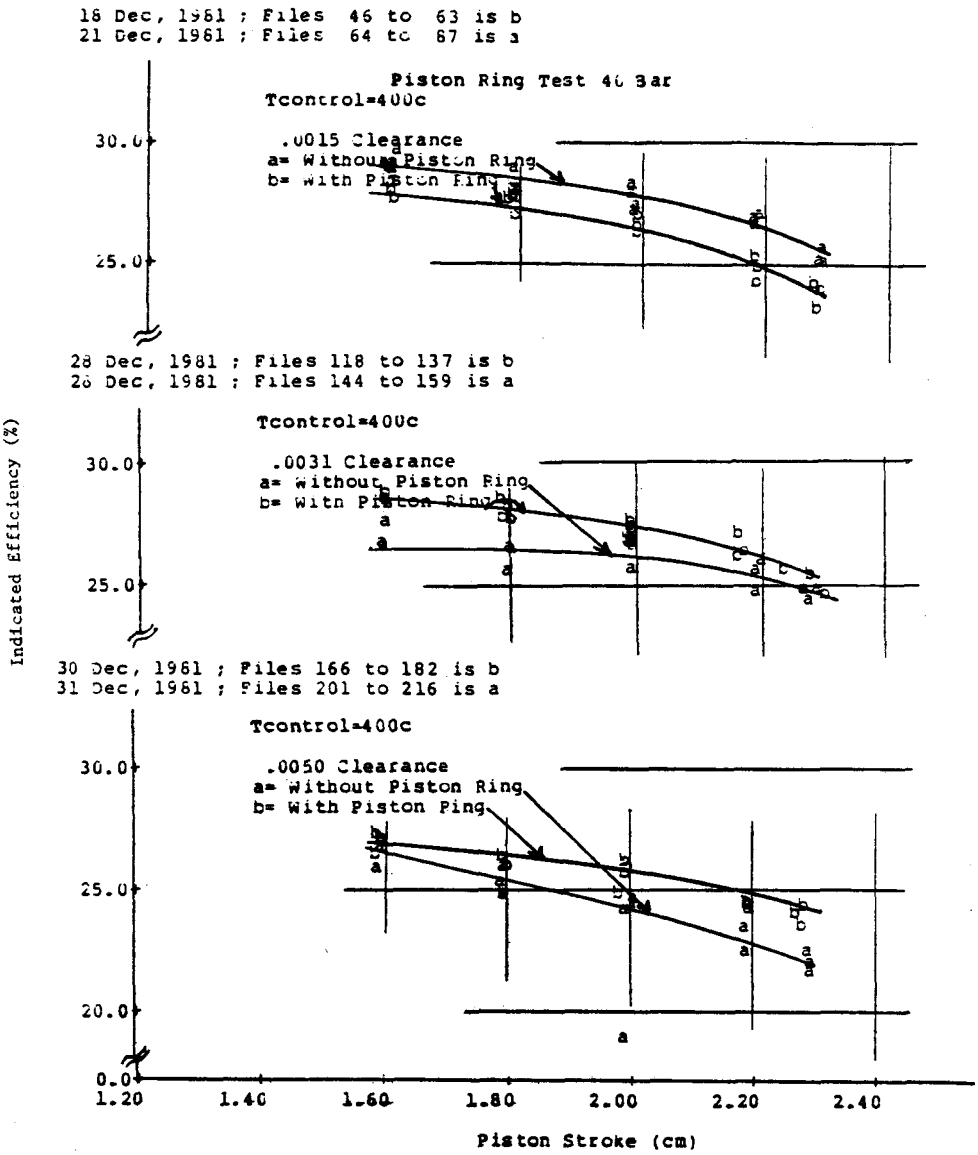

Fig. 1-9. Displacer Clearance Test: Indicated Efficiency Measurements at Various Clearances with and without Piston Rings

- Engines should be designed with a seal clearance of 0.002 in. or less.

- Analyses predict power and efficiency at small clearances, but do not account for enthalpy transport across the seal, so that power and efficiency at large displacer clearances are overpredicted.

1.3 CONCLUSIONS

This evaluation focused on loss mechanisms within free-piston engines without there being a requirement to achieve specific overall performance requirements; however, the knowledge gained as a direct result of the program will aid in the design and development of higher-efficiency machines. Focus of the experimental evaluation was directed toward performance level differences from test to test, not on absolute performance values.

This study concludes that within the limited range of existing experience, current design and analytical models for the evaluation of free-piston engines are adequate; however, care should be exercised when the analytical models are extended beyond this range of experience. The study also identified several technological areas that need to be explored further to improve the general state of knowledge of free-piston engines. Significant areas that require further evaluation include:

- Displacer convection and conduction losses;

- Compression-space hysteresis losses to isolate the effect on pressure, and obtain agreement with analytical models;

- Regenerator evaluation and testing to improve

  - regenerator flow distribution,
  - empirical data for pressure drop and heat transfer in periodic flow fields, and
  - alternative regenerative material;

- Compression-space seal leakage; and

- Improvements of the appendix gap model.

2. INTRODUCTION

Free-piston Stirling engines (FPSEs), a potentially important variant of Stirling-cycle machines, are hermetically sealed, and operate by an external heat source that causes motion of internal pistons. Useful work is obtained either by mounting magnets on the moving power piston to create alternating electric current by the movement of the magnets through electric windings, or by utilizing the movement of the power piston to pump a fluid. This latter embodiment could find application as the compressor of residential heat pumps operating on natural gas, while offering large energy savings and improved utilization of primary energy sources.

The objective of this analytical/experimental study is to improve the understanding of loss mechanisms of free-piston engine technology such that the information will provide the technical base from which further development and improvements will follow.

This report documents the results of an analytical/experimental evaluation of potential loss mechanisms within an existing and operating free-piston Stirling engine. The specific loss mechanism evaluated and results presented in this report include:

- Baseline operating parameters of the TDE (Section 4),
- Compression-space hysteresis loss (Section 5),
- Regenerator loss (Section 6),
- Displacer seal clearance loss (Section 7), and
- Displacer gap loss (Section 8).

The approach used in the study was to modify the TDE to highlight (either reduce or increase) the particular loss mechanism, and compare it before and after engine performance.

The TDE has been the primary workhorse FPSE technology-development tool at Mechanical Technology Incorporated (MTI). Its primary purposes are the validation, improvement, and development of analytical codes; technology improvement; and engine component development. The TDE has the necessary and sufficient instrumentation, and range of operating parameters, to be used as the test vehicle in the loss-mechanism evaluation study. A complete description of the TDE hardware is found in Section 3.

The test results, test data, and effects on engine performance (power, efficiency, displacer phase angle, and pressure wave) are contained in this report, along with conclusions and recommendations as to the significance of each loss mechanism.

3. HARDWARE

A complete and detailed description of the combustion-heated TDE-alternator system and its associated instrumentation is contained in the TDE Period Test Report.[1]

Instrumentation has been included in the system design to measure critical thermodynamic/mechanical dynamic parameters. Piston/displacer dynamics can be varied through adjustable gas spring characteristics.

Engine geometry is summarized by Figures 3-1 through 3-3. Figure 3-1 shows a general layout of the system, Figure 3-2 is a cutaway view of the engine gas path, and Figure 3-3 is a schematic view of the displacer drive geometry.

The adjustable nature of the displacer gas spring permits the TDE to operate over a wide range of displacer phase angles and displacer stroke ratios. Volume control rods (VCRs) are installed in the displacer gas spring such that opening of the VCR reduces its stiffness and, correspondingly, reduces the displacer phase angle. A valve is installed between the gas spring volume and bounce space to permit control of the displacer stroke ratio through increased gas spring damping. Both the VCR and damping valve can be adjusted routinely during testing to obtain specific engine dynamics.

The following section is a discussion of the geometry of selected critical components and their potential impact on engine performance, as well as the history of the engine component assemblies evaluated.

3.1 CRITICAL COMPONENTS AND CLEARANCES

3.1.1 Expansion-Space Clearance Volume

Figures 3-2 and 3-3 illustrate the critical components and clearances of the TDE section. The expansion-space clearance volume (generated by the differences in the radii of curvature between the displacer dome and displacer-cylinder sleeve radii, and the entrance region to the heater head heat transfer channels) is the volume that would not be swept by the displacer if the displacer were extended to its stroke limit into the hot end of the engine. The expansion-space clearance volume adds to the unswept expansion-space volume for a prescribed displacer stroke (referred to as the displacer-to-piston-stroke ratio) as expansion-space dead volume.

3.1.2 Appendix Gap

The appendix gap is the region between the displacer and the displacer cylinder wall, including the annular gap between the displacer seal region and the seal cylinder. In the actual hardware, there is a slight taper in the cylindrical portion of the displacer dome due to fabrication requirements. The displacer appendix gap is given as the mean radial cold clearance between the cylindrical portion of the dome and the displacer cylinder sleeve.

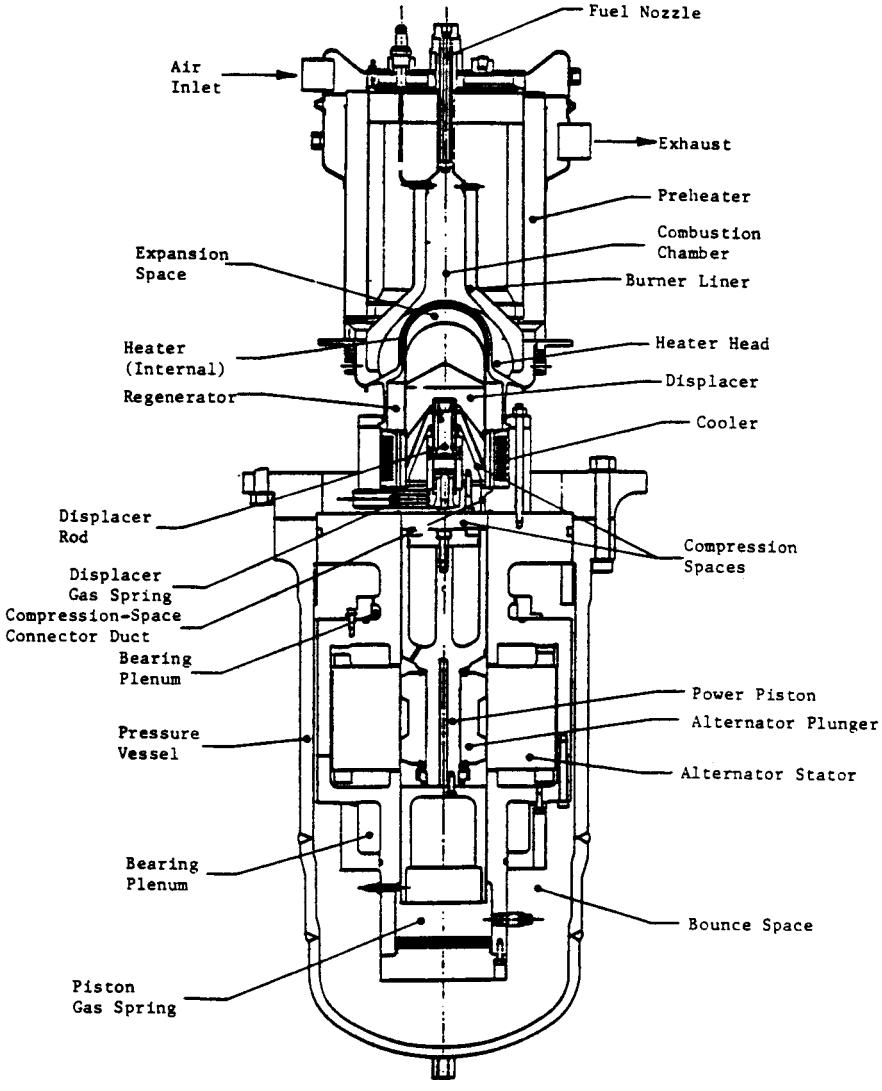

Fig. 3-1. TDE Layout

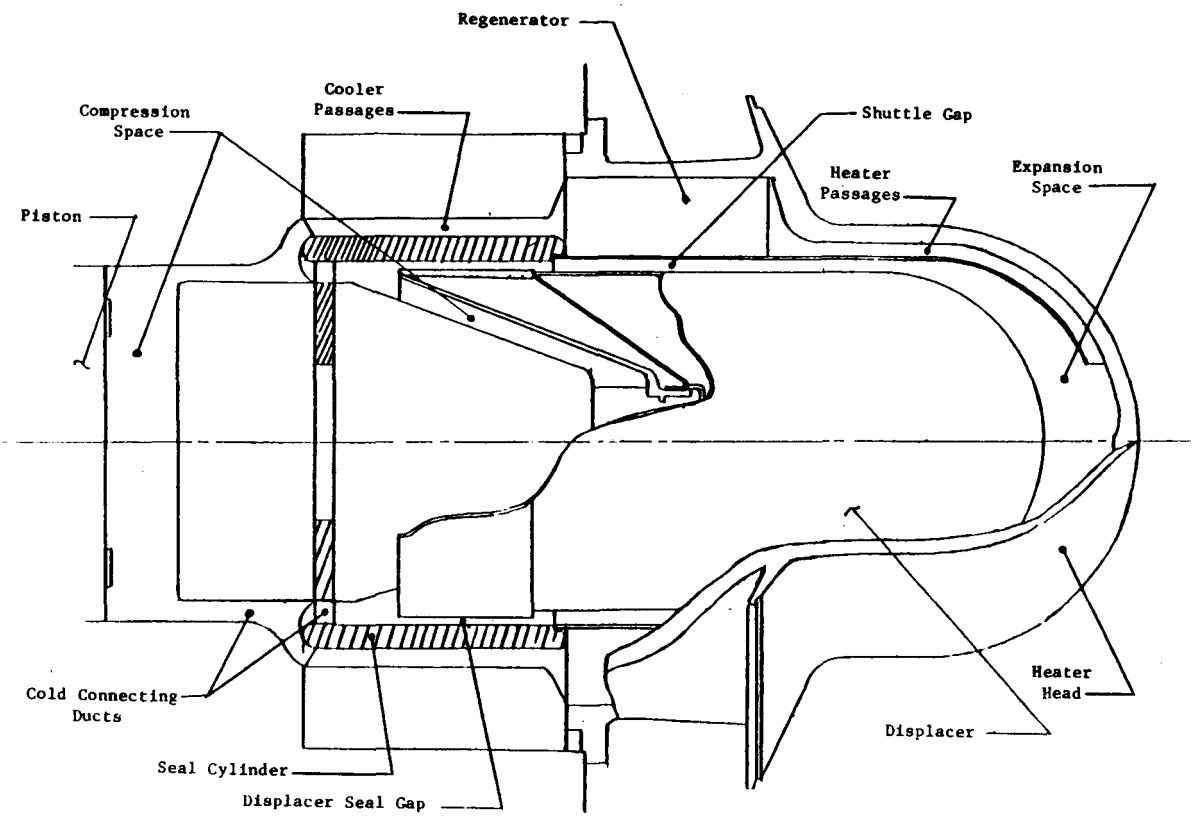

Fig. 3-2. TDE Gas Passages

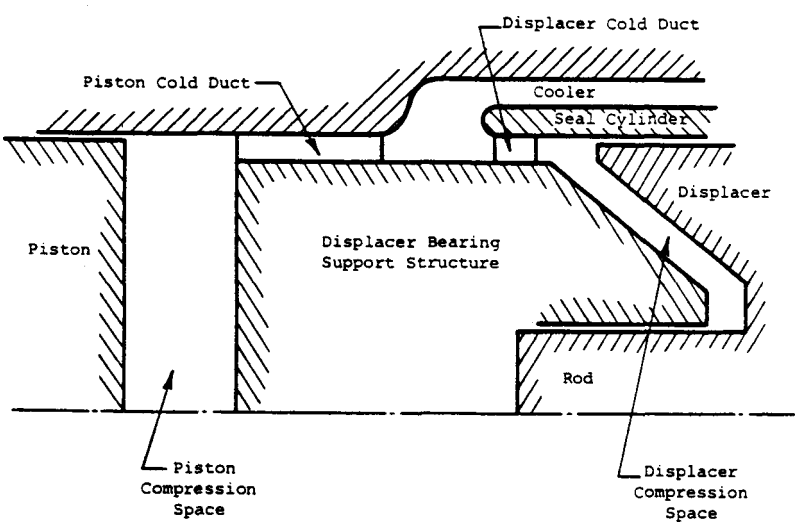

Fig. 3-3. TDE Compression-space Geometry

The displacer cylinder sleeve is a one-piece, thin-walled cylinder that forms the inside wall of the annular regenerator, separating the heater head heat transfer channels from the expansion space. The displacer dome is a thin-walled shell vented through the displacer rod to the bounce space. Two internal radiation shields are installed in the displacer dome to control radiation heat transfer. Internal convection currents resulting from both the motion of the displacer and the thermal gradient across it could cause significant heat transfer between the two radiation shields, as well as between the lower radiation shield and the displacer seal region.

3.1.3 Regenerator

The TDE base regenerator consists of approximately 1300 square-weave, 100-mesh, 0.001 in. diameter wire screens stacked together in the annular regenerator cavity between the heater head and the displacer cylinder sleeve. The entrance and exit regions of the regenerator are set by the heater head and cooler flow channels. The regenerator void volume accounts for a major portion of the engine dead volume.

3.1.4 Displacer Seal Gap

The displacer seal gap, which separates the hot expansion space from the cold compression space, is formed by the displacer seal skirt and seal cylinder.

3.1.5 Cold Connecting Duct

The compression space is separated into two regions identified as the displacer compression space and the piston compression space. The two compression spaces are connected by the cold connecting duct.

3.1.6 Displacer Drive Support

The displacer drive support (shown in Fig. 3-3) incorporates the cooler housing, gas bearing bore, and displacer support cone. This displacer drive packaging arrangement results in a relatively large wetted surface area in the compression space.

3.1.7 Compression Space

The compression space in the TDE is sealed from the bounce space by the clearance seal between the power piston and cylinder, and the clearance seal between the displacer rod and bearing. Although these clearances are small, the eccentricity in the clearances is unknown. The clearance seal coefficient (Dh^3/L) used in the analyses is given an eccentricity factor that assumes the piston and rod are 50% eccentric in their respective cylinders.

3.2 TDE BUILD HISTORY

Five basic tests were conducted:

- Baseline engine test,
- Compression-space hysteresis tests,

- Regenerator tests,
- Displacer appendix gap tests, and
- Displacer seal gap tests.

The TDE build history, showing the hardware combination and operating times for each of the five tests, is outlined in Table 3-1. Prior to this testing period, the TDE-alternator system accumulated a total of 335.8 operating hours. At the writing of this report, the system had accumulated 467.4 operating hours. Table 3-1 lists the major hardware components by serial number, shows the critical dimensions for each piece, and sequentially shows the engine configuration number relative to the first major engine build reported in Reference 1. The description of the engine build briefly defines major hardware component changes. The build number is the sequential assemblies of each engine configuration. Each hardware component is indicated in the table by the component number described in Table 3-2. The start date is the date that actual hardware assembly was initiated. Engine run time for each build is the total accumulated engine operating time for that assembly. The reasons for any disassembly (constituting a new build number) are indicated in the remarks column of Table 3-1.

Table 3.1. TDE Build History

Base Engine

ENGINE CONF.	DESCRIPTION	BUILD NO.	HEATER HEAD	DISPL. CYL.	DISPL.	DISPL. ROD	DISPL. BRG.	DISPL. SEAL	COOLER HOUSE	REGEN. HOUSE	BUMPER SUPPORT	REGEN.	PISTON & CAP	PISTON C/S CAP	START DATE	RUN TIME HOURS	REMARKS
21	Baseline TDE Gas-Fired, Large Rod Wear Couple	1	4	2	5	12	5	4	2	2	1	1	3	4	7Jul81	4.62	Fuel nozzle plug burner disassembled
		2	↓	↓	↓	↓	↓	↓	↓	↓	↓	↓	↓	↓	8Jul81	6.68	Burner disassembled, inspect for domes
		3	↓	↓	↓	↓	↓	↓	↓	↓	↓	↓	↓	↓	8Jul81	16.60	Engine teardown
		4	↓	↓	↓	↓	↓	↓	↓	↓	↓	↓	↓	↓	21Jul81	9.35	Engine unstable, o-rings
		5	↓	↓	↓	↓	↓	↓	↓	↓	↓	↓	↓	↓	30Jul81	5.07	Burner disassembled, VCR roll pin shimmed
		6	↓	↓	↓	↓	↓	↓	↓	↓	↓	↓	↓	↓	3Aug81	0.32	Burner disassembled, replaced combustor
		7	↓	↓	↓	↓	↓	↓	↓	↓	↓	↓	↓	↓	4Aug81	0.88	Engine unstable, liner damaged handling, replaced
		8	↓	↓	→6	↓	↓	↓	↓	↓	↓	↓	↓	↓	5Aug81	10.58	
																389.90	Total Engine Hours

Hysteresis Test

ENGINE CONF.	DESCRIPTION	BUILD NO.	HEATER HEAD	DISPL. CYL.	DISPL.	DISPL. ROD	DISPL. BRG.	DISPL. SEAL	COOLER HOUSE	REGEN. HOUSE	BUMPER SUPPORT	REGEN.	PISTON & CAP	PISTON C/S CAP	START DATE	RUN TIME HOURS	REMARKS
21	Base engine with probes replaced	10	4	2	5	12	4	4	2	2	1	1	3	4	29Sep81	0.73	Replaced wear-couple brg. with air bearing
26	Base engine air bearing	1	↓	↓	↓	↓	→16	↓	↓	↓	↓	↓	↓	↓	60ct81	0.20	Displacer ran biased to hot end
27	Base eng. C air brg shimmed back .021	1	↓	↓	↓	↓	↓	↓	↓	↓	↓	↓	↓	↓	70ct81	0.20	Displacer would not hold port
28	Base eng. with new wear-couple bearing	1	↓	↓	↓	↓	→17	↓	↓	↓	↓	↓	↓	↓	90ct81	1.53	Installed finned end cap
29	Hysteresis test finned plug	1	↓	↓	↓	↓	↓	↓	↓	↓	↓	↓	→4	↓	130ct81	0.52	Replaced piston to seal end cap bolt
29	Hysteresis test finned plug	2	↓	↓	↓	↓	↓	↓	↓	↓	↓	↓	↓	↓	140ct81	3.23	Installed unfinned plug
30	Hysteresis test unfinned plug	1	↓	↓	↓	↓	↓	↓	↓	↓	↓	↓	→5	↓	150ct81	6.07	
																430.60	Total Engine Hours

Appendix Gap Test

ENGINE CONF.	DESCRIPTION	BUILD NO.	HEATER HEAD	DISPL. CYL.	DISPL.	DISPL. ROD	DISPL. BRG.	DISPL. SEAL	COOLER HOUSE	BRG. HOUSE	BUMPER SUPPORT	REGEN.	PISTON & CAP	PISTON C/S CAP	START DATE	RUN TIME HOURS	REMARKS
28	Base eng. 28 modified for internal C/S bearing pump	2	4	2	5	12	17	4	2	2	7	1	3	4	230ct81	5.20	Installed redesigned displacer/air bearing
31	.5-mm shuttle gap engine, .0048 seal clearance	1	↓	↓	13	13	16	↓	↓	↓	↓	↓	↓	↓	5Nov81	2.70	Installed smaller diameter seal cylinder
32	.5-mm shuttle gap engine, .0015 seal clearance	1													11Nov81	2.18	Installed 1.1-mm shuttle gap displacer
33	1.1-mm shuttle gap engine, .0015 seal clearance	1			14	16									17Nov81	1.67	Reworked displacer rod for improved position signal
33	1.1-mm shuttle gap engine, .0015 seal clearance	2													20Nov81	2.75	Installed 2.3-mm shuttle gap displacer
34	2.3-mm shuttle gap engine, .0014 seal clearance	1			16	15									24Nov81	1.78	
																446.90	Total Engine Hours

Table 3.1. TDE Build History (Contd.)

Metex Regenerator Test

ENGINE CONF.	DESCRIPTION	BUILD NO.	HEATER HEAD	DISPL. CYL.	DISPL.	DISPL. ROD	DISPL. BRG.	DISPL. SEAL	COOLER HOUSE	BRG. HOUSE	BUMPER SUPPORT	REGEN.	PISTON & CAP	PISTON C/S CAP	START DATE	RUN TIME HOURS	REMARKS
21	Last TDE baseline ling engine build	8	4	2	5	12	6	4	2	2	1	1	3	4	5Aug81	10.58	Changed VCR & sleeve
21	VCR & sleeve replaced	9	↓	↓	↓	↓	↓	↓	↓	↓	↓	↓	↓	↓	24Aug81	5.20	Reworked probe feed through & relocated "blip" line
22	85%-porosity regen., .0025 wire	1	↓	↓	↓	↓	↓	↓	↓	↓	↓	→3	↓	↓	14Sep81	-	Igniter shorting at re-generator backing plate
22	85% regen., ignition lead short repaired	2	↓	↓	↓	↓	↓	↓	↓	↓	↓	↓	↓	↓	15Sep81	5.22	Regenerator removed
23	80% porosity regen., .0025 wire	1	↓	↓	↓	↓	↓	↓	↓	↓	↓	→4	↓	↓	16Sep81	2.00	Displacer C/S damping line failed
23	80% regen, C/S damping line replaced	2	↓	↓	↓	↓	↓	↓	↓	↓	↓	↓	↓	↓	17Sep81	3.77	Regen. removed, displacer bearing shimmed
24	75% porosity regen., .0025 wire	1	↓	↓	↓	↓	↓	↓	↓	↓	↓	→5	↓	↓	21Sep81	4.13	Regen. removed, combustor controller on line
25	70% porosity regen., .0025 wire	1	↓	↓	↓	↓	↓	↓	↓	↓	↓	→6	↓	↓	23Sep81	7.87	Reinstalled baseline regenerator
																418.10	Total Engine Hours

Regenerator Test

ENGINE CONF.	DESCRIPTION	BUILD NO.	HEATER HEAD	DISPL. CYL.	DISPL.	DISPL. ROD	DISPL. BRG.	DISPL. SEAL	COOLER HOUSE	BRG. HOUSE	BUMPER SUPPORT	REGEN.	PISTON & CAP	PISTON C/S CAP	START DATE	RUN TIME HOURS	REMARKS
	Base engine with reduced water in temp. & air brg.		4	2	5	12	16								25Nov81	1.50	Removed regenerator for Metex test
35	.002 seal clearance, .5-mm shuttle, 70% porosity, .0035 wire	1													3Dec81	1.283	Installed 75% regenerator
36	.002 seal clearance, .5-mm shuttle, 75% porosity, .0035 wire														3Dec81	1.617	Installed 80% regenerator
37	.002 seal clearance, .5-mm shuttle, 75% porosity, .0035 wire														4Dec81	2.38	Installed 85% regenerator
38	.002 seal clearance, .5-mm shuttle, 80% porosity, .0035 wire														8Dec81	1.37	
																455.10	Total Engine Hours

Displacer Seal Test

ENGINE CONF.	DESCRIPTION	BUILD NO.	HEATER HEAD	DISPL. CYL.	DISPL.	DISPL. ROD	DISPL. BRG.	DISPL. SEAL	COOLER HOUSE	BRG. HOUSE	BUMPER SUPPORT	REGEN.	PISTON & CAP	PISTON C/S CAP	START DATE	RUN TIME HOURS	REMARKS
39	1.1-mm shuttle gap displ. reworked for .0015 ring clearance	1	4	2	18	16									17Dec81	1.017	Removed displacer to remove piston ring
39	Conf. 39 without piston ring	2													21Dec81	1.23	Removed displacer for clearance rework
40	1.1-mm shuttle gap displ. reworked for .0031 ring clearance	1			19										24Dec81	2.17	Removed displacer to remove piston ring
40	Conf. 40 without piston ring	2													28Dec81	0.97	Removed displacer for clearance rework
41	1.1-mm shuttle gap disp. reworked for .0050 ring clearance	1			20										29Dec81	1.15	Removed displacer to remove piston ring
42	Conf. 41 without piston ring	2													31Dec81	0.75	Removed displ. to back piston ring with o-ring
42	Conf. 42 E o-ring-backed piston ring	3													4Jan82	4.82	
																467.36	Total Engine Hours

Table 3.2. TDE/ECUT Component Hardware Description

HEATER HEAD #4 - The TDE heater head is a monolithic, high-temperature pressure vessel with internal EDM'ed fins and 48 individual external fins brazed to the outside. The internal heat-exchanger passages are separated from the expansion space by a thin-walled shell that is electron-beamed welded to the internal fins.

DISPLACER CYLINDER #2 - Thin-walled hydroformed shells separate heater head heat-transfer channels from the expansion space, forming the appendix gap O.D.

Critical Dimensions: 1. Inside Diameter - 3.6984

DISPLACER #5 - One of the original DOE displacers reworked to accommodate different rods.

Critical Dimensions: 1. Mass (with rod assembly) - 0.8790 kg
2. Seal Skirt Diameter - 3.6749 nominal
3. Mid-Span Dome Diameter - 3.6583 nominal
4. Seal Skirt Length -
5. Effective Shuttle Gap - 0.50 mm

DISPLACER #13 - Displacer redesigned to eliminate rod cone to displacer seal skirt butt weld.

Critical Dimensions: 1. Mass (with rod assembly) - 0.9450 kg
2. Seal Skirt Diameter - 3.6771 nominal
3. Mid-Span Dome Diameter - 3.5934
4. Seal Skirt Length - 1.4220
5. Effective Shuttle Gap - 0.50 mm

DISPLACER #14 - Reduced dome diameter displacer.

Critical Dimensions: 1. Mass (with rod assembly) - 0.9300 kg
2. Seal Skirt Diameter - 3.6782
3. Mid-Span Dome Diameter - 3.5934
4. Seal Skirt Length - 1.4220
5. Effective Shuttle Gap - 1.10 mm

DISPLACER # 16 - Reduced dome diameter displacer.

Critical Dimensions: 1. Mass (with rod assembly) - 0.9720 kg
2. Seal Skirt Diameter - 3.6783
3. Mid-Span Dome Diameter - 3.5190
4. Seal Skirt Length - 1.4210
5. Effective Shuttle Gap - 2.30 mm

DISPLACER #18 - Displacer #14 reworked to accommodate a piston ring.

Critical Dimensions: 1. Mass (with rod assembly)
- without piston ring - 0.9120 kg
- with piston ring - 0.9220 kg
2. Seal Skirt Length - 3.6782

DISPLACER #19 - Displacer #18 reworked to reduce the seal skirt diameter.

Critical Dimensions: 1. Mass (with rod assembly)
- without piston ring - 0.8980 kg
- with piston ring - 0.9090 kg
2. Seal Skirt Diameter - 3.6751 nominal

DISPLACER #20 - Displacer #19 reworked to reduce the seal skirt diameter.

Critical Dimensions: 1. Mass (with rod assembly)
- without piston ring - 0.8940 kg
- with piston ring - 0.9040 kg
2. Seal Skirt Diameter - 3.6708

DISPLACER ROD #12 - Cr_2O_3 coated rod used in Displacer #5.

Critical Dimensions: 1. Rod Diameter - 1.1793 nominal

DISPLACER ROD #13 - Cr_2O_3 coated rod used in Displacer #13.

Critical Dimensions: 1. Rod Diameter - 1.1790 nominal

DISPLACER ROD #16 - Cr_2O_3 coated rod used in Displacer #14.

Critical Dimensions: 1. Rod Diameter - 1.1790 nominal

DISPLACER ROD #15 - Cr_2O_3 coated rod used in Displacer #16.

Critical Dimensions: 1. Rod Diameter - 1.1785 nominal

DISPLACER BEARING #4 - Hardened steel wear couple bearing.

Critical Dimensions: 1. Bearing Bore - 1.1810
2. Compression-Space Engine Seal Length - 1.4400

DISPLACER BEARING #5 - Hardened steel wear couple bearing.

Critical Dimensions: 1. Bearing Bore - 1.1808 nominal
2. Compression-Space Engine Seal Length - 1.4400

DISPLACER BEARING #6 - Hardened steel wear couple bearing.

Critical Dimensions: 1. Bearing Bore - 1.1806
2. Compression-Space Engine Seal Length - 1.4400

DISPLACER BEARING #17 - Hardened steel wear couple bearing.

Critical Dimensions: 1. Bearing Bore - 1.1808
2. Compression-Space Engine Seal Length - 1.4400

DISPLACER BEARING #16 - Hydrostatic air bearing.

Critical Dimensions: 1. Bearing Bore - 1.1804
2. Compression-Space Engine Seal Length - 0.4720

DISPLACER SEAL CYLINDER #2 - Baseline seal cylinder.

Critical Dimensions: 1. I.D. of Seal Diameter - 3.6845

DISPLACER SEAL CYLINDER #3 - Cr_2O_3 coated seal cylinder (original DOE).

Critical Dimensions: 1. I.D. of Seal Diameter - 3.6811

DISPLACER SEAL CYLINDER #4 - New seal cylinder fabricated for piston ring tests.

Critical Dimensions: 1. I.D. of seal diameter - 3.6811

COOLER HOUSING #2 - Original DOE cooler housing reworked for hardware interchangeability.

BEARING HOUSING #2 - Original displacer bearing housing.

PISTON END CAP #3 - Redesigned piston end cap.

PISTON END CAP #4 - Finned end cap for hysteresis tests.

Critical Dimensions: 1. Surface Area - 0.220 in^2

PISTON END CAP #5 - Unfinned end cap for hysteresis tests.

Critical Dimensions: 1. Surface Area - 0.160 in^2

PISTON GAS SPRING CAP #4 - Redesigned to remove velocity probe.

4. BASELINE ENGINE TESTS

4.1 TEST OBJECTIVES

The baseline geometry of the TDE was tested during July/August, 1981, in the Stirling engine test laboratory at MTI's New Karner Road facility. Test objectives were to:

- Establish the performance of the baseline TDE geometry,
- Define the engine operating envelope, and
- Establish performance repeatability.

Performance data generated over a wide range of thermodynamic/mechanical dynamic operating conditions will provide a data base for evaluating the results of subsequent loss mechanism tests, as well as demonstrate the suitability of the TDE for operation as a general Stirling engine test bed.

4.2 TEST METHODS

Three series of tests were performed with a charge pressure of 40 bar. During the first series--to investigate performance variation of the baseline TDE with heater temperature/piston stroke and establish its operating envelope--both the VCR and damping valve were closed to permit operation at maximum displacer phase and corresponding maximum stroke ratio. The second series of tests investigated the performance variation with VCR setting and piston stroke at a fixed heater control temperature of 500°C, permitting high-power operation over a wide range of piston strokes. The third series investigated the performance variation with displacer stroke ratio and phase angle at a fixed mean heater temperature of 450°C, and a fixed piston stroke of 2.2-cm.

4.2.1 Test Series 1

Initial testing focused on determination of engine performance variation with stroke at heater control temperatures (T/C #12) of 400 and 500°C. The engine was operated at a 2.0-cm piston stroke while being heated to a 400°C control temperature. After the engine was stabilized at this temperature level, the piston stroke was varied in discrete steps over its operating range. Performance data were recorded at each discrete piston stroke, and limiting piston strokes were established. The lower limit corresponded to an engine instability at a 1.4-cm piston stroke. The instability was characterized by a large oscillation in stroke amplitude with an approximate frequency of 2-3 Hz.

A similar procedure was used to characterize the engine performance at a 500°C control temperature. The maximum piston stroke again corresponded to the maximum design stroke, while the minimum piston stroke corresponded to an engine stroke instability. The onset of instability, however, occurred at a 1.6-cm piston stroke.

An alternative procedure was used to investigate the temperature dependence of this engine instability. Starting at a control temperature of 400°C, the engine was heated at fixed stroke until either the combustor facility airflow limit was reached, or an engine instability occurred. The required stroke was held constant during the heat input process by increasing the engine load. The heat input process was accomplished in small step changes to permit the acquisition of performance data at intermediate heater temperatures. During operation at piston strokes of 2.2- and 2.4-cm, the combustor facility limit was reached before instability occurred (at a control temperature of 580°C). After establishing the repeatability of this behavior at the 2.0-cm stroke, the procedure was applied at successively lower strokes to determine the temperature dependence of the low-stroke instability.

In summary, Test Series 1 investigated the variation of TDE performance with heater control temperature and piston stroke, and established the TDE operating envelope. Performance curves based on these test results are presented in Section 4.3. The operating limits are defined by a temperature-dependent, low-stroke instability; the combustor facility airflow limit; and the 2.5-cm maximum design stroke curves.

4.2.2 Test Series 2

Performance variation with piston stroke was investigated for nominal VCR settings of 50 and 100% open. Opening the VCR increased both the mean volume and wetted surface area of the gas spring, correspondingly reducing both its stiffness and damping. The reduced gas spring stiffness caused the displacer phase angle to decrease. Reduction in both the displacer phase angle and gas spring damping lowered the total damping on the displacer, causing the displacer stroke ratio to increase. Insufficient displacer damping will permit the displacer to impact the engine structure at each end of its stroke range. The gas spring damping valve was adjusted to control the total displacer damping, and to maintain the stroke ratio within an acceptable operating range.

The following procedure was followed to adjust the damping valve for each VCR setting: After stabilizing the engine at a 400°C heater control temperature and a 2.2-cm piston stroke, the damping valve was opened until the stroke ratio corresponded to the value measured during the closed VCR test. The damping valve setting was maintained constant while performance variation with stroke was investigated. Testing at each VCR setting followed the appropriate procedure from Test Series 1. Performance curves based on these test results are presented in Section 4.3.

4.2.3 Test Series 3

Performance variation with displacer stroke ratio and phase angle was investigated for a mean heater temperature of 450°C and a piston stroke of 2.2-cm. The displacer stroke ratio and phase angle were varied by simultaneous adjustments of the VCR and damping valve. Data were recorded for operation at discrete displacer stroke ratios and phase angle settings. A thermodynamic map based on the test results is presented in Section 4.3.

4.3 TEST RESULTS

4.3.1 Performance Mapping

The results for the first test series, shown in Figures 4-1 through 4-6, include indicated power and efficiency, average heater head temperature, displacer stroke ratio, displacer phase angle, and engine frequency. Engine operating limits observed during the tests are identified in Figures 4-1 through 4-3. Performance variations with stroke at the 400 and 500°C control temperatures were measured directly; however, performance variations with stroke at these control temperatures were interpolated from test data measured during heating at fixed stroke.

Test results for the second test series (see Figs. 4-7 through 4-12) include indicated power and efficiency, average heater temperature, displacer stroke ratio, displacer phase angle, and engine frequency. Test results for the third test series are shown in Figure 4-13 as a thermodynamic map of indicated power versus efficiency. Performance variation with displacer stroke ratio and phase angle demonstrates the influence of engine dynamics on engine thermodynamics. Table 4-1 summarizes the actual test conditions used to generate this map.

4.3.2 System Repeatability

Thermodynamic performance was repeatable for cases of equivalent mean heater temperature and equivalent dynamics. Figures 4-14 and 4-15, respectively, compare the variations of indicated power and efficiency with piston stroke that were measured from engine Builds 21-1 and 21-4. The following disassembly procedures were performed between these builds:

- Burner disassembly to clear a restricted fuel nozzle,
- Burner removal to inspect for heater head dome cracks, and
- Complete engine disassembly and rebuild to evaluate performance repeatability.

Figures 4-16 and 4-17, respectively, compare the variations of indicated power and efficiency with mean heater temperature between engine Builds 21-4 and 21-8. Scatter at each temperature principally reflects small variations in displacer stroke ratio and phase angle. The following disassembly procedures were performed between these builds:

- Teardown to replace gas spring sealing O-rings,
- Burner removal to repair a sheared roll pin in the VCR,
- Burner disassembly to replace a cracked combustor liner, and
- Burner/engine disassembly to replace a damaged combustor liner and a worn displacer bearing.

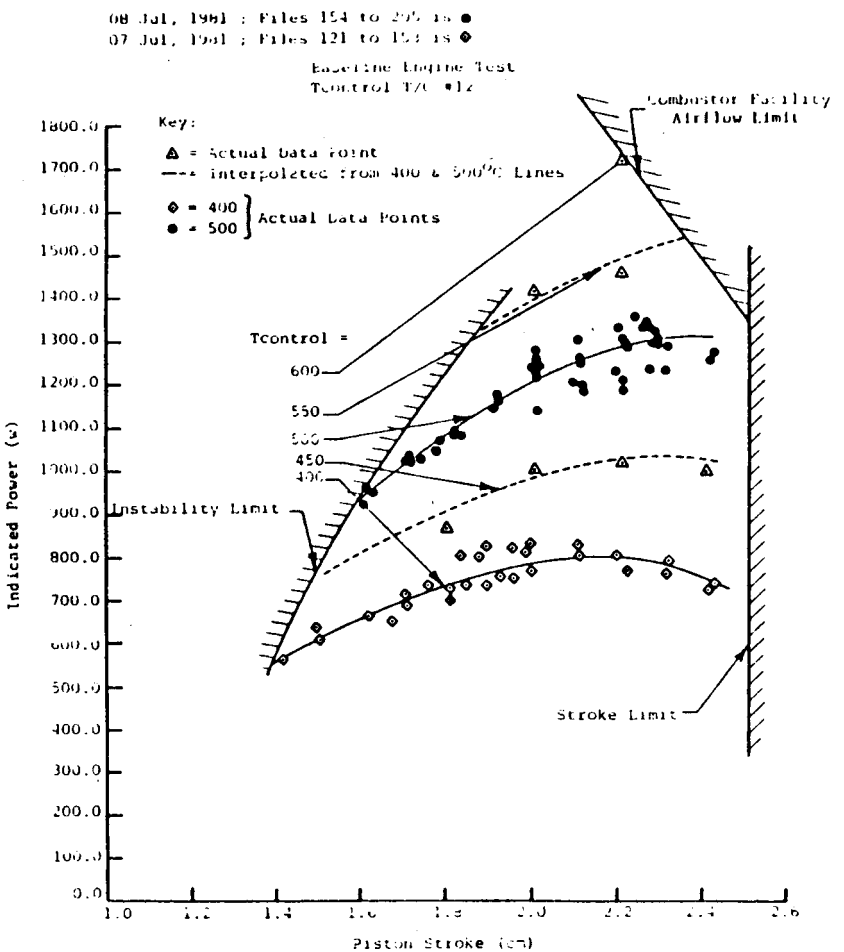

Fig. 4-1. Power Range for Test Series 1

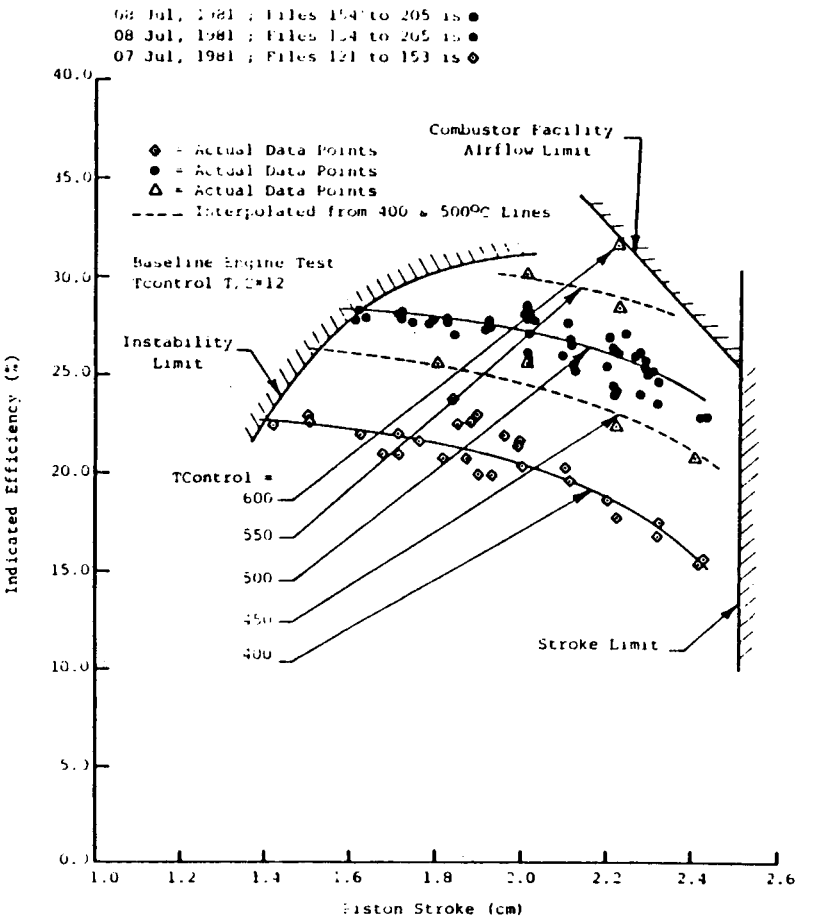

Fig. 4-2. Efficiency Range for Test Series 1

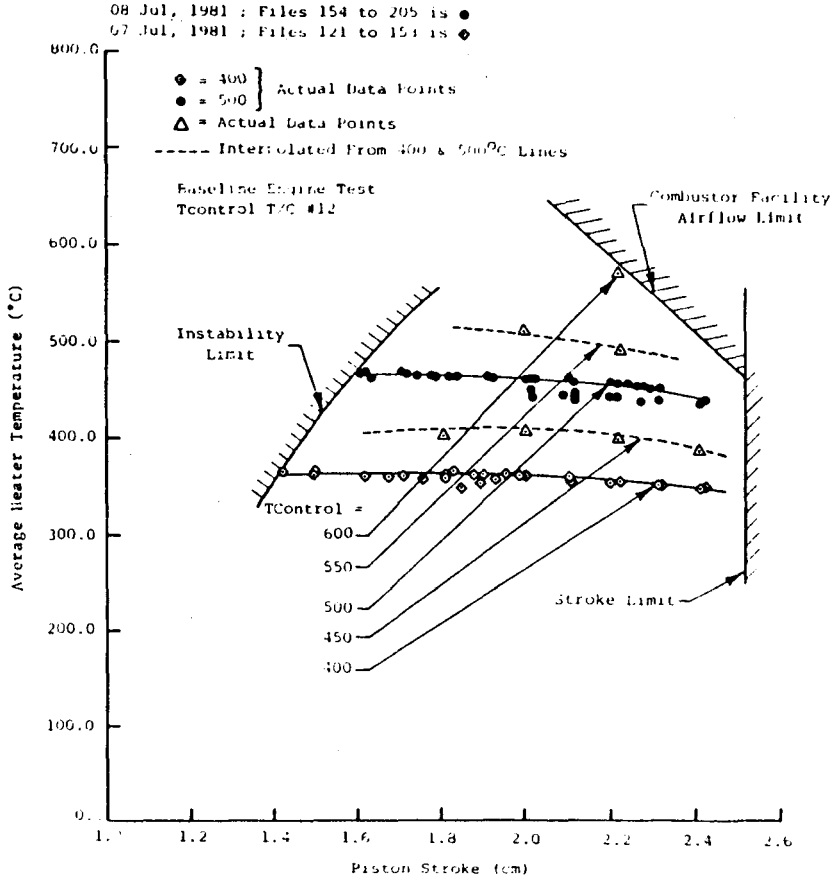

Fig. 4-3. Temperature Range for Test Series 1

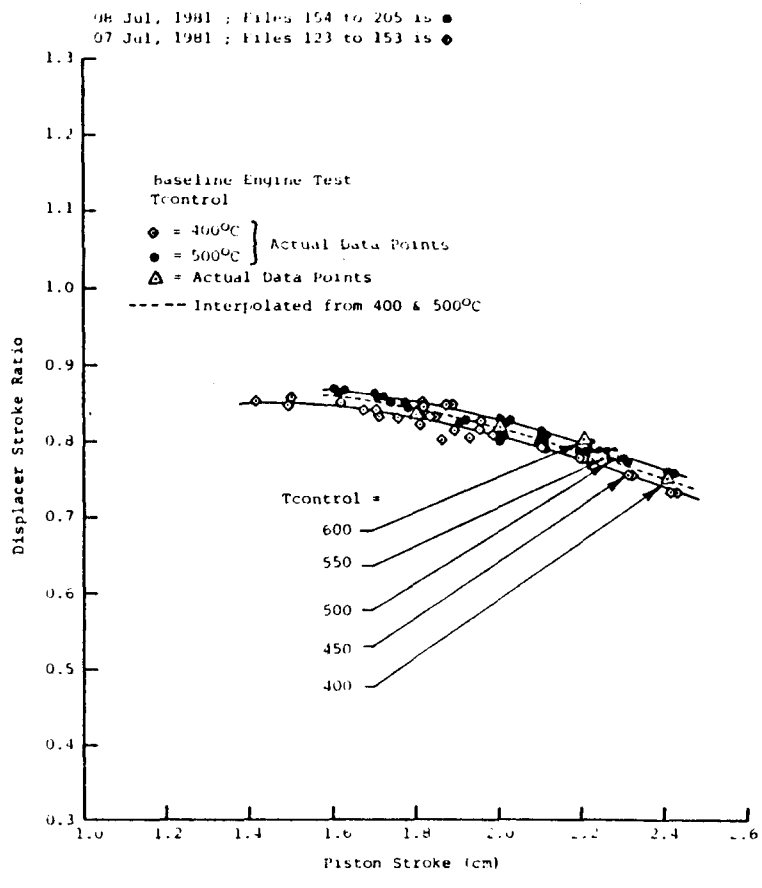

Fig. 4-4. Displacer Stroke Ratio Range for Test Series 1

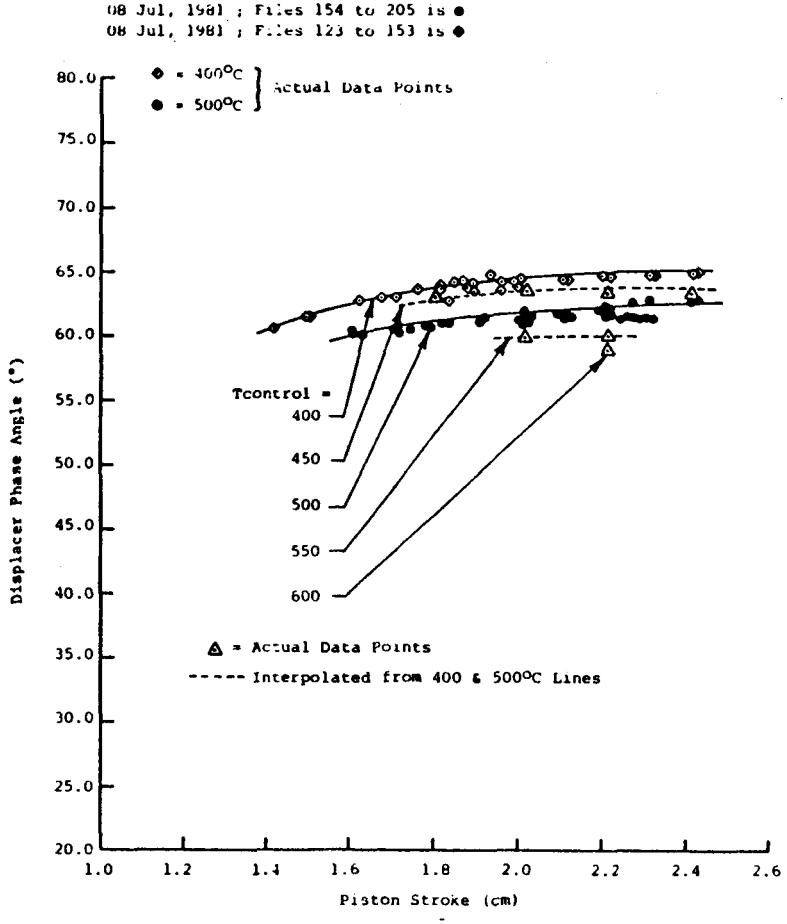

Fig. 4-5. Displacer Phase Angle Range for Test Series 1

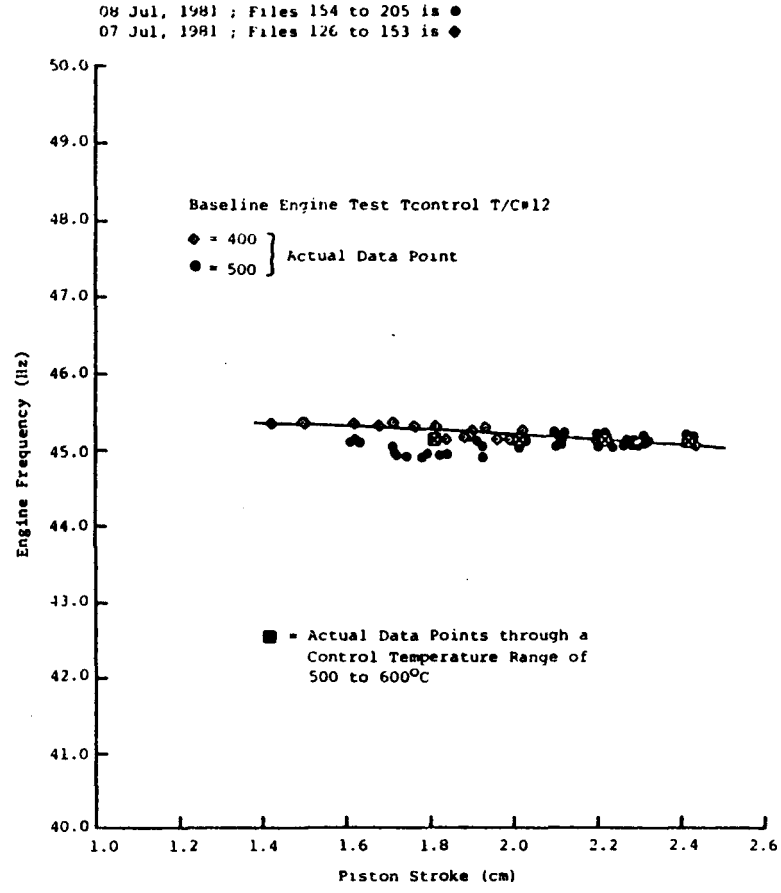

Fig. 4-6. Engine Frequency Range for Test Series 1

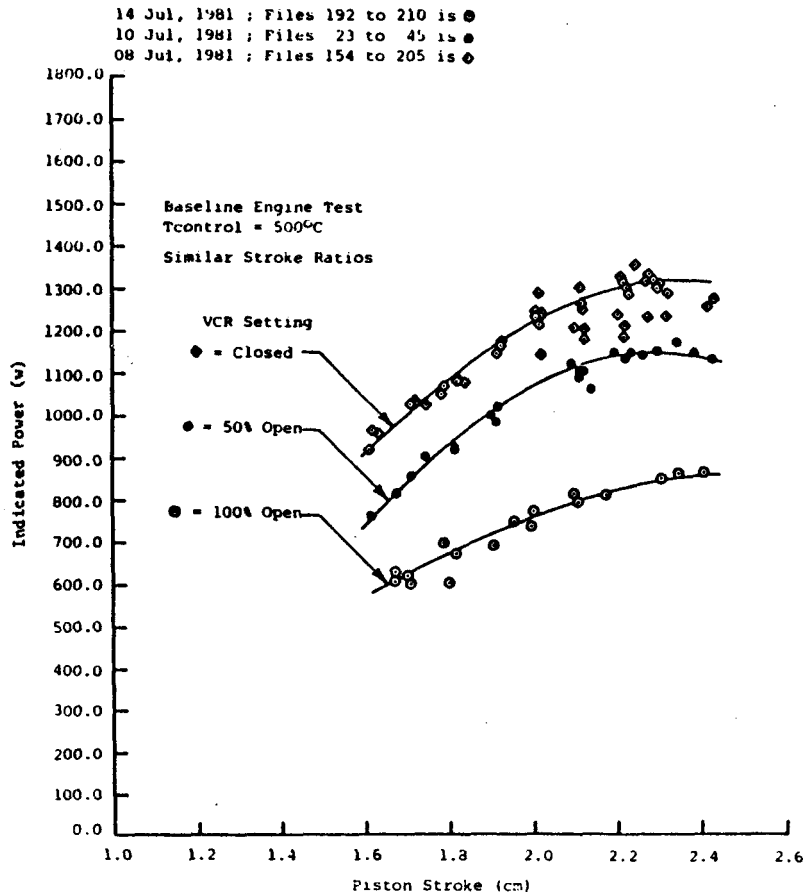

Fig. 4-7. Power Range for Test Series 2

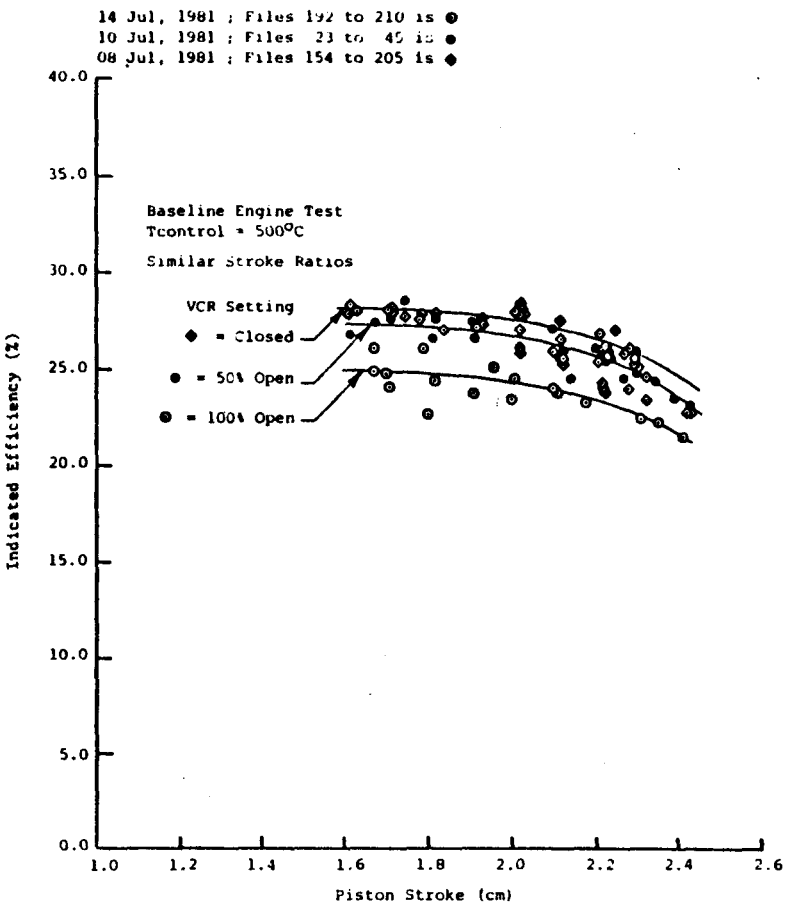

Fig. 4-8. Efficiency Range for Test Series 2

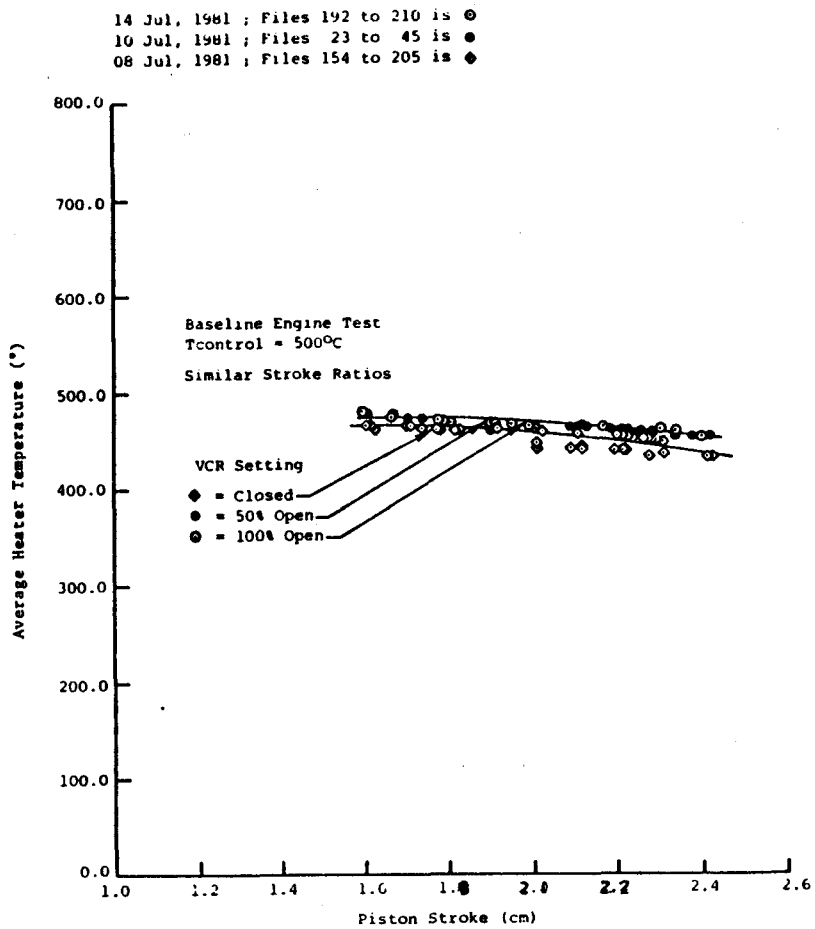

Fig. 4-9. Heater Temperature Range for Test Series 2

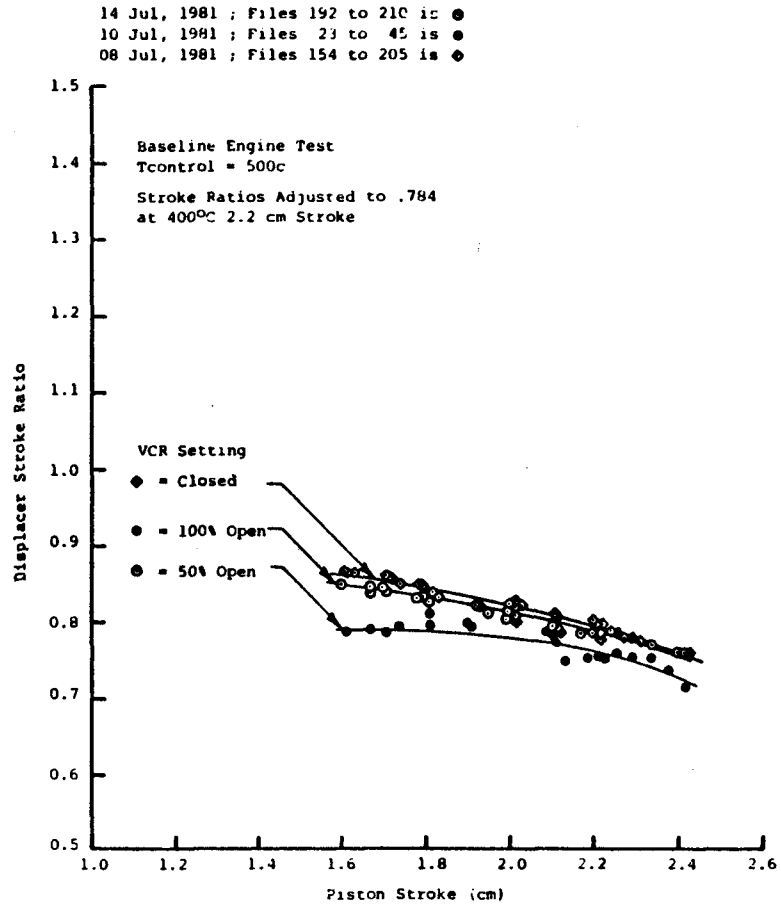

Fig. 4-10. Displacer Stroke Ratio Range for Test Series 2

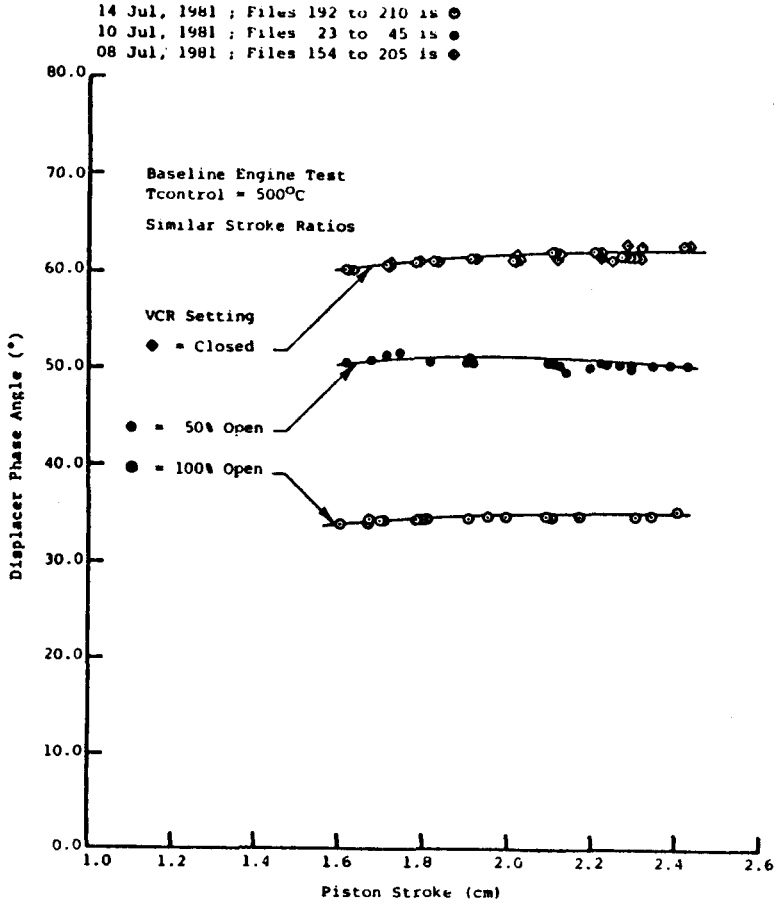

Fig. 4-11. Displacer Phase Angle Range for Test Series 2

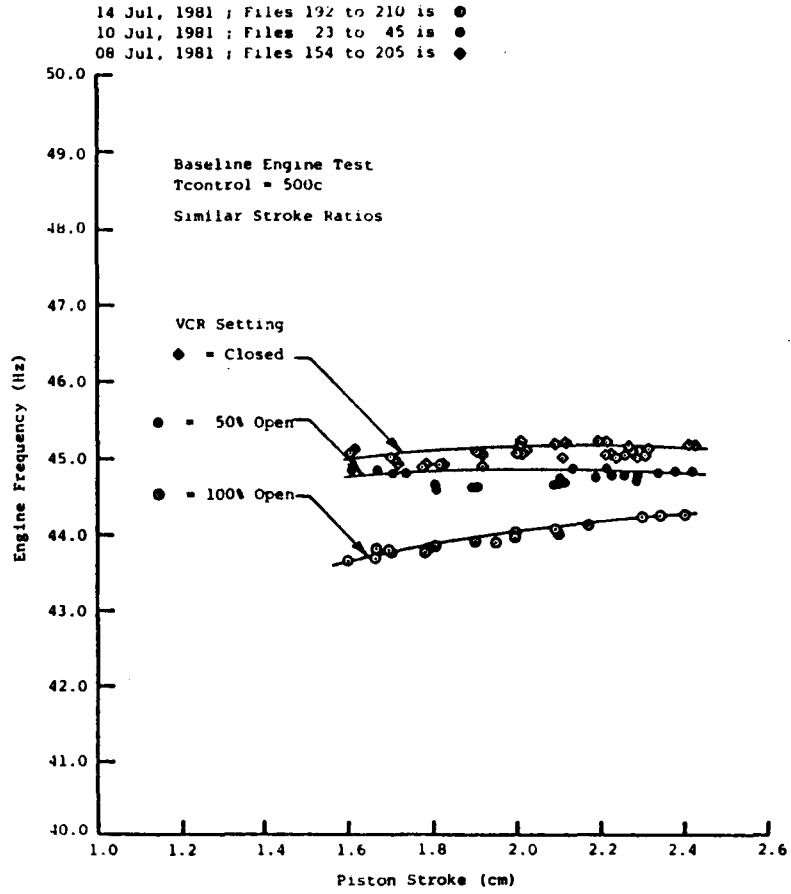

Fig. 4-12. Engine Frequency Range for Test Series 2

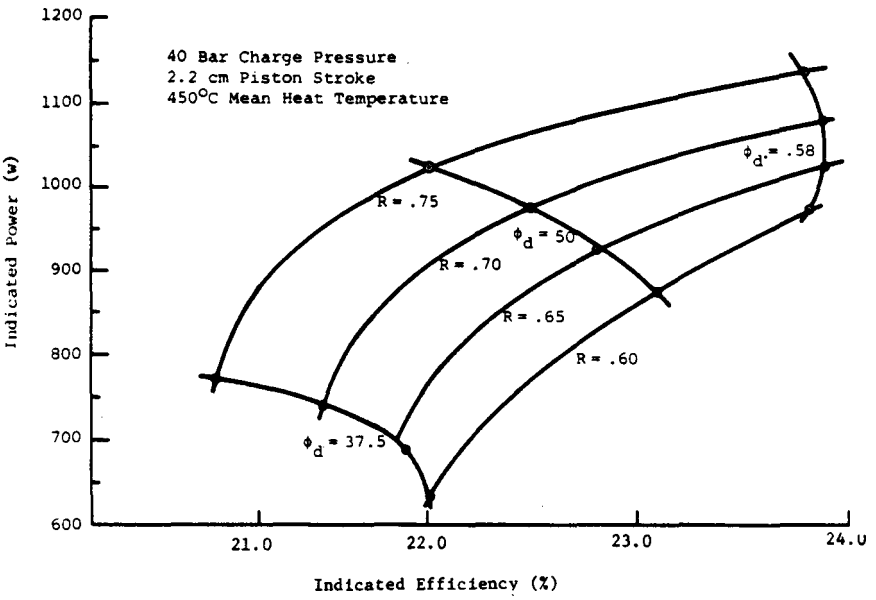

Fig. 4-13. Operating Envelope for Test Series 3

Table 4-1. Test Conditions for Generating Thermodynamic Map of Indicated Power vs. Efficiency
(T_{mean} = 450°C, X_p = 2.2 cm, P_m = 40 Bar)

Test Date 1981	Files	Tape #	PRWN (W)	η TOT (%)	Stroke Ratio	Displacer Phase (deg)
Jul 28	18-57	35	1,000.00 +27.9 -35.0	23.720	.620 +0.004 -0.010	58.99
Jul 30	63-105	35	1,023.00 +37.5 -34.6	23.720 +0.23 -0.93	.661 +0.015 -0.013	58.23 +0.05 -0.76
Jul 30	110-143	35	995.30 +21.0 -27.9	24.186	.637 +0.006 -0.010	58.23 +0.50 -0.26
Jul 30	187-223	35	1,083.70 +23.6 -41.8	24.186 +1.16 -0.47	.695 +0.008 -0.090	58.35 +0.75 -0.38
Jul 30	152-181	35	1,032.60 +37.2 -32.6	24.190 +0.46 -0.93	.657 +0.009 -0.011	57.97 +0.89 -0.47
Jul 30	1-37	36	1,113.95 +41.9 -37.2	23.720	.730 +0.017 -0.017	57.72 +0.38 -0.25
Aug 4	41-56	36	890.70 +32.6 -32.6	23.260 +1.39 -0.91	.618	51.77 +0.51 -0.38
Aug 5	99-129	36	932.56 +32.6 -18.6	22.560	.644 +0.008 -0.007	50.25
Aug 6	130-166	36	946.51 +27.9 -32.6	22.790	.677 +0.005 -0.006	48.99
Aug 6	1-35	37	741.86 +18.6 -27.9	20.700	.761 +0.014 -0.015	35.44 +0.51 -0.64
Aug 6	44-67	37	727.91 +20.9 -18.6	21.630	.675	37.97
Aug 7	73-101	37	730.23 +20.9 -20.9	21.400	.659 +0.006 -0.006	39.11

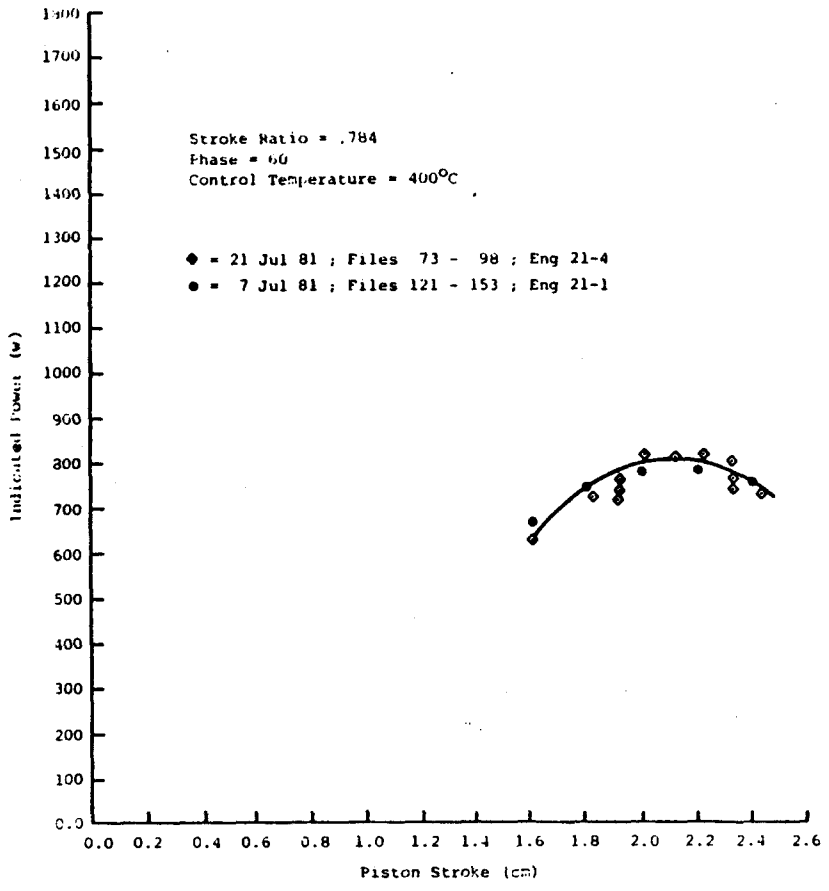

Fig. 4-14. Power Dependence on Piston Stroke, Builds 21-1 and 21-4

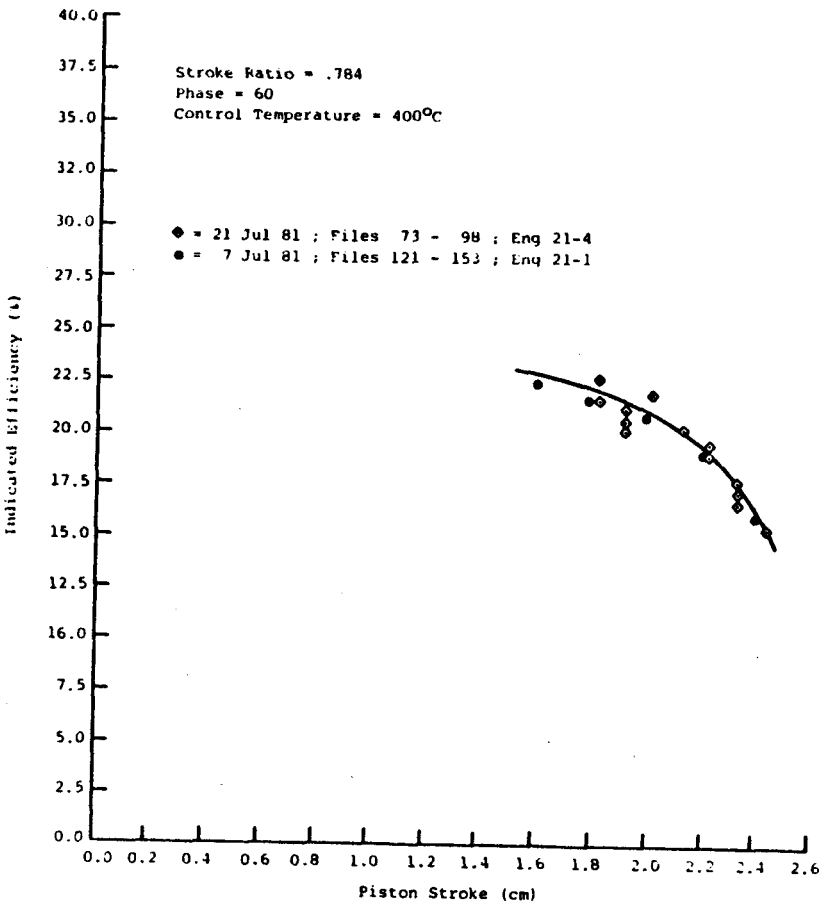

Fig. 4-15. Efficiency Dependence on Piston Stroke, Builds 21-1 and 21-4

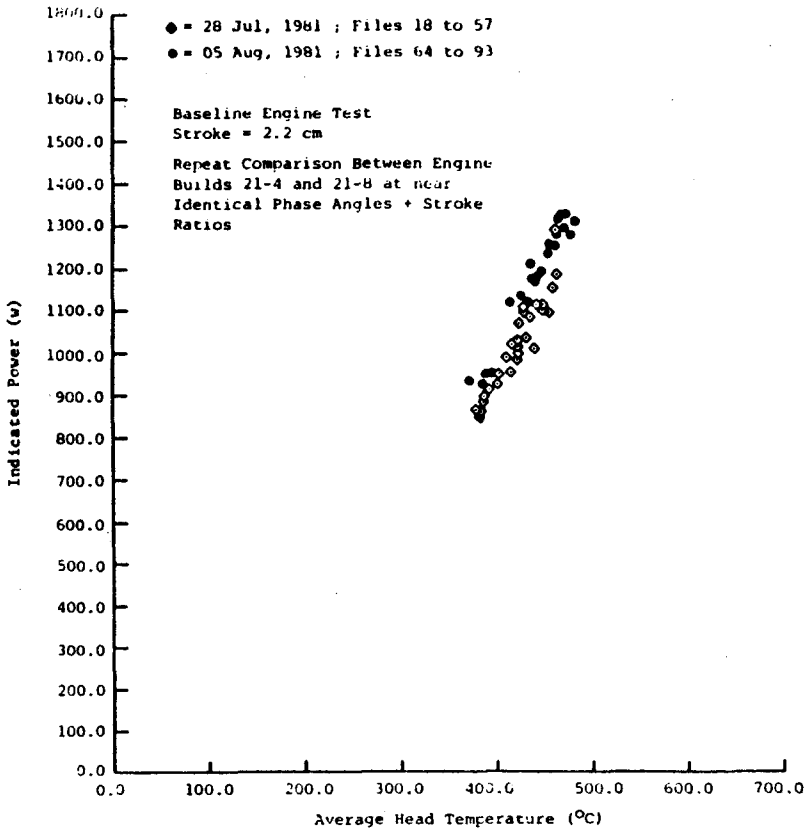

Fig. 4-16. Power Dependence on Temperature, Builds 21-4 and 21-8

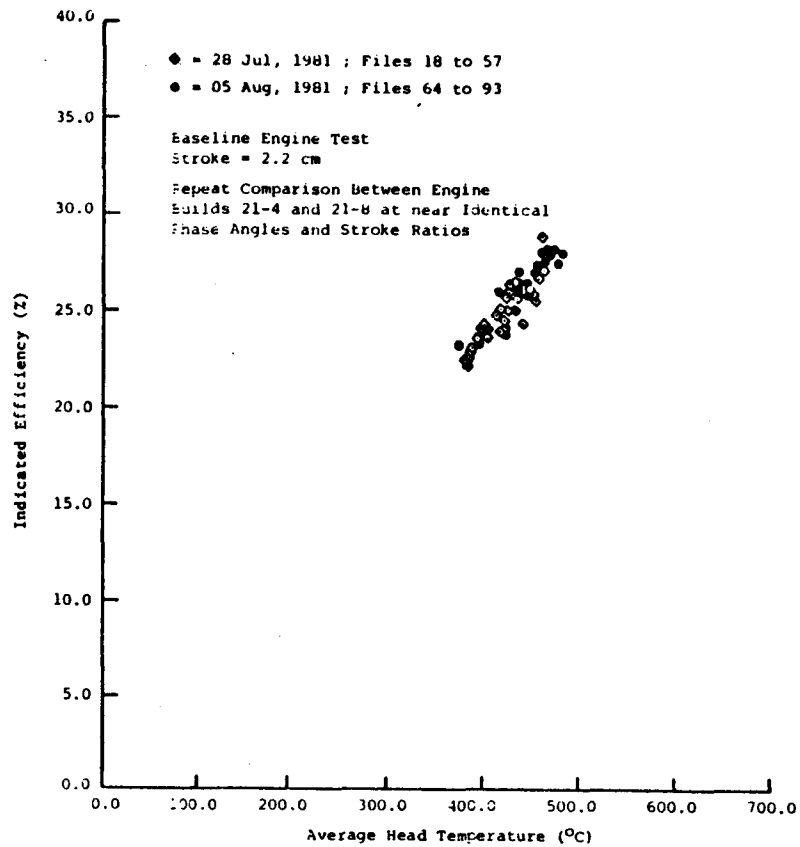

Fig. 4-17. Efficiency Dependence on Temperature, Builds 21-4 and 21-8

In both comparisons, thermodynamic performance was repeatable within a nominal experimental error of +5%.

4.4 ANALYTICAL COMPARISON

Thermodynamic performance of the baseline TDE operating at a control temperature of 500°C was evaluated by comparing measured power and efficiency data with corresponding predictions from MTI's proprietary computer code. The influences of engine dynamics and heat exchanger thermal boundary conditions on the comparison were minimized by basing performance predictions on measured values for piston stroke, displacer stroke ratio, displacer phase angle, operating frequency, heater temperatures, and mean coolant temperature. Typical measured variations of the piston/displacer dynamics parameters and the mean combustor-side heater temperature with piston stroke and VCR setting are shown in Figures 4-9 through 4-12. Because the predictions for each correlation point were based on actual measured parameters, they exhibit scatter about a mean curve similar to the test data. The magnitude of the scatter was minimized by selecting correlation points with approximately the same heater control temperature, and without obvious operating anomalies.

Initial predictions of indicated power and efficiency during operation with the closed VCR settings are compared with baseline test results in Figure 4-18. Measured power correlated well with predicted power for piston strokes less than 2.0-cm, but dropped off relative to predicted power for larger strokes. Measured efficiencies, however, were significantly less than predicted values at all correlation points.

Poor efficiency correlation (particularly at low strokes) suggested the presence of an additional parasitic heat flow. Because predicted heat input is calculated as the sum of heat transferred to the working gas and all modeled parasitic losses, the difference between measured and predicted heat input provided an estimate of this heat flow (shown as a function of stroke in Fig. 4-19).

The influence of this heat flow was approximated in the theoretical model as a constant thermal conductance (1.5 W/°C) between the expansion- and compression-space gasses. The resulting prediction yielded much better correlation between measured and predicted efficiency. Inclusion of the thermal conductance, however, caused a 5% drop in predicted power through changes in the expansion- and compression-space temperatures.

Indicated power and efficiency predictions, including the effect of the 1.5 W/°C conductance, are compared to baseline test data in Figure 4-20. The variation of indicated power with piston stroke was similar for each VCR setting, showing a drop-off in measured power at high strokes. The onset and magnitude of the "power drop-off" were both dependent on the VCR setting or, equivalently, on the displacer phase angle. The piston stroke corrseponding to the onset of the "power drop-off" decreased as the VCR opened and the displacer phase angle decreased. The magnitude of the "power drop-off" increased with increasing piston stroke and decreasing phase angle.

The variation of indicated efficiency with stroke showed an "efficiency drop-off" corresponding to the "power drop-off." Correction of the predicted

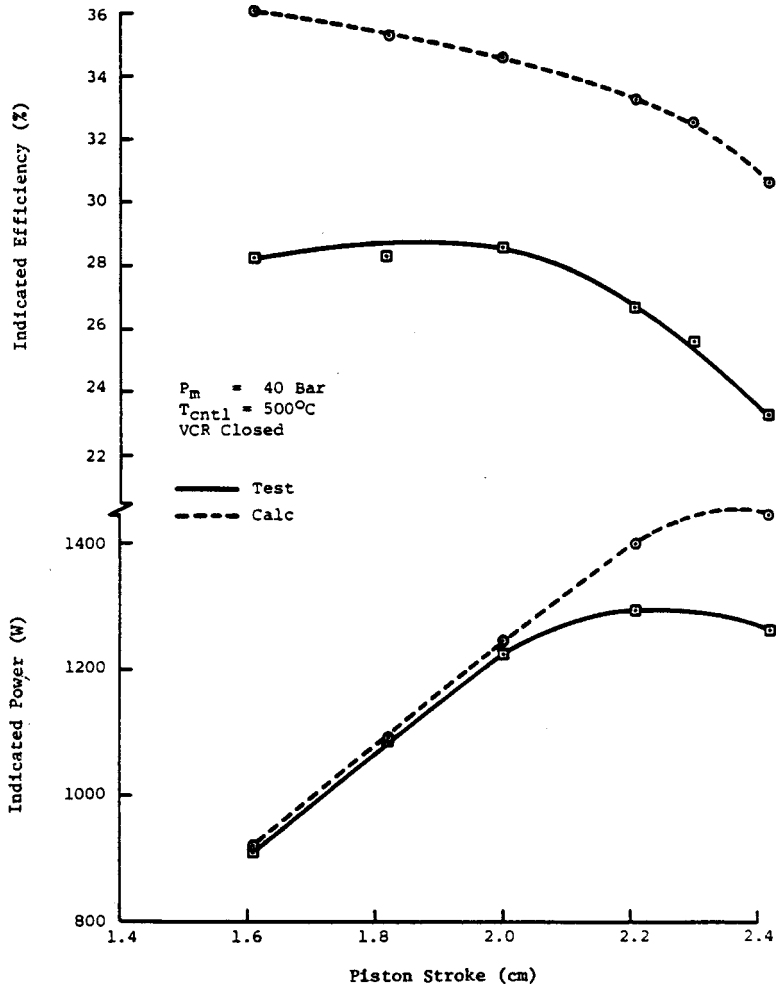

Fig. 4-18. Comparison of Indicated Power and Efficiency Predictions (VCR closed) for Baseline Engine Test

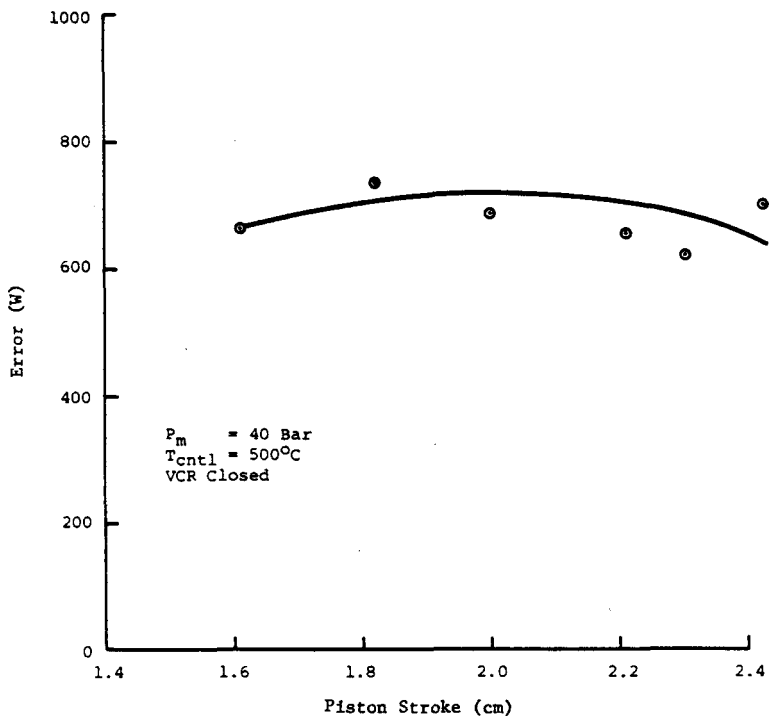

Fig. 4-19. Error between Measured and Predicted Heat Input for Baseline Test

efficiencies by the ratio of measured-to-predicted power formed the basis for the comparison in Figure 4-21. Correlation measurements were less than 10%. This residual correlation error was attributed to inaccurate modeling of the additional parasitic heat flow. The magnitude of this thermal loss was reestimated from the difference between the measured and predicted heat inputs, and from the heat flow across the assumed 1.5 W/°C thermal conductance. Its variation with piston stroke is shown in Figure 4-22. The curves showing the stroke and phase dependence of the heat flow were obtained from the predicted heat input and normalized heat input difference.

4.4.1 Power Drop-Off and Efficiency Loss Mechanisms

Potential causes of the discrepancies between the measured and predicted values for power and efficiency include:

- Increased compression-space leakage losses due to inaccurate modeling leakage path resistances,
- Increased frictional pumping losses, particularly in the cold connecting duct region,
- Increased appendix gap losses due to leakage flows across the displacer seal,

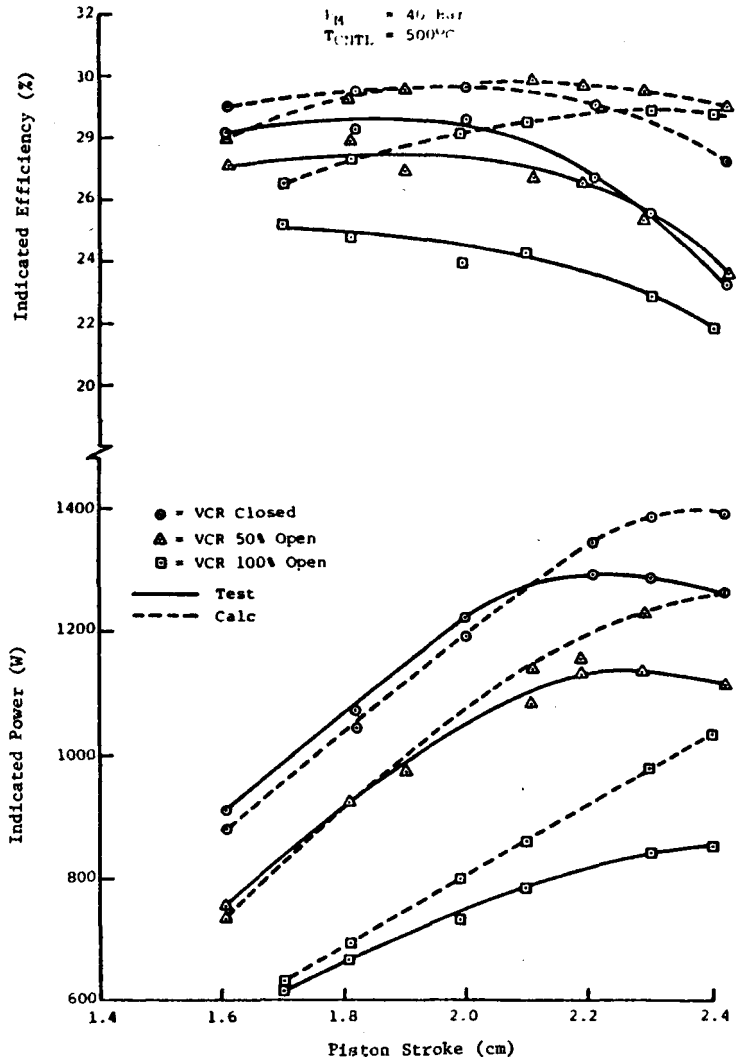

Fig. 4-20. Comparison of Indicated Power and Efficiency Predictions with Revised Engine Model for Baseline Test

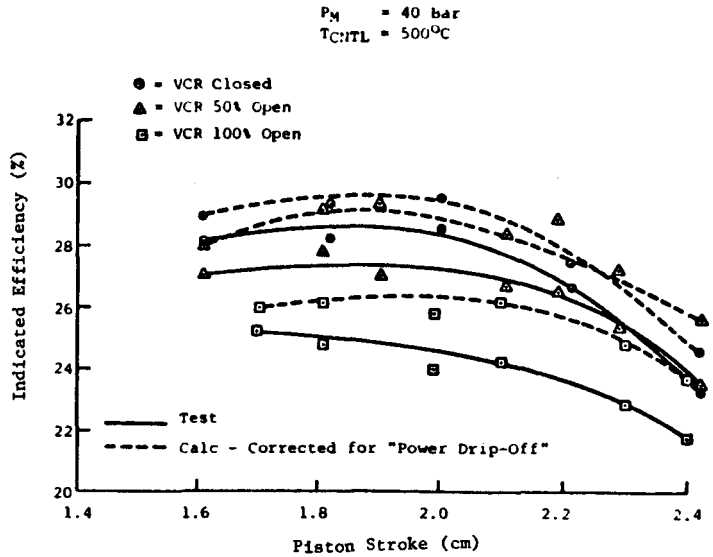

Fig. 4-21. Comparison of Indicated Efficiency Predictions After Adjustment for "Power Drop-Off" for Baseline Test

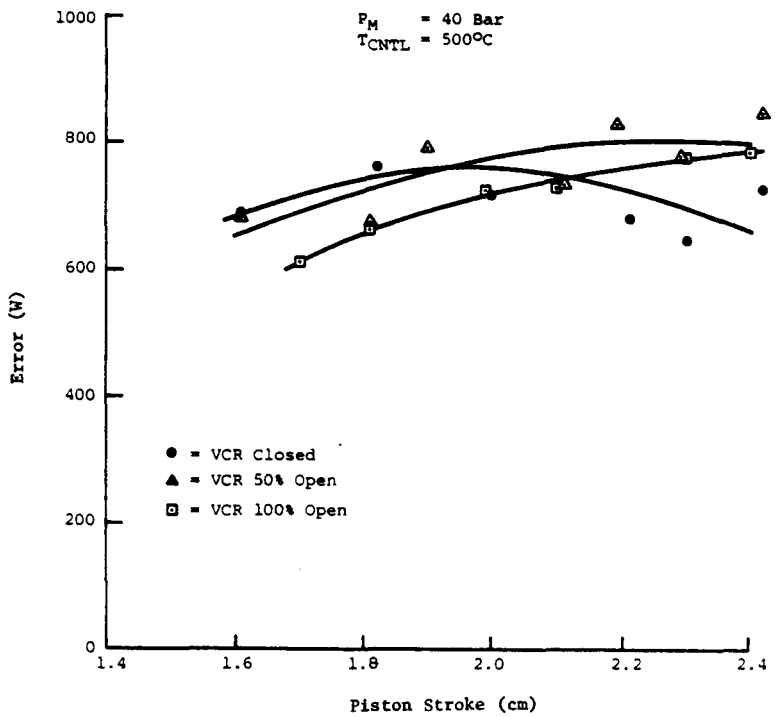

Fig. 4-22. Error between Measured and Predicted Heat Input for Baseline Test

- Increased regenerator thermal hysteresis due to inaccurate regenerator matrix friction and heat-transfer correlations, and
- Heat transfer through the displacer due to internal convection currents between the hot and cold ends of the displacer.

An evaluation of each mechanism resulted in the conclusions discussed below.

Compression-space leakage losses depend principally on pressure-wave amplitude and leakage-path flow resistance. Significant errors in predicting each of these parameters would be required to account for the observed power drop-off. A comparison of measured and predicted compression-space pressure amplitudes (Fig. 4-23) indicated good agreement. While high eccentricity of the piston in its bore and 10% error in the assumed seal clearance will significantly alters the leakage-path flow resistance, the resulting flow resistance would not depend strongly on displacer phase angle. The expected insensitivity of compression-space leakage to displacer angle indicated that it was not a major contributor to the observed power drop-off.

Higher-than-anticipated pumping losses in the cold ducts joining the cooler to the displacer and piston compression spaces are the most probable cause for the measured power drop-off. Typical engine geometry in the vicinity of the compression spaces is shown in Figure 4-24. Three different flow paths are:

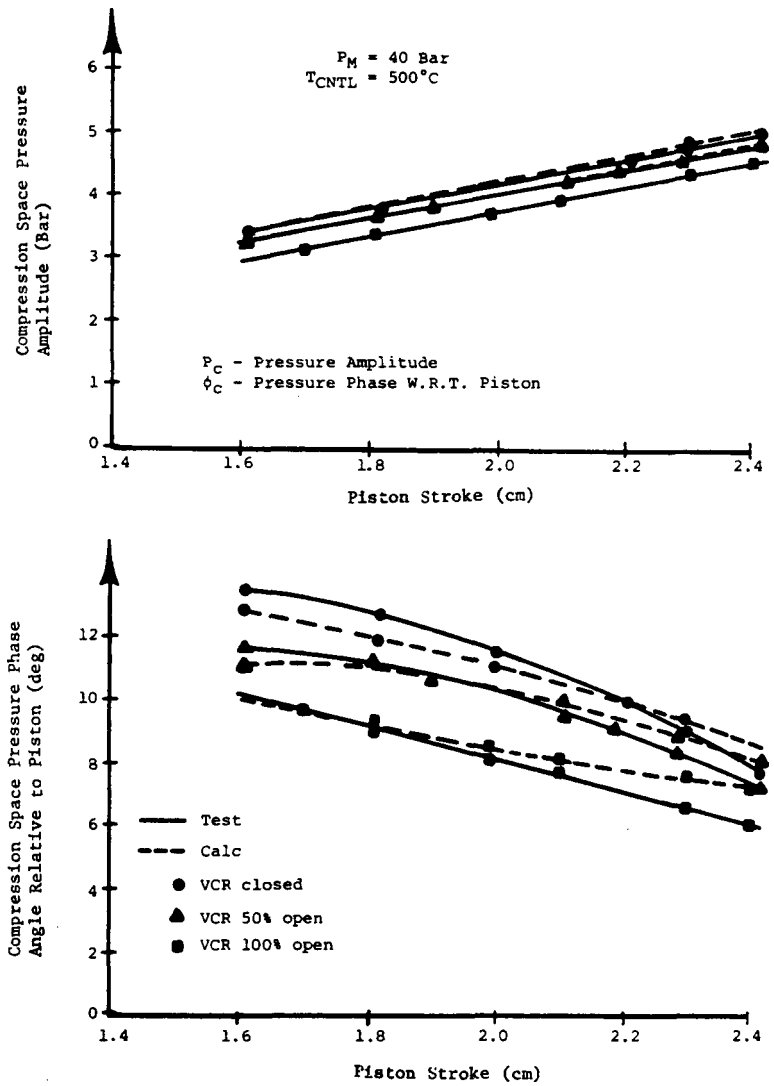

Fig. 4-23. A Comparison between Measured and Predicted Pressure Amplitude and Phase Angle

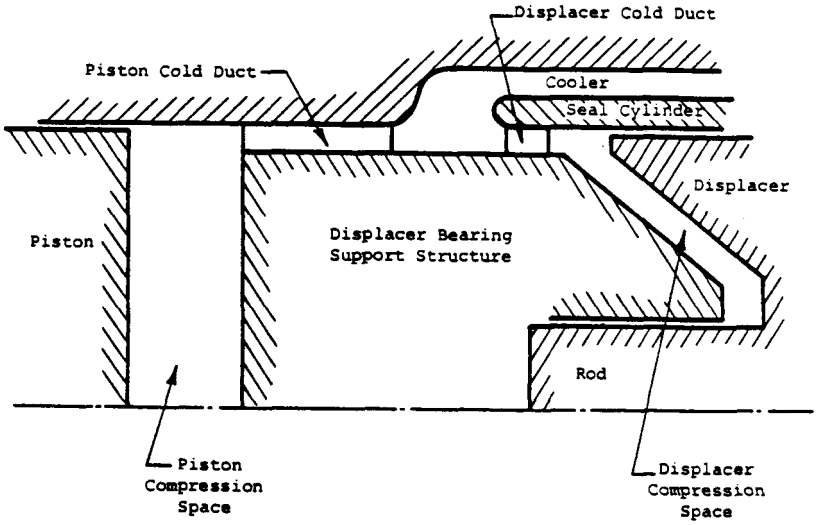

Fig. 4-24. TDE Compression-Space Geometry

- Flow from the cooler into the piston compression space through the piston cold duct,
- Flow from the cooler into the displacer compression space through the displacer cold duct, and
- Flow between the piston and displacer compression spaces through the cold ducts.

This analysis calculates cold duct pumping losses based only on the periodic flow into the total compression-space volume through the first flow path; actual pumping losses result from the interaction of all three flow paths. Because such losses increase approximately with the cube of piston stroke, analytical model deficiencies become more significant at large strokes. Losses associated with periodic flow between the two compression-space volumes were estimated assuming:

- No interaction with flow between the cooler and compression space,
- Blasius turbulent friction correlation applied to the cold duct with a period flow enhancement factor of 2.0, and
- 0.75 velocity head pressure loss at each cold duct entrance/exit.

Calculations for operation at 40 bar and 2.4-cm piston stroke yielded losses that increased with decreasing phase angle, and approach 100 W in magnitude. Accurate prediction of the stroke and phase dependence of these losses requires a more detailed analysis of the cold duct region. The importance of these periodic flow losses can be reduced substantially by

increasing the flow area in the cold connecting ducts. Since the magnitude of these losses varies approximately with the cube of the cold duct velocity, increasing the cold duct flow area by factor of two or more should reduce them to acceptable levels. The cold duct flow areas of the TDE could be increased significantly.

Increased appendix gap losses due to displacer seal leakage are considered a major contributor to the discrepancy between measured and predicted efficiencies, and also could contribute significantly to the measured power drop-off. The appendix gap region generally encompasses the clearance space between the displacer and its cylindrical bore (shown in Fig. 4-25).

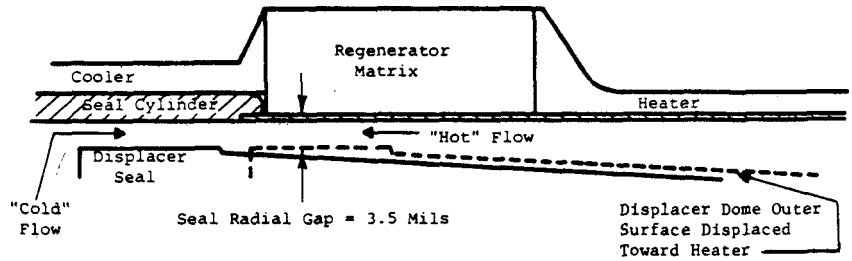

Fig. 4-25. Typical TDE Displacer Seal and Appendix Gap Geometry

Three modes of heat transfer are associated with the appendix gap losses:

- Direct conduction along the displacer wall,
- Shuttle heat transfer between the displacer wall and cylindrical bore, and
- Enthalpy flux associated with the gas flow between the expansion space and displacer seal region.

The latter two mechanisms, which generally dominate the appendix gap losses, exhibit opposite dependencies on gap size, i.e., shuttle heat transfer decreases with gap, while enthalpy flux losses increase with gap. Enthalpy flux losses also increase significantly with displacer seal flow because periodic flow across the displacer seal transfers heat into the cooler through the seal cylinder.

As the magnitude of these losses increases, their potential interaction with the expansion space conditions also increases. The engine pressure wave is affected both by reduction in expansion-space mean temperature and a modification of expansion-space temperature variation (amplitude and/or phase).

The analysis used to predict these losses assumes zero leakage across the displacer seal, identical temperature gradients along the cylinder and displacer walls, and a constant clearance in the appendix gap region; however, all three of these assumptions are violated in the TDE. Periodic flow across the displacer seal for the current 3.5-mil clearance was predicted to approach 5% of the flow entering the heater channels, and could significantly enhance the net enthalpy flux by altering the cylinder wall temperature gradient and increasing the net heat transfer into the appendix gap.

The influence of displacer seal leakage on engine performance, studied during subsequent testing with different displacer seal clearances, is reported in Section 8, Displacer Clearance Seal Test. Significant performance improvement with decreasing seal clearance was expected and verified by subsequent testing.

Increased regenerator thermal hysteresis can account for about 100-150 W of additional heat flow. A recent MTI test[2] of an unsintered woven-screen matrix sample yielded friction and heat-transfer correlations suggesting that standard code correlations underpredicted heat transfer and overpredicted friction. Engine performance predictions based on regenerator test correlations showed reduced regenerator efficiency due to increased mass flow through the regenerator. The regenerator hysteresis loss prediction increased from 80 to 200 W as regenerator efficiency dropped. Decreasing the porosity of the regenerator should, in this case, improve regenerator efficiency and reduce this thermal loss.

The magnitude of heat transfer due to internal convection paths within the displacer is more difficult to assess. Two conical radiation shields are installed in the displacer dome to control radiation heat transfer. Internal convection currents, resulting from both the motion of the displacer and the thermal gradient across it, can cause significant heat transfer between the two radiation shields, as well as between the lower radiation shield and displacer seal region. Fabrication of a displacer with thermal insulation between the two radiation shields will effectively limit the amount of heat reaching the lower radiation shield and control this heat loss mechanism.

4.5 CONCLUSIONS AND RECOMMENDATIONS

The baseline engine tests established the operating characteristics of the baseline TDE configuration, and demonstrated repeatable thermodynamic performance within the nominal experimental error. Operating experience with the engine and evaluation of the test results suggested unexpected losses in the baseline TDE that resulted in a "power drop-off" at high piston strokes, and a reduced efficiency at all piston strokes. A preliminary analysis of these losses led to an improved understanding of free-piston Stirling engine loss mechanisms.

The power drop-off was tentatively related to additional cold connecting duct pumping losses and enhanced appendix gap losses, while the reduced efficiency was tentatively related to enhanced appendix gap losses, reduced generator thermal efficiency, and displacer internal convection. The following analytical/experimental studies are recommended for improved understanding of these loss mechanisms:

- Modification of TDE test instrumentation to measure the pressure wave in both the piston and displacer compression spaces, and then a retest of the baseline TDE (measurement of the displacer compression-space pressure wave should be relative to the piston compression-space pressure wave);

- Enlargement of the cold connecting duct flow areas, followed by a series of performance tests;

- TDE tests with alternative displacer seal/appendix gap geometries (reported in Section 8);

- Evaluation of regenerator friction and heat transfer correlations for Metex regenerator samples spanning a broad range of wire diameters, porosities, and weave geometry;

- TDE testing with an insulated displacer to help quantify the importance of displacer internal convection;

- Modification of the thermodynamic cycle analysis to model the interaction of separate piston and displacer compression spaces with their respective cold connection ducts; and

- Development of an improved appendix gap loss analysis that considers displacer seal leakage, variable gap geometry, and unequal cylinder/displacer temperature gradients.

5. COMPRESSION-SPACE HYSTERESIS LOSS TESTS

The working space hysteresis loss is attributed to irreversible thermal transfers in the boundary layers on the various working space surfaces whenever the bulk gas in the working space undergoes a pressure variation similar to the hysteresis losses that have been analytically and experimentally studied for simple gas springs. Because of the high degree of turbulence in the TDE working spaces (due to the inflow of gas from the engine heat exchangers), and because the packaging requirements of the displacer drive system in the TDE tend to significantly increase the wetted surface area in the compression space, compression-space hysteresis losses were evaluated experimentally to verify that the analytical procedure does not significantly underestimate the hysteresis losses in the TDE.

5.1 TEST OBJECTIVES

The objective of the hysteresis tests was to evaluate compression-space hysteresis loss effects on engine performance as the compression-space wetted surface area was increased from 0.16 m^2 to 0.22 m^2. Pretest analysis (Table 5-1) indicated only a small change in engine performance with significant changes in compression-space wetted surface area.

5.2 TEST METHODS

Compression-space hysteresis losses are analytically modeled as a function of stroke squared, mean pressure squared, and wetted surface area. To evaluate the effects of stroke, an engine map was generated at constant temperature over the range of piston stroke. To evaluate the mean pressure effect, engine maps at a constant set temperature-versus-piston-stroke were generated for mean engine pressures of 30, 35, and 40 bar. To evaluate the effects of engine wetted surface area, the base engine piston end cap was replaced with a finned plug, resulting in a compression-space wetted surface area of 0.22 m^2. The installation of the finned plug also resulted in an increase in compression-space dead volume. To eliminate the effects of the increased dead volume, a plug without surface area extensions was designed and fabricated, yielding a compression-space wetted surface area of 0.16 m^2, and having the same compression-space dead volume as the finned plug. Engine tests were run first with the finned plug; the unfinned plug was then installed and the test points repeated to eliminate the dead volume effects.

From pretest engine analysis, a control temperature of 400°C was selected to accomplish stable engine operation over the 30- and 40-bar test range. From the baseline engine tests, the TDE was shown to exhibit performance sensitivity to changes in the engine dynamic parameters of displacer-to-piston-stroke ratio and phase. To reduce the effects of different operating conditions, similar dynamics between tests with the finned and unfinned piston end cap plugs were maintained.

The engine was started at the 30-bar pressure point, stroked to a 2.2-cm piston stroke, and stabilized. After stabilizing at the initial point, the engine was stroked in 0.1-cm increments with three and four data scans taken for each point, completing the map of performance versus stroke for the 30-bar

Table 5-1. Pretest Analysis of Hysteresis Losses

TDE ECUT HYST. TEST--T=400C. AWC=.22M**2--PRETEST — Finned Test

5 8 3

'XP-M'	'PRWN-W'	'ETAC-%'	'PRWD-W'	'THED-K'	'XRAT'	'PHID-DEG'	'FREQ-HZ'
'40 BAR'							
8.00000D-03	6.26450D+02	2.43960D-01	1.46990D+02	6.29280D+02	8.18540D-01	6.66050D+01	4.45200D+01
9.00000D-03	7.34300D+02	2.44360D-01	1.79380D+02	6.25030D+02	8.04150D-01	6.64500D+01	4.45080D+01
1.00000D-02	8.34870D+02	2.40270D-01	2.13670D+02	6.20640D+02	7.90280D-01	6.63160D+01	4.44930D+01
1.10000D-02	9.22690D+02	2.32310D-01	2.49330D+02	6.15980D+02	7.76510D-01	6.61840D+01	4.44770D+01
1.20000D-02	9.92160D+02	2.21170D-01	2.85470D+02	6.11420D+02	7.62090D-01	6.59820D+01	4.44590D+01
'XP-M'	'PRWN-W'	'ETAC-%'	'PRWD-W'	'THED-K'	'XRAT'	'PHID-DEG'	'FREQ-HZ'
'35 BAR'							
8.00000D-03	5.41770D+02	2.36300D-01	1.22300D+02	6.31820D+02	8.53300D-01	6.68110D+01	4.16650D+01
9.00000D-03	6.39990D+02	2.39540D-01	1.49560D+02	6.28160D+02	8.39130D-01	6.66790D+01	4.16570D+01
1.00000D-02	7.33690D+02	2.38300D-01	1.78520D+02	6.24350D+02	8.25430D-01	6.65670D+01	4.16470D+01
1.10000D-02	8.19690D+02	2.33410D-01	2.08910D+02	6.20310D+02	8.12140D-01	6.64750D+01	4.16350D+01
1.20000D-02	8.94580D+02	2.25410D-01	2.40510D+02	6.16040D+02	7.99190D-01	6.64000D+01	4.16210D+01
'XP-M'	'PRWN-W'	'ETAC-%'	'PRWD-W'	'THED-K'	'XRAT'	'PHID-DEG'	'FREQ-HZ'
'30 BAR'							
8.00000D-03	4.28990D+02	2.20620D-01	9.67870D+01	6.35050D+02	8.39260D-01	6.75770D+01	3.86200D+01
9.00000D-03	5.11680D+02	2.27670D-01	1.18940D+02	6.32130D+02	8.27300D-01	6.74450D+01	3.86110D+01
1.00000D-02	5.92950D+02	2.30250D-01	1.42630D+02	6.29070D+02	8.15690D-01	6.73340D+01	3.86010D+01
1.10000D-02	6.70180D+02	2.29010D-01	1.67660D+02	6.25790D+02	8.04360D-01	6.72440D+01	3.85890D+01
1.20000D-02	7.41040D+02	2.24700D-01	1.93880D+02	6.22320D+02	7.93280D-01	6.71710D+01	3.85760D+01

TDE ECUT HYST. TEST--T=400C.AWC=.16M**2--PRETEST — Unfinned Test

5 8 3

'XP-M'	'PRWN-W'	'ETAC-%'	'PRWD-W'	'THED-K'	'XRAT'	'PHID-DEG'	'FREQ-HZ'
'40 BAR'							
8.00000D-03	6.36840D+02	2.48120D-01	1.46870D+02	6.29290D+02	8.18380D-01	6.64430D+01	4.45100D+01
9.00000D-03	7.47630D+02	2.48890D-01	1.79240D+02	6.25040D+02	8.04010D-01	6.62820D+01	4.44980D+01
1.00000D-02	8.51530D+02	2.45150D-01	2.13520D+02	6.20450D+02	7.90170D-01	6.61420D+01	4.44840D+01
1.10000D-02	9.43070D+02	2.37510D-01	2.49190D+02	6.15990D+02	7.76420D-01	6.60030D+01	4.44690D+01
1.20000D-02	1.01670D+03	2.26690D-01	2.85330D+02	6.11430D+02	7.62030D-01	6.57950D+01	4.44520D+01
'XP-M'	'PRWN-W'	'ETAC-%'	'PRWD-W'	'THED-K'	'XRAT'	'PHID-DEG'	'FREQ-HZ'
'35 BAR'							
8.00000D-03	5.51080D+02	2.40480D-01	1.22170D+02	6.31840D+02	8.53080D-01	6.66400D+01	4.16540D+01
9.00000D-03	6.51840D+02	2.44130D-01	1.49520D+02	6.28170D+02	8.38940D-01	6.65010D+01	4.16460D+01
1.00000D-02	7.48630D+02	2.43260D-01	1.78360D+02	6.24370D+02	8.25270D-01	6.63820D+01	4.16370D+01
1.10000D-02	8.38000D+02	2.38710D-01	2.08750D+02	6.20320D+02	8.12010D-01	6.62820D+01	4.16260D+01
1.20000D-02	9.16630D+02	2.31040D-01	2.40350D+02	6.16050D+02	7.99090D-01	6.62010D+01	4.16130D+01
'XP-M'	'PRWN-W'	'ETAC-%'	'PRWD-W'	'THED-K'	'XRAT'	'PHID-DEG'	'FREQ-HZ'
'30 BAR'							
8.00000D-03	4.37280D+02	2.25020D-01	9.66650D+01	6.35060D+02	8.38990D-01	6.73860D+01	3.86070D+01
9.00000D-03	5.22310D+02	2.32530D-01	1.18800D+02	6.32140D+02	8.27060D-01	6.72460D+01	3.85990D+01
1.00000D-02	6.06240D+02	2.35530D-01	1.42480D+02	6.29080D+02	8.15490D-01	6.71280D+01	3.85900D+01
1.10000D-02	6.88440D+02	2.34680D-01	1.67510D+02	6.25810D+02	8.04190D-01	6.70320D+01	3.85790D+01
1.20000D-02	7.66062D+02	2.30730D-01	1.93720D+02	6.22340D+02	7.93130D-01	6.69510D+01	3.85670D+01

NOMENCLATURE FOR TABLES OF PRETEST DATA

XP	= PISTON STROKE (M)
PRWN	= TOTAL INDICATED THERMODYNAMIC POWER (W)
ETAC	= TOTAL INDICATED THERMODYNAMIC EFFICIENCY (-)
PRWD	= DISPLACER POWER (W)
THED	= MEAN HEATER HEAD TEMPERATURE (K)
XRAT	= STROKE RATIO - DISPLACER STOKE / PISTON STROKE (-)
PHID	= DISPLACER PHASE ANGLE W.R.T. PISTON (DEG)
FREQ	= ENGINE OPERATING FREQUENCY (HZ)
TCNTRL	= HEATER HEAD CONTROL TEMPERATURE (K)

pressure point. The map was generated while maintaining the control temperature fixed at 400°C. The engine was stroked back to 2.2-cm and held at this stroke by varying the field control gain; control temperature was measured at 400°C, and the pressure was increased to 35 bar. The engine map versus stroke was generated at 35 bar, and the procedure was repeated for an engine map at 40 bar.

The engine was disassembled, and the finned plug was removed and replaced with the unfinned plug with a reduced surface area, but comparable dead volume. The engine was started at 30 bar and stroked to a 2.2-cm piston stroke where the stroke ratio and displacer phase angle were tuned to match with the finned plug dynamics while maintaining stroke and mean head temperature. The mean heater temperatures, displacer stroke ratios, and displacer phase angles between the finned and unfinned tests are shown in Figures 5-1 through 5-3, respectively.

The area weighted mean temperature (Fig. 5-1) was found from the baseline tests to adequately represent the hot-end engine temperature, and was constant for both the finned and unfinned tests. As the controls for the displacer stroke ratio and phase angle are to some extent interactive (increased displacer gas spring volume for a lower phase results in lowered displacer damping and higher stroke ratio for a constant drive power), a trade between an exact match of stroke ratio and phase between tests was established. The stroke ratio set point in Figure 5-2 was established at a 2.2-cm stroke and 30-bar pressure. The stroke ratio was set to the same value established during the finned test, with a small penalty in phase (Fig. 5-3). The stroke ratio (Fig. 5-3) was seen to deviate from the set point with increasing pressure for the unfinned tests.

The differences in displacer phase and stroke ratio indicate that an exact dynamic match between unfinned and finned can be obtained, and therefore influences analytical evaluation.

5.3 EXPERIMENTAL RESULTS

Because pressure was one of the parameters for the hysteresis loss test, the results revealed not only engine behavior due to compression-space hysteresis losses, but also as a function of pressure and stroke. The tests results have been broken down to indicate:

- Engine power and power parameter trends with pressure and stroke,
- Power trends for the finned and unfinned plug tests,
- Power parameters for the finned and unfinned tests,
- Thermodynamic efficiency trends with pressure, and
- Efficiency trends for the finned and unfinned tests.

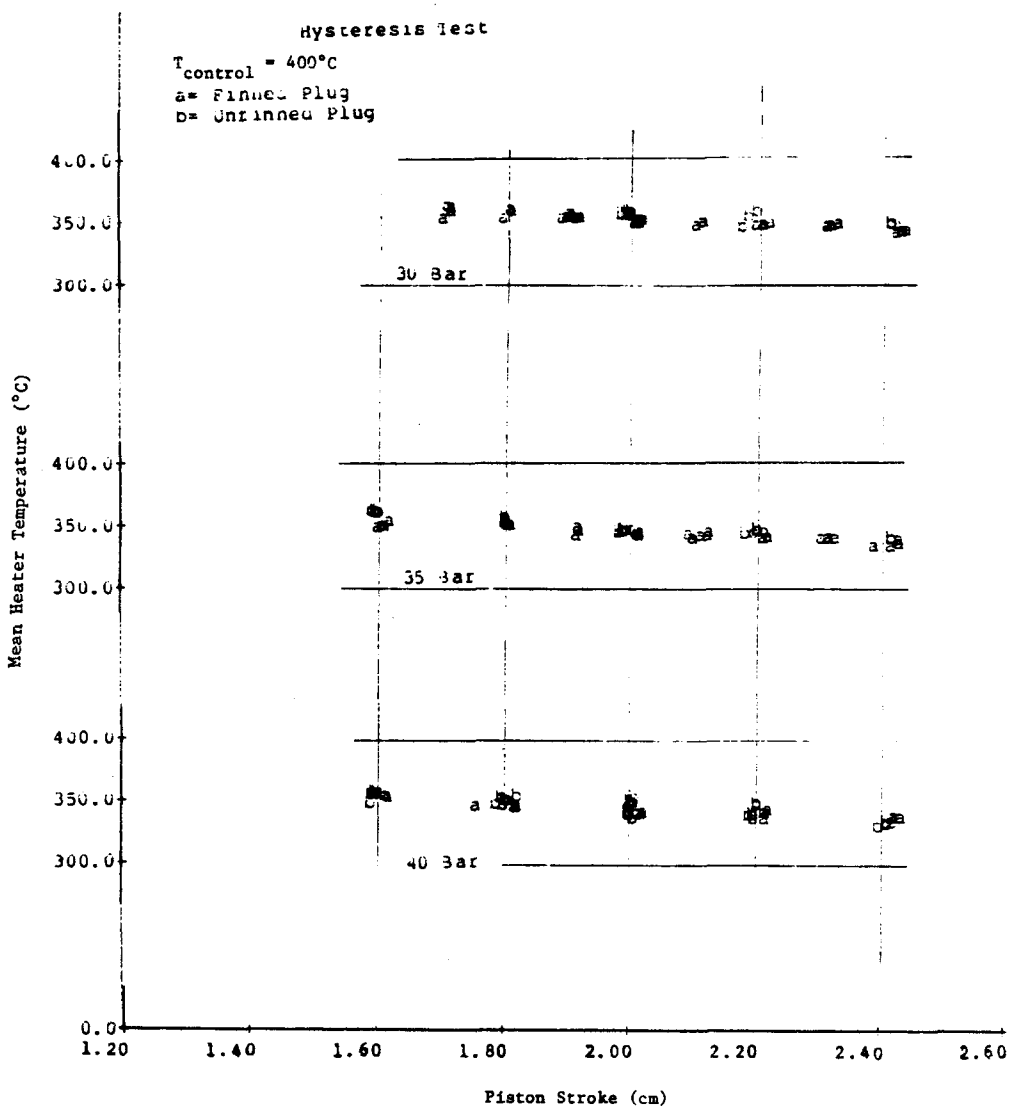

Fig. 5-1. Hysteresis Test: Area Mean Temperature

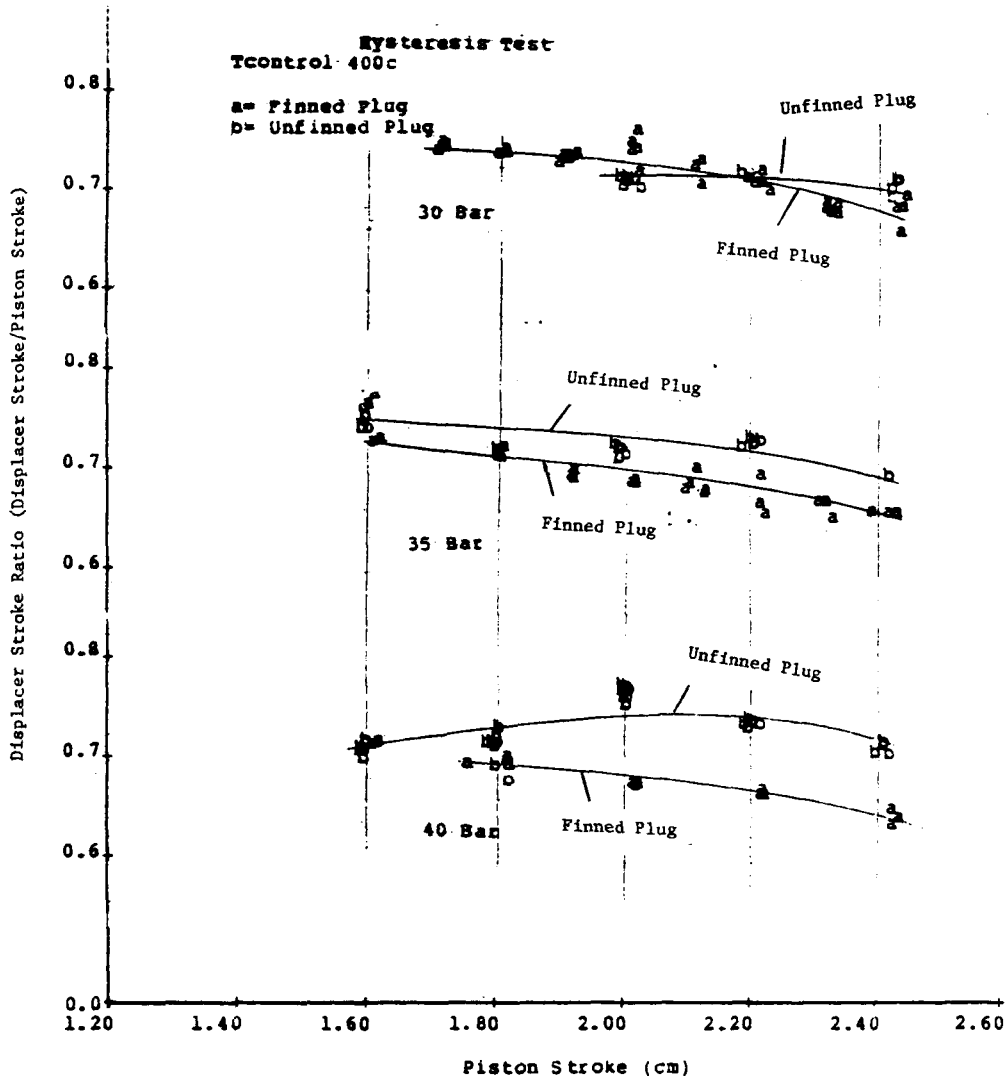

Fig. 5-2. Hysteresis Test: Effect of Pressure on Displacer Stroke Ratio

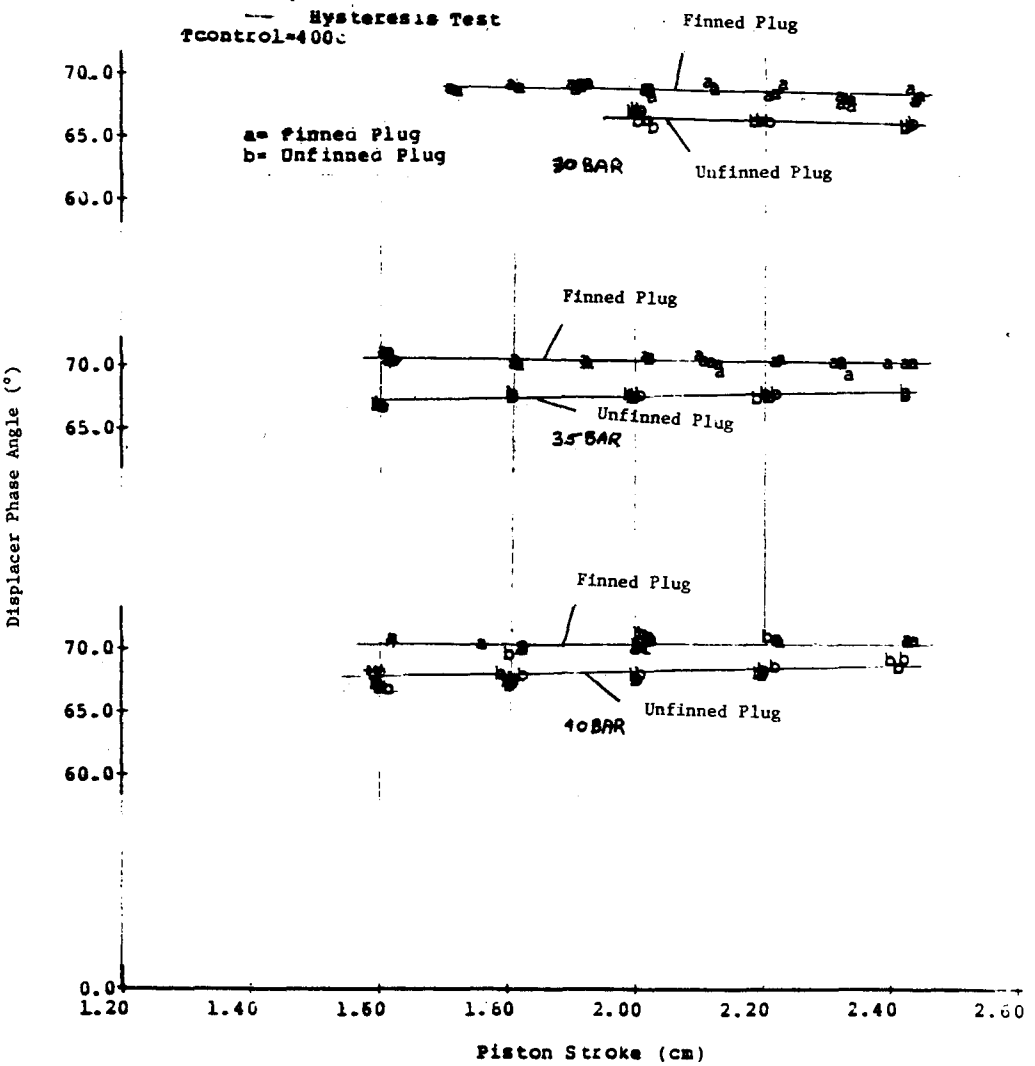

Fig. 5-3. Hysteresis Test: Effect of Pressure on Displacer Phase Angle

5.3.1 Indicated Power Trends with Pressure and Stroke

Indicated power for the TDE system is defined as that thermodynamic power produced by the Stirling cycle at the expense of internal losses such as hysteresis, compression-space leakage, and heat exchanger pumping. The net cycle power after internal losses is divided between the power required to overcome the displacer gas spring losses and the power to drive the loaded piston. Figure 5-4 shows the TDE power flow. Because external damping is imposed artificially on the displacer gas spring from test to test to maintain comparable operating dynamics, comparisons of the indicated power allow a direct comparison of the engine cycle power performance as internal engine changes are made and dynamics held the same. Indicated power is then the sum of piston P-V power plus displacer gas spring loss power, and is the power delivered to the piston if the displacer gas springs are ideal.

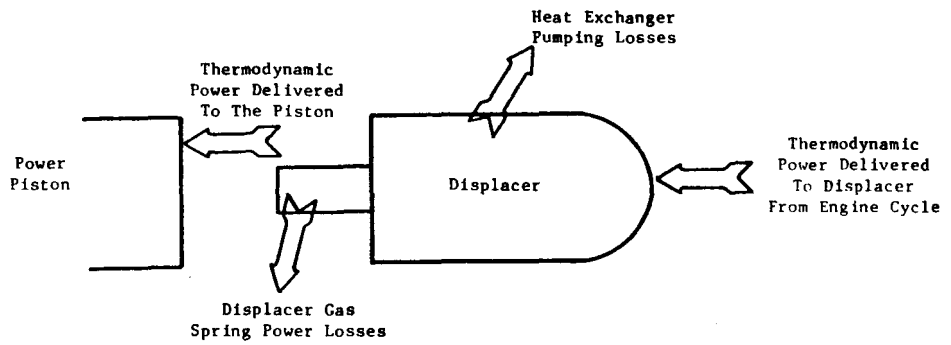

Fig. 5-4. TDE Power Flow

Indicated power is determined from the fundamental harmonic of the dynamic pressure and position measurements by the following:

$$P_I = P_{p-v} + P_{dg/s}$$

$$= \pi f(Ap\ p_c\ X_p \sin\theta_c - Ar\ p_{dg/s}\ X_D \sin\xi)$$

where P_I = indicated power,

P_{p-v} = piston P-V power

$P_{dg/s}$ = power dissipated in displacer gas spring

π = 3.1416,

f = engine frequency,

A_p = area of piston

p_c = compression-space pressure amplitude,

X_p = piston position amplitude

θ_c = phase angle

Ar = area of displacer rod

$p_{dg/s}$ = pressure amplitude of displacer gas spring

X_D = displacer position amplitude

ξ = phase angle between $p_{dg/s}$ and X_D

Figure 5-5 shows indicated power versus piston stroke for mean engine pressures of 30, 35, and 40 bar. By considering the separate effects that determine indicated power, the following trends can be shown:

- Engine frequency increases with pressure, is essentially constant with stroke (Fig. 5-6) as the stiffness associated with both the displacer and piston gas springs increase with pressure. An increase in frequency will result in an increase in power for a given stroke.

- Compression-space pressure amplitude increases with pressure and stroke at constant temperature (Fig. 5-7). As the nominal pressure increases, the total mass of the gas in the engine increases, resulting in greater changes in pressure amplitude for the same changes in engine swept volume. An increase in pressure amplitude results in an increase in power for a given stroke.

- With respect to the piston, the compression-space pressure-wave phase angle decreases with pressure and stroke (Fig. 5-8). The decline in pressure phase for fixed operating dynamics and temperatures is due to internal losses in the engine. As the losses increase with pressure and stroke, the pressure phase decreases. Behavior of the pressure phase angle is an indication of internal losses in the engine such as the compression-space hysteresis loss.

5.3.2 Finned Plug versus Unfinned Plug Power Trends

Figures 5-9 through 5-11 compare the indicated power results between tests run with the finned piston end cap plug (0.22-m^2 hysteresis surface area) and the unfinned piston end cap plug (0.16-m^2 hysteresis surface area) for mean pressures of 30, 35, and 40 bar, respectively. Results indicate that as stroke and pressure increase, deviation in power between the two tests increases. Cross-plotting the fitted results for piston strokes of 2.0 and 2.4 cm versus mean pressure (Fig. 5-12) shows that indicated power for the unfinned tests exceeds the results from the finned tests. The power parameters of frequency, compression-space pressure amplitude, and pressure phase to the piston position are plotted in Figures 5-13 through 5-15, comparing the finned and unfinned test results at 40 bar. The deviation in

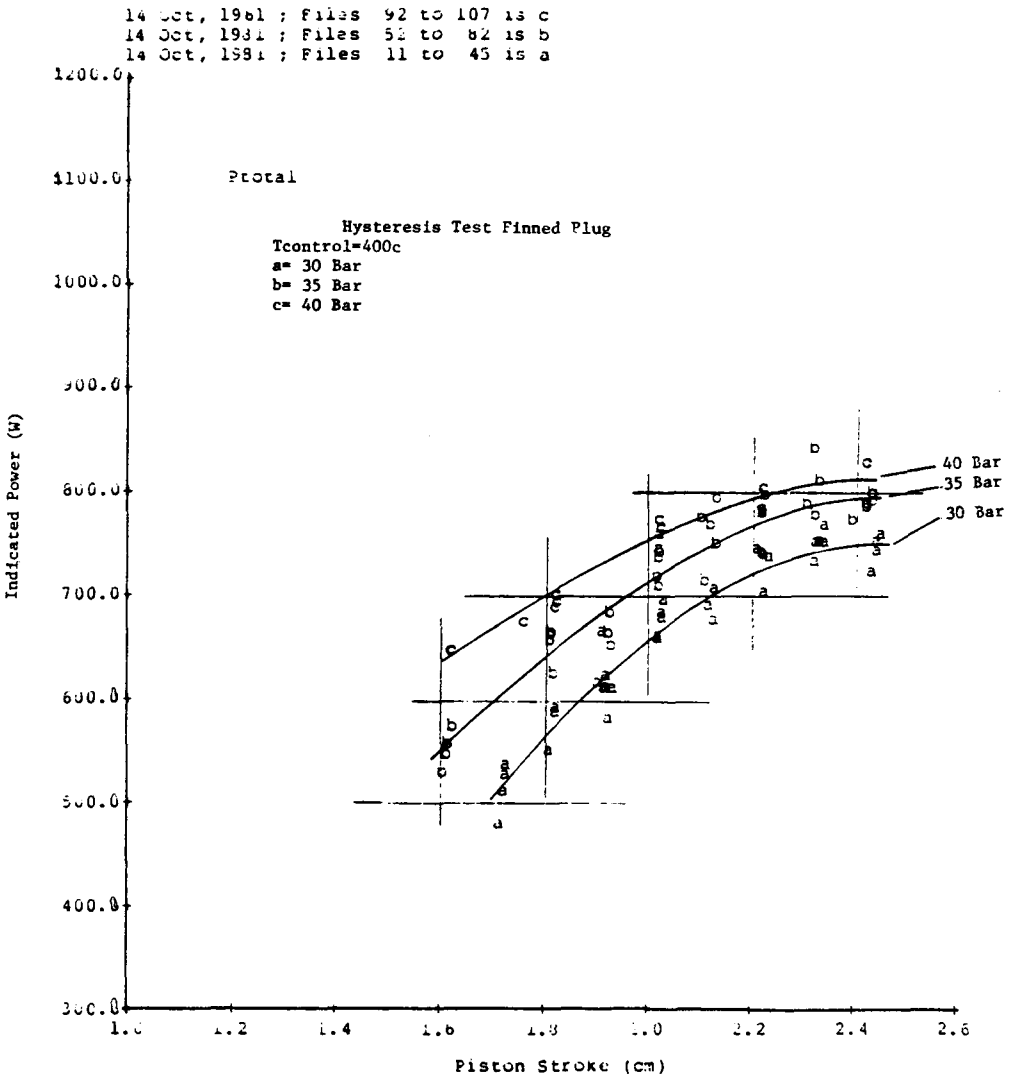

Fig. 5-5. Hysteresis Test: Effect of Pressure on Indicated Power

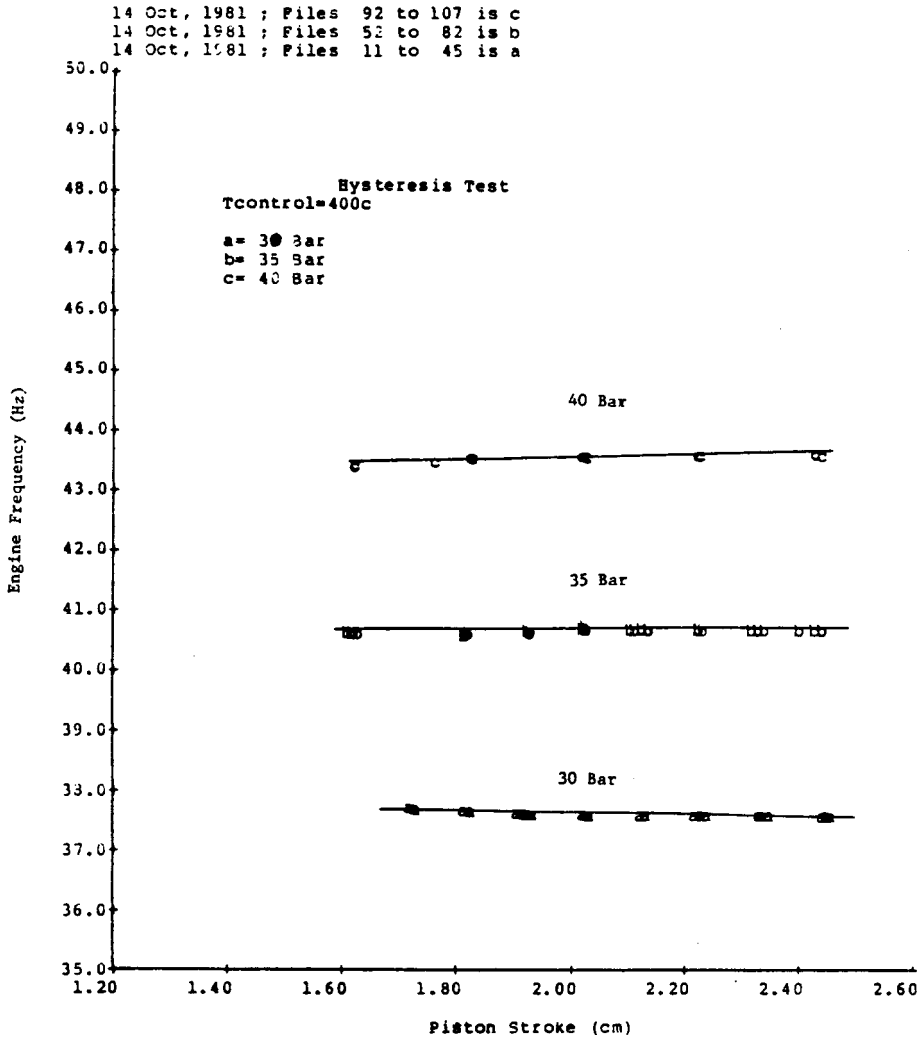

Fig. 5-6. Hysteresis Test: Engine Frequency Variation with Pressurization

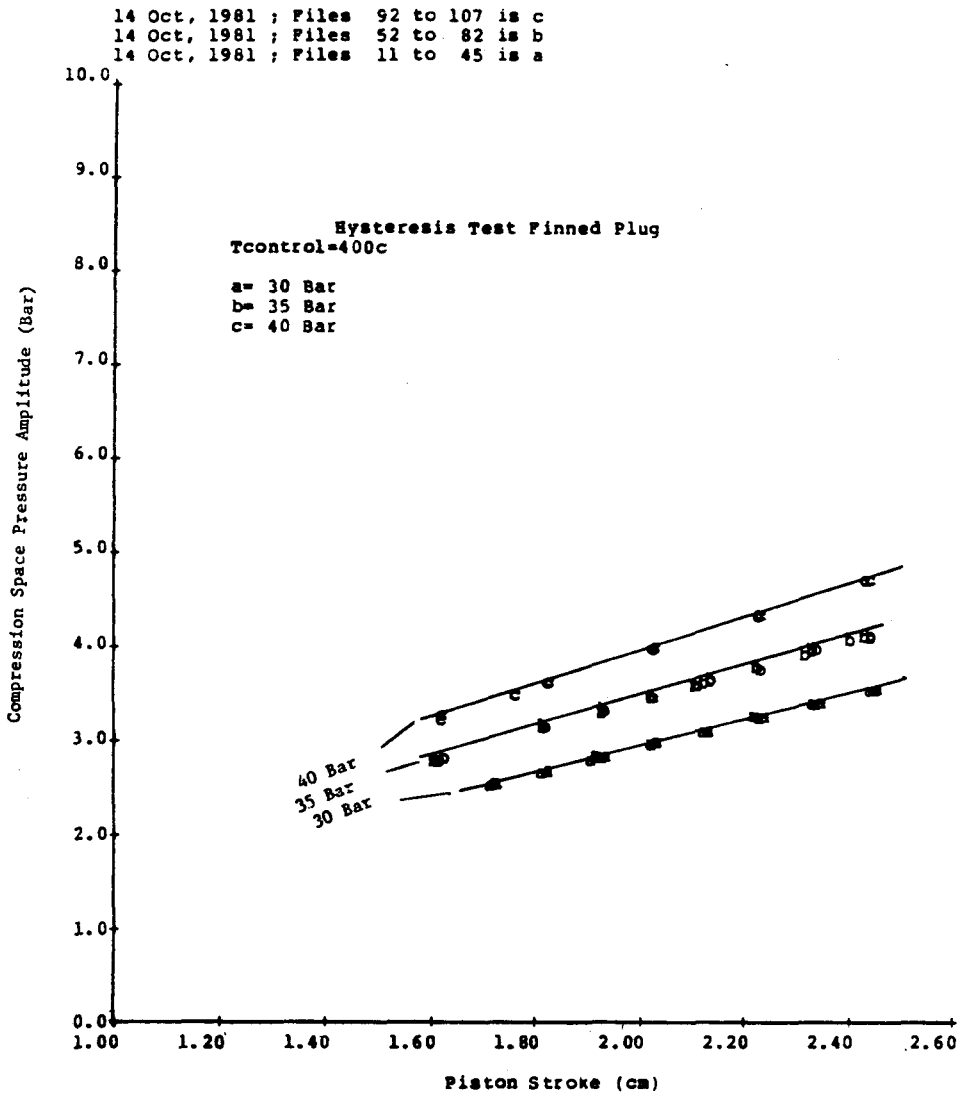

Fig. 5-7. Hysteresis Test: Engine Pressure Amplitude Variation with Pressurization

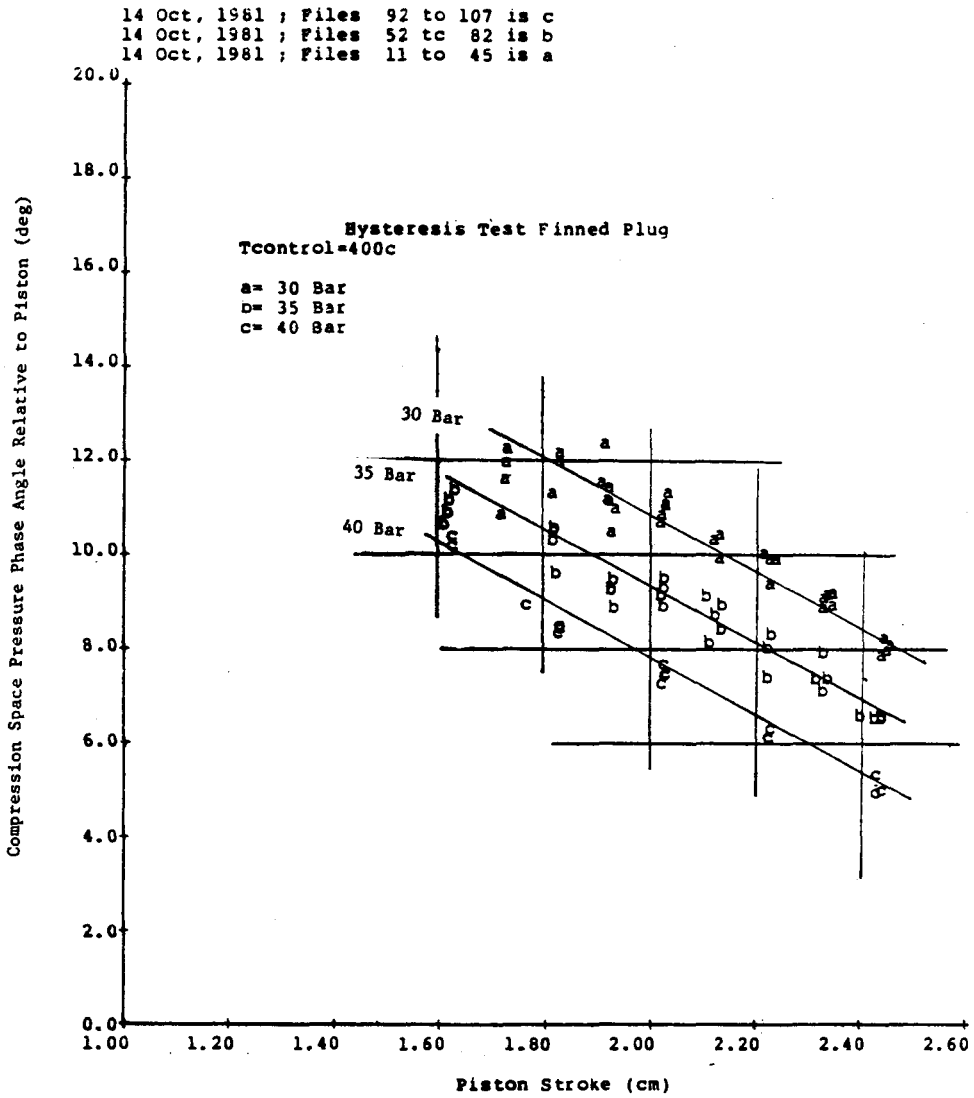

Fig. 5-8. Hysteresis Test: Engine Pressure Angle Variation with Pressurization

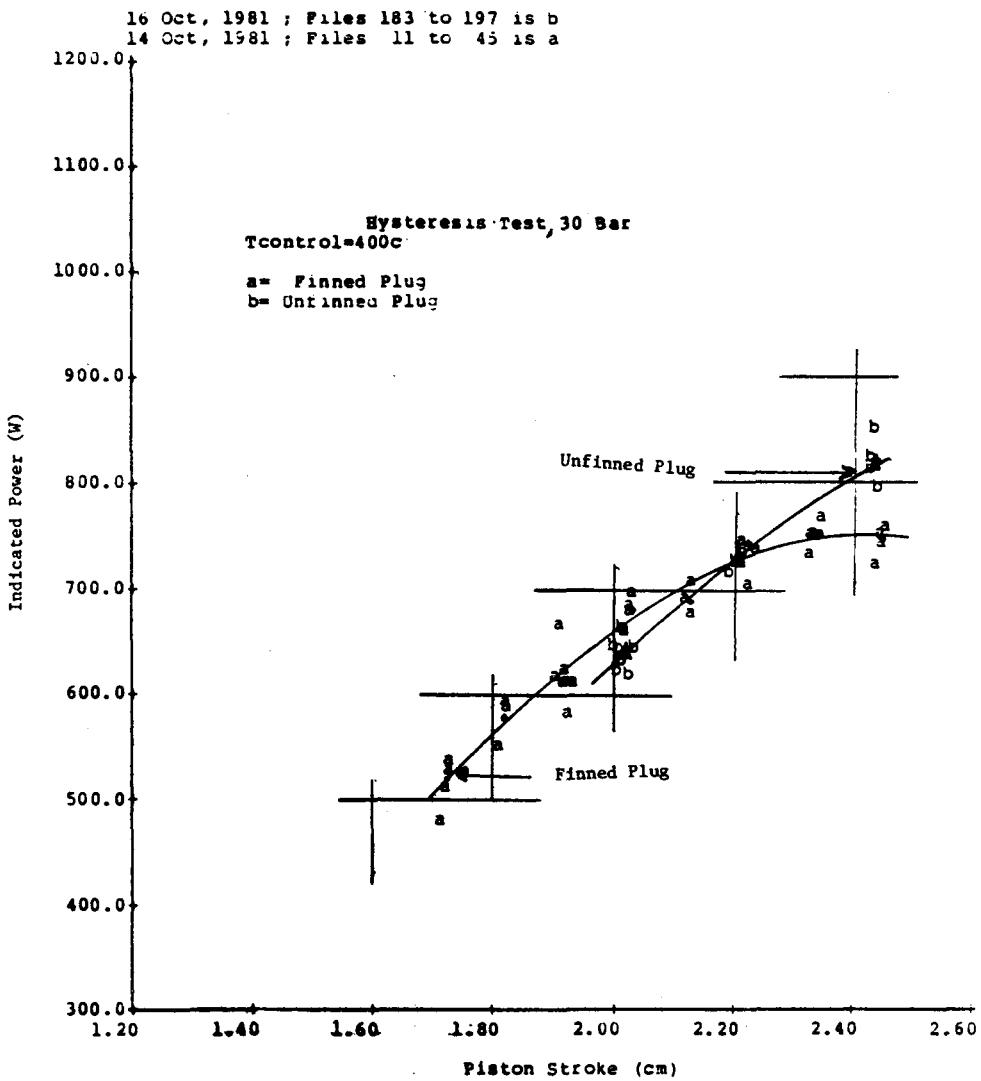

Fig. 5-9. Hysteresis Test: Indicated Power Measurements at 30 Bar

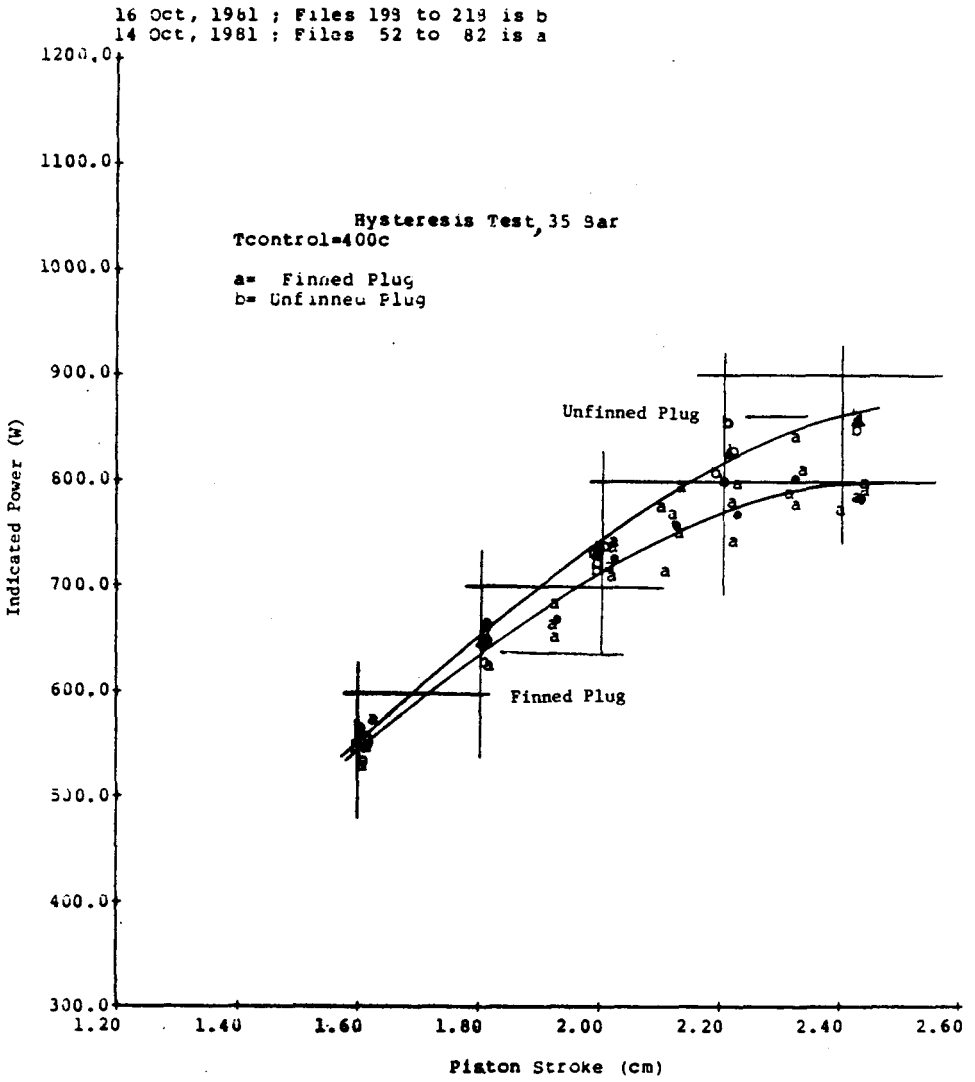

Fig. 5-10. Hysteresis Test: Indicated Power Measurements at 35 Bar

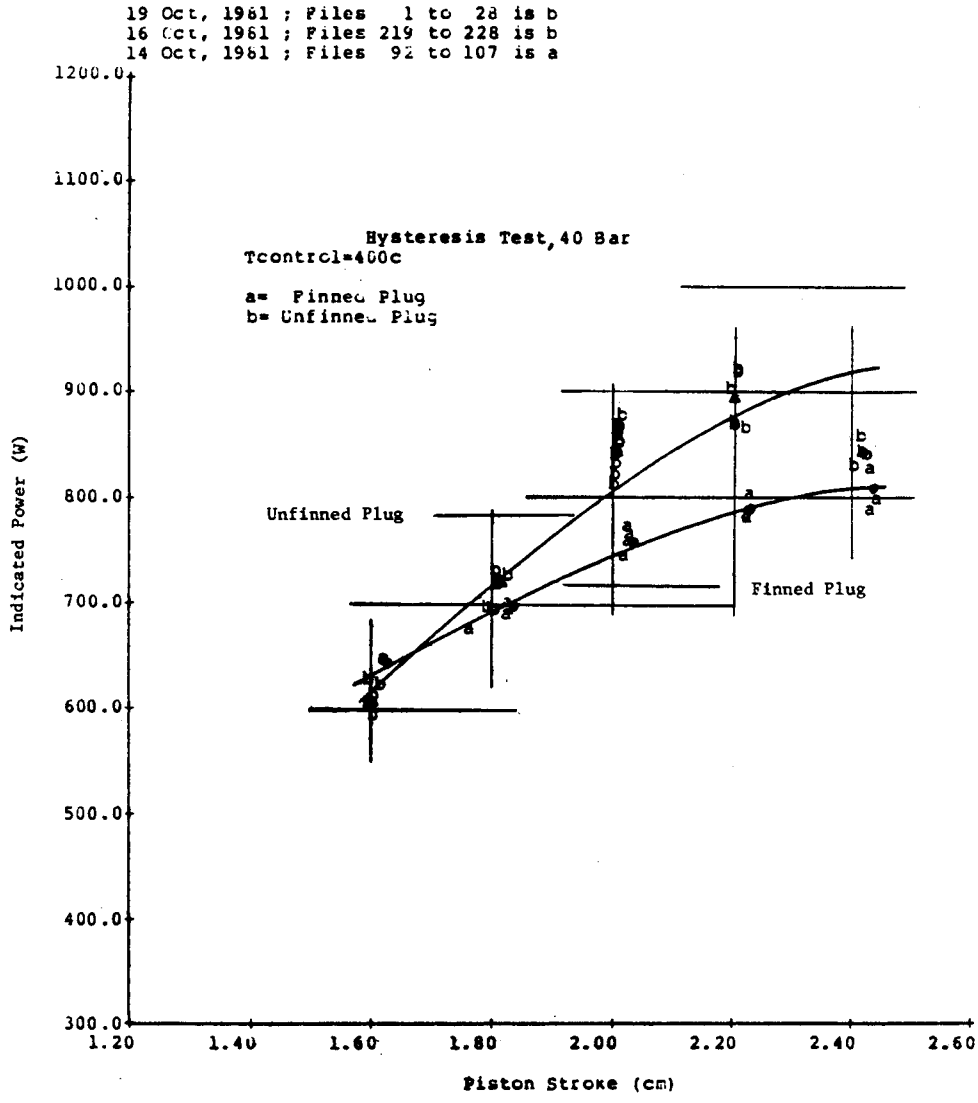

Fig. 5-11. Hysteresis Test: Indicated Power Measurements at 40 Bar

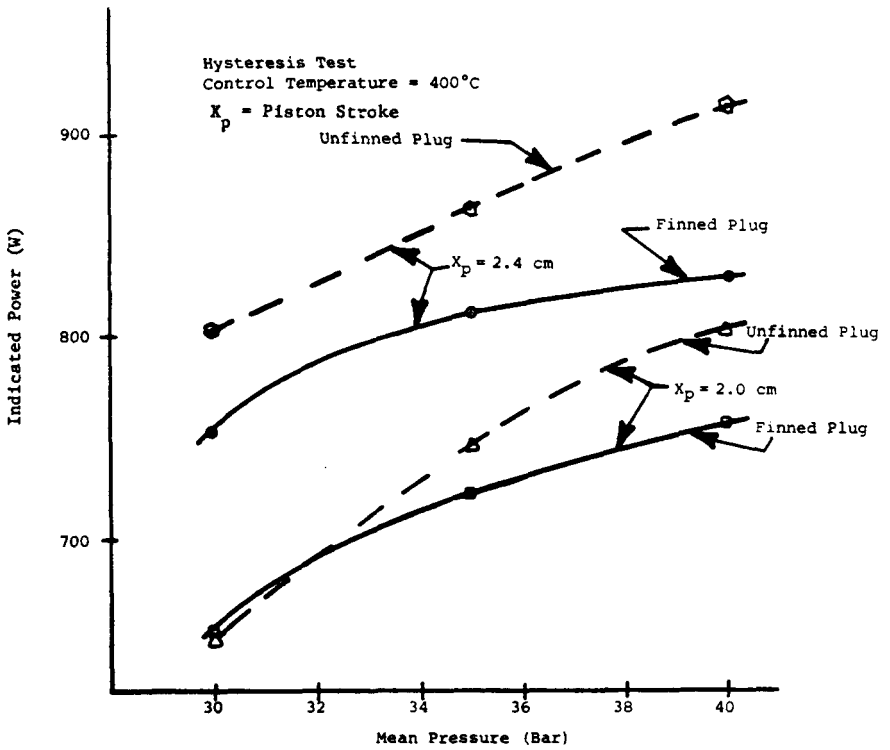

Fig. 5-12. Hysteresis Test: Indicated Power Variation with Pressure at Fixed Piston Stroke

power between the two tests is attributed to the deviation in pressure phase. Separating the effects of displacer gas spring power (Fig. 5-16) from the indicated power results in the piston P-V power shown in Figure 5-17. The effect of the higher pressure phase for the unfinned test versus the finned test results in the higher power.

Hysteresis loss effects can be studied by investigating causes for the deviation in the compression-space phase angle. Basic pressure phase is set by the reduced volume vector resultant, which is a function of operating dynamics and temperature. The TDE does not have direct expansion-space temperature instrumentation, so it will be assumed that the heater head surface temperature is representative of the expansion-space temperature. A cold-space thermocouple exists as part of the TDE instrumentation, and is plotted in Figure 5-18. Because operating temperatures, heat exchanger pumping compression-space leakage, and compression-space dead volume are evaluated to be the same, the remaining causes for the deviation in pressure phase angle between the two tests with the above assumptions and results are: compression-space hysteresis losses, or deviations in operating dynamics, or a combination of both.

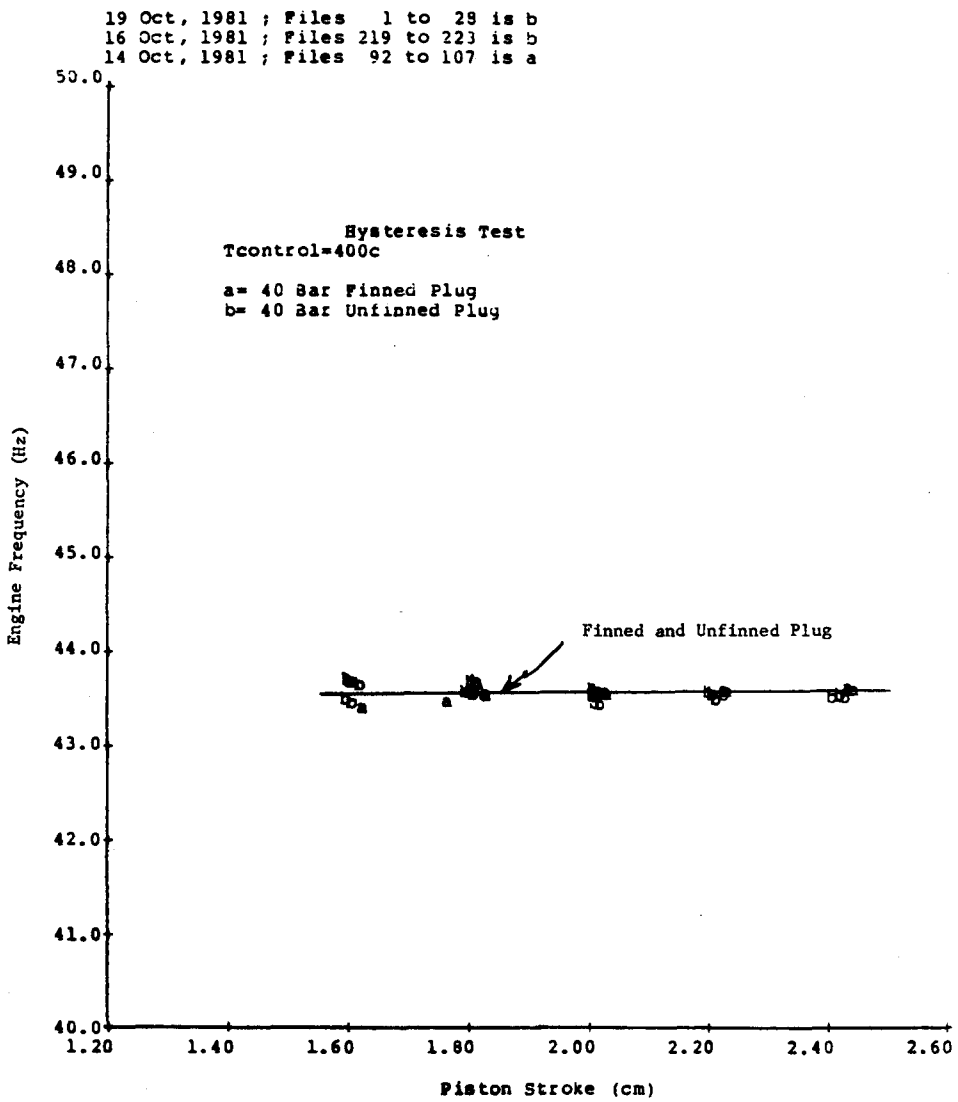

Fig. 5-13. Hysteresis Test: Engine Frequency Measurements

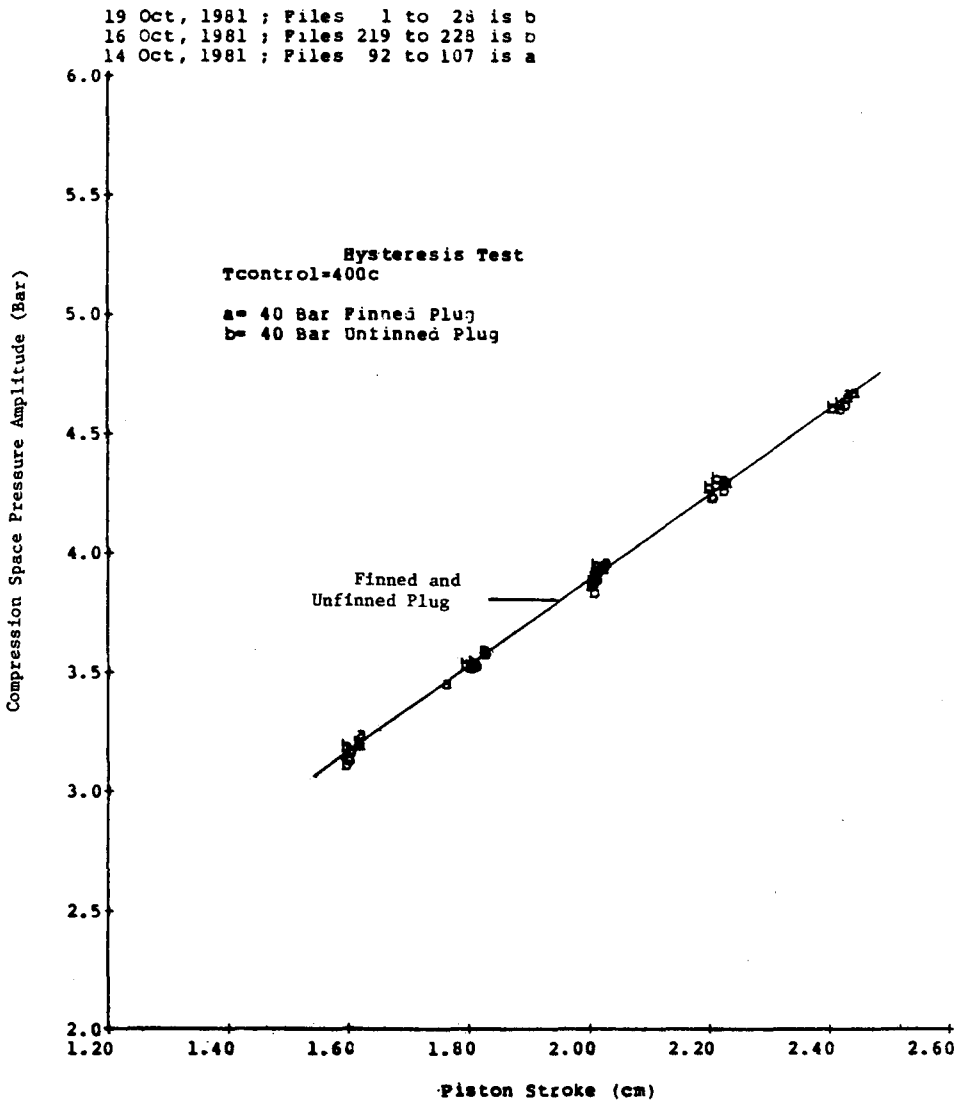

Fig. 5-14. Hysteresis Test: Compression Space Pressure Amplitude Measurements

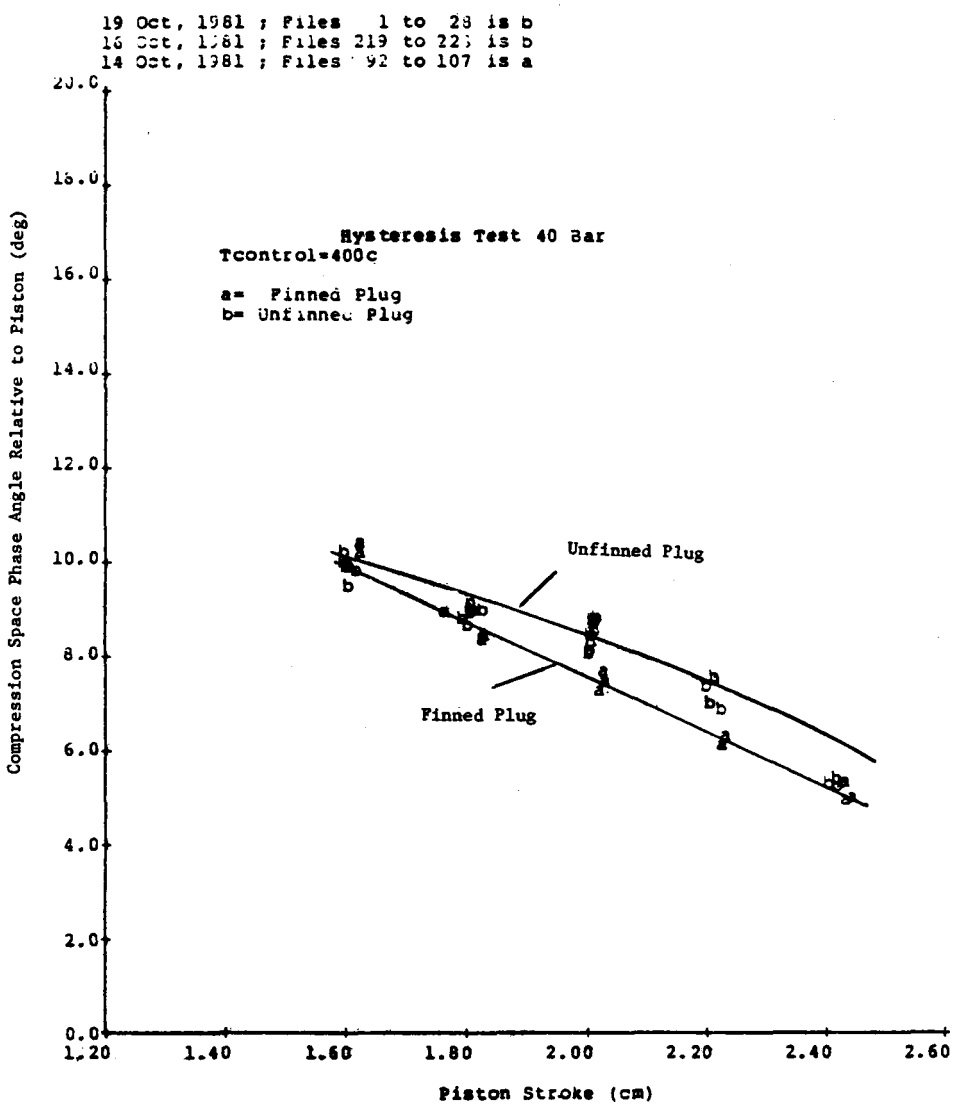

Fig. 5-15. Hysteresis Test: Compression Space Phase Angle Measurements

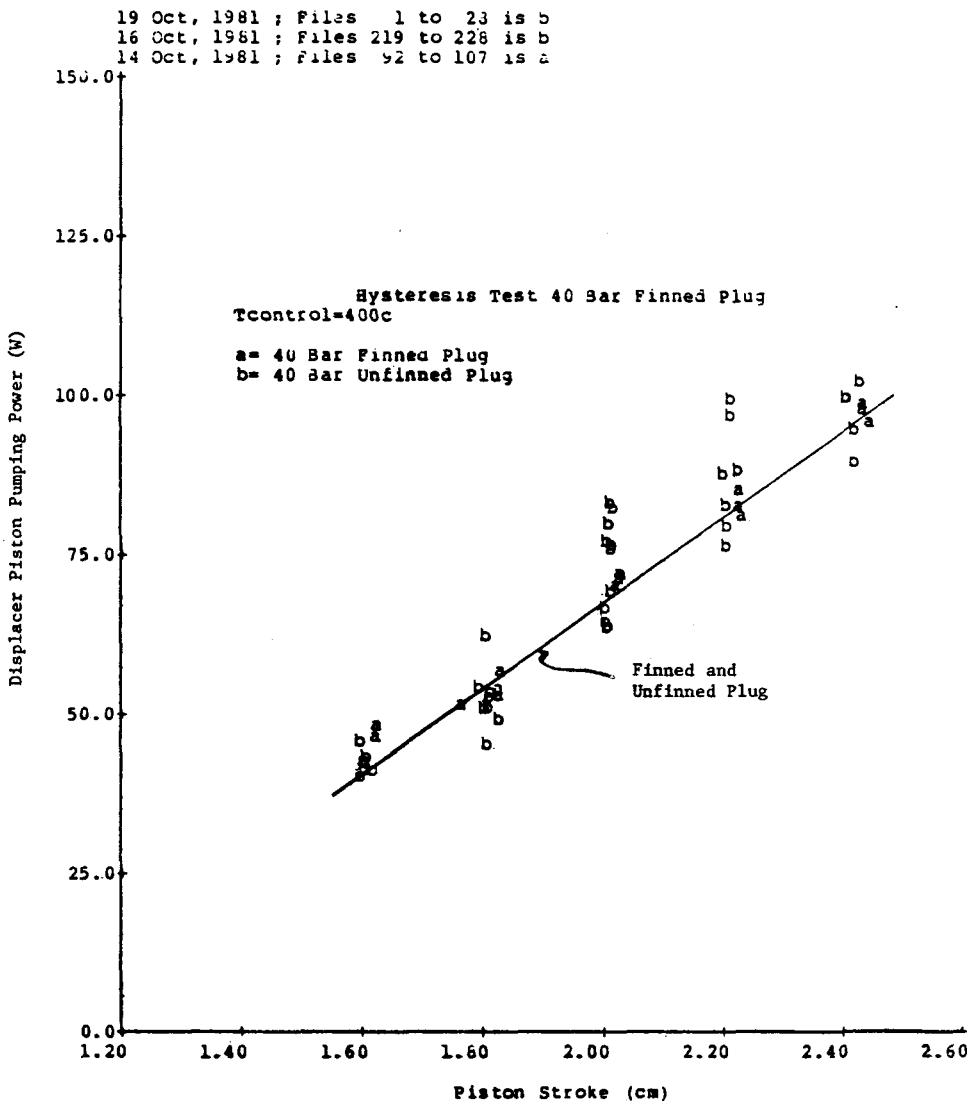

Fig. 5-16. Hysteresis Test: Displacer Power Measurements

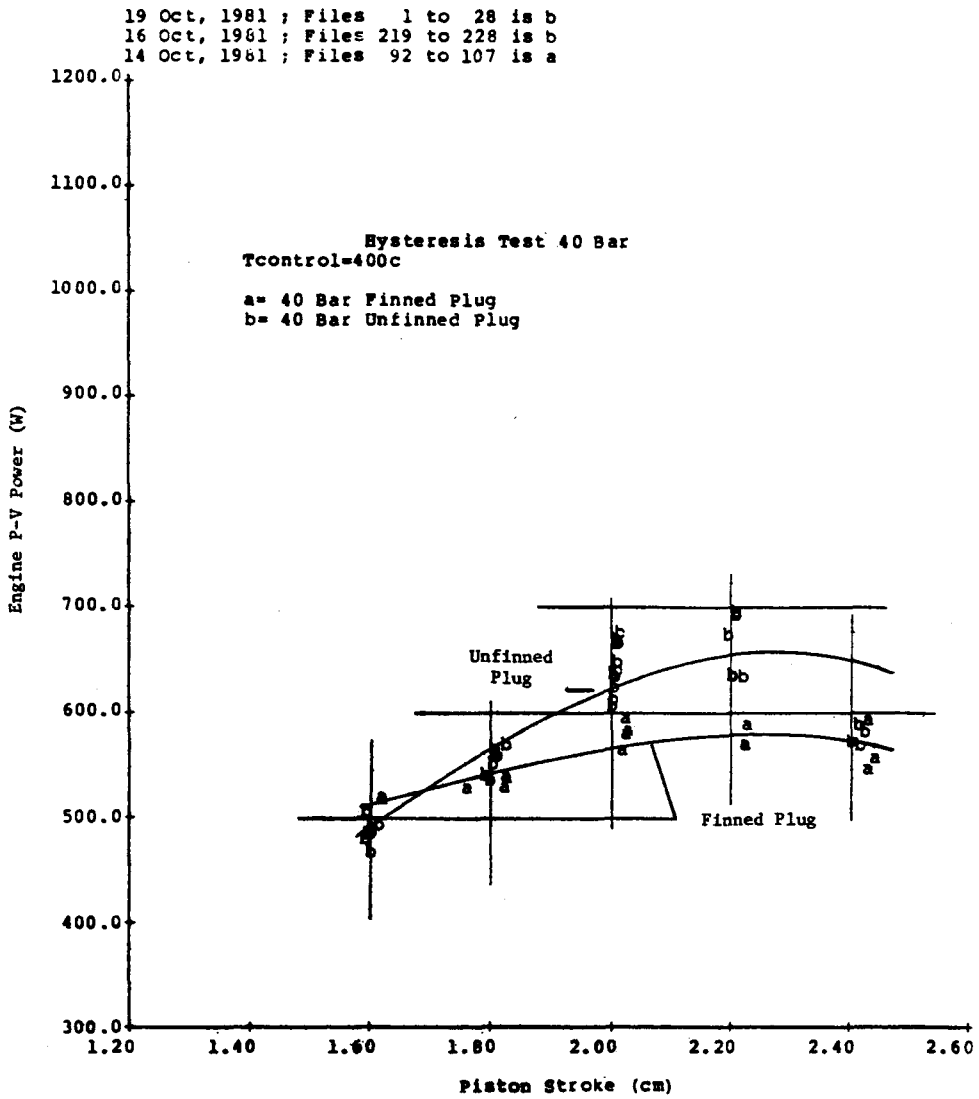

Fig. 5-17. Hysteresis Test: Engine P-V Power Measurements

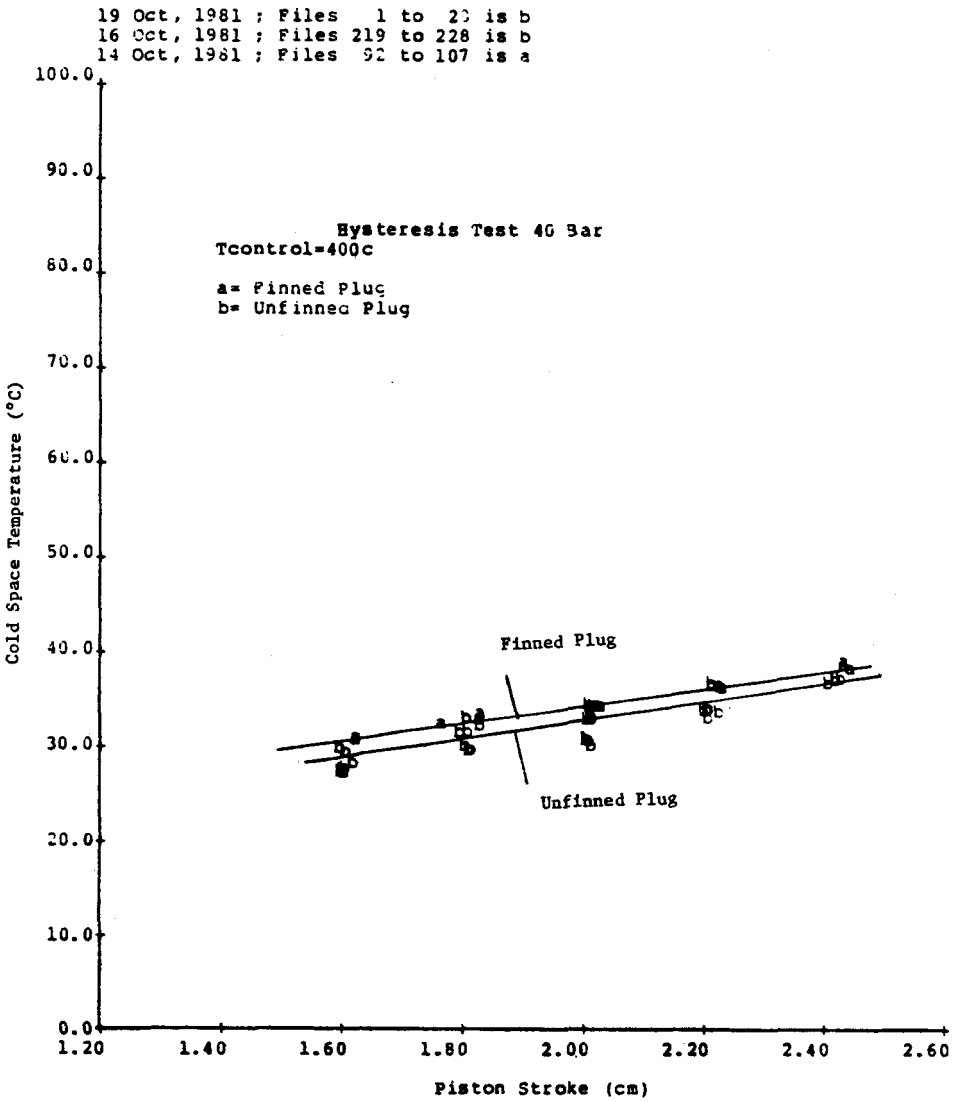

Fig. 5-18. Hysteresis Test: Cold-Space Temperature Measurements

Figure 5-3 showed that the operating displacer phase angle for the unfinned test was slightly lower than for the finned test for each pressure. Tests at 40 bar revealed a reduction in power with a reduction in displacer phase angle (Baseline Engine Test Summary Report).[3] Figure 5-2 showed an increasing deviation in the displacer-to-piston-stroke ratio as the pressure was increased. Tests have shown that power increases with increasing stroke ratio. Comparing the trends of the stroke ratio and phase angle deviations with the power deviations suggests that the reduction in power is a result of the deviating stroke ratio. A normalized power factor, defined as

$$PF = \frac{P\text{-}V}{f\ P_m \frac{X_D}{X_P} X_P{}^2 \sin \theta d}, \qquad 5.1$$

where $P\text{-}V$ = P-V piston power (W),

f = frequency (Hz),

P_m = mean pressure (bar),

X_D = displacer stroke (cm)

X_P = piston stroke (cm), and

θd = displacer phase angle (°),

normalizes the piston P-V power with respect to small deviations in stroke ratio and phase angles. The power factor for the finned and unfinned tests at 40 bar (where the power deviations are more readily apparent) is plotted in Figure 5-19. Small pressure phase angle effects on the displacer power are small; accordingly, Figure 5-19 indicates that the power deviations between the tests were due to operating dynamics, and hysteresis loss effects could not be determined from the test data.

5.3.3 Indicated Efficiency Trends

Indicated efficiency is defined as indicated power divided by heat input. Heat input to the TDE is in the form of chemical energy from natural gas supplied by a local utility. Because the heating value of the utility-supplied natural gas is not monitored with on-line instrumentation, and the combustion system mass requires long-term operation before an energy balance closure for the combustion system is approached the following ssumptions were made to determine heat input:

- All the heat generated by alternator inefficiencies and the piston gas spring is dissipated by free convection to the environment through the alternator pressure vessel,
- Internal losses in the displacer gas spring due to seal leakage and hysteresis are dissipated through the cooler, and
- All parasitic conduction losses from the hot space to the cold space are dissipated by the cooler because the regenerator wall is insulated.

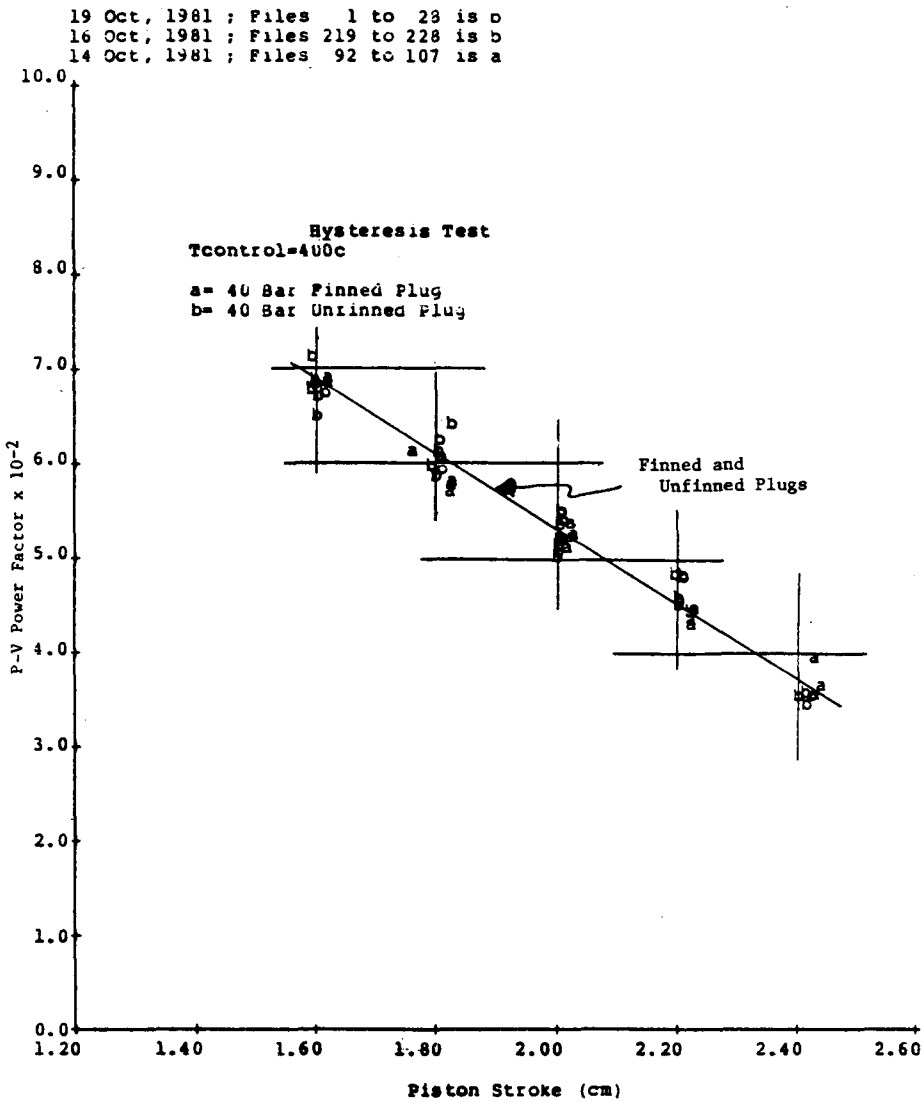

Fig. 5-19. Hysteresis Test: Insensitivity of Power to Hysteresis Effects

With these assumptions regarding the thermodynamic envelope, heat input to the engine is piston P-V power plus engine heat rejection. The measurement of engine heat rejection is obtained by a precision flow meter in the water line and by the use of a precision RTD bridge network for coolant ΔT.

Figure 5-20 compares indicated efficiency results between the finned and unfinned tests. Considering that heat rejection (Fig. 5-21) between the two tests was essentially the same, the deviations in indicated efficiency shown are due to deviations in the indicated power.

A secondary result of the uncertain hysteresis losses is the fact that indicated efficiency increased with decreasing mean pressure. A subsequent test of the compression-to-expansion-space displacer seal leakage revealed a strong dependency of engine performance on the seal gap. Because the power still increased as the pressure was increased, the decline in efficiency shown in Figure 5-20 is primarily a parasitic loss. A very likely candidate for this loss is the displacer seal gap losses resulting from enthalpy transport from the appendix gap to the cooler through the large seal clearance.

5.4 ANALYTICAL COMPARISON

The First-Order Harmonic Engine Analysis Code is structured to allow two modes of analysis-fixed and free-dynamics. Free-piston Stirling engine analysis as a free oscillator is accomplished by establishing the proper spring damping values in the dynamic matrix, and by allowing the code to iterate to a solution by coupling the two mass-system dynamics with the resulting thermodynamics. The pretest analysis was accomplished in this manner. A second option with the First-Order Code is to establish engine operating dynamics as obtained from testing, and then calculate engine predicted performance from the fixed dynamics input equal to the engine operating dynamics. The latter option of using fixed dynamics to study code correlation with engine data eliminates any uncertainties in the dynamics matrix, either measured or calculated, and gives a one-to-one correlation of the code's ability to predict engine thermodynamic performance. To assist the analysis, a data reduction routine was written that retrieves actual engine data stored on data tapes, and lists the input dynamics and temperatures as they are to be used in the code, with some of the pertinent calculated results for comparison.

5.4.1 Power Correlation

The absolute power correlation between engine test results and predicted power is shown in Figures 5-22 and 5-23 for the finned and unfinned tests. The predicted results, calculated (using the fixed dynamics option) by using the measured dynamics at each point shown, show that the code underpredicts the power, with the discrepancy increasing as pressure decreases. Because the engine frequency, displacer stroke ratio, displacer phase angle, and temperature were fixed parameters in the code, study of the calculated pressure amplitude and phase will show the discrepancy in power correlation. Figure 5-24 shows that correlation of the pressure amplitude is nearly exact for each pressure point, indicating that engine volumes and calculated gross temperatures are modeled correctly. Figure 5-25 indicates that the discrepancy in power correlation as pressure is reduced is due to underprediction

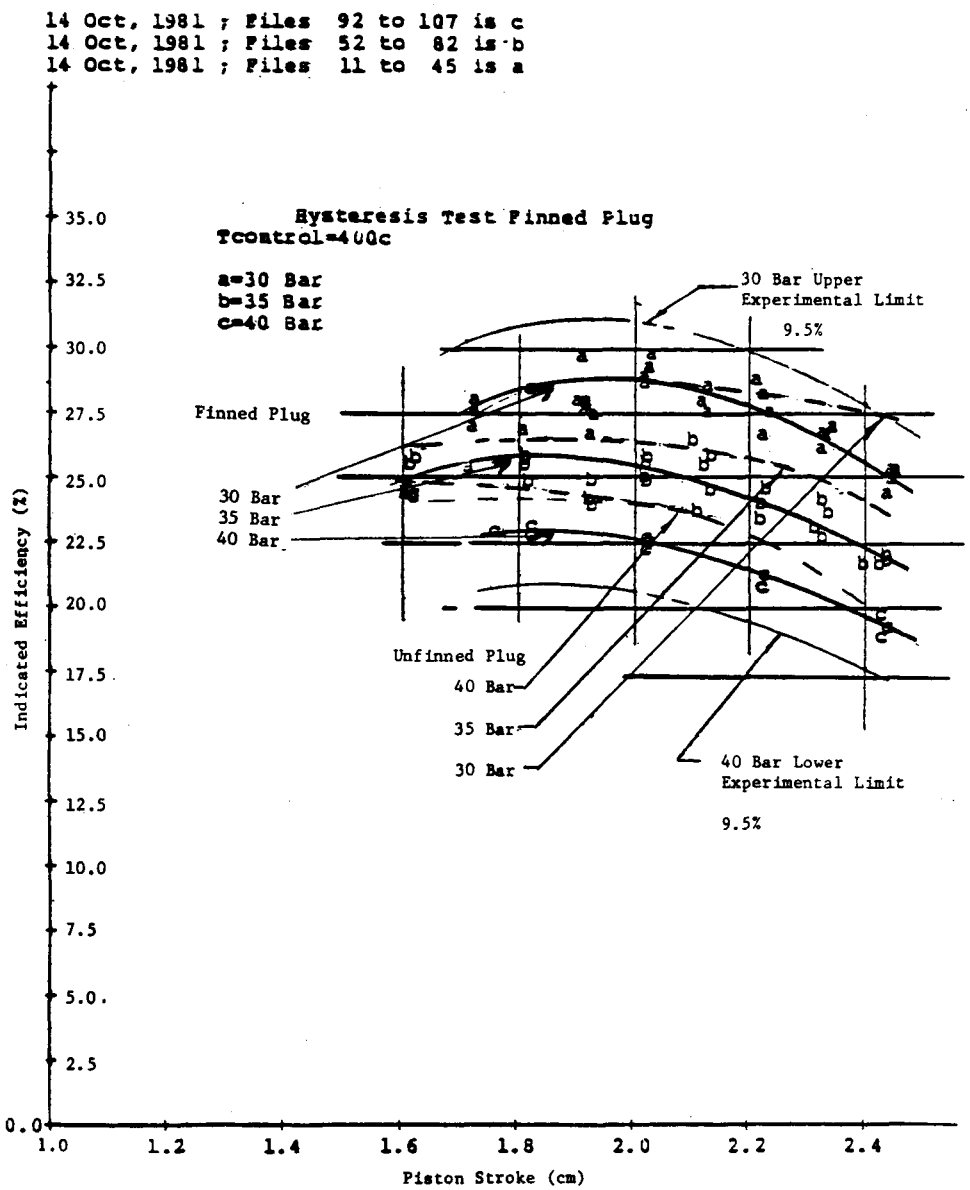

Fig. 5-20. Hysteresis Test: Indicated Efficiency Measurement Summary

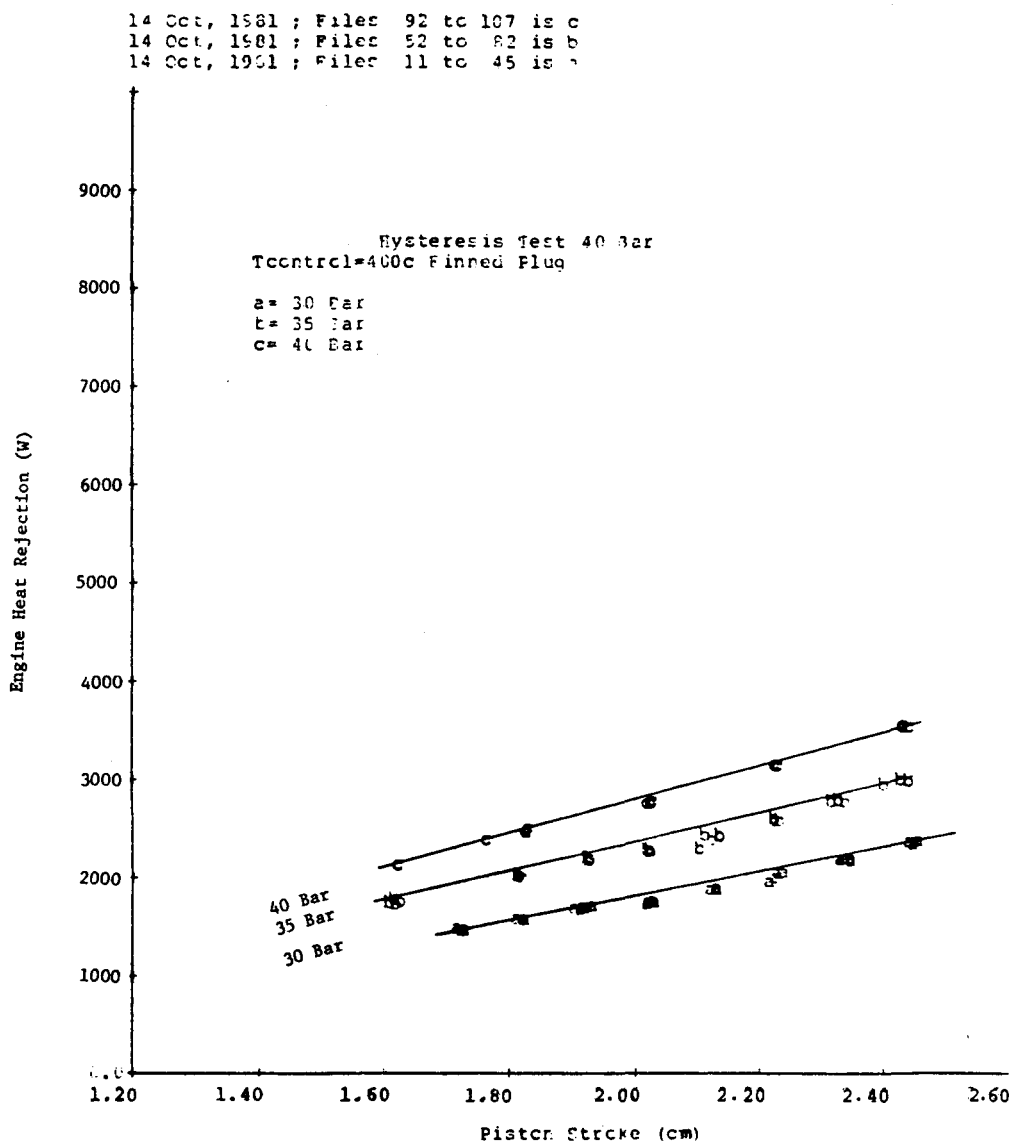

Fig. 5-21. Hysteresis Test: Effect of Pressurization on Engine Heat Rejection

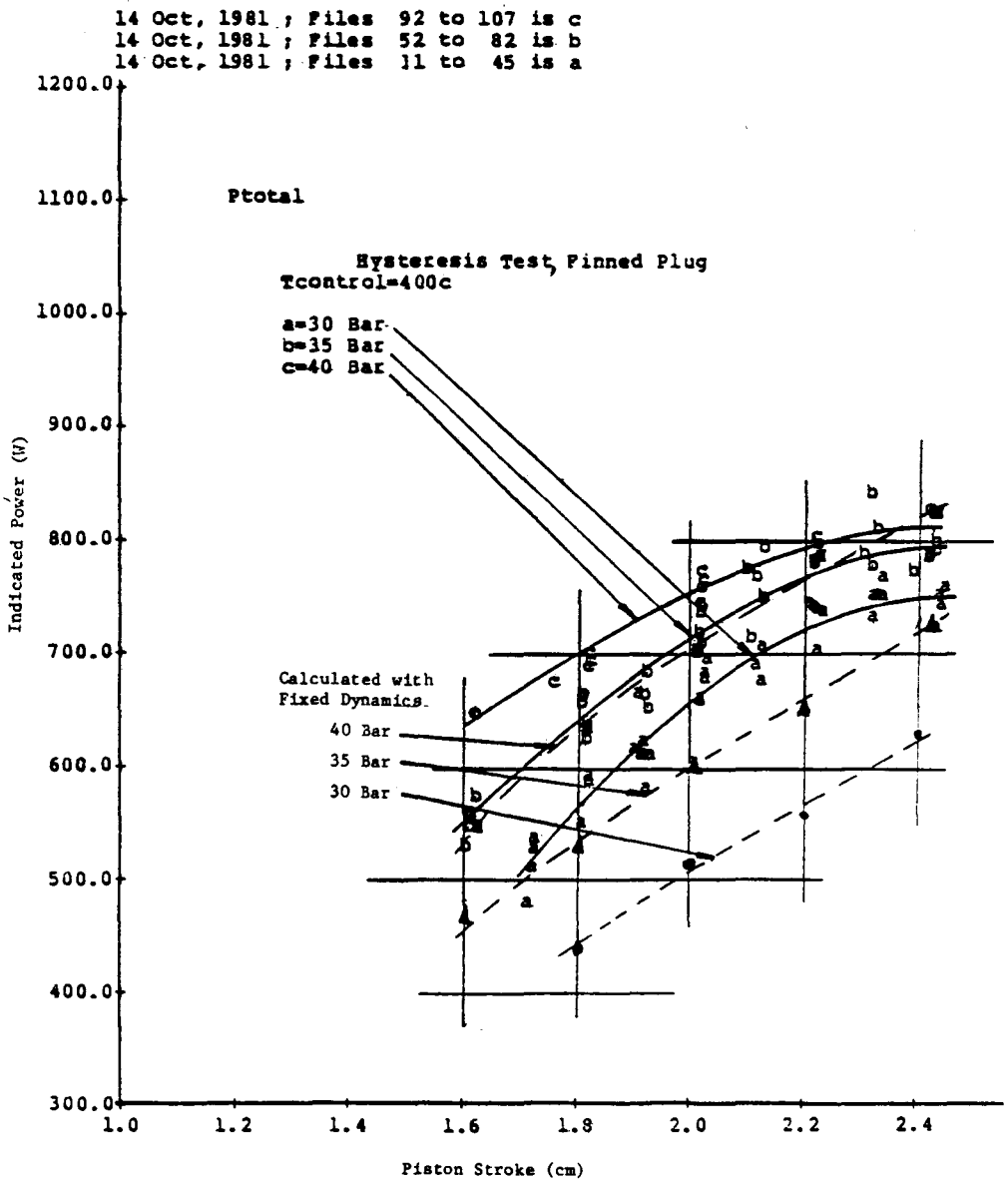

Fig. 5-22. Hysteresis Test: Comparison between Measured and Predicted Power, Finned Plug

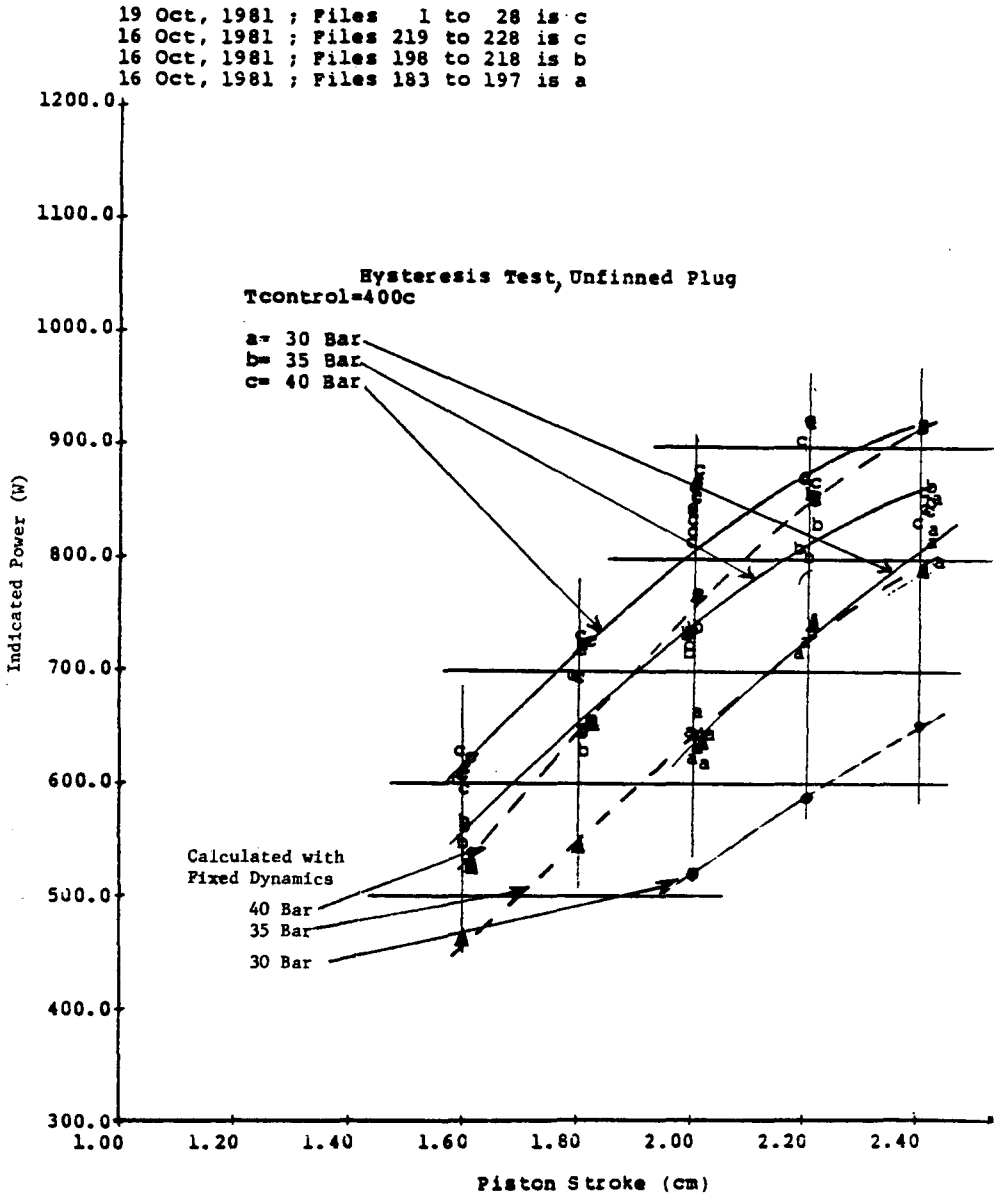

Fig. 5-23. Hysteresis Test: Comparison between Measured and Predicted Power, Unfinned Plug

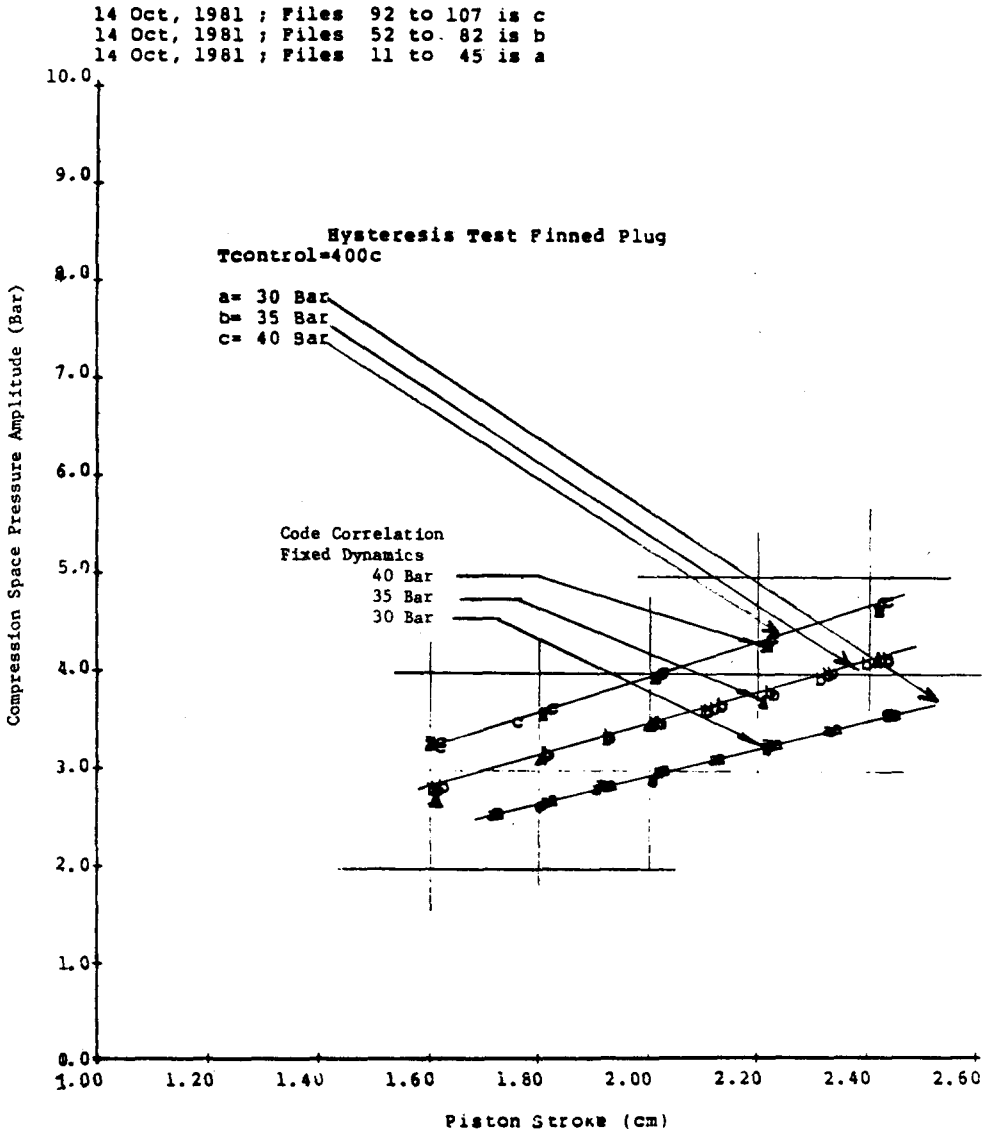

Fig. 5-24. Hysteresis Test: Comparison between Measured and Predicted Pressure Amplitude, Finned Plug

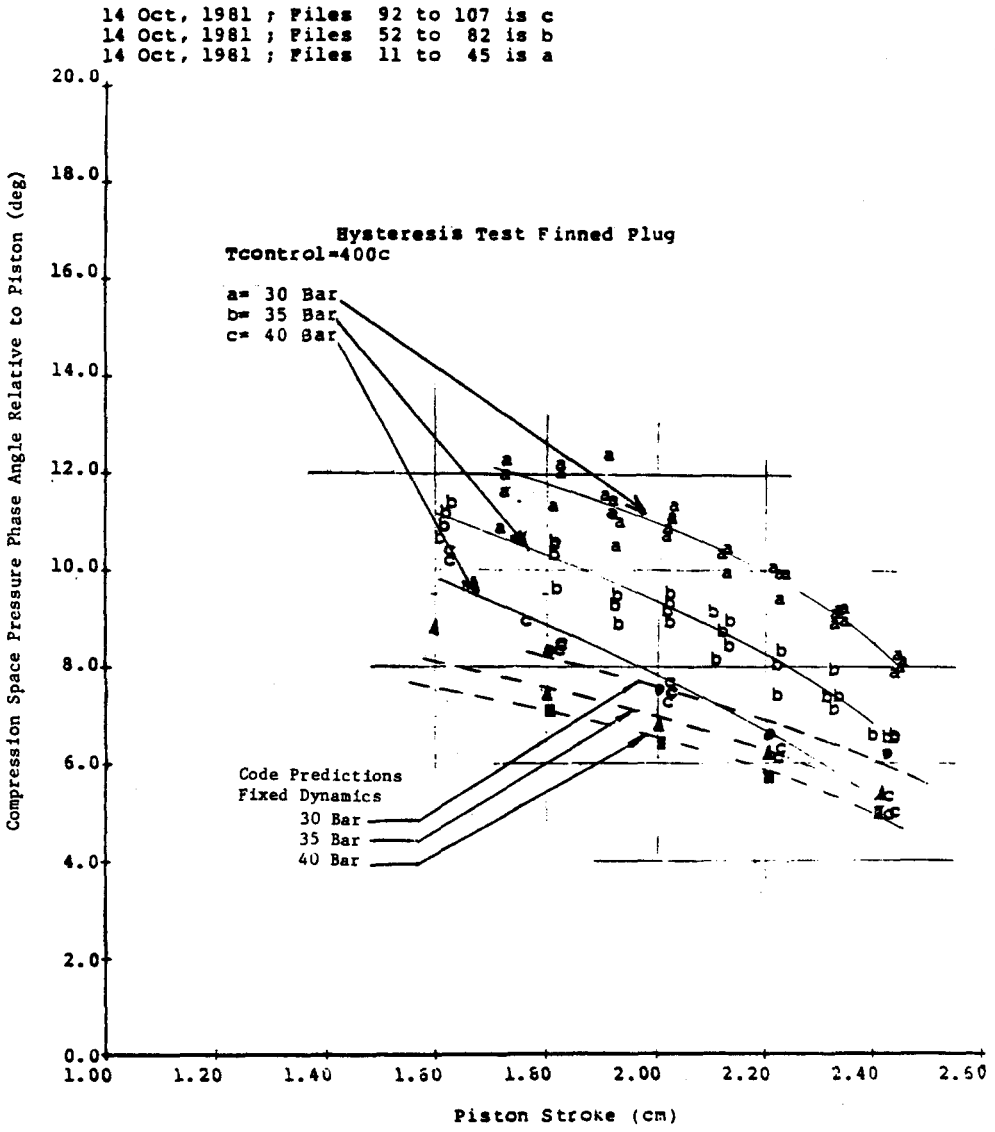

Fig. 5-25. Hysteresis Test: Comparison between Measured and Predicted Compression Space Phase Angle

of the pressure phase angle. Figure 5-26 shows that the heat exchanger pressure-drop amplitude calculation slightly underpredicts the measured results, but follows the measured trends. Because the trend of the calculated compression-space pressure phase does not follow the measured results where the δP trends do, and because the δP amplitude is slightly underpredicted (underprediction will result in an overprediction of pressure phase), the error in the calculated pressure phase trends with pressure is not due to heat exchanger pumping modeling.

The remaining avenues to explore for an explanation of the deviations in calculated pressure phase and trends are: compression-space leakage, expansion-space gas temperature calculation (cold-space temperature was fixed by the input) due to effects of excessive expansion-to-compression-space seal clearance, erroneous hysteresis loss predictions, or a combination of all these effects. Figure 5-27 shows the relative correlation between measured and calculated test results for the run with the finned and unfinned plugs, as well as the correlation deviations for a given pressure and stroke point, to be small between the two tests, although the absolute trend in correlation deviated more with decreasing mean pressure. Also, from the experimental results, the difference in power performance was shown to be small between the two tests. From these two observations, it can be concluded that significant code correlation deviations from the actual test data as the pressure was reduced are not due to erroneous hysteresis loss predictions.

The compression-space leakage coefficient was derived from actual hardware clearances with a conservative 50% eccentricity factor applied. The same coefficient was used for correlation of engine data for the base engine test. Producing calculated results that will correlate to the 30 bar data by artificially increasing the compression-space leakage coefficient will result in an impractical clearance. The discrepancy in the power correlation trend is then due to erroneous expansion-space temperature calculations, perhaps because of the excessive expansion-space-to-compression-space leakage, which is not modeled by the code.

The same trends between measured and calculated correlation for finned and unfinned configurations of efficiency are shown in Figures 5-28 and 5-29. A comparison of the relative correlation in Figure 5-30 shows a small discrepancy beteen the two tests for a given pressure and significant absolute discrepancy as a function of pressure. Relative trends with efficiency correlation are consistent with power correlation trends, indicating that the basic discrepancy is in the predicted power due to an erroneous pressure phase calculation.

5.5 CONCLUSIONS AND RECOMMENDATIONS

5.5.1 Conclusions

- Hysteresis losses are not underestimated by the code, and the hysteresis analysis is adequate.
- Engine P-V power drops off with increasing pressure due to the dominant affect of decreasing compression-space pressure phase angle. (This may be due to excessive displacer seal leakage.)

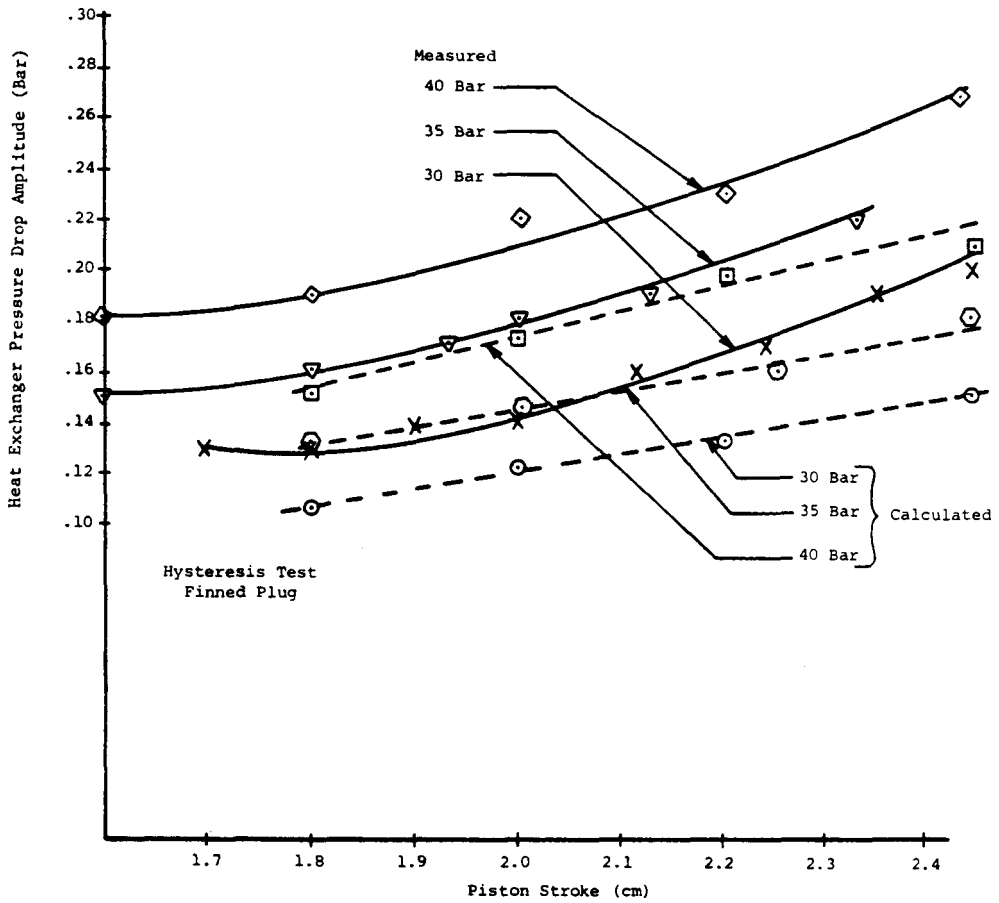

Fig. 5-26. Hysteresis Test: Comparison between Measured and Predicted Heat Exchanger Pressure Drop Amplitude

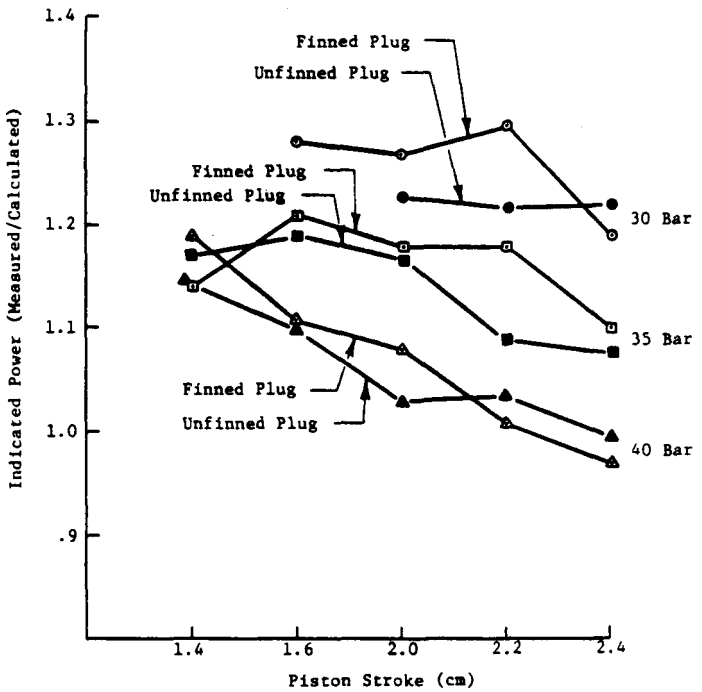

Fig. 5-27. Hysteresis Test: Correlation between Measured and Predicated Power

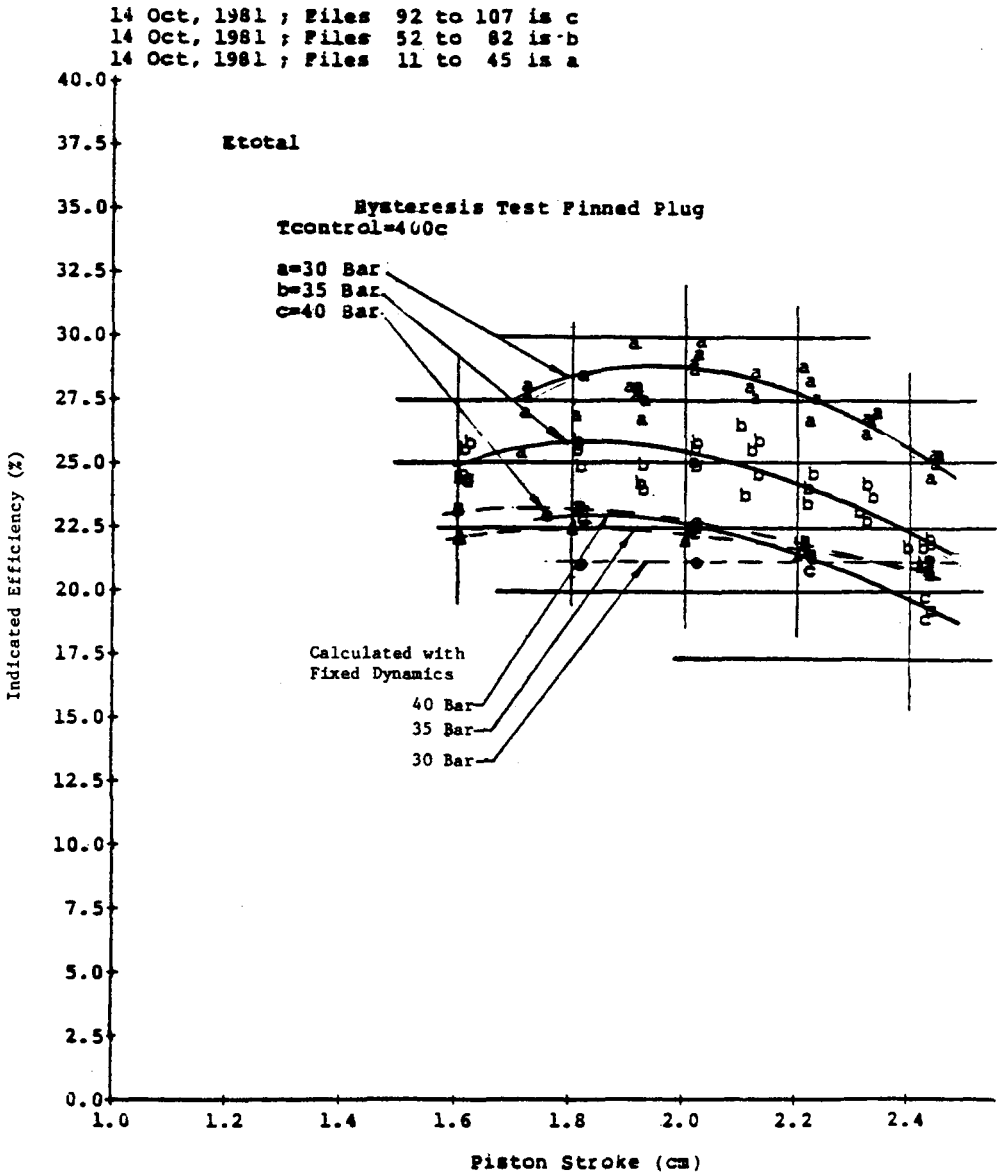

Fig. 5-28. Hysteresis Test: Comparison between Measured and Predicted Indicated Efficiency, Finned Plug

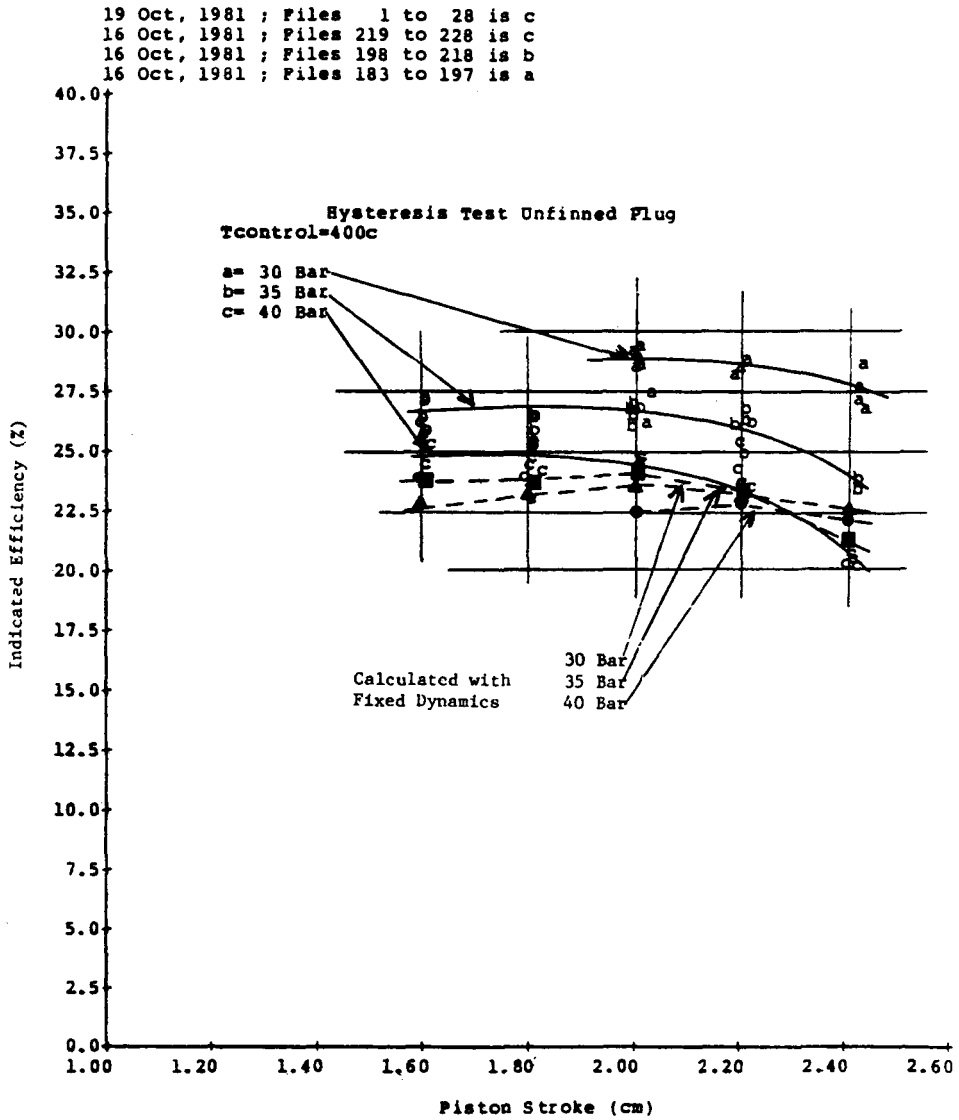

Fig. 5-29. Hysteresis Test: Comparison between Measured and Predicted Indicated Efficiency, Unfinned Plug

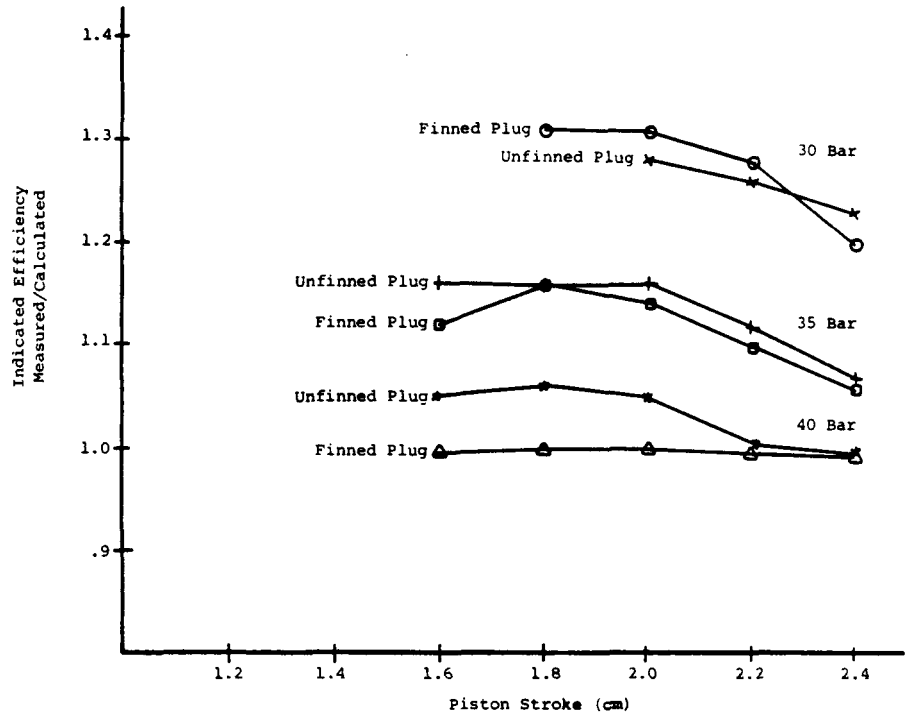

Fig. 5-30. Hysteresis Test: Correlation between Measured and Predicted Indicated Efficiency

- For a constant stroke ratio, the displacer gas spring power loss increases with engine pressure, lessening the available power to be delivered to the piston.

- The analytical code does not track the engine power trends as a function of pressure, underpredicting the power at lower pressures due to underprediction of the compression-space pressure phase.

- The code tracks the heat-exchanger pressure drop as a function of pressure.

5.5.2 Recommendations

- Conduct a test with a close-clearance seal to evaluate the effects of pressure on engine performance.

- Generate a thermodynamic map, similar to the one generated during the baseline tests, with a close-clearance displacer seal at different pressures.

- Improve the alternator feedback field controller circuit to compensate for the nonlinearity at higher field currents to allow stable operation at higher powers/lower pressures and strokes.

- Explore increasing compression-space seal leakage clearances on engine performance.

6. REGENERATOR MATRIX TEST

6.1 TEST OBJECTIVE

Regenerator ineffectiveness results from numerous, complex, and often interacting phenomena such as matrix-to-gas friction/heat transfer, axial/radial gas and matrix thermal conduction, cycle gas pressure variation during regenerator process, regenerator bypass leakage, and regenerator gas flow maldistribution.

Selection of a regenerator matrix involves trade-offs between pumping, thermal, and void volume loss effects to provide an optimal geometry and porosity for a specified matrix wire size. The objective of this test was to aid in assessing the accuracy of the present regenerator analytical model, and to study the effects of varying regenerator porosity using woven-wire screens of different sizes and densities.

6.2 TEST METHODS

The TDE baseline engine regenerator is composed of ~1300 annular-shaped, wire-mesh (100 mesh), 0.001-in. wire diameter screens. The packed wire-screen matrix has a 91% porosity when installed. Two tests series were conducted with the knitted-weave Metex* regenerators. The first series was run with regenerator screens of 0.0025-in. diameter wire and porosities of 70, 75, 80, and 85%; however, they were conducted with a displacer/displacer seal clearance combination that yielded a 0.0048-in. clearance. To eliminate the effects of the large displacer seal clearance from engine performance results, the regenerator tests were rerun with a close-clearance displacer seal using regenerator screens that had a 0.0035-in. diameter wire with porosities of 70, 75, 80, and 85%.

The engine was first assembled with the 70% Metex regenerator, and performance maps versus stroke were run for control temperatures of 400 and 500°C. The engine was disassembled and the regenerator replaced with successive regenerators of increasing porosity. Testing the lower porosities first allowed retuning the engine to comparable dynamics for successive tests since displacer damping power decreases with increasing porosity, andthe additional damping required to set the stroke ratio could be met by adjusting gas spring damping valve. Figures 6-1 through 6-3 show the area weighted mean heater temperature, displacer stroke ratio, and displacer-to-piston phase angle for the four tests at 400°C. The operating temperature and dynamics for each test were set at a piston stroke of 2-cm and a control temperature of 400°C. The area weighted mean head temperature, displacer stroke ratio, and displacer-to-piston phase angle for the 500°C performance tests are shown in Figures 6-4 through 6-6.

*Reference to any specific commercial product, process, or service by trade name, trademark, manufacturer, or otherwise, does not necessarily constitute or imply its endorsement, recommendation, or favoring by the United States Government or any agency thereof.

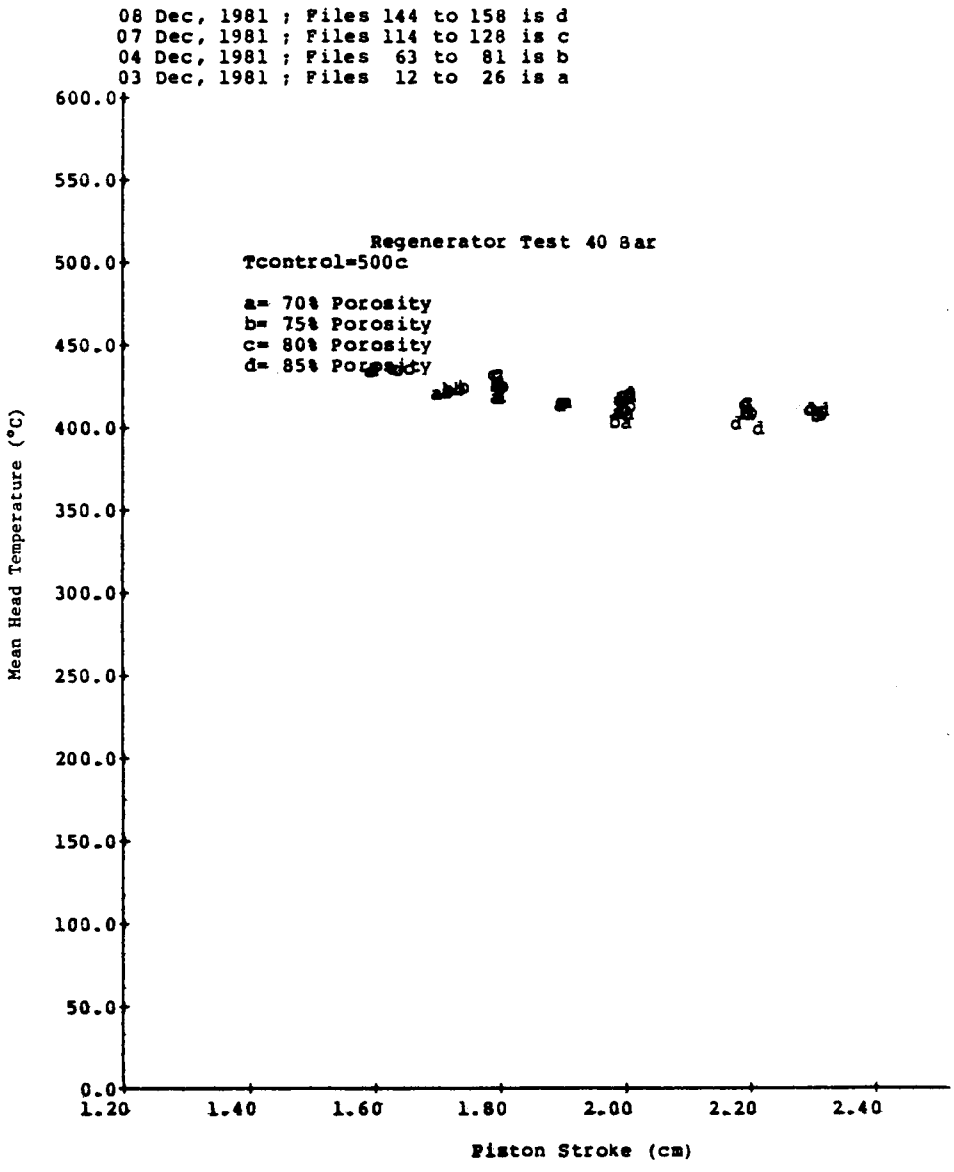

Fig. 6-1. Regenerator Test: Mean Head Temperature Measurements, Tcontrol=500°C

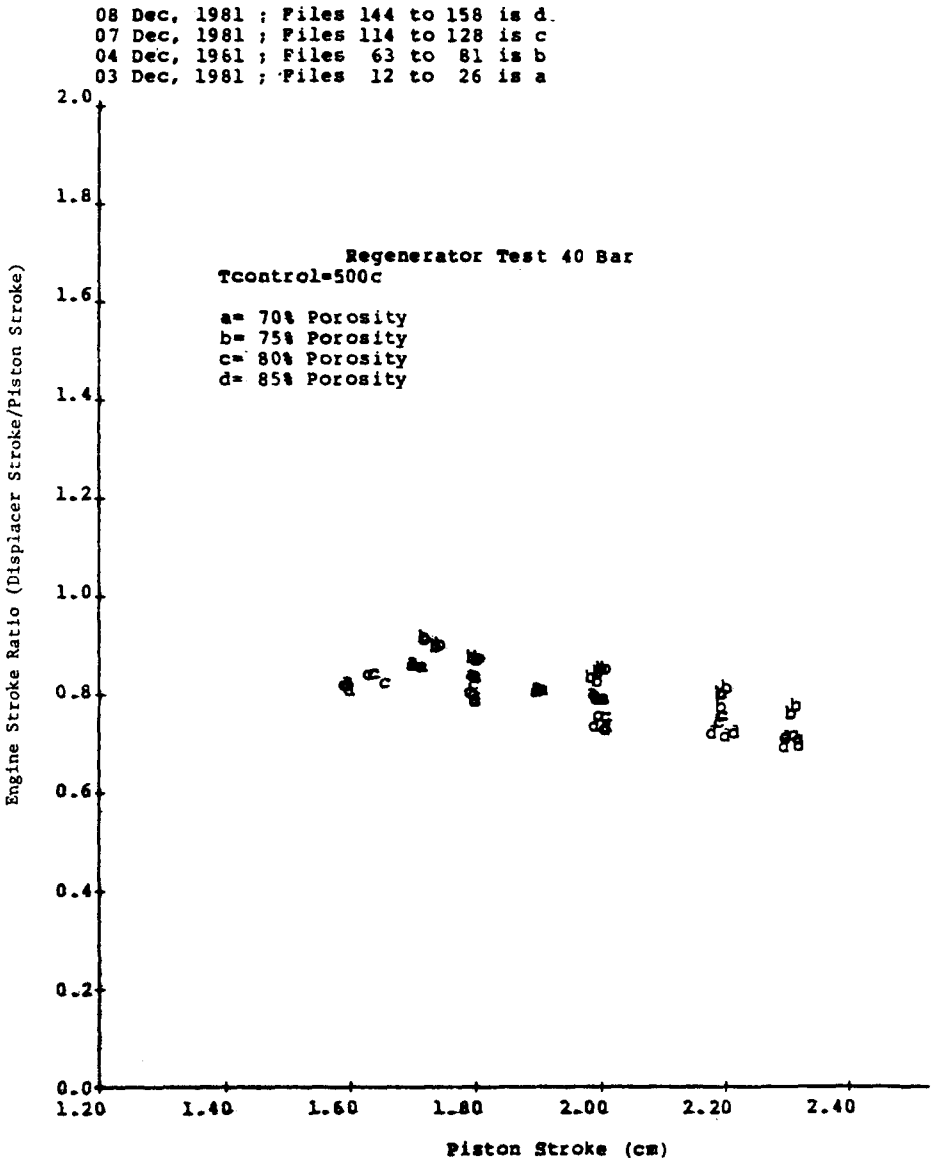

Fig. 6-2. Regenerator Test: Engine Stroke Ratio Measurements, Tcontrol=500°C

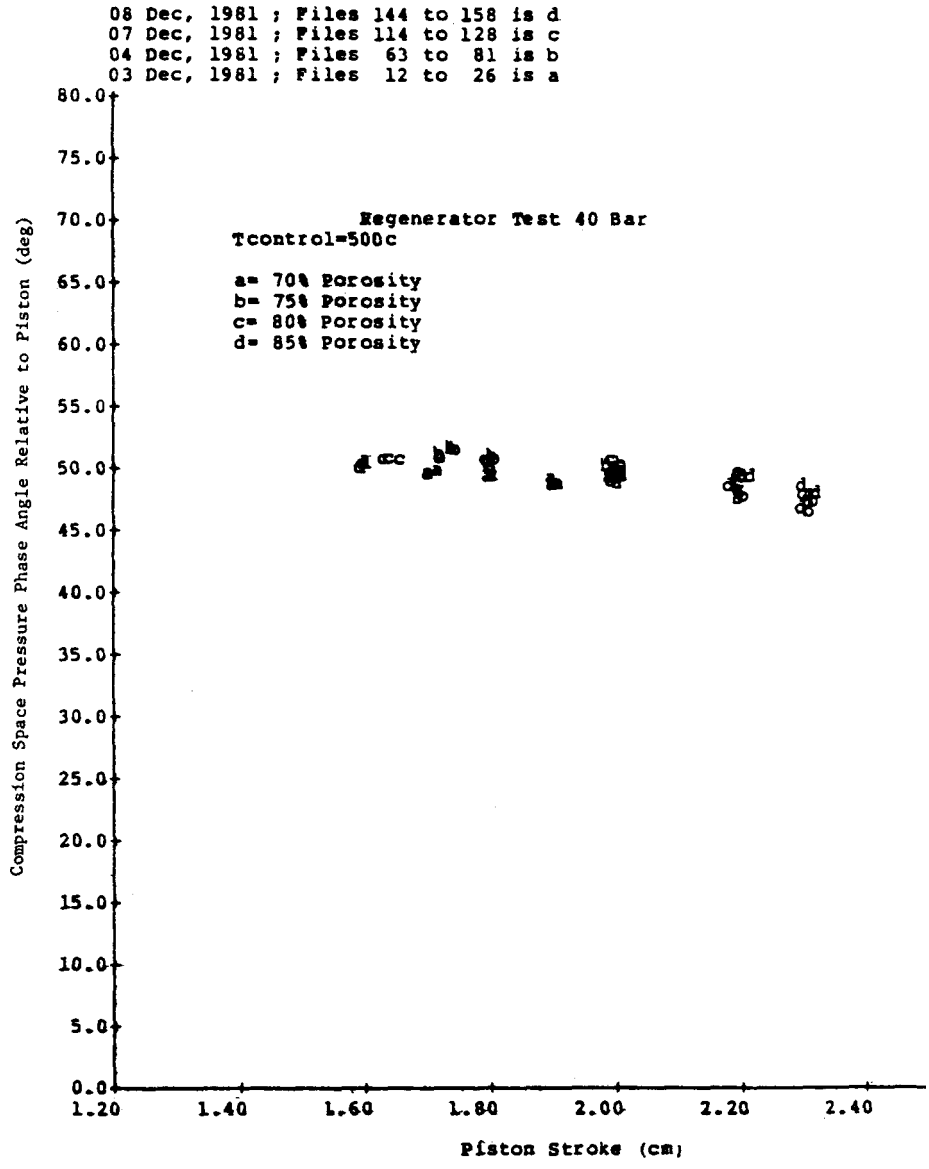

Fig. 6-3. Regenerator Test: Engine Phase Angle Measurements, Tcontrol=500°C

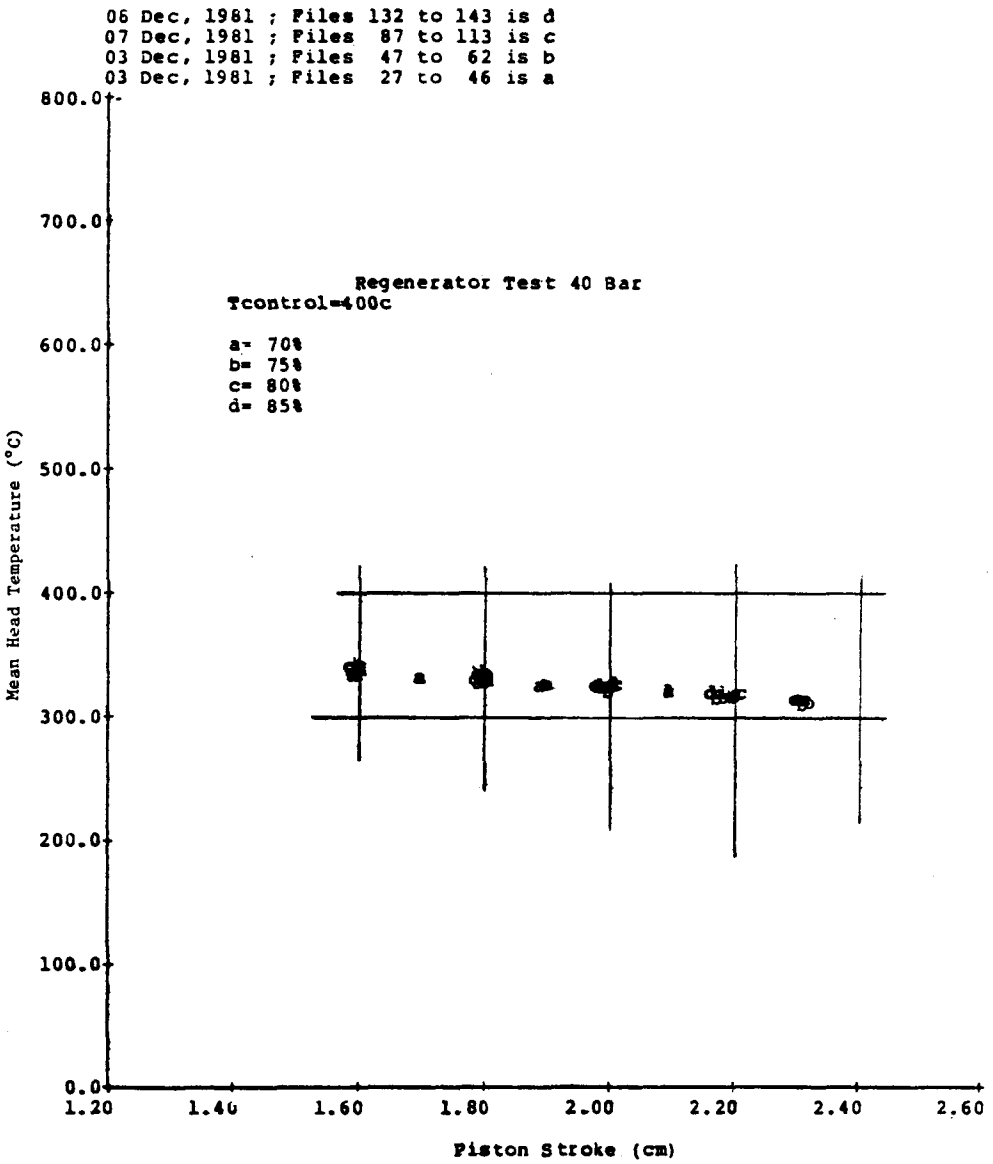

Fig. 6-4. Regenerator Test: Mean Head Temperature Measurements, Tcontrol=400°C

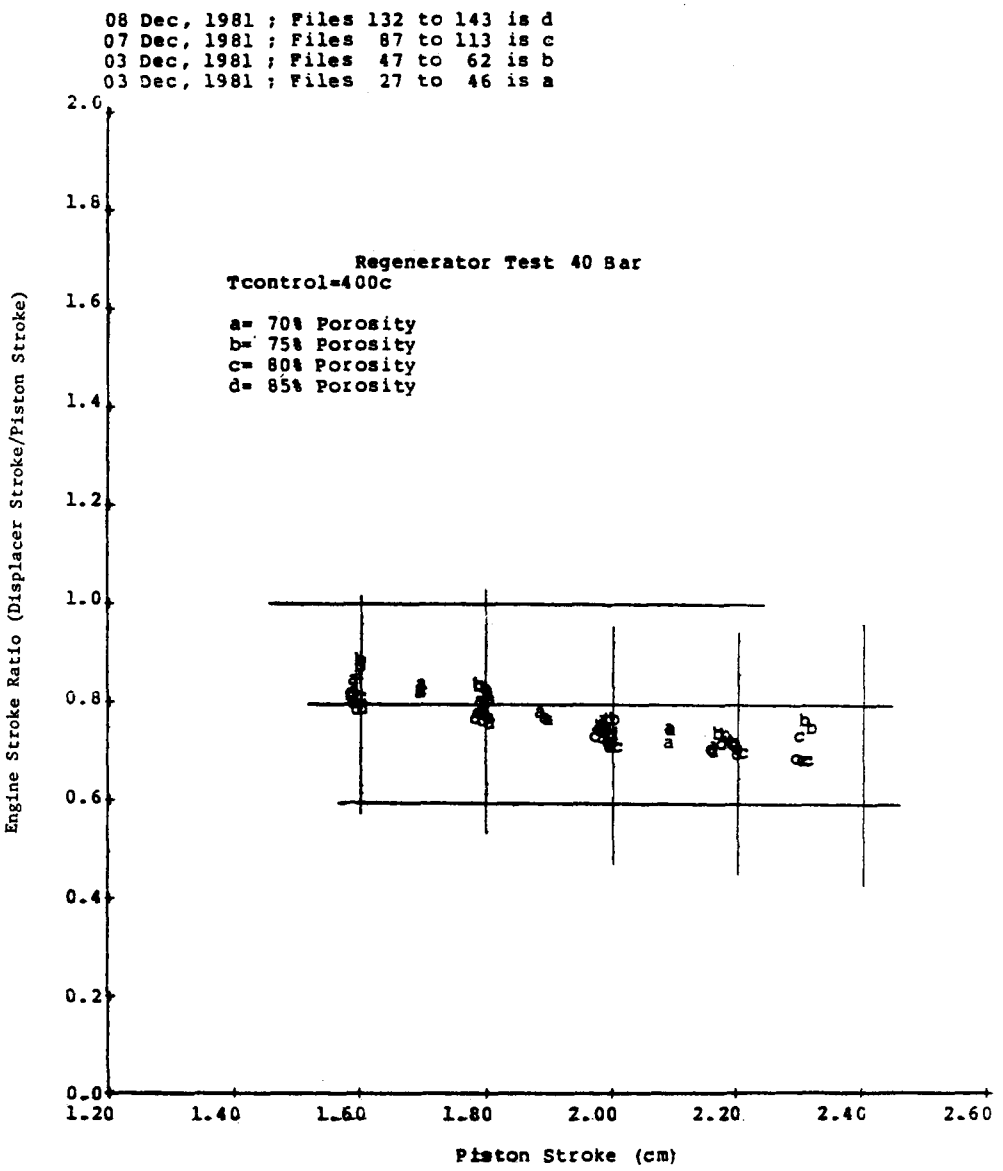

Fig. 6-5. Regenerator Test: Engine Stroke Ratio Measurements, Tcontrol=400°C

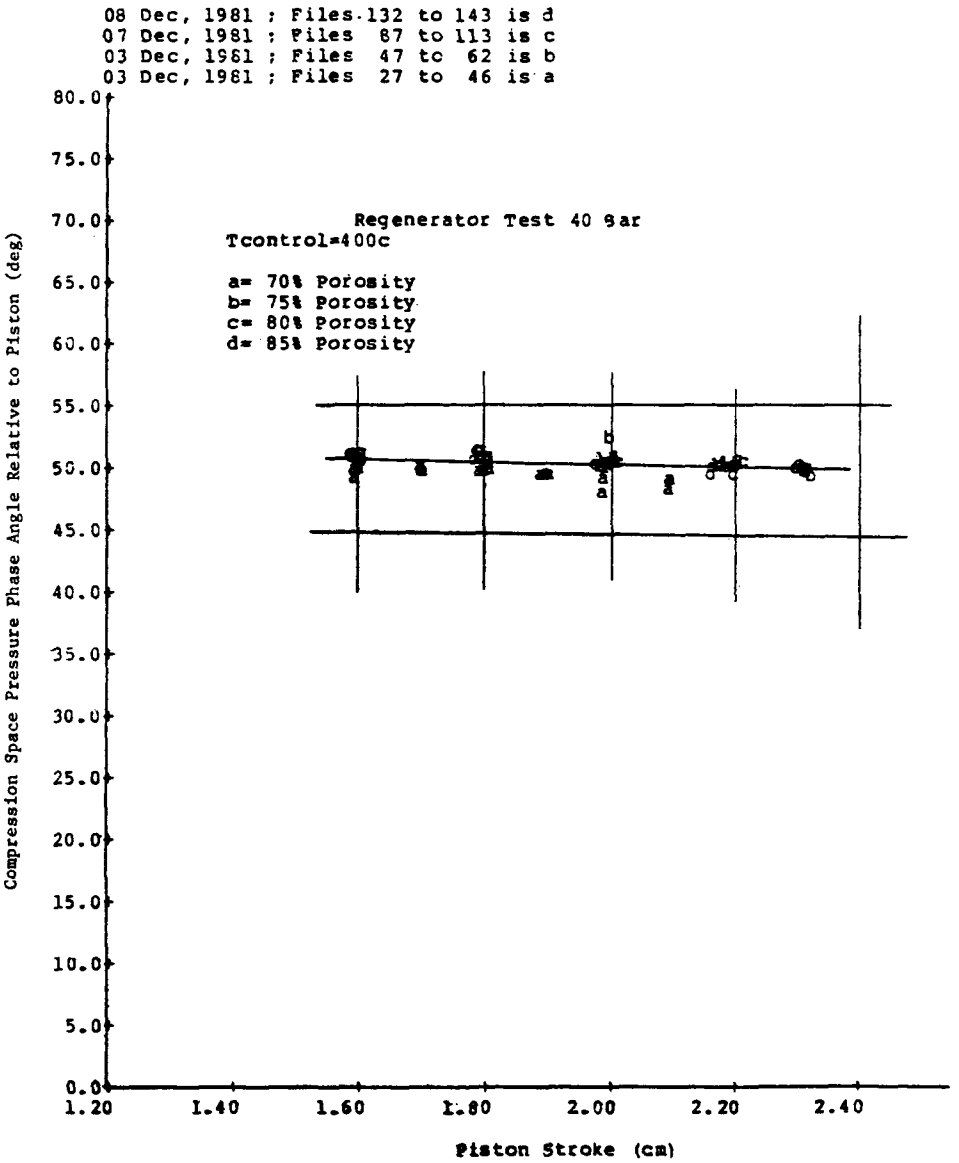

Fig. 6-6. Regenerator Test: Engine Phase Angle Measurements, Tcontrol=400°C

6.3 EXPERIMENTAL RESULTS

The test results presented in this section apply to the tests run with Metex knitted-weave regenerator screens having a 0.0035-in. wire diameter. All tests were run with a displacer/displacer seal cylinder combination yielding a 0.002-in. seal clearance.

6.3.1 Indicated Power Results

Indicated power (see Section 5.3.1) for the 400 and 500°C control temperatures is plotted versus stroke in Figures 6-7 and 6-8 for the four porosities of 70, 75, 80, and 85%. These results, cross-plotted versus porosity in Figure 6-9 for a constant stroke of 2.0-cm at 400°C, show decreasing power with increasing porosity, with an optimum power somewhere below the 70% porosity mesh that was run. Two effects may explain the reduction in power with increasing porosity. The most obvious is the increasing dead volume as regenerator porosity is increased; the second is the subtle interaction of regenerator pressure drop and effectiveness, which affects the thermodynamics of the engine cycles. In Section 5.3.1, the important power parameters were shown to be compression-space pressure amplitude, engine frequency, compression-space pressure phase, and the power split between displacer gas spring power and piston P-V power. Separating the displacer gas spring power (Figs. 6-10 and 6-11) and the piston P-V power (Figs. 6-12 and 6-13) from the indicated power reveals a nearly constant displacer gas spring power with a slight reduction at the lower porosities. The significant reduction in power as a function of porosity is in the piston P-V power parameters, as shown in Figures 6-12 and 6-13.

Figures 6-14 and 6-15 show compression-space pressure amplitude at 400 and 500°C versus stroke and regenerator porosity. As porosity increases (void volume increases), compression-space pressure amplitude decreases due to increased engine volume. Reductions in pressure amplitude with increasing regenerator porosity will result in a reduction of engine power. A reduction in compression-space pressure amplitude will also result in a reduction of the engine spring component, reducing engine frequency (Figs. 6-16 and 6-17).

The compression-space pressure has a spring force component that acts on both the piston and displacer. Reduction in the pressure amplitude reduces the system stiffness and, therefore, the system frequency. A reduction in system frequency will rseult in a reduction of engine power.

Figures 6-18 and 6-19 show the trends of compression-space pressure phase as stroke and regenerator porosity are varied. Compression-space pressure phase generally decreases with increasing porosity for a given stroke, except when there is a slight rise in pressure phase angle between the 70 and 75% tests. Because the dynamics between these two tests were the same, this slight reversal in pressure phase trend (shown to be more distinct for the 500°C case in Fig. 6-19) suggests that thermodynamic interaction of the regenerator on engine power performance becomes more significant with a reduction in regenerator porosity. With a further reduction in regenerator porosity from 70%, reductions in pressure phase due to thermodynamic affects will become more dominant over the dead volume affects of increasing pressure amplitude and frequency, resulting in a reduction of power. The reversal in

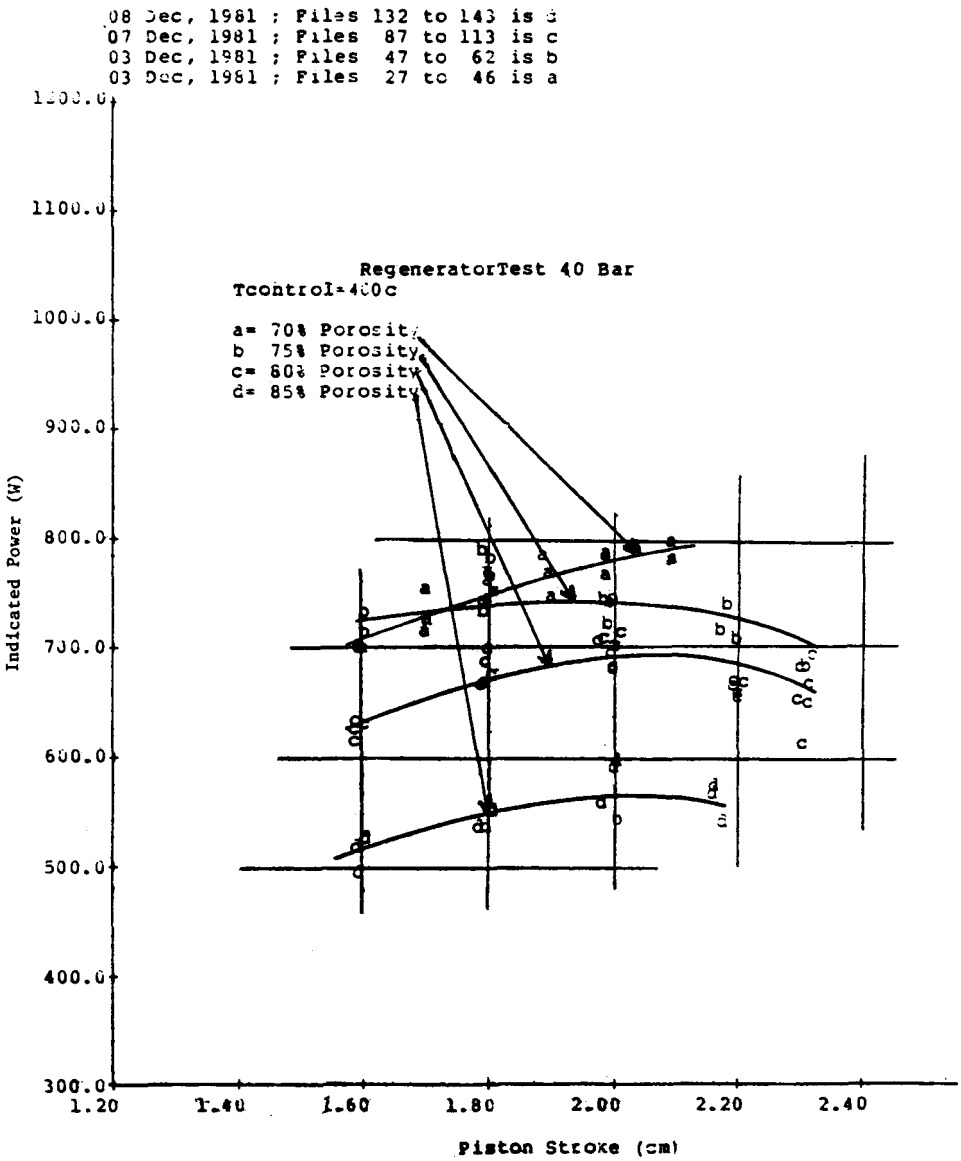

Fig. 6-7. Regenerator Test: Indicated Power Measurements, Tcontrol=400°C

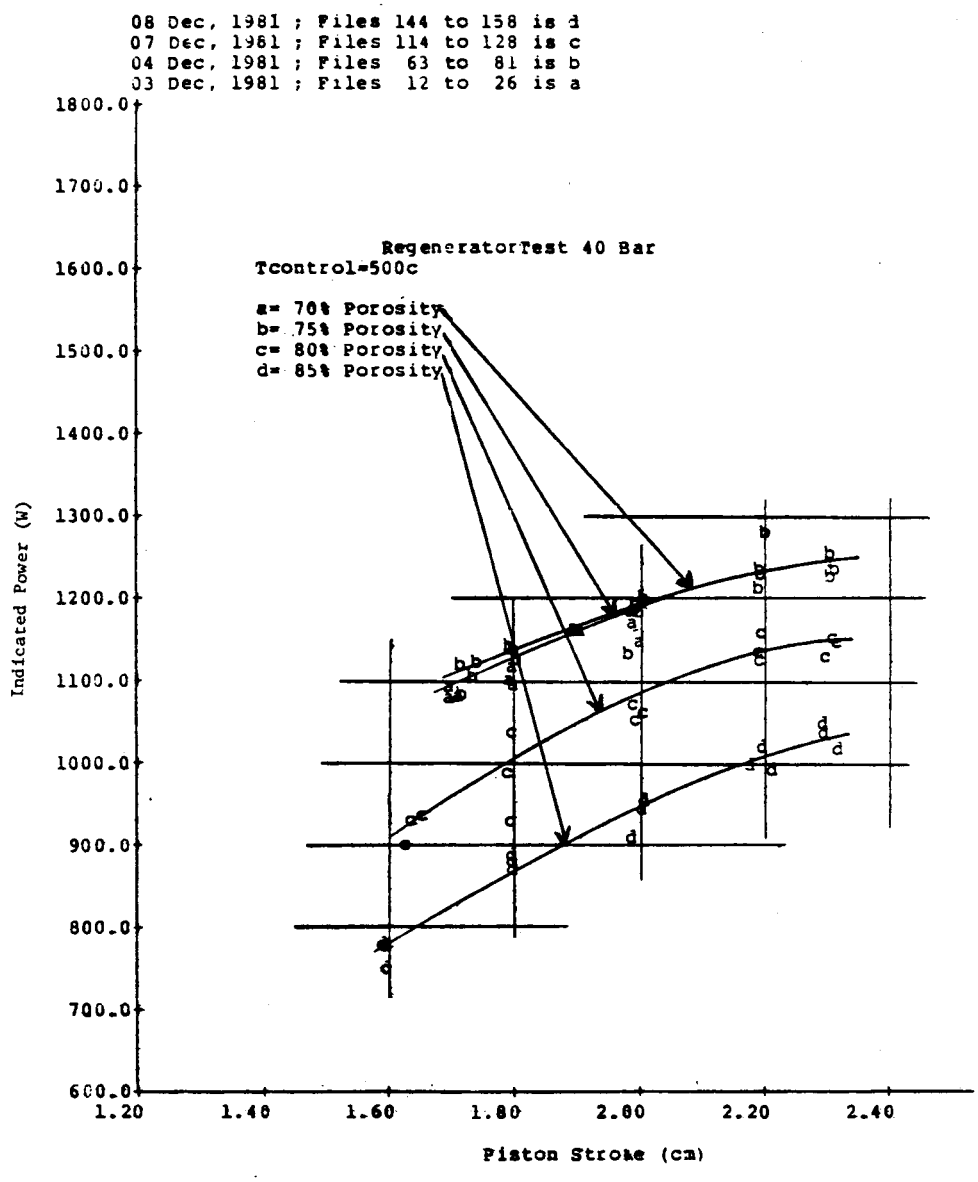

Fig. 6-8. Regenerator Test: Indicated Power Measurements, Tcontrol=500°C

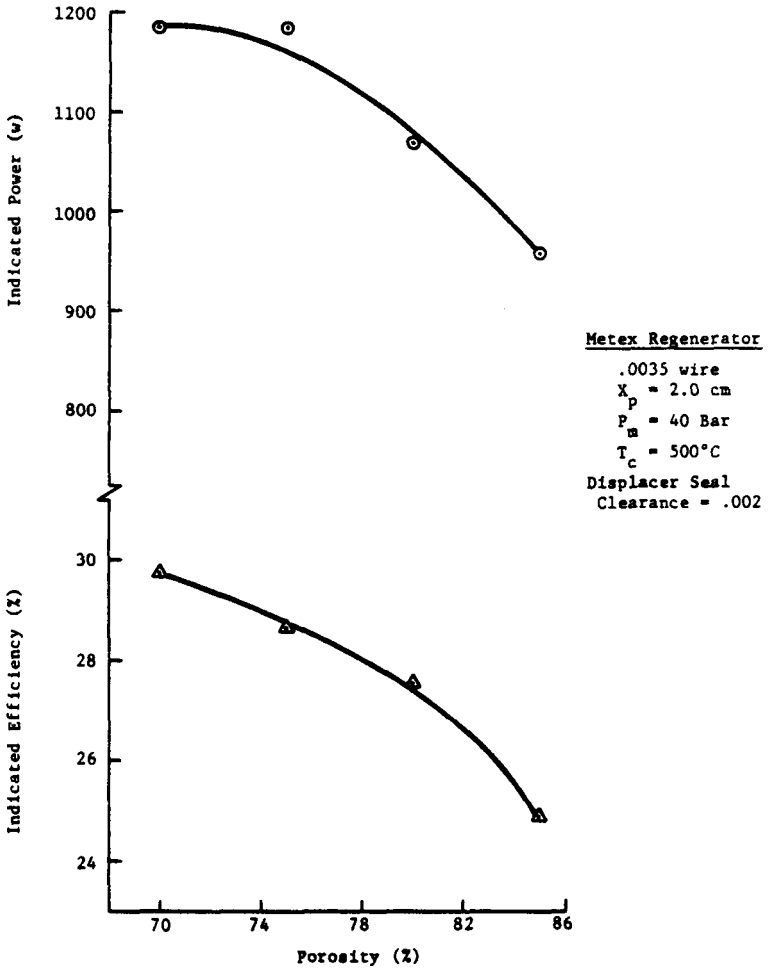

Fig. 6-9. Regenerator Test: Indicated Power and Efficiency Measurements at Constant Piston Stroke

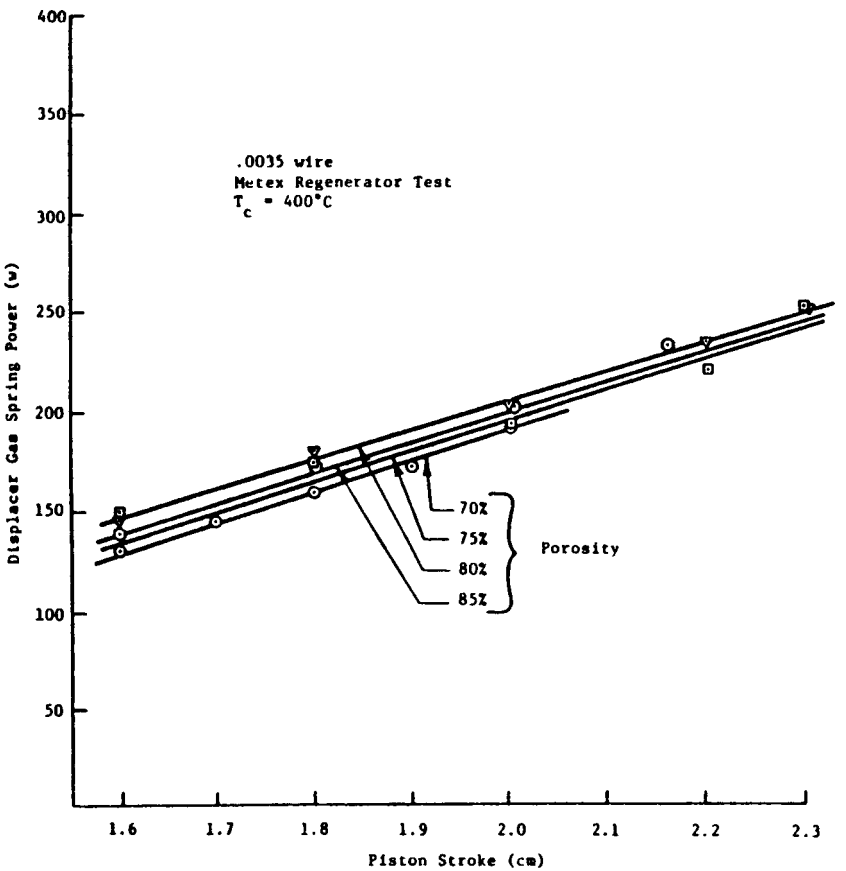

Fig. 6-10. Regenerator Test: Displacer Gas Spring Power Measurements, Tcontrol=400°C

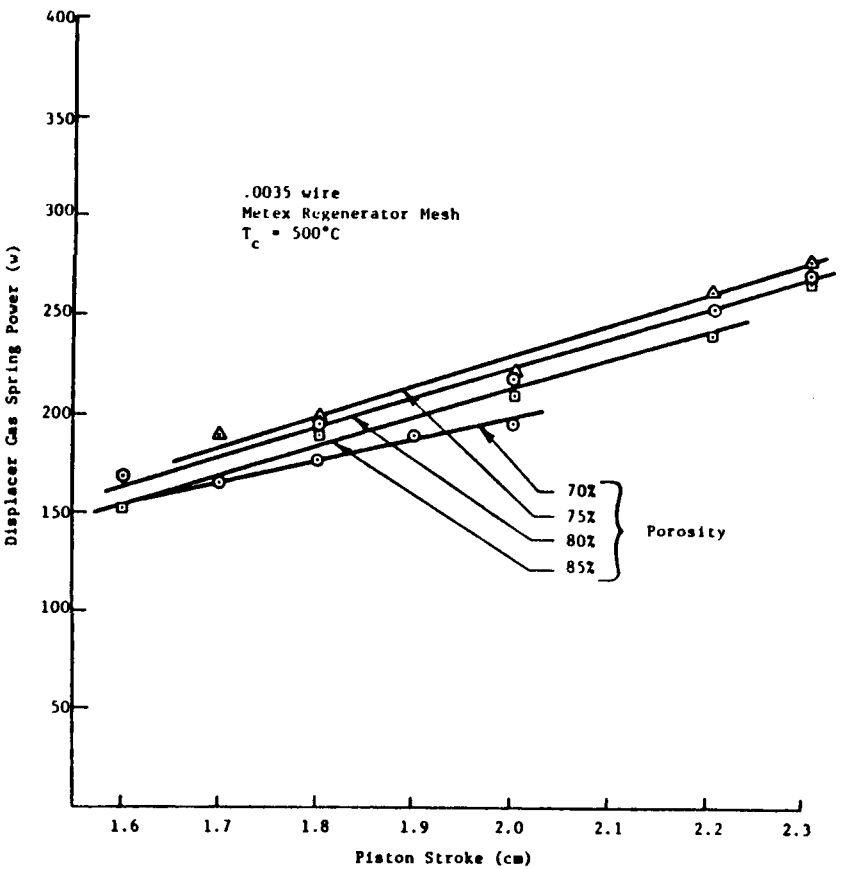

Fig. 6-11. Regenerator Test: Displacer Gas Spring Power Measurements, Tcontrol=500°C

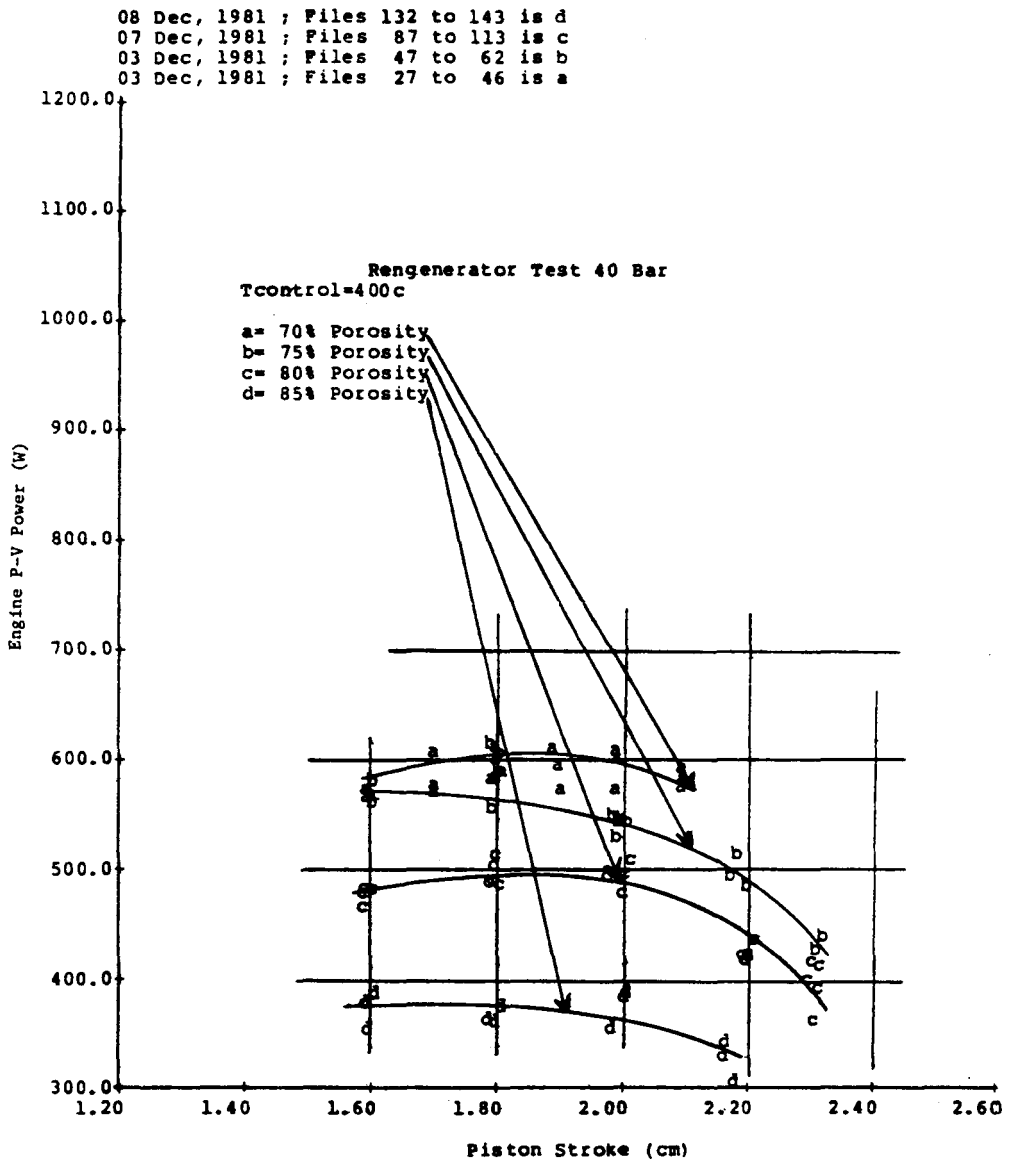

Fig. 6-12. Regenerator Test: Engine P-V Power Measurements, Tcontrol=400°C

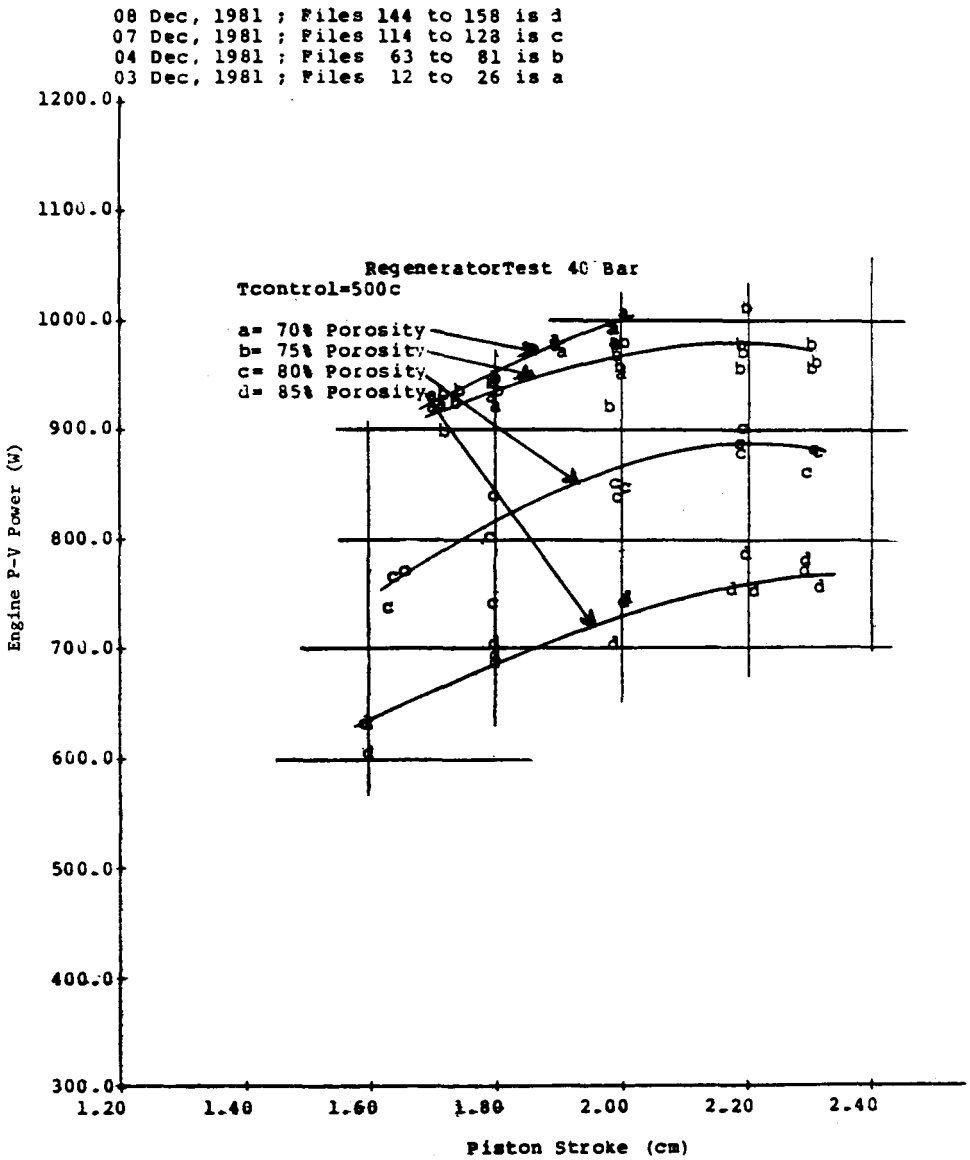

Fig. 6-13. Regenerator Test: Engine P-V Power Measurements, Tcontrol=500°C

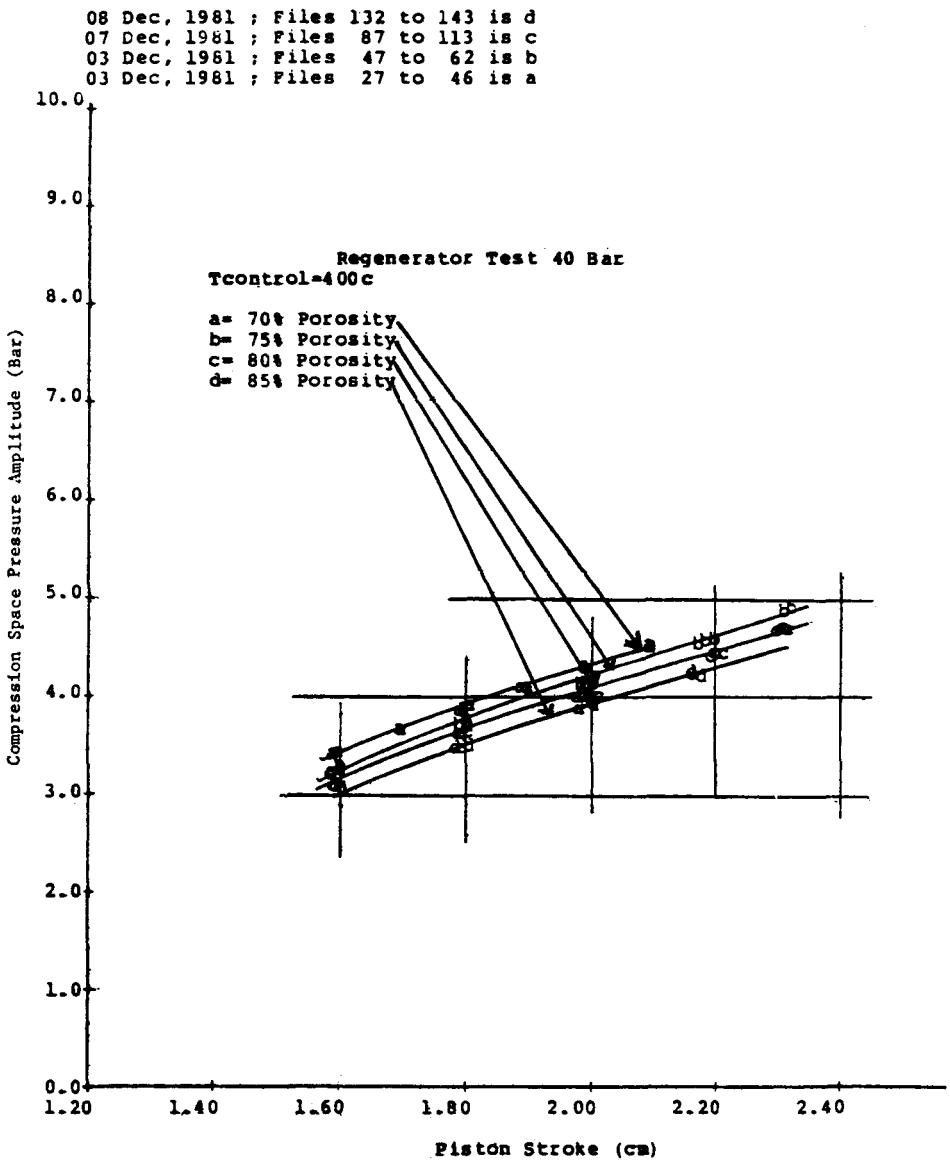

Fig. 6-14. Regenerator Test: Engine Pressure Amplitude Measurements, Tcontrol=400°C

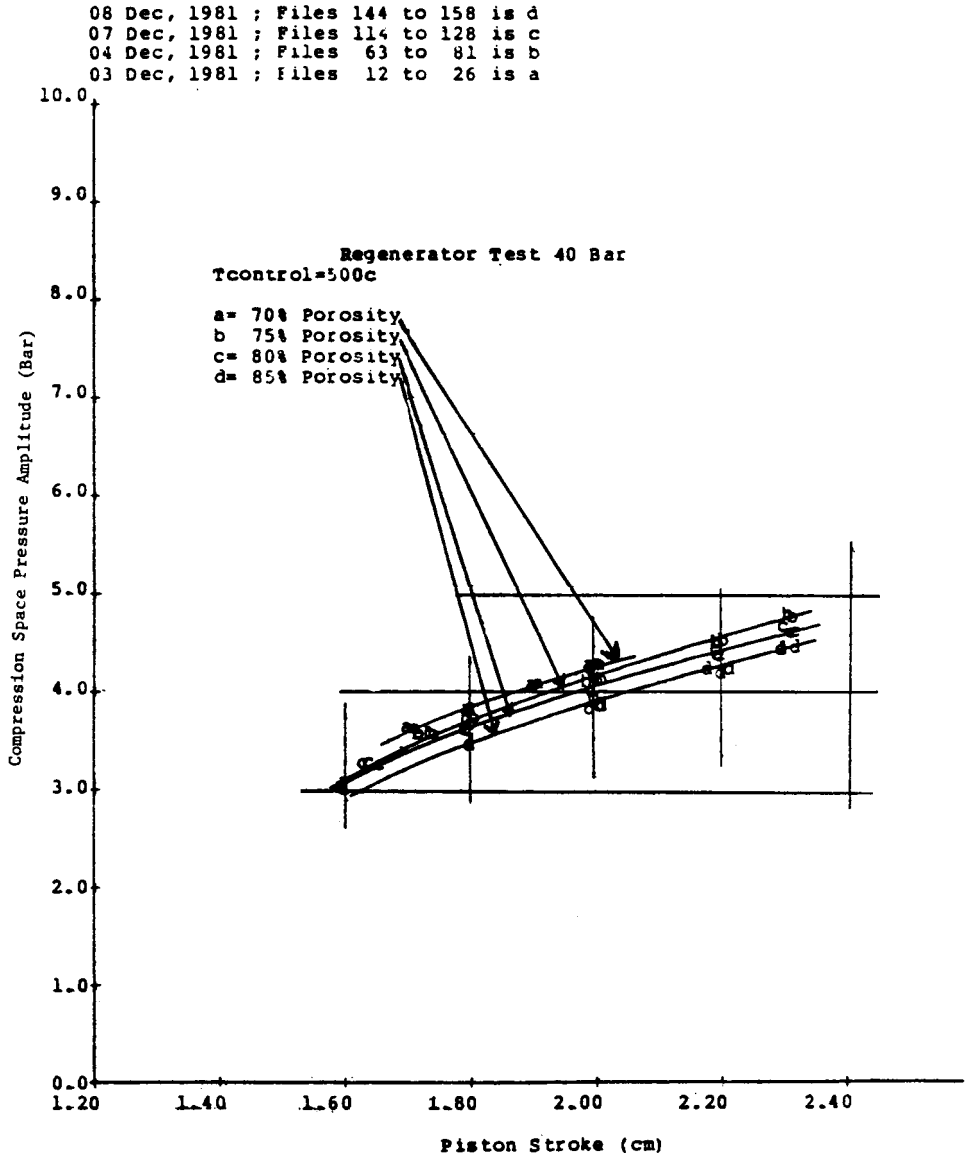

Fig. 6-15. Regenerator Test: Engine Pressure Amplitude Measurements, Tcontrol=500°C

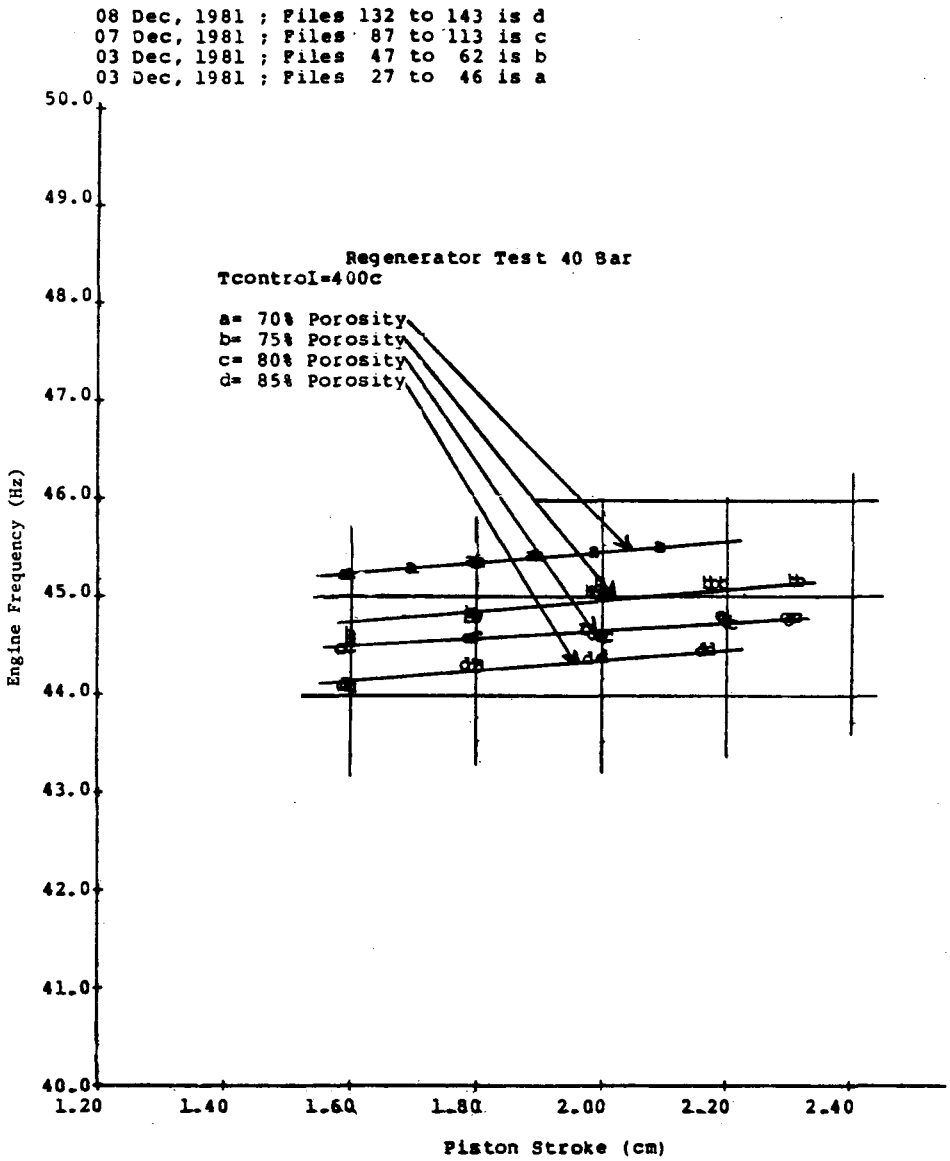

Fig. 6-16. Regenerator Test: Engine Frequency Measurements, Tcontrol=400°C

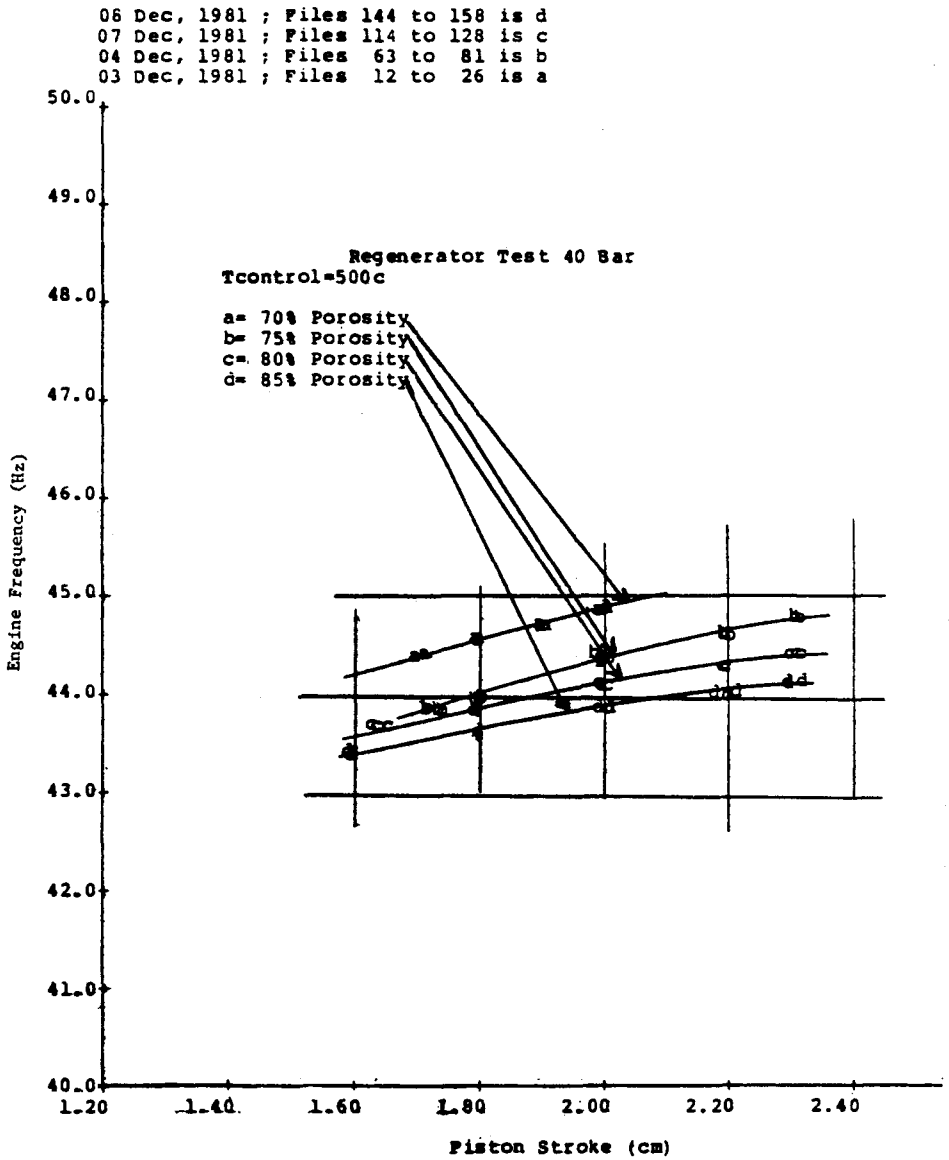

Fig. 6-17. Regenerator Test: Engine Frequency Measurements, Tcontrol=500°C

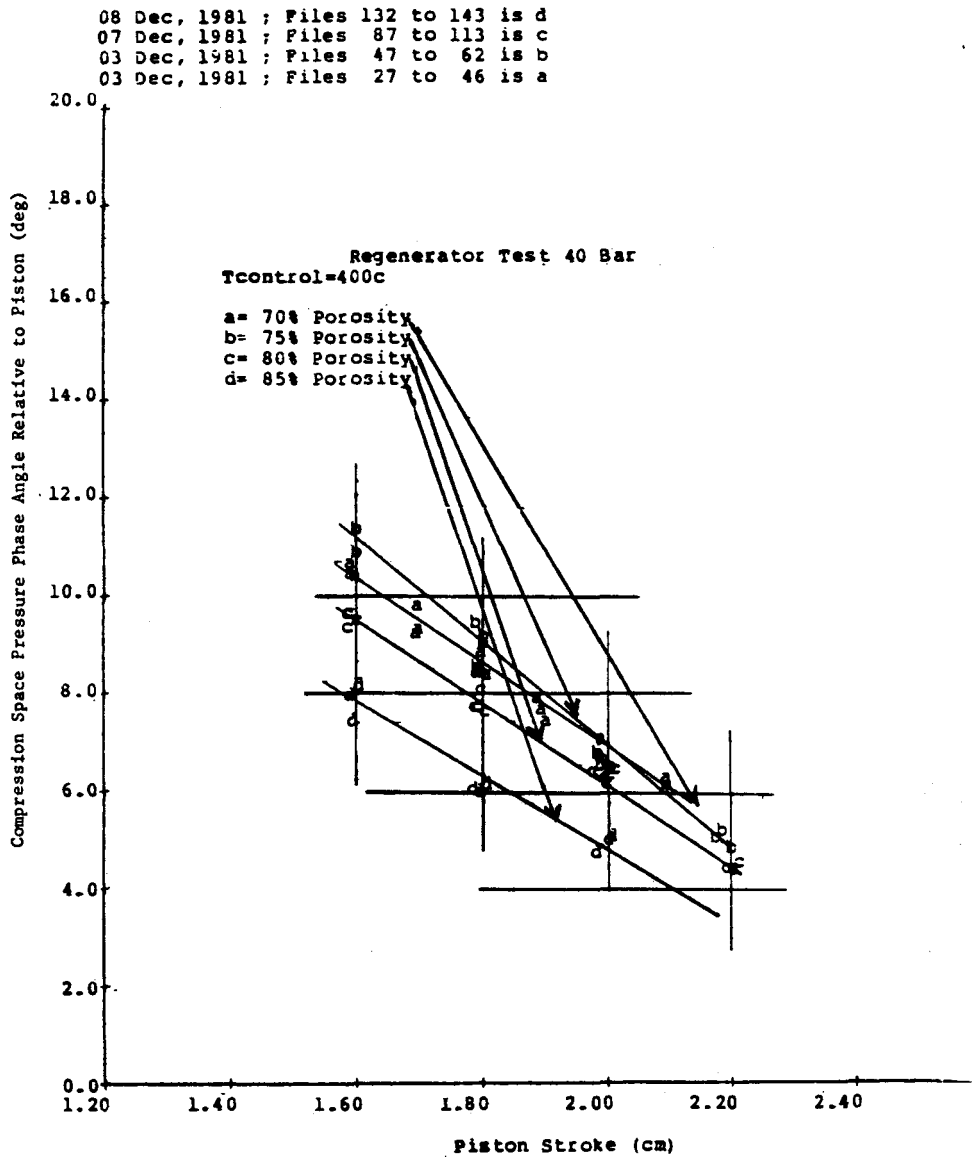

Fig. 6-18. Regenerator Test: Engine Pressure Angle Measurements, Tcontrol=400°C

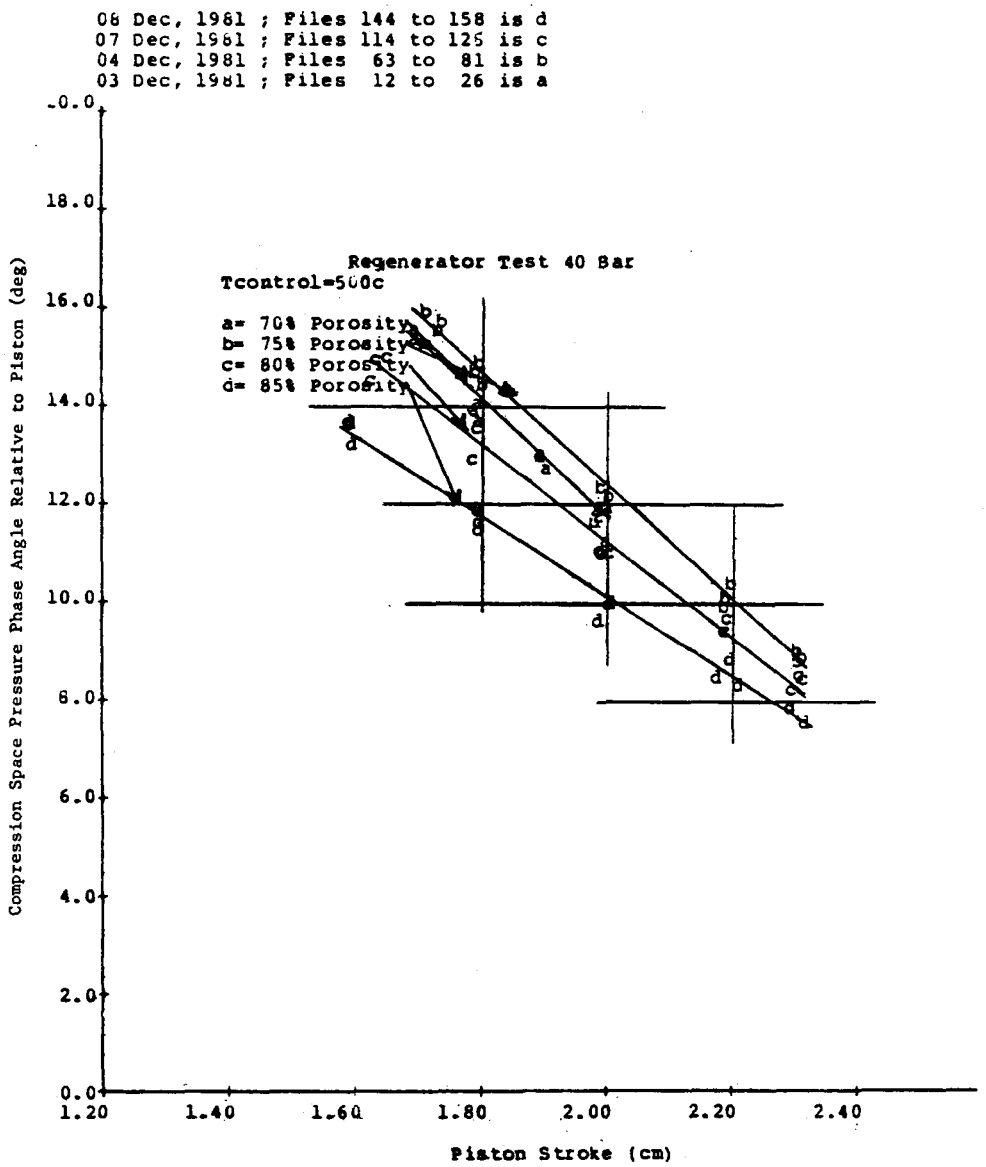

Fig. 6-19. Regenerator Test: Engine Pressure Angle Measurements, Tcontrol=500°C

the pressure phase trend between the 70 and 75% tests indicates that optimum regenerator porosity for the TDE, at the prescribed operating dynamics, is approached with a regenerator porosity slightly less than 70% for the Metex knitted-weave mesh with a 0.0035-in. wire.

Parameters that set the pressure phase angle are the expansion/compression-space temperatures, hysteresis/leakage losses, and heat exchanger pumping losses. Figures 6-20 and 6-21 reveal that the cold-space temperatures are the same for each test at 400 and 500°C. An indication of the expansion-space temperature is the heater head dome temperature. The dome area of the heater head is insulated from the combustion gases by a ceramic cap, and does not have surface area extensions, so little to no heat transfer (aside from conduction via the head and expansion-space gas) occurs in this dome area.

With the assumption that dome temperature is representative of expansion-space temperature (Figs. 6-22 and 6-23), the plot of dome temperature versus piston stroke for each porosity indicates that the expansion-space temperature for each test was nearly constant. Because the same hardware (other than regenerator changes) was used for each test, compression-space leakage and hysteresis losses were assumed the same for each test. Also, test results from the hysteresis test revealed that large changes in compression-space surface area resulted in insignificant changes in engine power performance. With these assumptions, the remaining parameter influencing the compression-space pressure phase is the heat exchanger pumping power. Since the TDE is not instrumented to record expansion-space pressure amplitude and phase, heat exchanger pumping power is inferred from displacer power balance, or from the power delivered to the displacer from the compression-space minus the power dissipated by the displacer gas spring. The results of the heat exchanger pumping power (Figs. 6-24 and 6-25), as determined from the above force balance, increase with decreasing porosity. This trend should result in a continually decreasing pressure phase angle as regenerator porosity is reduced. The pressure phase angle (shown in Figs. 6-18 and 6-19) increases with increasing porosity until the porosity is reduced to 70-75%.

The opposing trend of the pressure phase angle (from what the pumping power suggests) may be explained by the assumption that the heater head dome is nearly adiabatic, and there is, in fact, a reduction in expansion-space temperature due to regenerator interaction with the thermodynamics. Interaction of the regenerator with the thermodynamics will be expected to affect the heater and cooler temperatures. Figures 6-26 and 6-27 show plots of all heater head thermocouple readiness versus heater head axial location of each T/C; they do not show any significant temperature maldistributions as a function of porosity. Also, gas temperature on the regenerator side of the cooler (Figs. 6-28 and 6-29) does not indicate a significant thermodynamic shift with regenerator porosity. Further work is required to develop a good understanding of the current variations of compression-space pressure-wave phase angle with porosity.

6.3.2 Indicated Efficiency Test Results

Indicated efficiency results versus piston stroke for porosities of 70, 75, 80, and 85% from the Metex regenerator tests are plotted in Figures 6-30

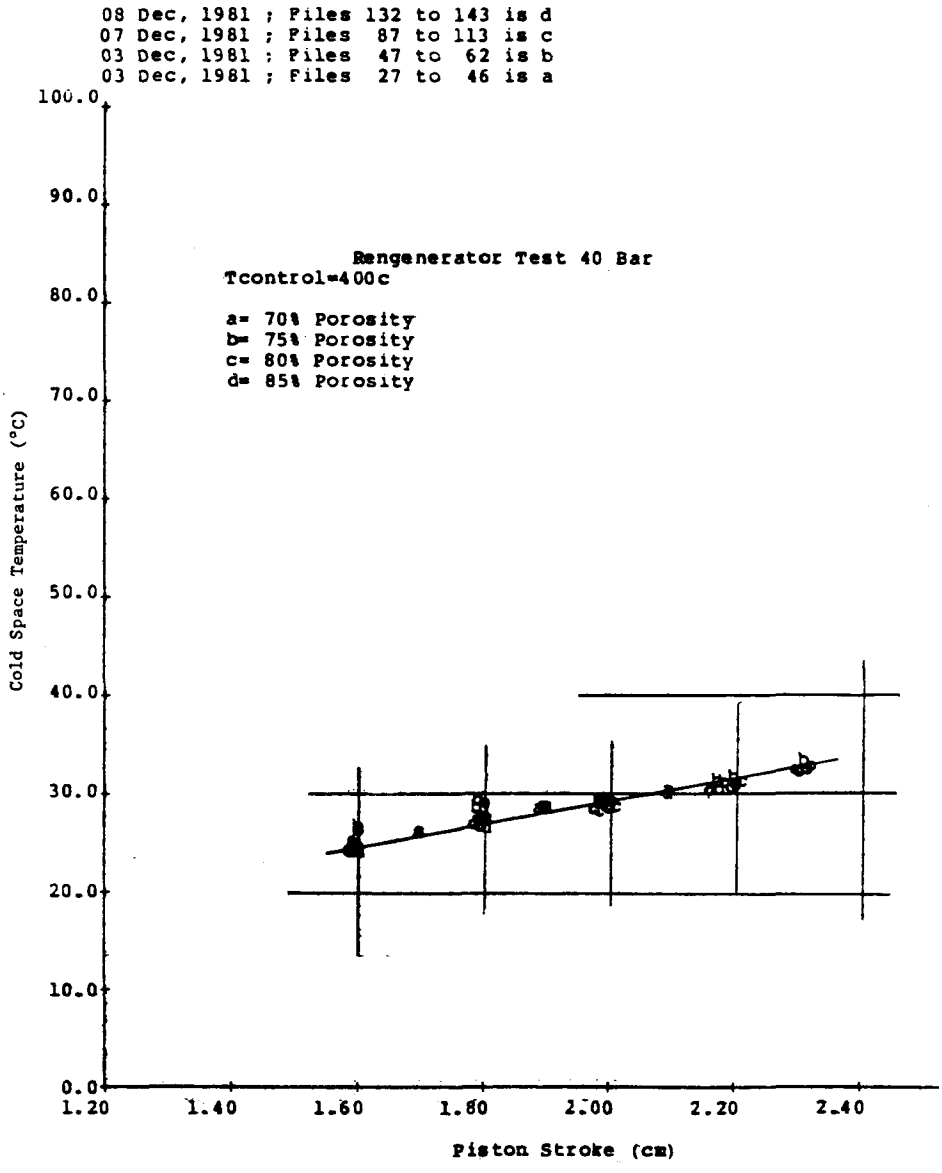

Fig. 6-20. Regenerator Test: Cold Temperature Measurements, Tcontrol=400°C

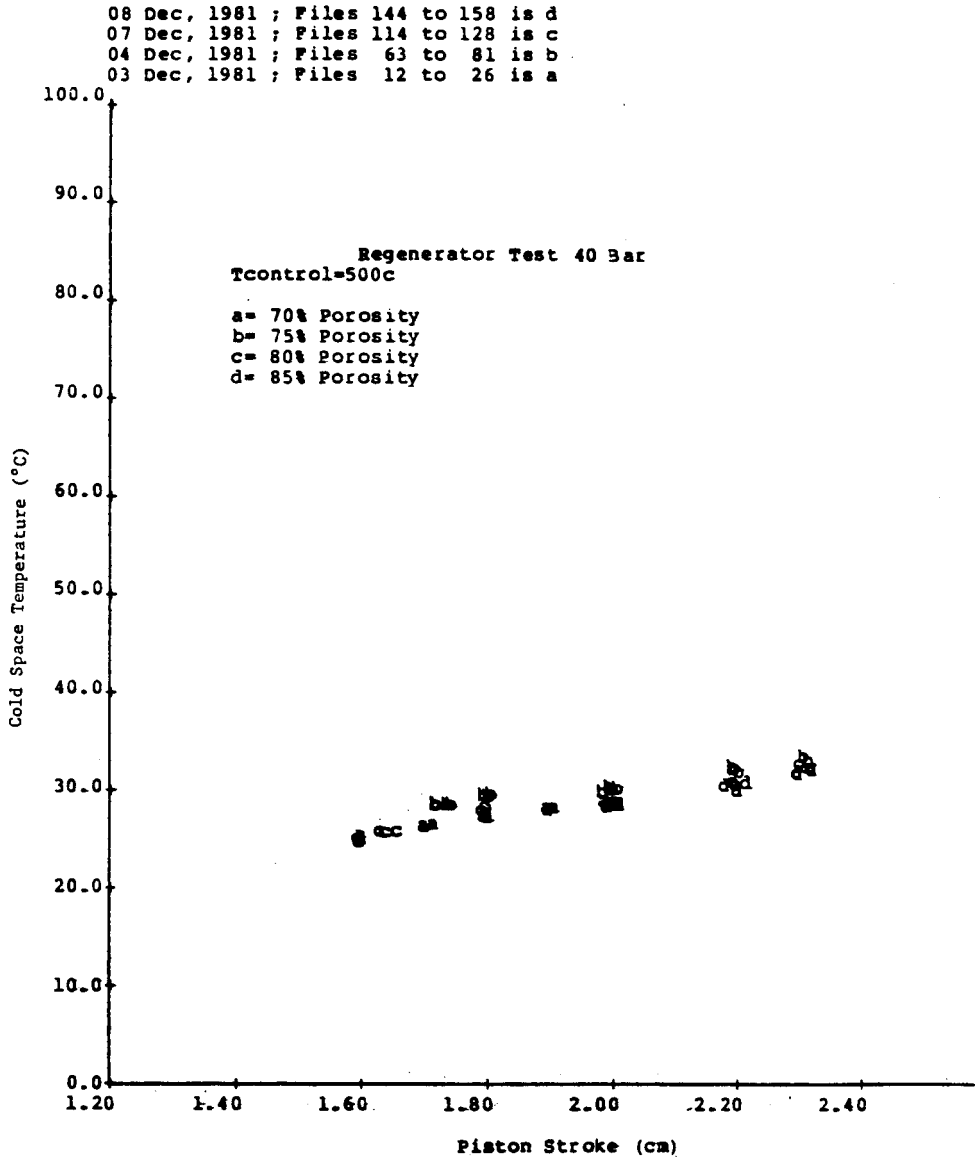

Fig. 6-21. Regenerator Test: Cold Temperature Measurements, Tcontrol=500°C

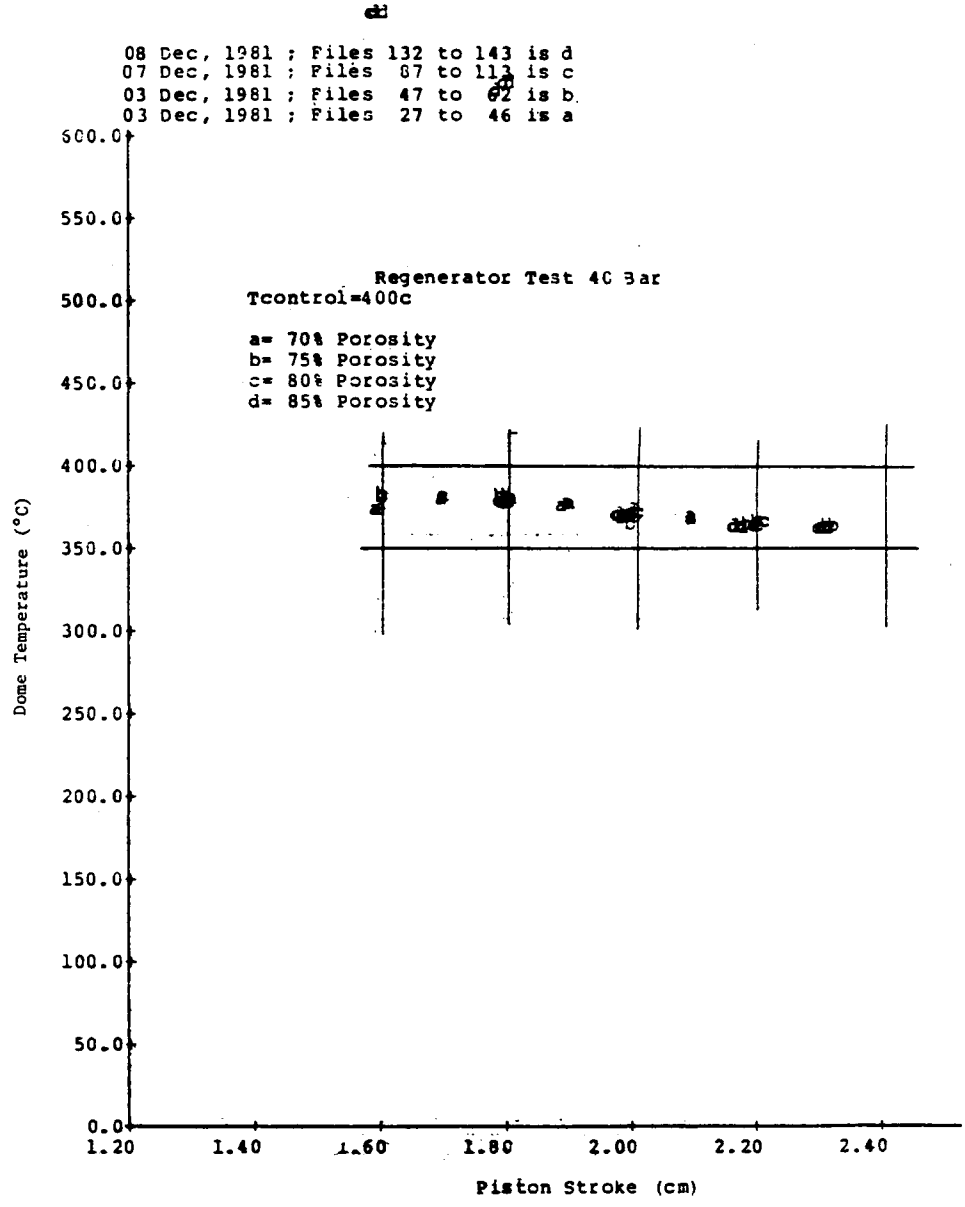

Fig. 6-22. Regenerator Test: Dome Temperature Measurements, Tcontrol=400°C

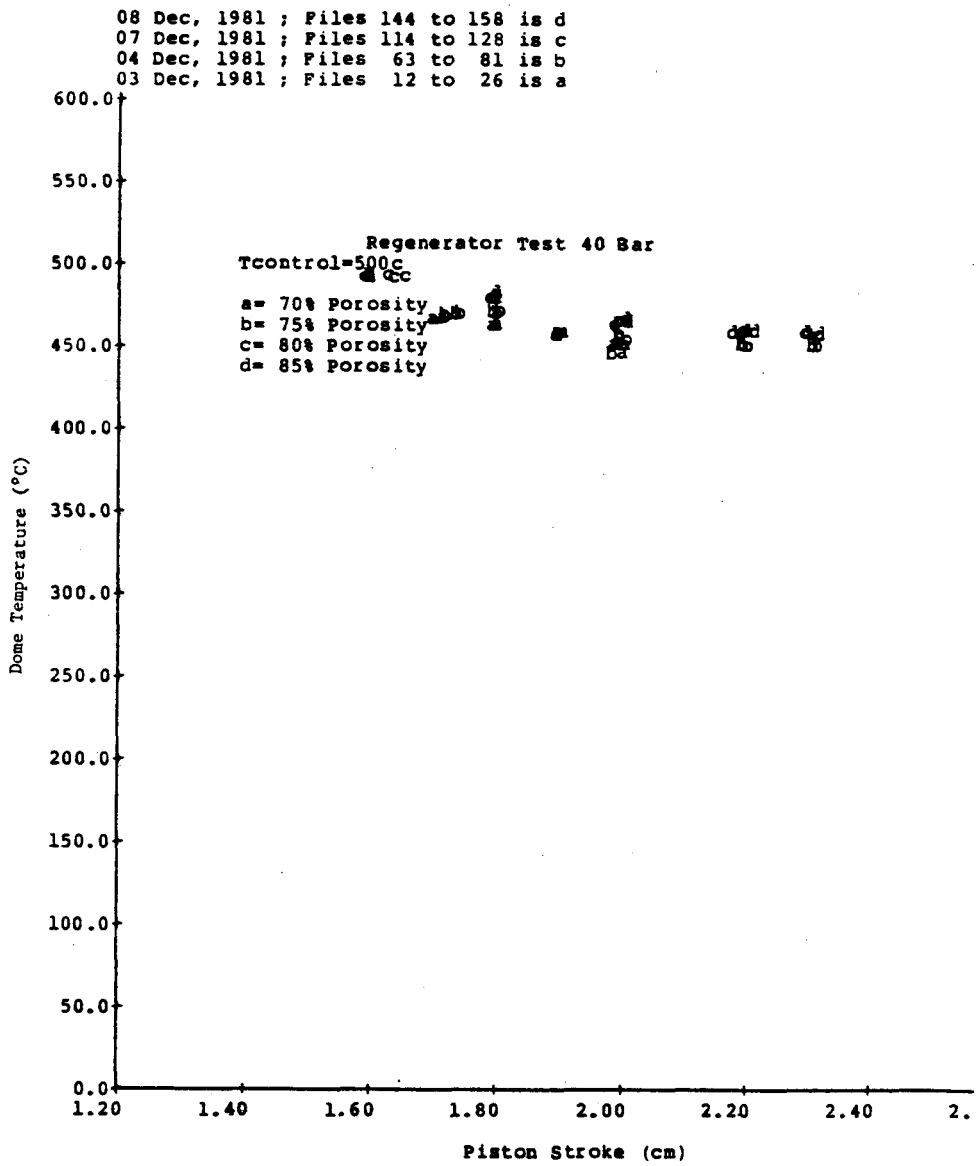

Fig. 6-23. Regenerator Test: Heater Dome Temperature Measurements, Tcontrol=500°C

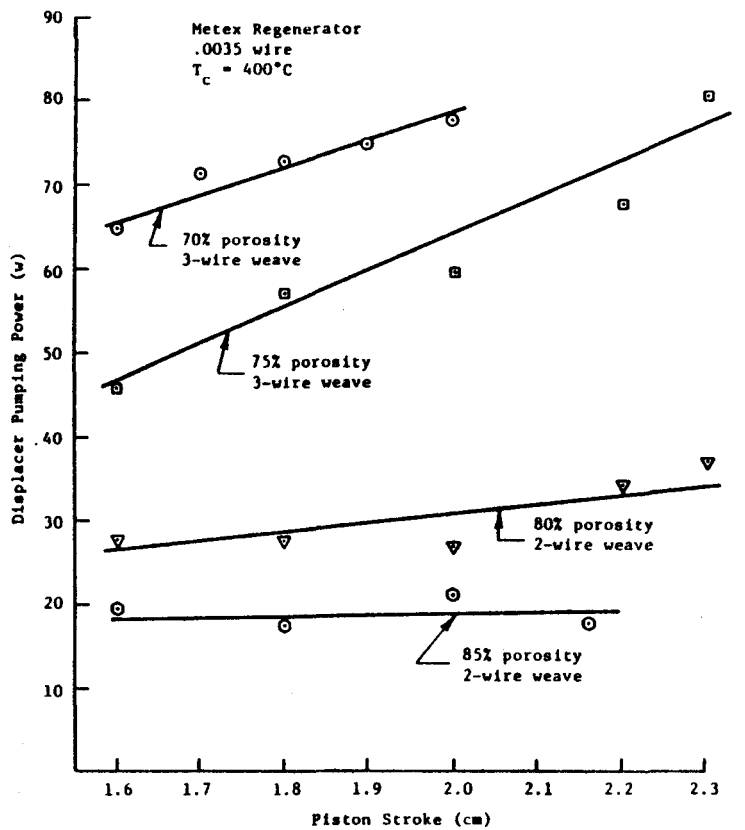

Fig. 6-24. Regenerator Test: Displacer Pumping Power Measurements, Tcontrol=400°C

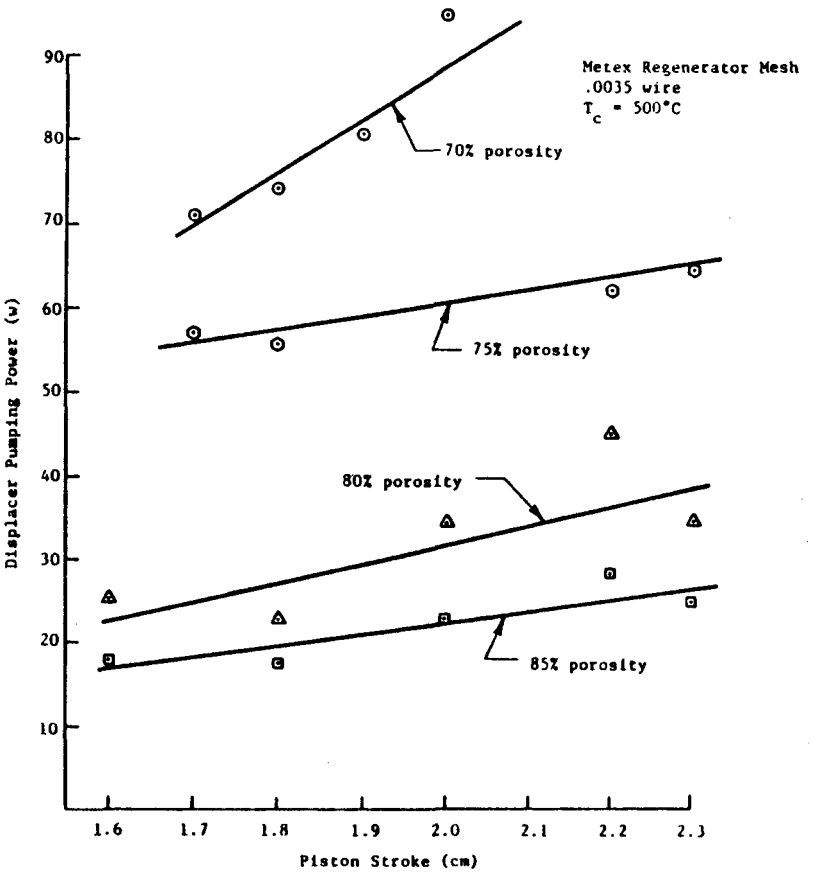

Fig. 6-25. Regenerator Test: Displacer Pumping Power Measurements, Tcontrol=500°C

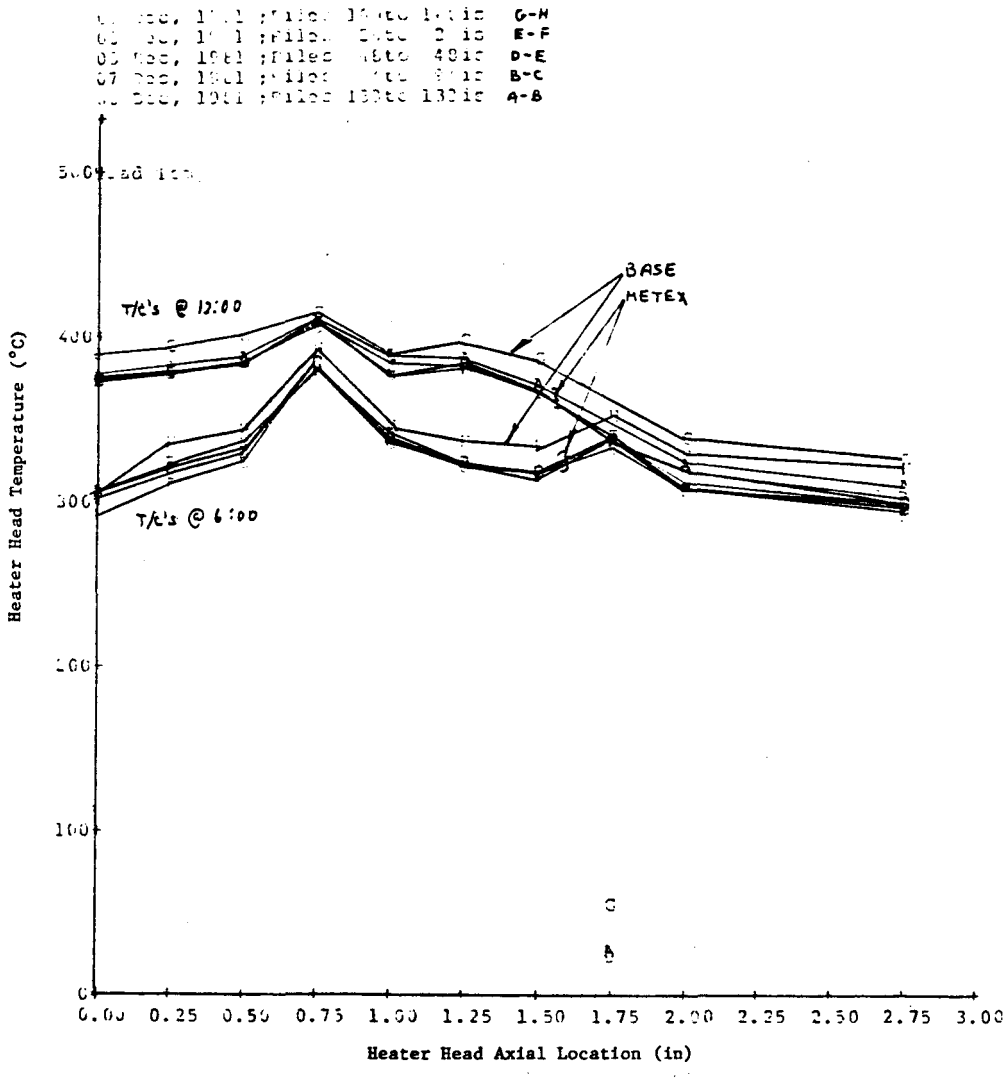

Fig. 6-26. Regenerator Test: Heater Head Temperature Distribution, Tcontrol=400°C

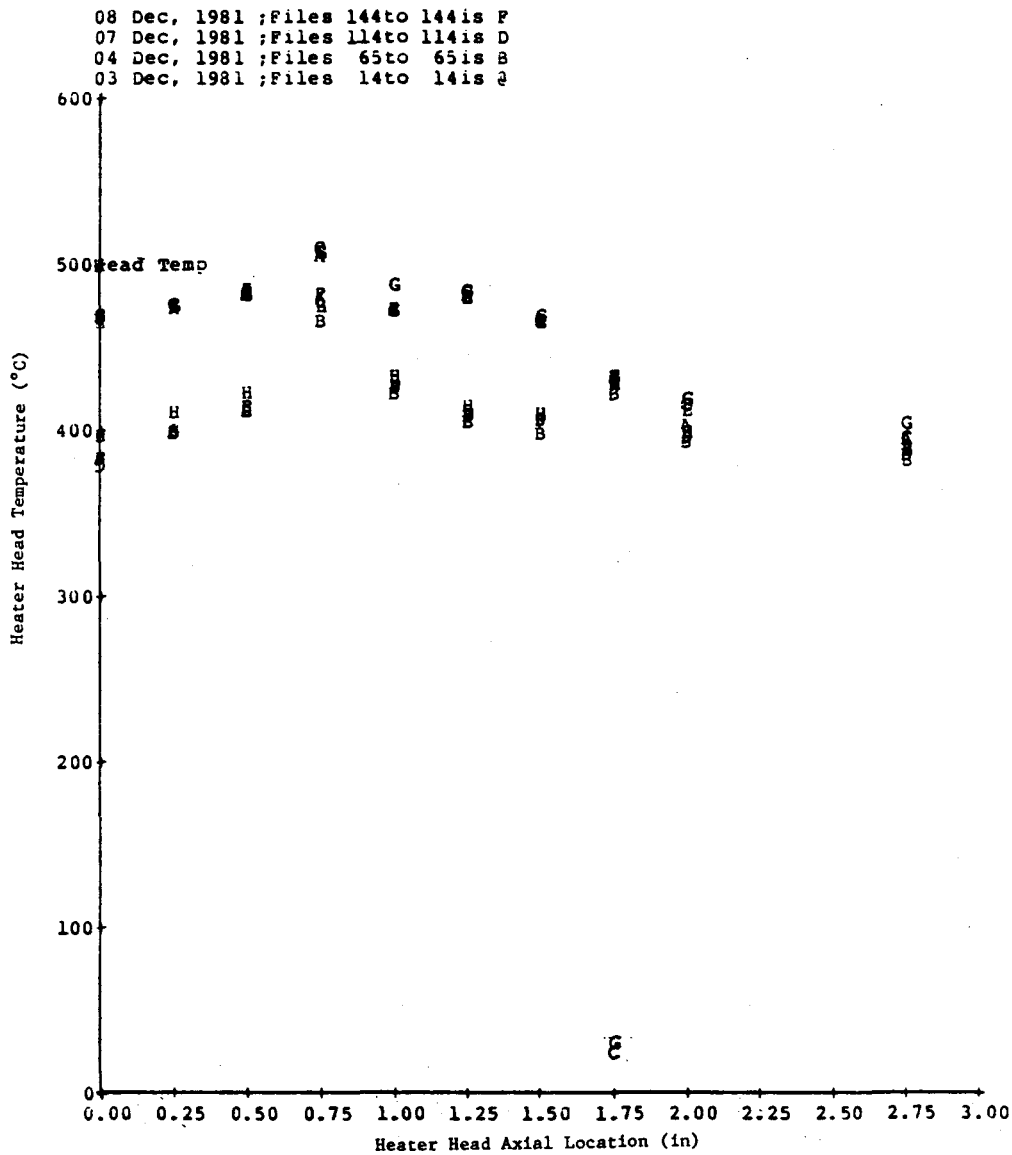

Fig. 6-27. Regenerator Test: Heater Head Temperature Distribution, Tcontrol=500°C

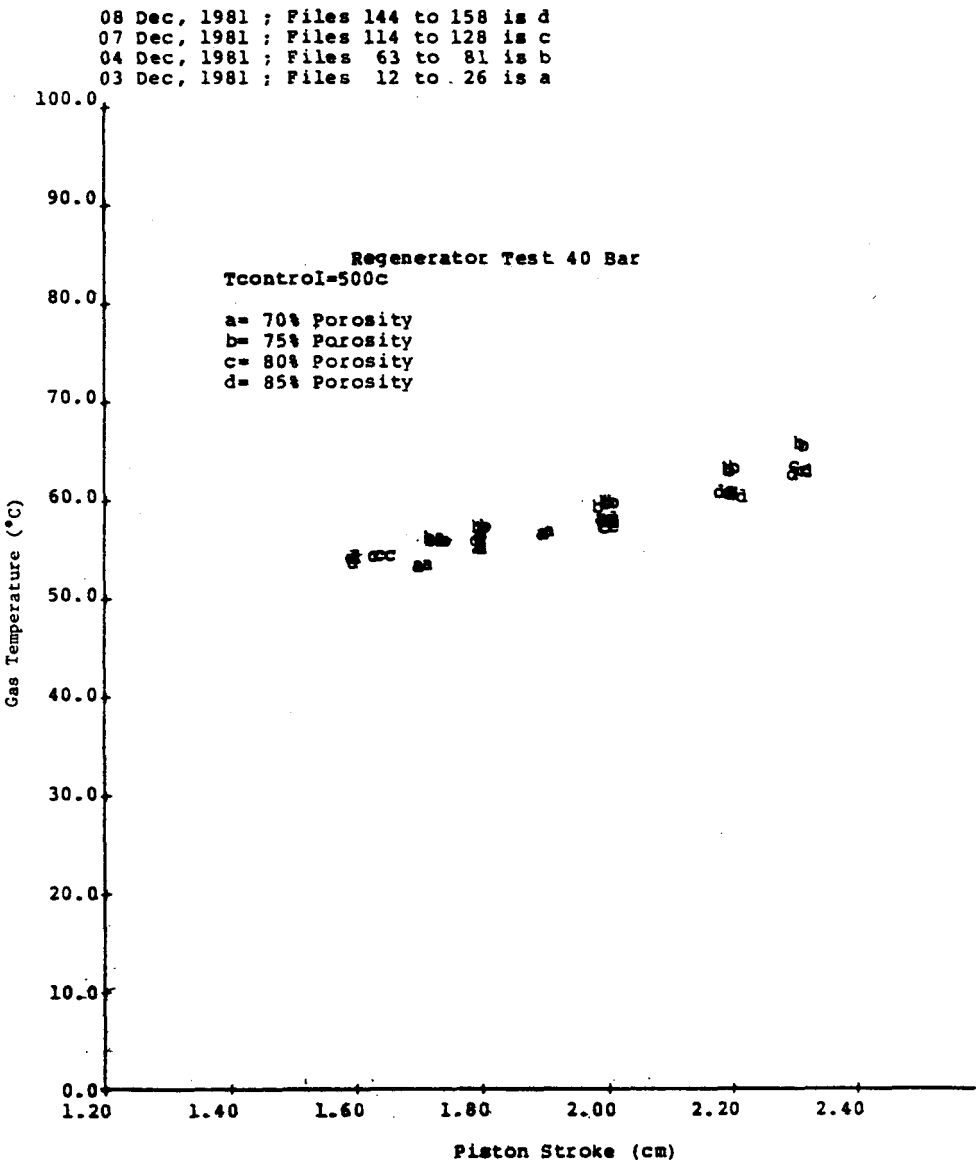

Fig. 6-28. Regenerator Test: Temperature Measurements at Cold Side of Regenerator, Tcontrol=500°C

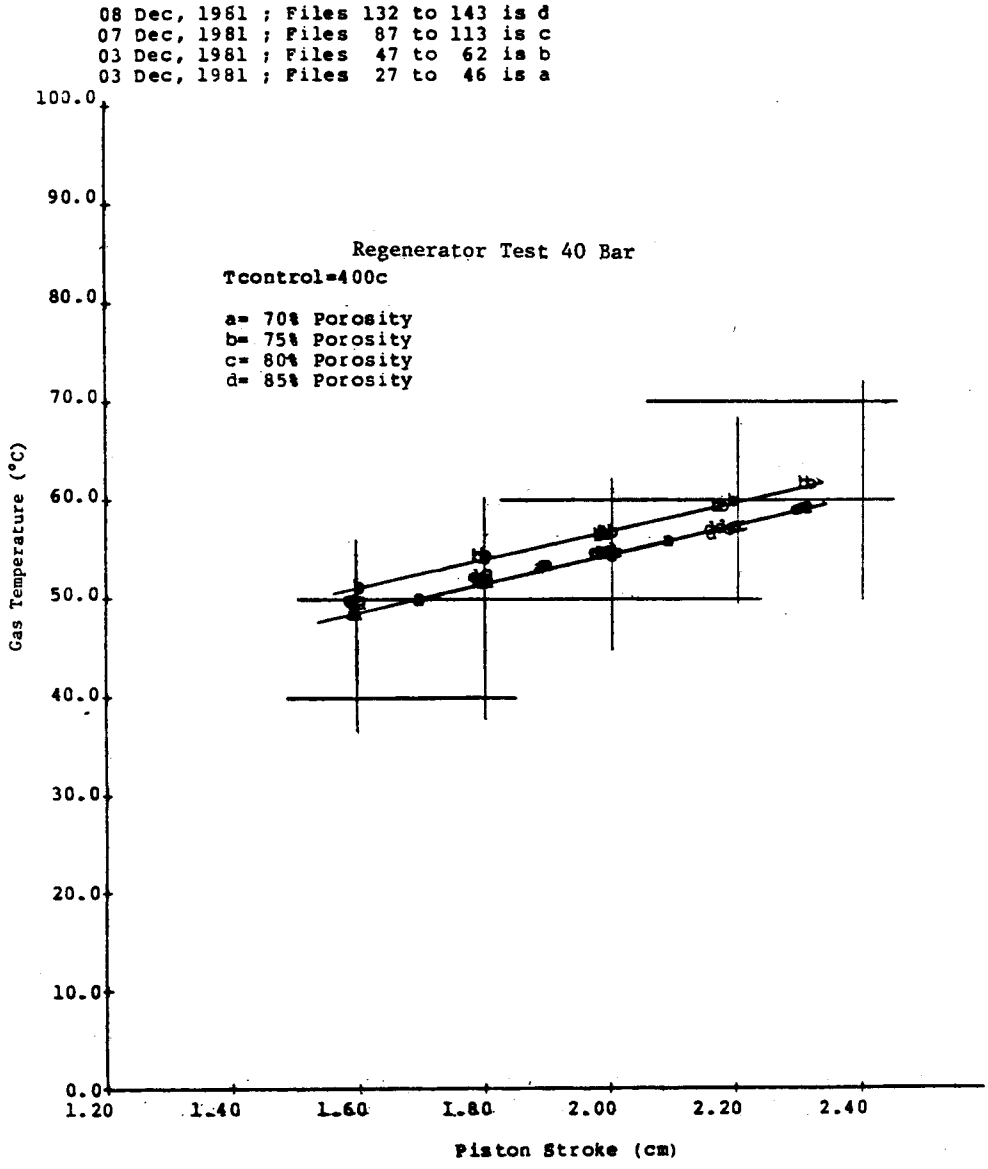

Fig. 6-29. Regenerator Test: Temperature Measurements at Cold Side of Regenerator, Tcontrol=400°C

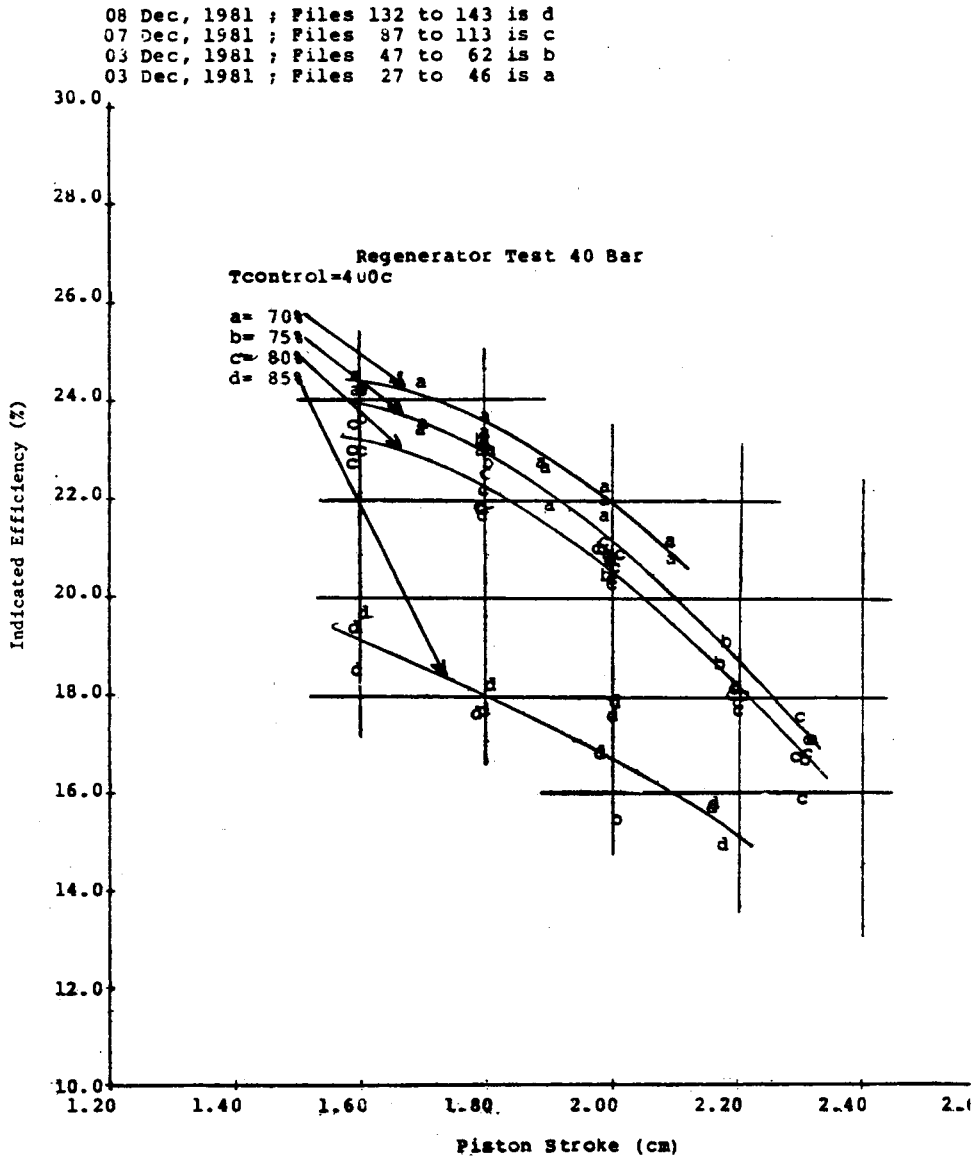

Fig. 6-30. Regenerator Test: Indicated Efficiency Measurements, Tcontrol=400°C

and 6-31. The results, if cross-plotted versus porosity, show decreasing engine efficiency with increasing porosity. Figures 6-32 and 6-33 show that engine heat rejection was nearly constant for each test. Because of this and a continuous decline in engine power with increasing porosity, the drop in efficiency was due to drop in power, and the parasitic losses in the engine were nearly constant. This is discussed in greater detail in Section 6.4.

6.4 ANALYTICAL COMPARISON

Similar to the procedures outlined in Section 5.4, the Regenerator Matrix Test, analytical comparison was performed by using the fixed dynamics option, which eliminates any discrepancies between calculated and measured results that might occur due to errors in the calculated dynamics. With any discrepancies due to erroneous dynamics eliminated, the calculated thermodynamic results can be compared directly with the measured results.

Figure 6-34 compares calculated/measured power with efficiency for the 400°C control temperature data at a piston stroke of 2.0-cm. A significant power discrepancy is especially evident at the higher porosities. Calculated power generally decreases with increasing porosity, but does not show the curving decline in power as do the engine data. Calculated efficiency shows an optimum near 79% porosity, while engine data show that the optimum was not achieved for the porosities tested. Corrected efficiency (shown in Fig. 6-36) is the predicted efficiency reduced by the ratio of measured to predicted power. With the efficiency thus corrected for deviations in power, the optimum point is shown to move from 79 to 75%--more in line with engine data.

Measured and calculated values of compression-space pressure amplitude and phase angle for a 2.0-cm stroke are shown in Table 6-1 at the porosities tested. Comparison of these results shows that pressure amplitude is closely predicted, indicating that engine volume and gross temperatures are modeled closely. Discrepancy in the power calculations is shown as a discrepancy in pressure phase angle calculation; declining power predictions with increasing porosity are due primarily to calculated dead-volume effects. Calculate pressure phase angle is seen to increase with increasing porosity (a trend opposite the measured results). Figure 6-35 is a plot of heat exchanger pressure drop, as calculated from the displacer force balance, with calculated points for a 2.0-cm stroke; the figure shows that pressure drop is underpredicted, which would result in an increase in calculated phase angle.

Pressure drop and heat-transfer characteristics used for the code calculations are derived from empirical correlations from a single-blow test using a Metex knitted mesh test sample with a 65.3% porosity and a 0.006-in. wire diameter. Subsequent to the engine test program, additional Metex knitted mesh regenerator samples with a 0.0035-in. wire diameter and 60-80% porosity ranges were tested with the single-blow test rig. Preliminary results from these data reveal a small change in friction factor between samples of different porosities, and an increase in Nusselt Number with increasing porosity at a constant Reynolds Number. Time precluded incorporating these new data into the code for further evaluation of engine test results.

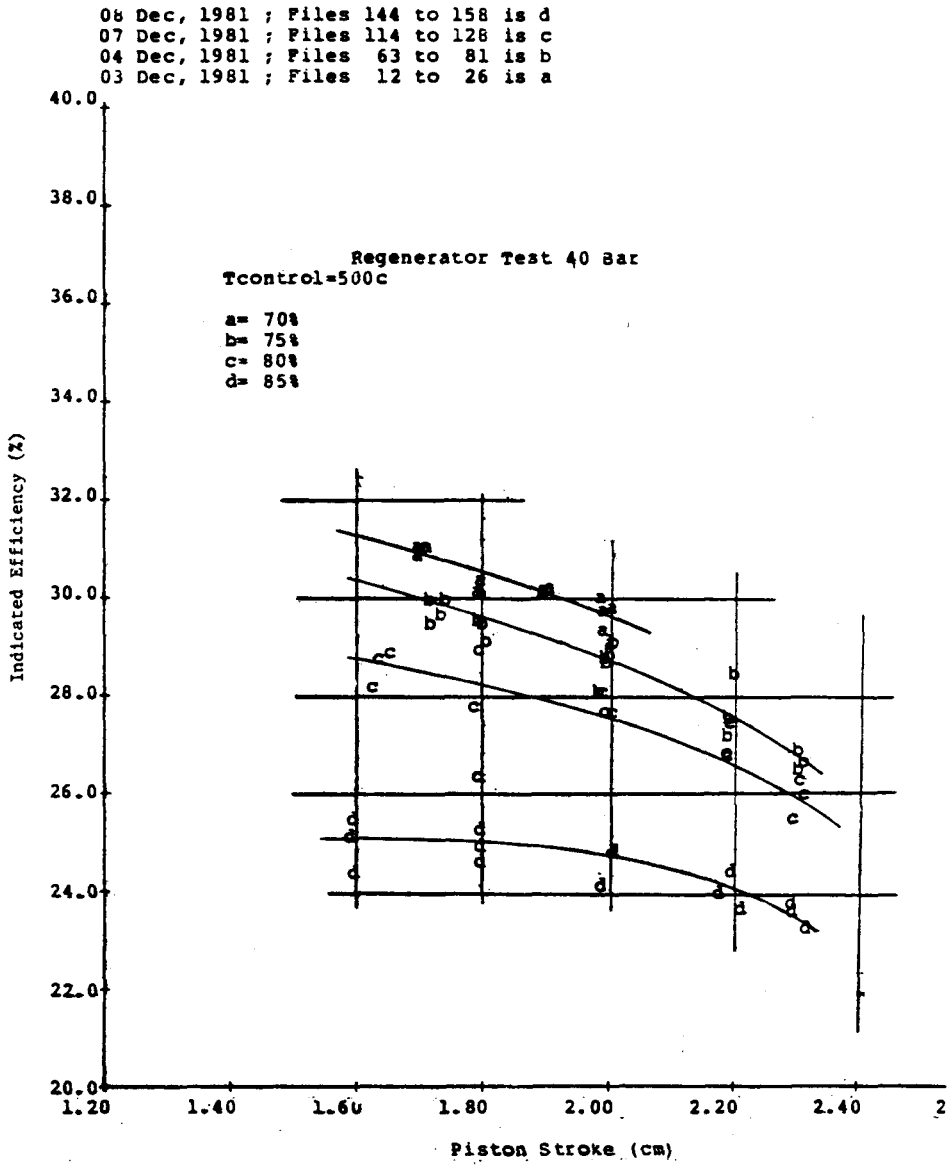

Fig. 6-31. Regenerator Test: Indicated Efficiency Measurements, Tcontrol=500°C

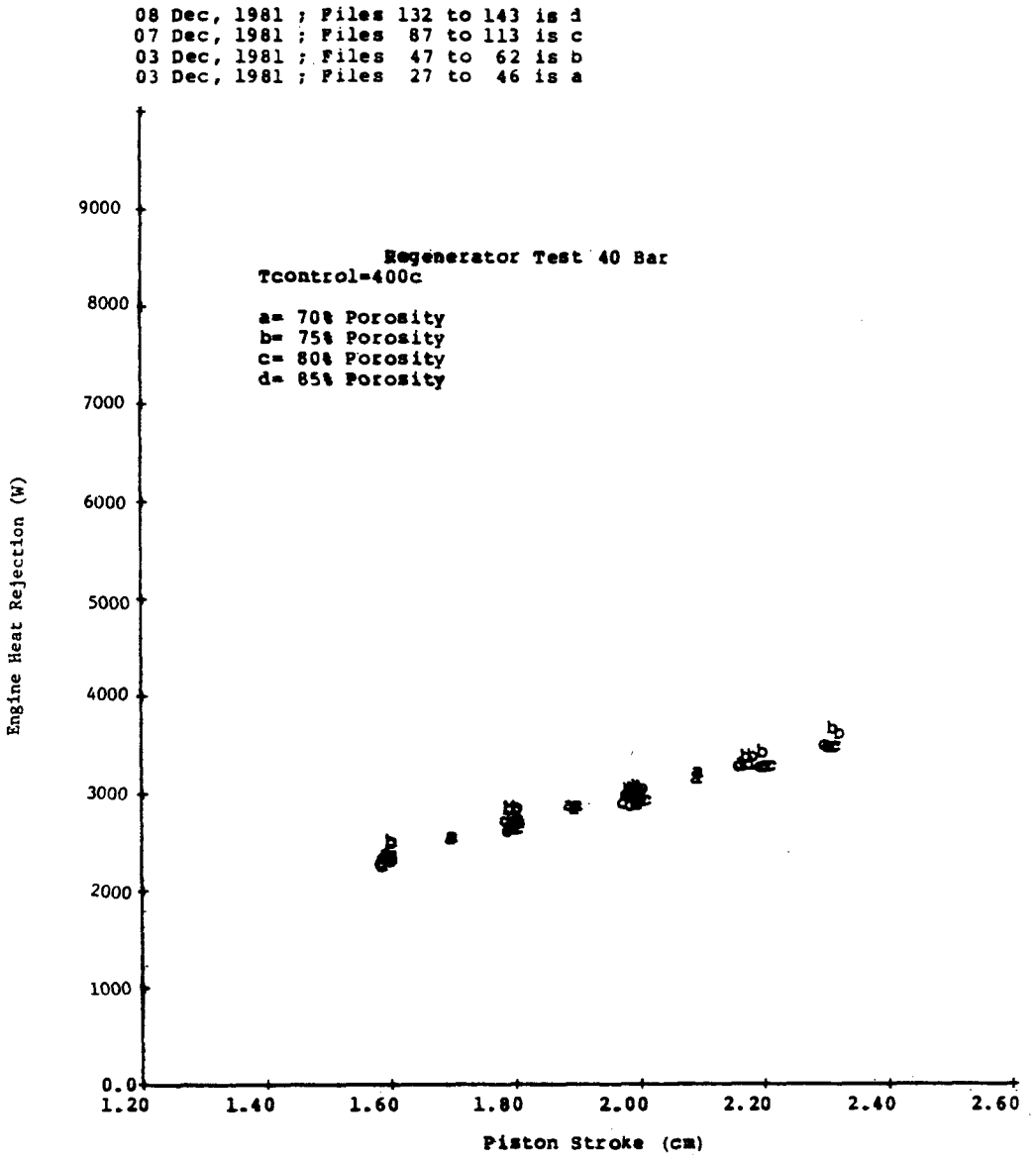

Fig. 6-32. Regenerator Test: Heat Rejection Measurements, Tcontrol=400°C

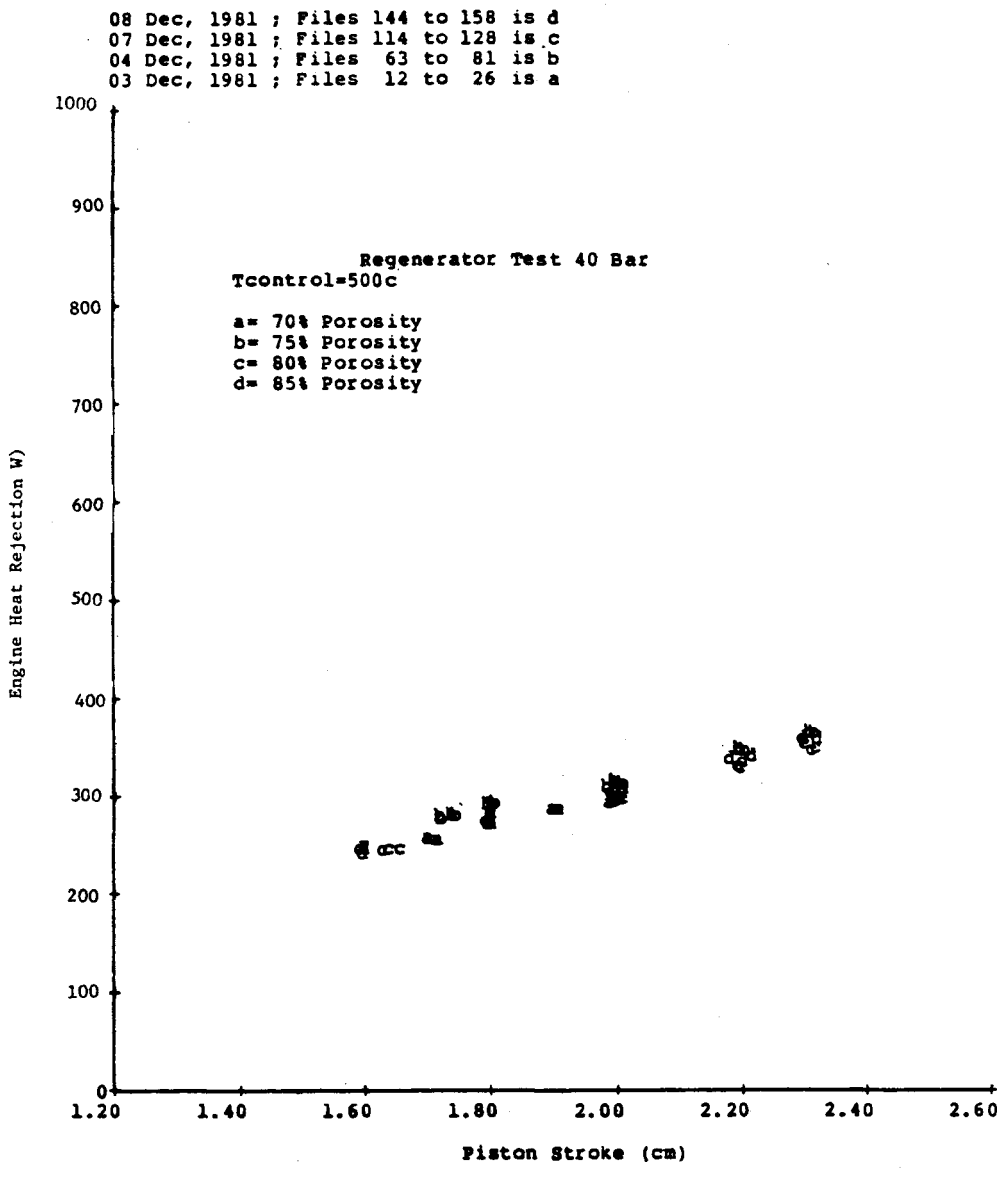

Fig. 6-33. Regenerator Test: Heat Rejection Measurements, Tcontrol=500°C

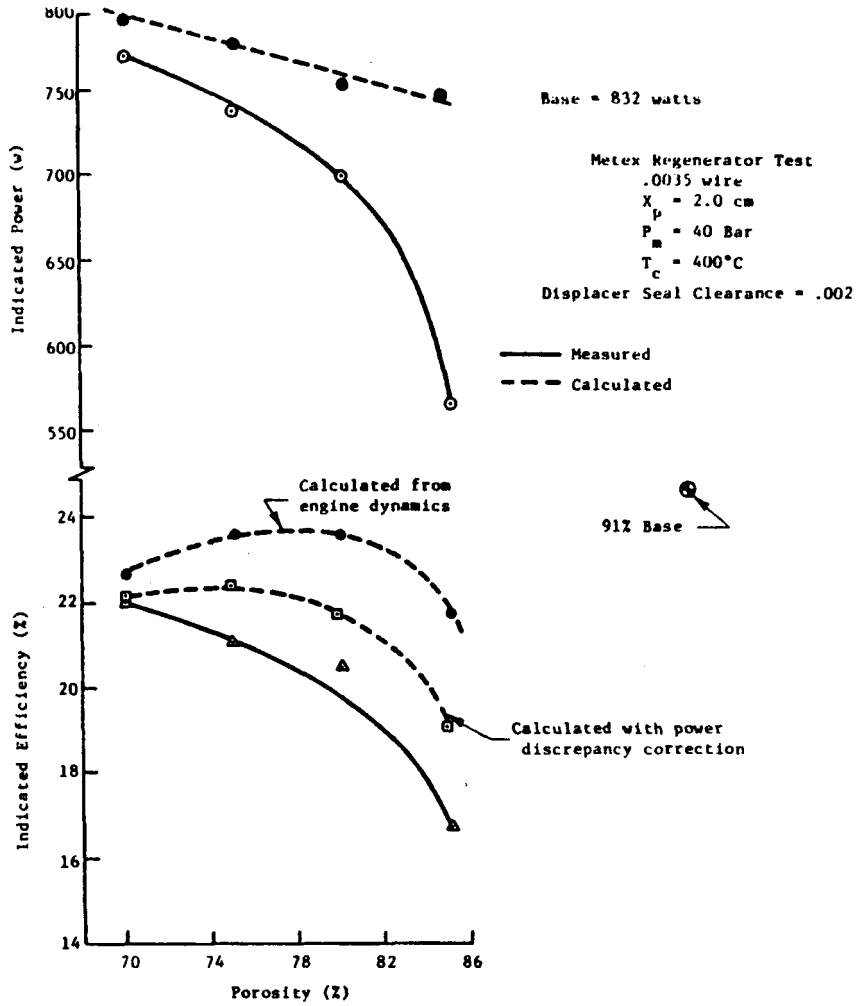

Fig. 6-34. Regenerator Test: Summary of Regenerator Porosity Effect on Power and Efficiency

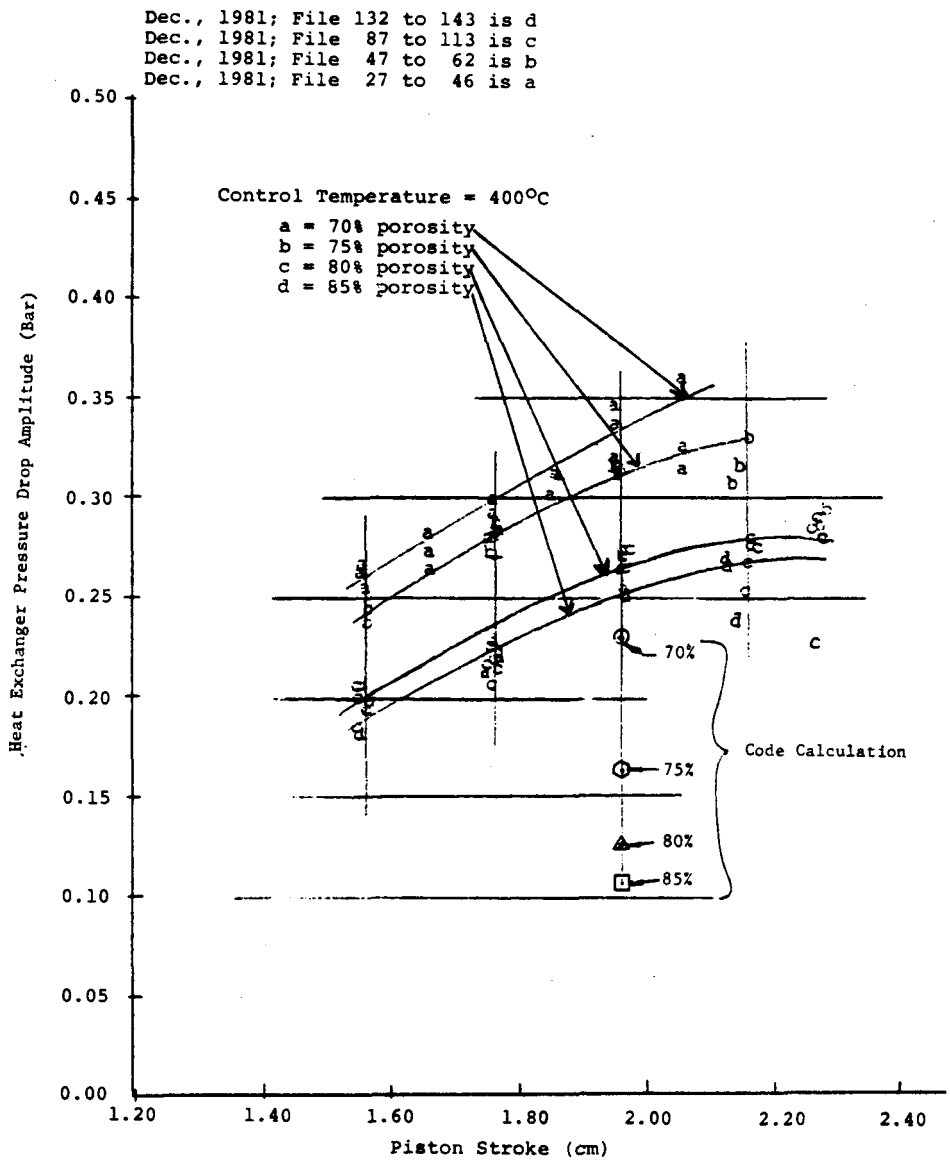

Fig. 6-35. Regenerator Test: Heat Exchanger Pressure Drop Measurements

Table 6-1. Effect of Porosity on Compression-Space Pressure Amplitude and Phase*

Porosity, %	P_c		Q_c	
	Measured	Calculated	Measured	Calculated
70	4.32	4.587	6.9	6.06
75	4.24	4.249	6.9	6.63
80	4.10	4.193	6.04	6.43
85	3.94	4.08	4.80	6.62

* X_p = 2.0-cm, P_m = 40 Bar, $T_{control}$ = 400°C

6.5 CONCLUSIONS AND RECOMMENDATIONS

6.5.1 Conclusions

- Reducing Metex (0.0035-in. wire diameter) regenerator porosities results in improved performance.
- Overall, performance of the Metex weave regenerators did not exceed the performance obtained with the 91%, 0.001-in. wire diameter, 100-mesh square-weave regenerators.
- Degradation in power performance with increasing porosity is due in part (12%) to an increase in dead volume. The dominant effect is due to a reduction in compression-space phase angle--a thermodynamic effect.
- Heater head axial temperature distribution does not reflect regenerator effectiveness effects.
- The code overestimates power performance for the Metex regenerator mesh due to overprediction of pressure phase angle.
- The code, when corrected for measured power degradation, yields an optimum porosity at 75% for best efficiency.
- The code underestimates heat-exchanger pressure-drop amplitude due to overestimation of compression-space phase prediction.

6.5.2 Recommendations

- Instrument the heater head to determine the expansion-space mean temperature.

- Perform wire-screen regenerator flow maldistribution tests.
- Vary the regenerator porosity in one build to evaluate the effects of hot- and cold-end volume distribution.
- Conduct a test where the regenerator void volume is reduced for a given porosity.
- Further reduce the Metex regenerator porosity to obtain optimum porosity.
- Incorporate the empirically generated friction and heat-transfer characteristics into the code.
- Conduct a test where a reduced regenerator void volume is shifted to the cold side.
- Explore regenerator material alternatives.

7. DISPLACER APPENDIX GAP TEST

7.1 TEST OBJECTIVE

The appendix gap is the thin working gas annulus between the displacer dome and the engine cylinder. Losses are associated with heat and mass transport in this gap region as the displacer reciprocates. The objective of the appendix gap test is to study the appendix gap loss effects as the gap is varied.

7.2 METHOD OF EXECUTION

To provide hardware resulting in varying appendix gaps without impacting heater head geometry, three separate displacers were fabricated with varying dome diameters. Each of the displacer seal skirts were final-machined during the displacer/displacer rod assembly to yield as close a running clearance to the displacer seal cylinder as possible.

The tests were conducted by running the 0.5-mm dome gap first, using a 2.2-cm piston stroke/400°C control temperature as the set point at which the succeeding tests with 1.1-mm and 2.3-mm gap domes were run. Area weighted mean temperature, displacer-to-piston stroke ratio, and displacer-to-piston angle for the tests are plotted in Figures 7-1 and 7-2, indicating that head temperature and stroke ratio were essentially constant between tests. Figure 7-3 shows that the displacer phase angle for the 2.3-mm gap test deviated from the trends of the previous test after the set point was established.

7.3 EXPERIMENTAL RESULTS

7.3.1 Indicated Power and Efficiency Trends

Indicated power is plotted versus piston stroke in Figure 7-4 for the three tests with displacer appendix gaps of 0.5, 1.1, and 2.3 mm, showing a dramatic decline in indicated power as appendix gap is increased significantly. To correct for the effects of differing displacer phase angle (Fig. 7-3) in the 2.3-mm tests, P-V power factor is plotted in Figure 7-5, showing the same significant power drop for the 2.3-mm tests. Alternator AC electrical power in Figure 7-6 confirms power reduction with increasing appendix gap.

This power reduction results from variations in pressure-wave amplitude and phase angle. Figure 7-7 shows that pressure amplitude for the 2.3-mm test was slightly higher than for the 0.5- and 1.1-mm tests, while the corresponding pressure phase angle was significantly lower (Fig. 7-8). This rise (~5%) in pressure amplitude may be due to the appendix gap volume exhibiting distinctly nonisothermal characteristics, resulting in a reduced effective volume and a corresponding increased pressure amplitude. The rise in pressure amplitude, coupled with the reduced pressure phase angle, increased the engine spring component acting on the power piston, thus increasing engine operating frequency (Fig. 7-9). Because increased pressure amplitude and frequency tend to increase output power, reduction in pressure phase angle clearly dominates engine power output.

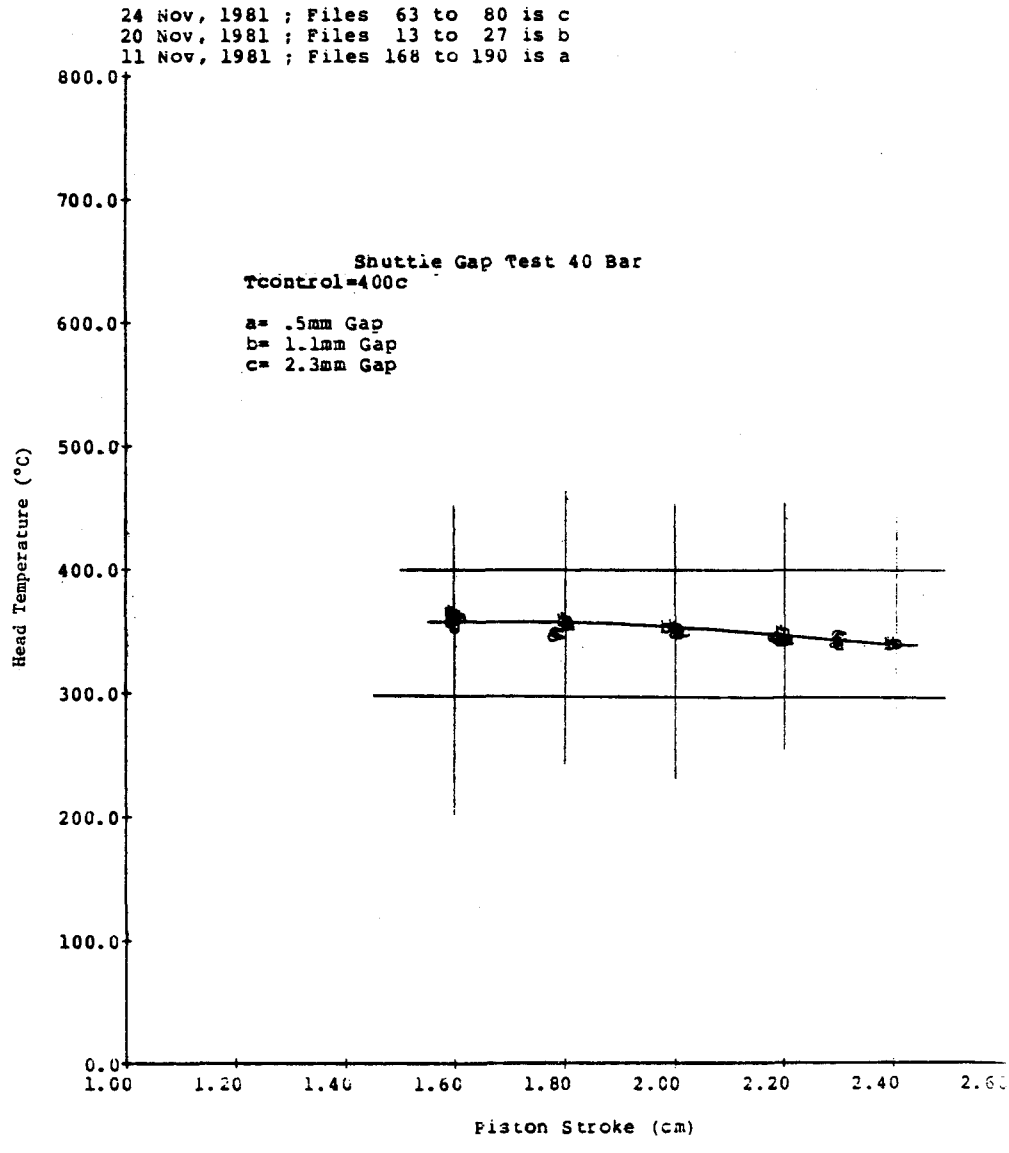

Fig. 7-1. Displacer Appendix Gap Test: Mean Head Temperature Measurements

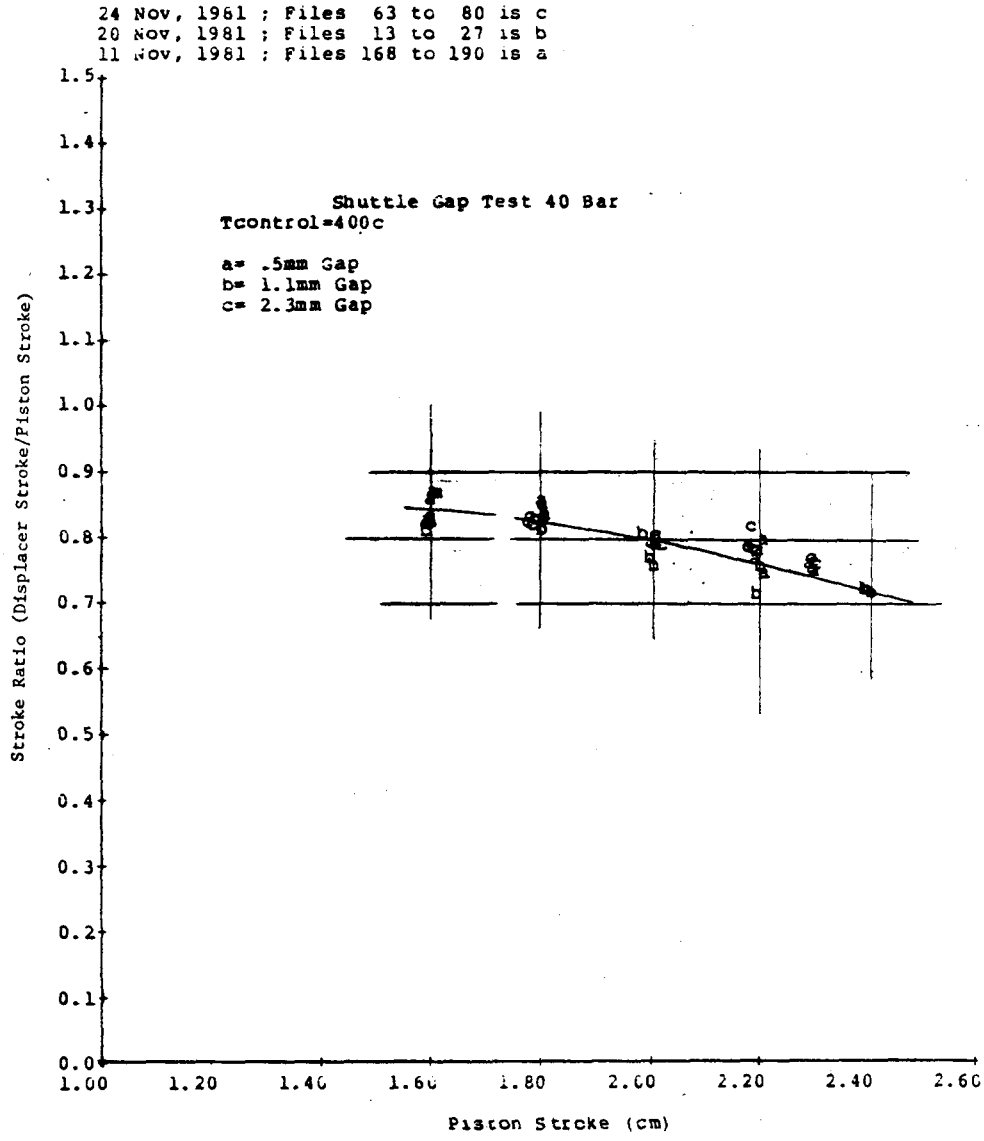

Fig. 7-2. Displacer Appendix Gap Test: Stroke Ratio Measurements

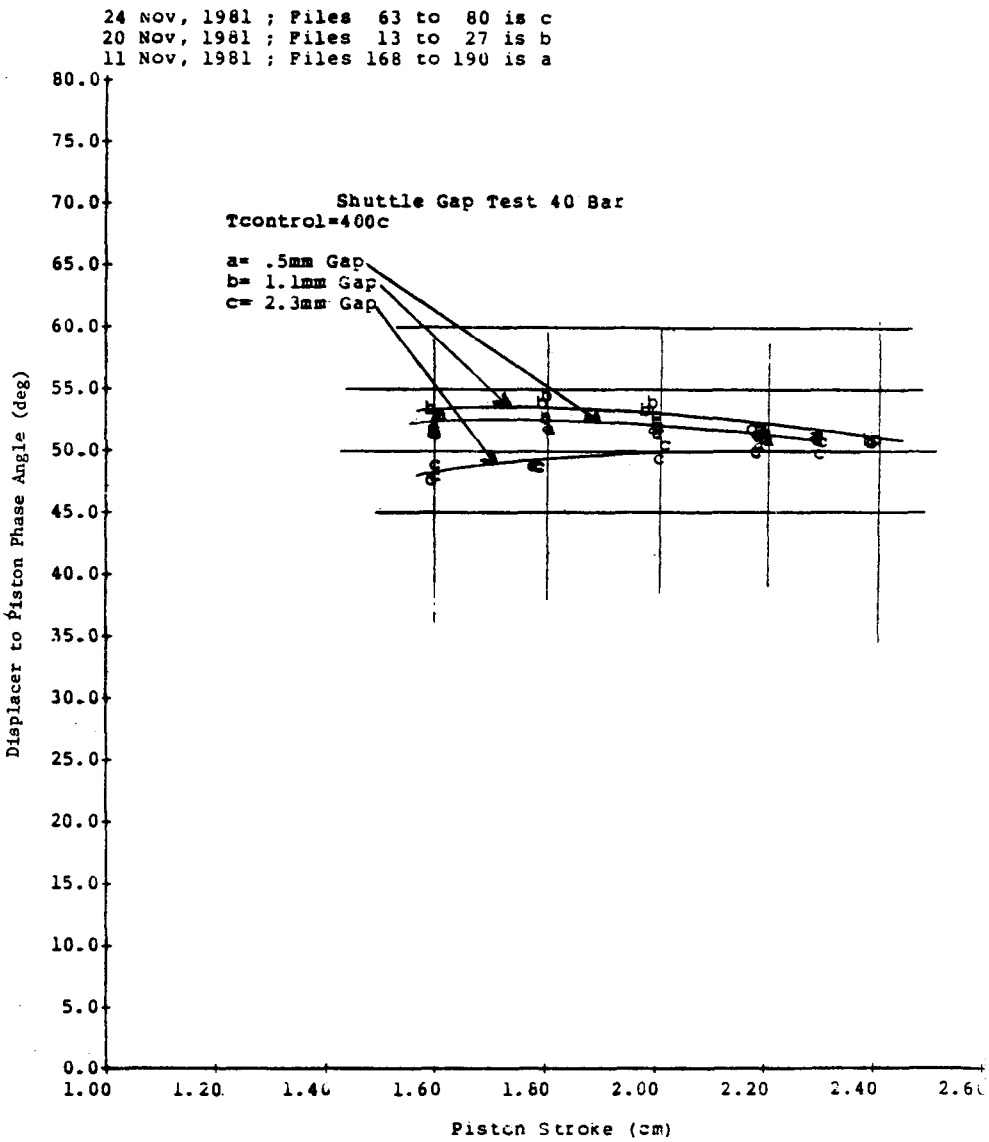

Fig. 7-3. Displacer Appendix Gap Test: Phase Angle Measurements

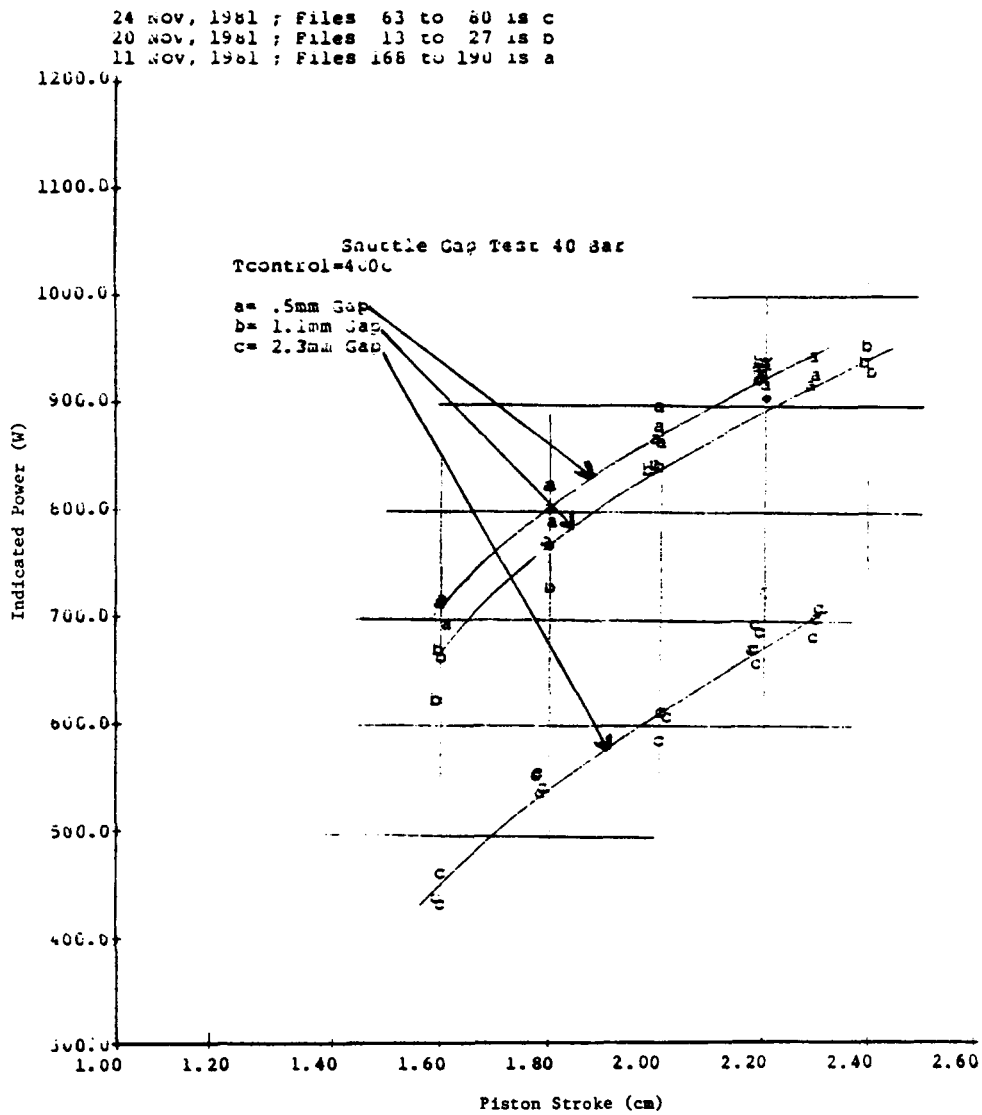

Fig. 7-4. Displacer Appendix Gap Test: Indicated Power Measurements

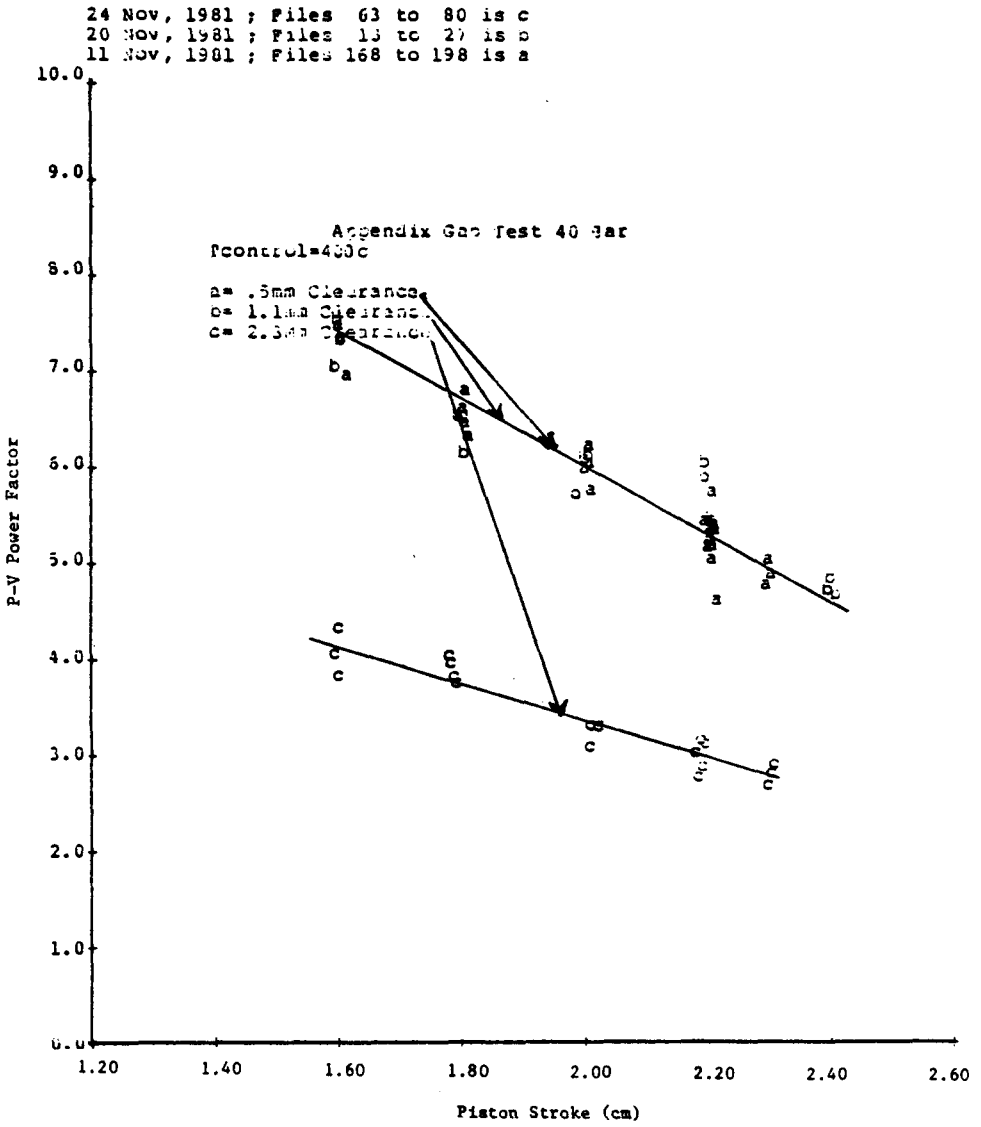

Fig. 7-5. Displacer Appendix Gap Test: P-V Power Factor (Equation 5.1) Measurements

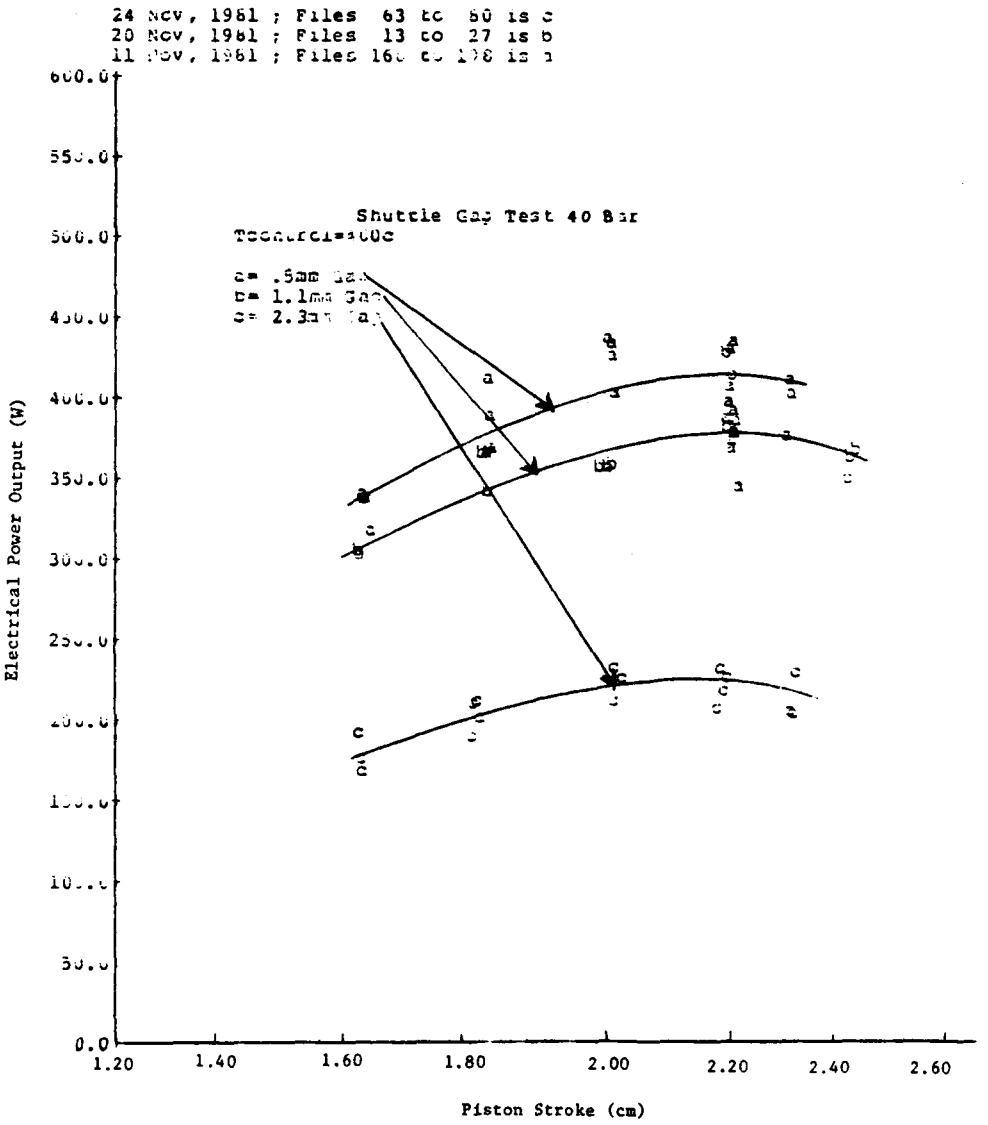

Fig. 7-6. Displacer Appendix Gap Test: AC Power Measurements

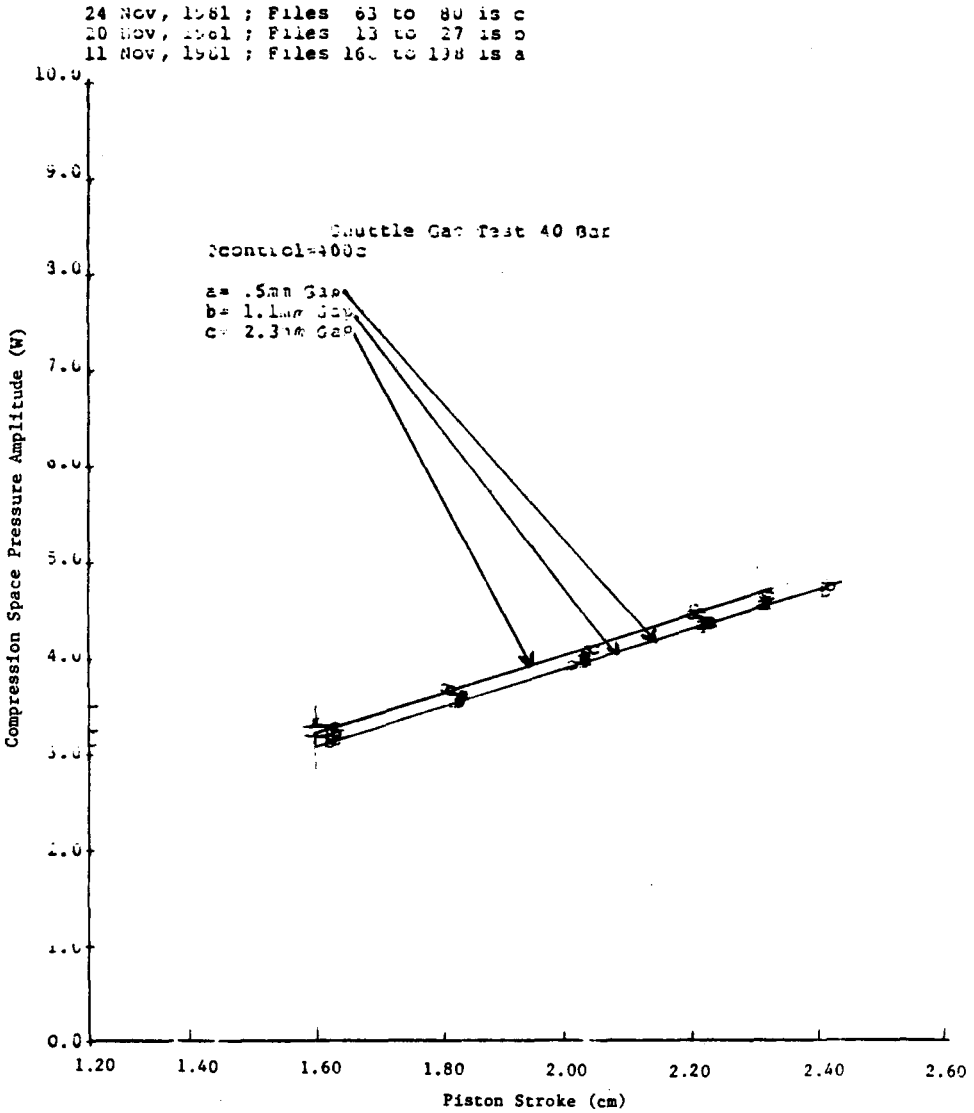

Fig. 7-7. Displacer Appendix Gap Test: Engine Pressure Amplitude Measurements

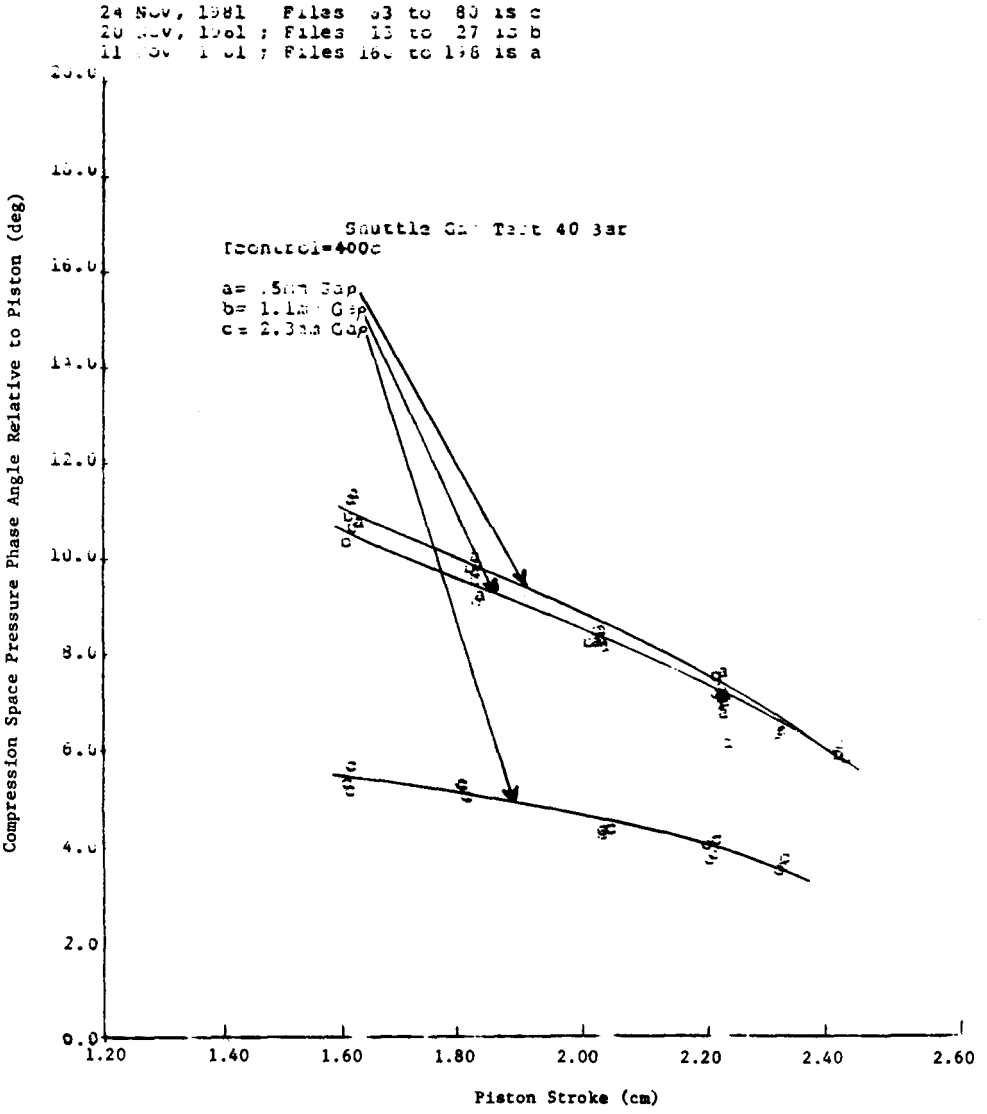

Fig. 7-8. Displacer Appendix Gap Test: Engine Pressure Angle Measurements

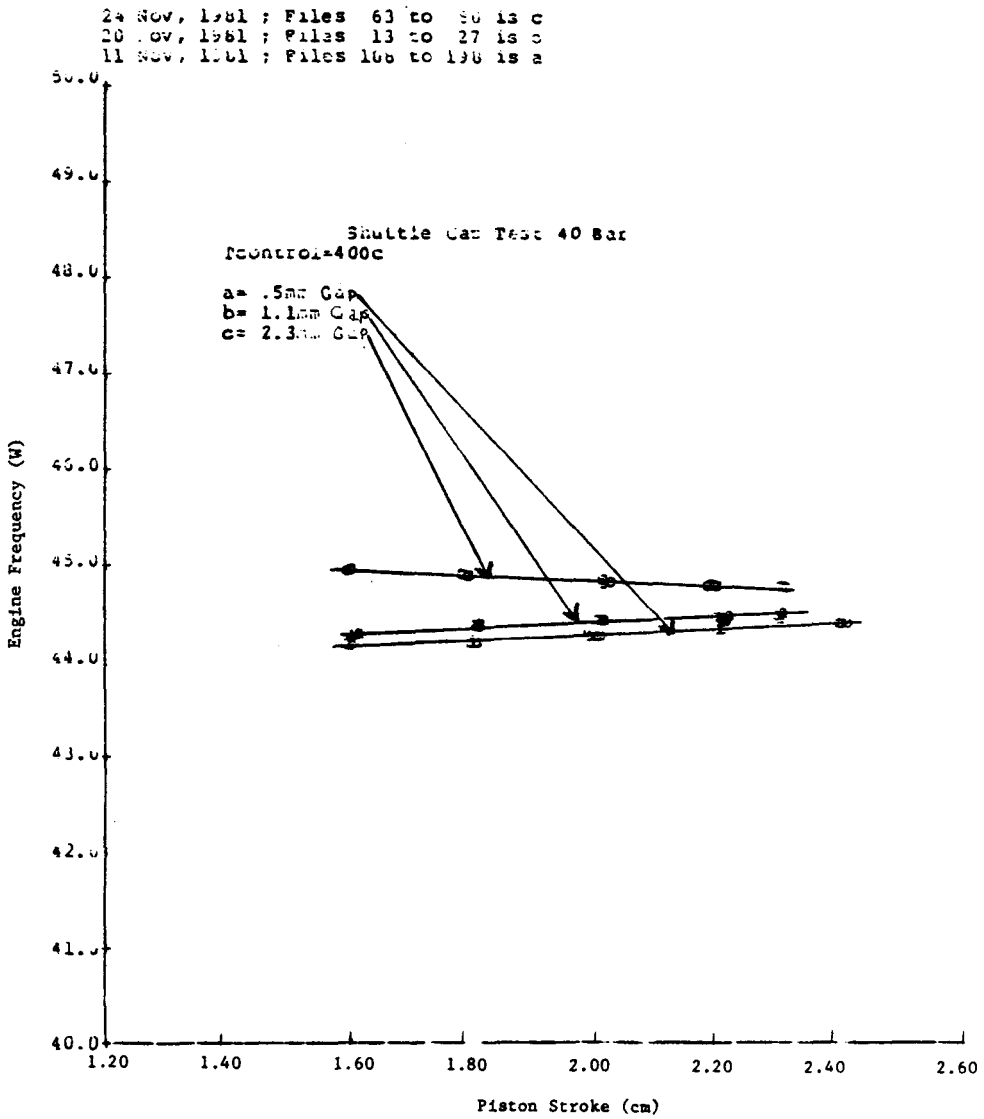

Fig. 7-9. Displacer Appendix Gap Test: Engine Frequency Measurements

The reduction in pressure-wave phase angle can result from a variety of effects; reduction in expansion-space mean temperature or increase in compression-space mean temperature will lower the pressure-wave phase angle. Figures 7-10 and 7-11 compare the variations of heater head dome temperature and compression-space temperature from the three gap tests. Assuming that dome temperature is an accurate measure of expansion-space temperatures, these variations suggest an increased pressure-wave phase angle for the large shuttle gap. Increased heat exchanger losses also will lower pressure-wave phase angle. Figure 7-12 compares the pumping power, pressure-drop phase angle, and pressure-drop amplitude calculated for the heat exchanger loop from the displacer force balance parameters. The lower losses associated with 2.3-mm gap test again suggest an increased pressure-wave phase angle. A shift in the expansion-space temperature wave, such that it lagged the corresponding pressure wave, also would reduce the pressure-wave phase angle. Transient pressure/temperature measurements for the expansion space, however, were not available to evaluate this mechanism or to verify the assumed correlation between heater head dome temperature and mean expansion-space temperature.

Figure 7-13 compares the variation of indicated efficiency with piston stroke for the three gap tests. There was a consistent drop in efficiency with increasing appendix gap, indicating that parasitic losses per unit of heat input increased with appendix gap width. The significant reduction in efficiency at low piston strokes for the 2.3-mm gap test indicated the importance of appendix losses at such operating points.

In summary, appendix gap losses were shown to influence both engine power and efficiency. A degradation in both parameters was observed as appendix gap width increased. The reduction in power indicated that the appendix gap losses altered the basic thermodynamics of the machine.

7.4 ANALYTICAL COMPRESSION

The influence of geometry and operating conditions was investigated by approximating the appendix gap losses.[4] The overall loss is considered to be the net effect of three separate contributions--shuttle heat transfer, pumping losses, and hysteresis heat transfer. The shuttle loss is, in effect, a conduction loss down the wall enhanced by the oscillatory motion of the piston. Figure 7-14 indicates that when the piston is at top dead center, the piston wall has a lower local temperature than the corresponding cylinder wall temperature at any point x; thus, heat is transferred to the piston. Conversely, when the piston is at bottom dead center, the temperature relationship between the piston and cylinder is reversed so that heat is transferred from the piston to the cylinder. Therefore, for the part of the cycle in which the piston has a lower temperature than the cylinder, heat moves from the cylinder to the piston, and is carried by the piston and transferred back to the cylinder at a different axial location during the part of the cycle when the piston has a higher temperature than the cylinder. The piston motion thus serves to shuttle heat from the hot end to the cold end. This heat transfer mechanism was first analyzed in the literature by Zimmerman and Longsworth.[5]

Pumping loss is simply the net enthalpy transport down the gap by virtue of the working gas motion, pressure, and temperature. Finally, hysteresis

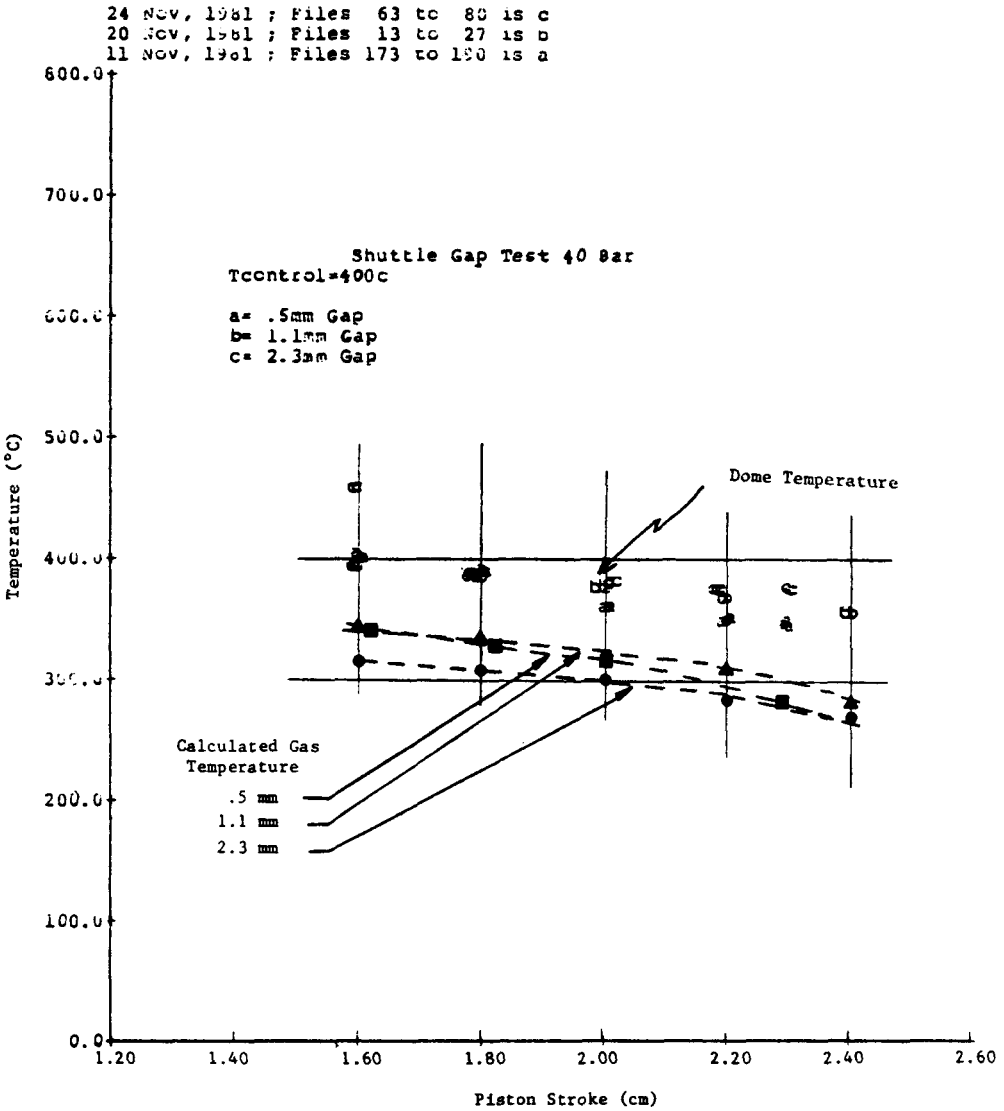

Fig. 7-10. Displacer Appendix Gap Test: Average Dome Temperature Measurements and Calculated Expansion Space Gas Temperatures

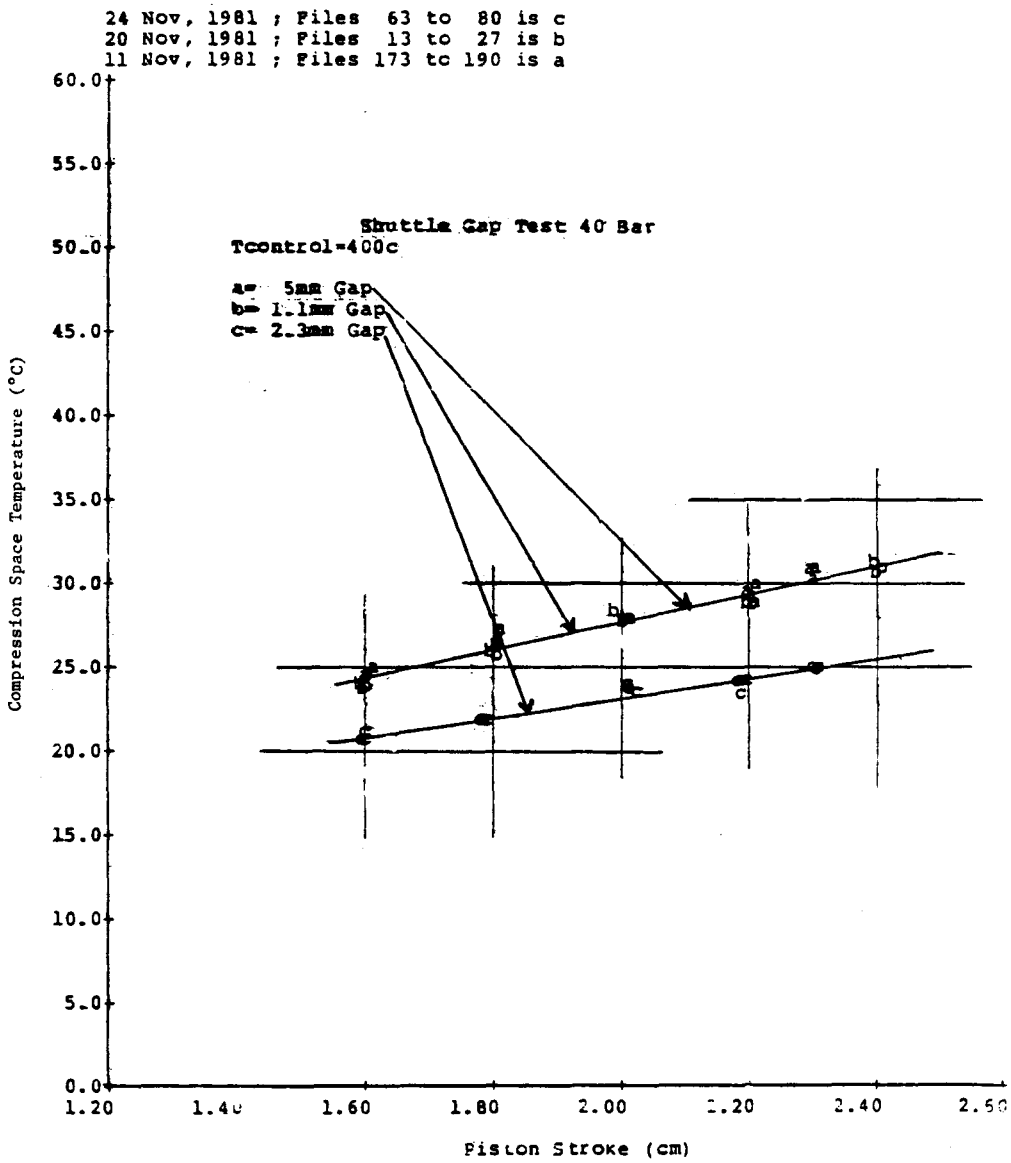

Fig. 7-11. Displacer Appendix Gap Test: Compression-Space Temperature Measurements

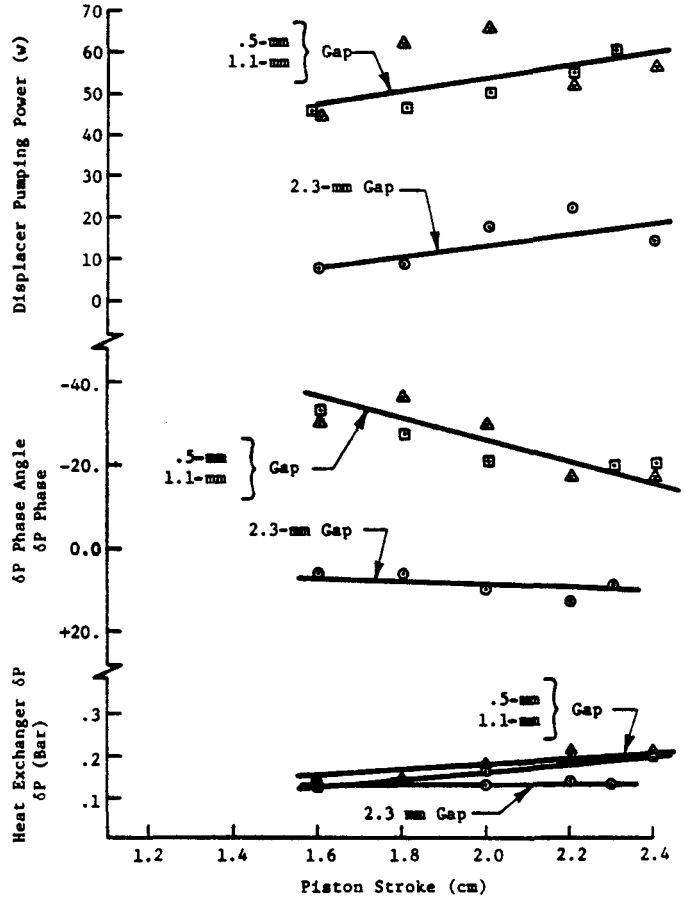

Fig. 7-12. Displacer Appendix Gap Test: Displacer Pumping Power/δP Phase Angle/Heat Exchanger δP

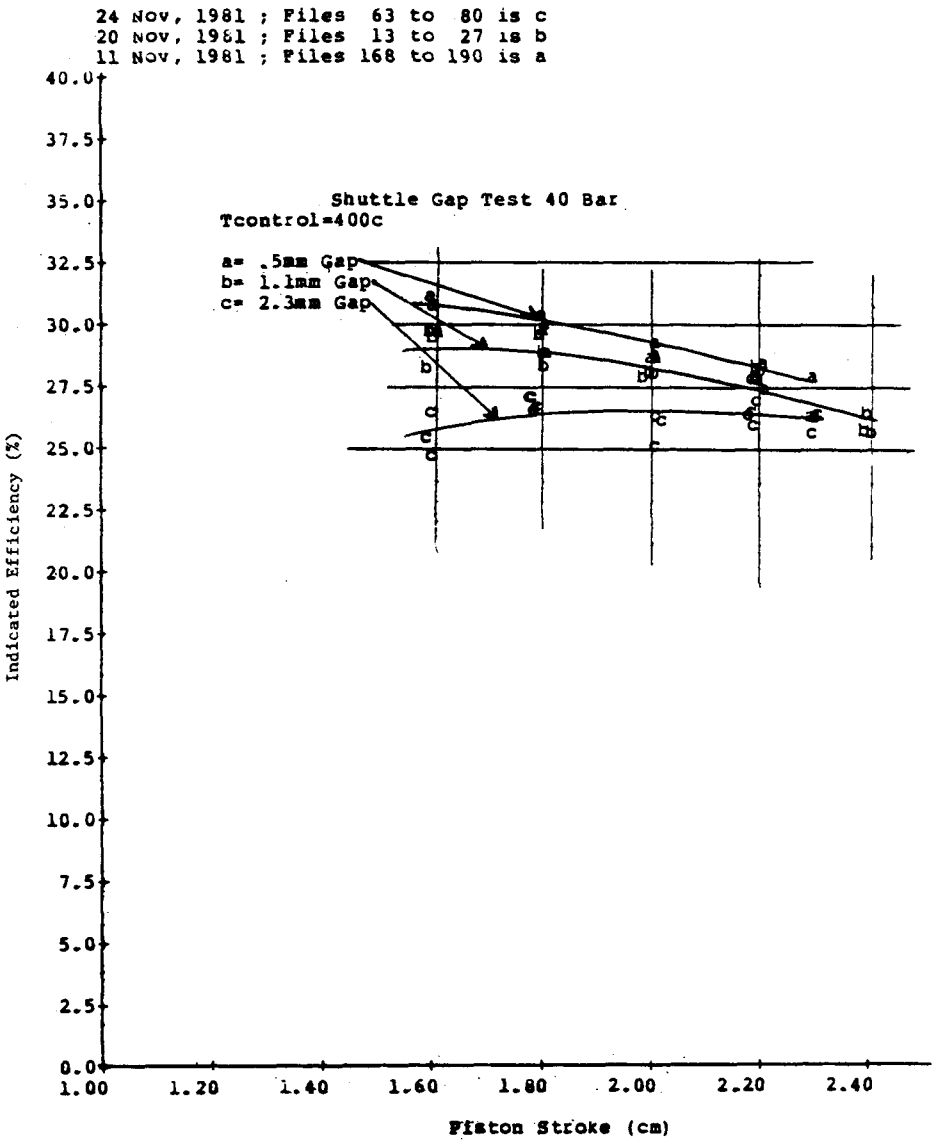

Fig. 7-13. Displacer Appendix Gap Test: Indicated Efficiency Measurements

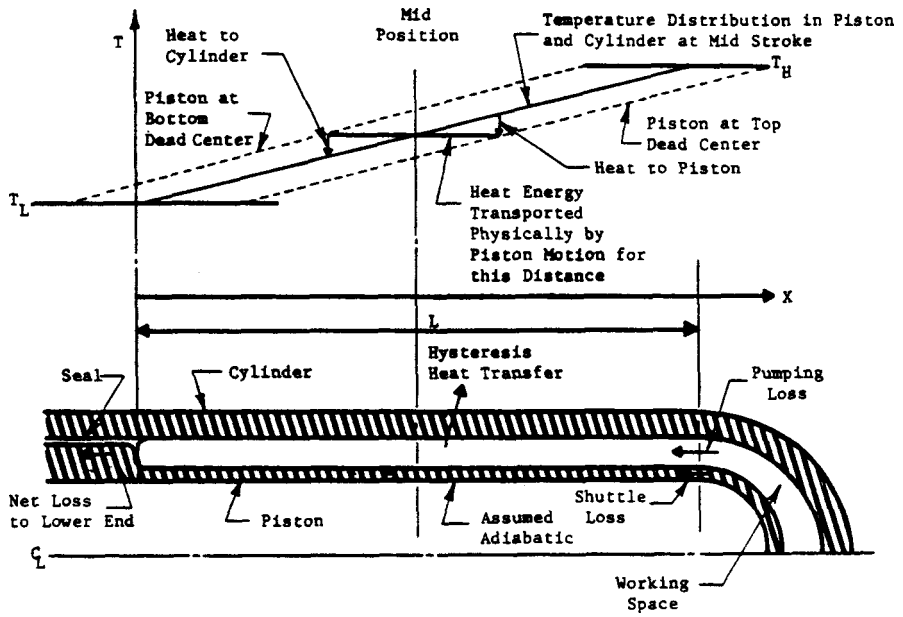

Fig. 7-14. Displacer Appendix Gap Test: Shuttle Loss Mechanism and Control Volume

loss is the net heat transfer from the gas to the cylinder due to the out-of-phase relationship of pressure and temperature. Hysteresis heat transfer does not contribute directly to total thermal loss from the working space; however, to determine the heat transferred to the lower end of the piston, it is necessary to form an energy balance for the appendix volume. To this end, it is necessary to know the hysteresis heat transfer.

Rios[6] improved the Zimmerman/Longsworth calculation by obtaining a less limited, closed-form solution that is simple to apply. Rios included the effects of radial temperature distribution in the walls, as well as the effects of higher harmonics in all the periodic terms. Like the Longsworth/Zimmerman analysis, Rios' results indicated that the losses might always be reduced by making the gap as large as practically possible. The present analysis extends Rios' work by including gas momentum effects and solving the gas wall temperature fields for plausible boundary conditions. Furthermore, an imposed pressure variation with time to simulate the changing working gas pressure is included. Results of this analysis indicate the existence of a particular gap size for which the losses might be minimized.

The appendix gap loss analysis predicts the losses in Figure 7-15 for TDE test conditions where the appendix gap was varied (0.5, 1.1, and 2.3 mm). Figure 7-16 compares calculated indicated power with measured indicated power from the appendix gap test results. For small appendix gaps, the code correlates very well; for the 2.3-mm gap, the code overpredicts the power.

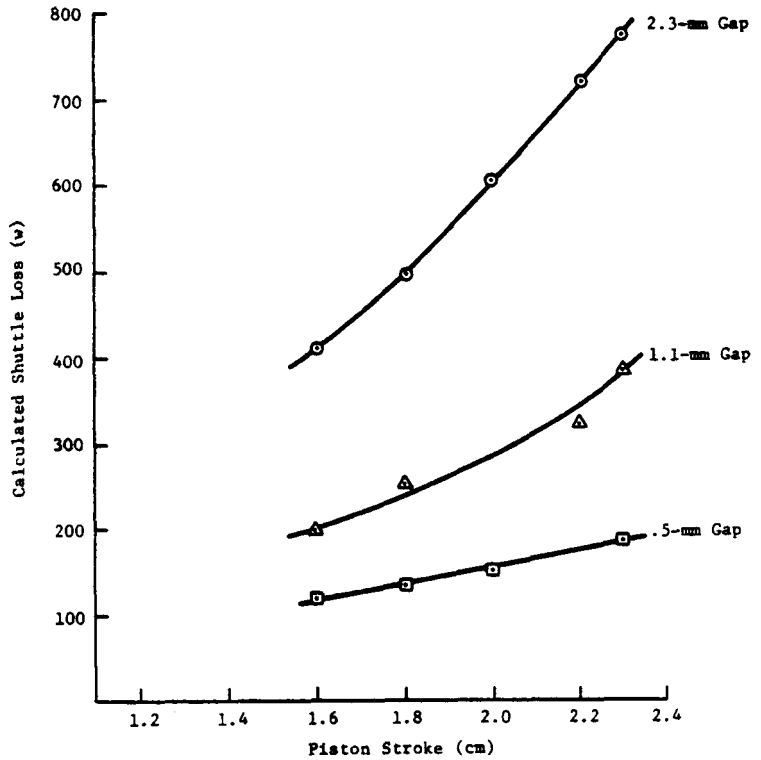

Fig. 7-15. Displacer Appendix Gap Test: Calculated Appendix Gap Losses

Compression-space pressure amplitude and phase correlation are shown in Figure 7-17. The code slightly underpredicts the pressure amplitude for the 2.3-mm tests, due to assumed isothermal expansion-space dead volume, which (from the data) appears more adiabatic. For small gaps, the code effectively predicts the compression-space pressure phase, and overpredicts the compression-space phase for the large 2.3-mm gap. Table 7-1 indicates that calculated phase is insensitive to expansion-space dead volume. Pumping effects associated with the large appendix gap are believed to be stronger than anticipated for the appendix gap boundary conditions in the real engine. The overall trend is consistent in that engine losses increase with increasing appendix gap. Figure 7-18 shows the code correlation with measured efficiency results for the appendix gaps tested. Efficiencies at the smaller gaps are tracked closely by the code; for the large gap, the code underpredicts the efficiency, revealing that the appendix gap parasitic loss is overestimated by the code.

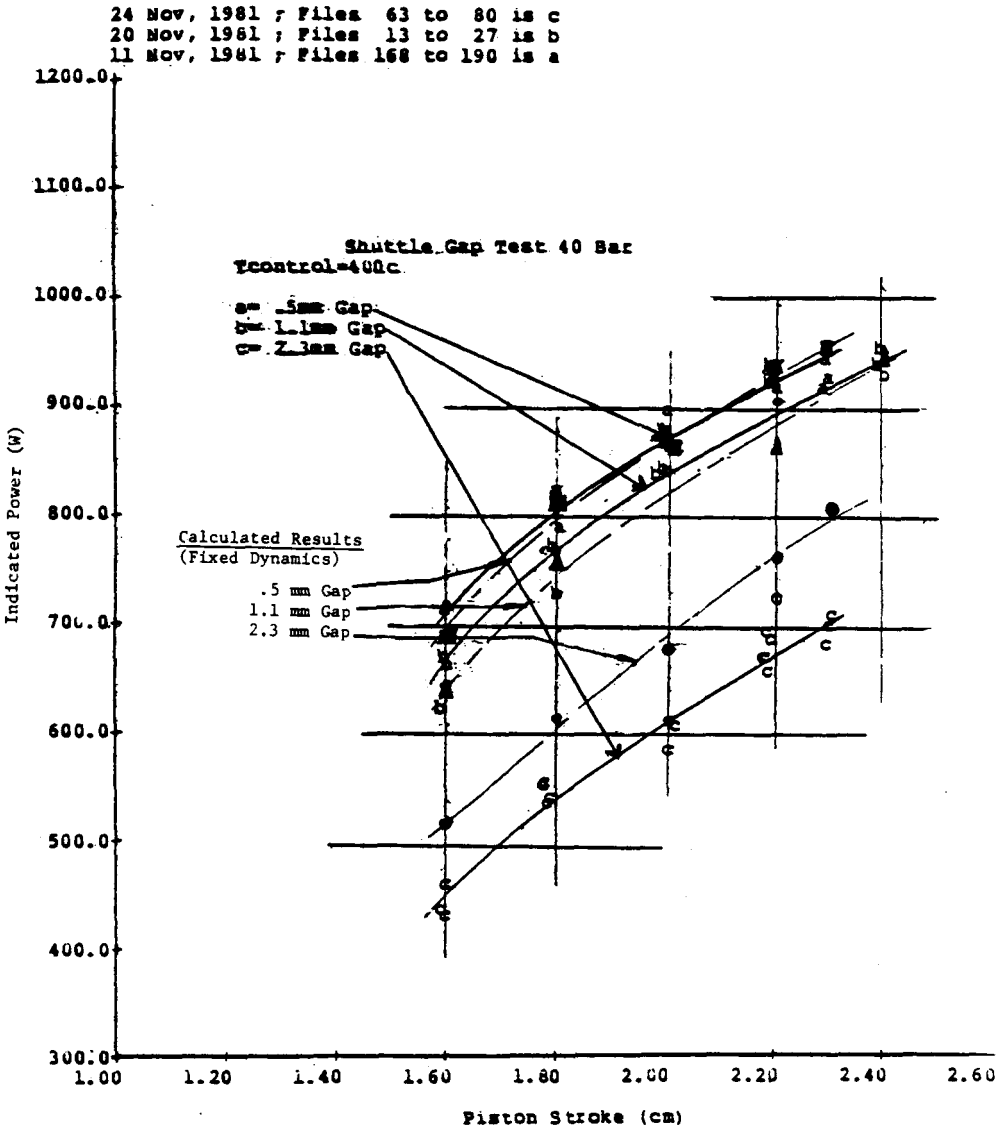

Fig. 7-16. Displacer Appendix Gap Test: Comparison between Measured and Calculated Indicated Power

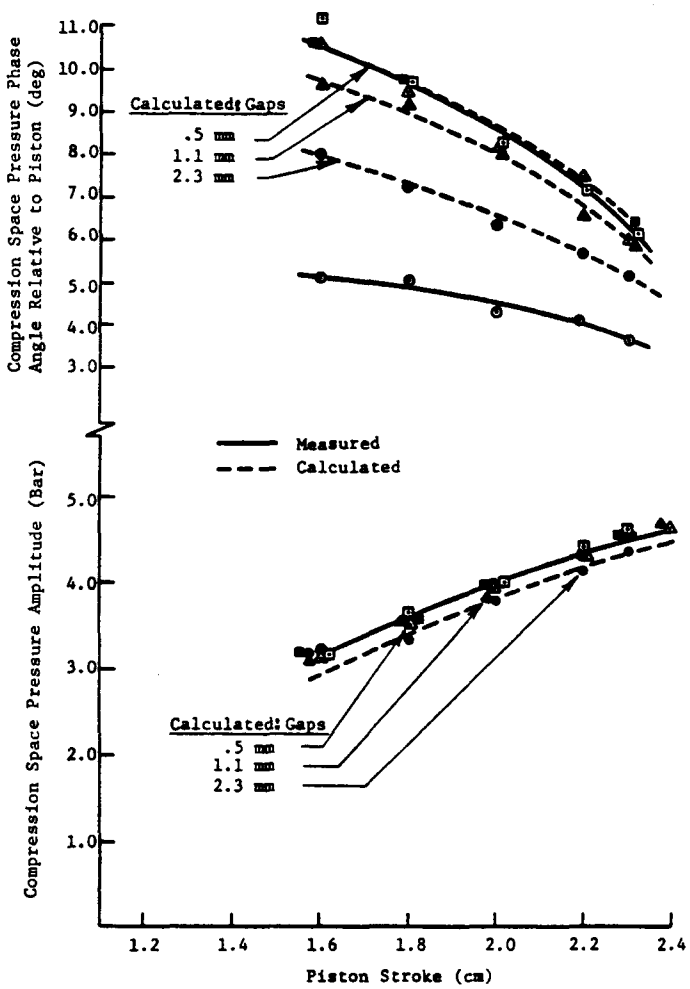

Fig. 7-17. Displacer Appendix Gap Test: Comparison between Measured and Calculated Compression Space Pressure Amplitude and Phase Angle

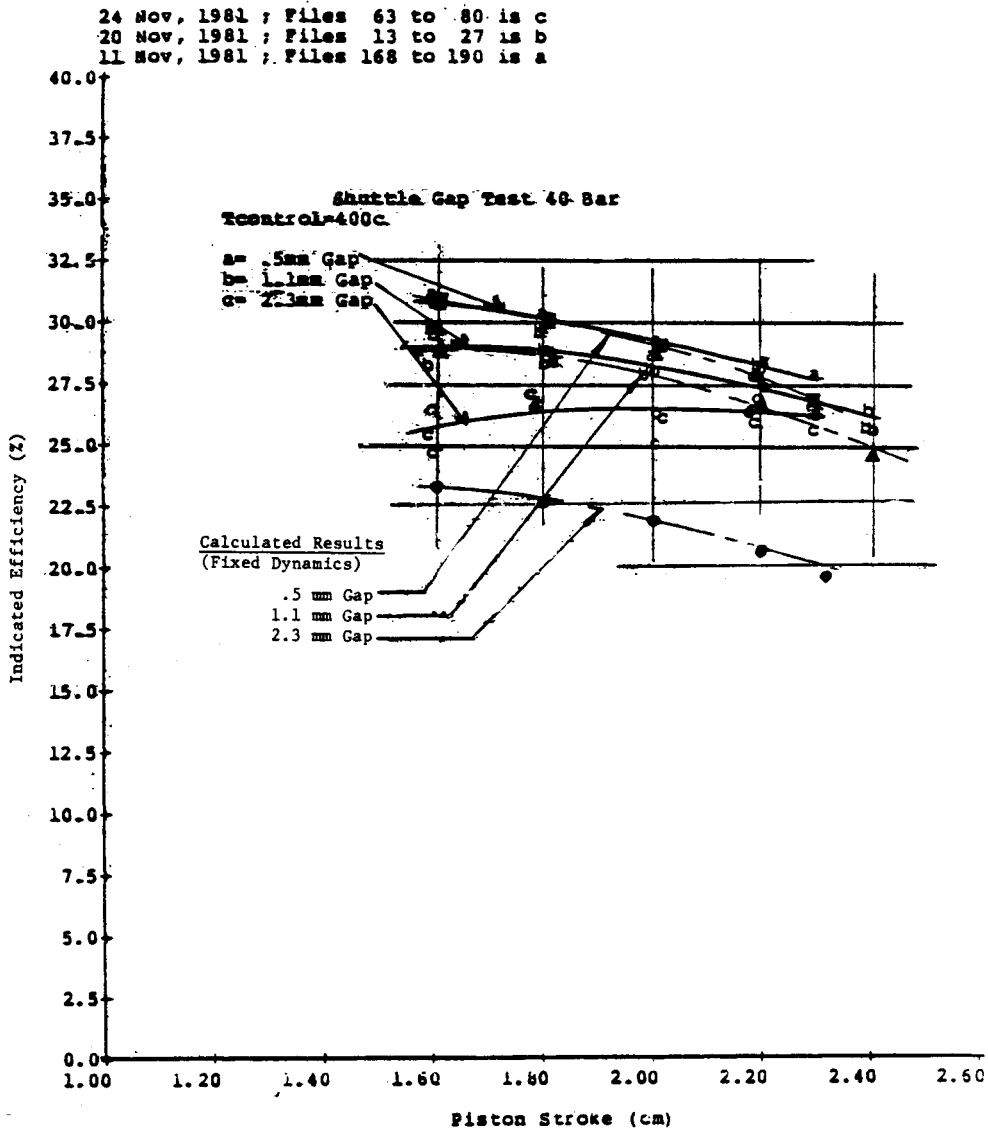

Fig. 7-18. Displacer Appendix Gap Test: Comparison between Measured and Calculated Indicated Efficiency

Table 7-1. Effect of Dead Volume on Compression-Space Pressure and Phase

Expansion-Space Dead Volume (cc)	Calculated Pressure Amplitude, P_c	Calculated Pressure Phase Angle, θ_c
64.43 (base)	4.037	6.570
100	3.975	6.585
130	3.892	6.685
1500	2.520	6.262

7.5 CONCLUSIONS AND RECOMMENDATIONS

7.5.1 Conclusions

- Engine power is significantly reduced at large appendix gaps.
- For the large appendix gap, the δP angle shifts such that the expansion-space pressure wave leads compression-space pressure wave.
- The code effectively matches engine performance for reasonably small appendix gaps, but overpredicts power at the large gap due to overprediction of the pressure phase.
- As indicated by the predicted pressure phase angle, expansion-space dead volume has little effect on the pressure phase.
- The calculated efficiency is underpredicted at the large appendix gaps, indicating a deficiency in the appendix gap model, which calculates too high a parasitic loss at large gaps.

7.5.2 Recommendations

- Design engines with as small an appendix gap as possible.
- Explore effects of expansion-space dead volume on engine performance with a fixed appendix gap (although judged as not important).

- Conduct a test with a fourth appendix gap intermediate to the 1.1-mm and 2.3-mm gaps that were run.

- Investigate further improvements to the appendix gap model.

- Explore different displacer dome geometries.

- Conduct a sensitivity study with the code to determine effects of operating dynamics on appendix gap losses. (If the losses are shown insensitive to dynamics, conduct a test at constant power to evaluate appendix gap losses by generating data as a function of engine heat rejection.)

8. DISPLACER CLEARANCE SEAL TEST

8.1 OBJECTIVES

The seal between the displacer piston skirt and cylinder wall is accomplished in the TDE by a close clearance. Flow through this seal results in parasitic pumping losses and a potential thermal energy transfer from the hot expansion-space working gas directly to the cooler. The objective of this test is to evaluate the effects of displacer seal clearance on engine performance.

8.2 METHOD OF EXECUTION

Ten separate tests were run with the TDE to evaluate the effects of displacer seal gap on engine performance. The first three tests, conducted with hardware combinations resulting in displacer clearance seal gaps of 0.0048, 0.0029, and 0.002 in. were conducted to evaluate the effects on engine performance without a piston ring present. The clearance gap tests were conducted with displacer domes having a 0.5-mm shuttle gap.

The first test was run with a displacer/seal cylinder combination that yielded a 0.0029-in. clearance gap. The dynamics for this test were taken from one of the baseline tests, which yielded dynamics that were close enough to be reestablished by the 0.0029-in. clearance tests. Hardware differences between the previous test and this test were the displacer mass and bearing engine seal coefficient.

The 0.0029-in. clearance test was conducted by generating a performance map versus stroke for a constant control temperature of 400°C. The seal/displacer combination was then changed to yield a 0.002-in. seal clearance, and the performance test at a 400°C control temperature was repeated after tuning the dynamics at a 2.2-cm piston stroke equivalent to the 0.0029-in. test. Tests from the previous baseline test (run during the summer of 1981) were rerun; these tests had a seal clearance of 0.0048-in. and a wear couple bearing for which the 0.002-in. and 0.0029-in. test dynamics were set. The 0.0048-in. tests were run with the displacer air bearing used for the 0.002/0.0029 in. tests. Because several hours had been accumulated with the 0.0048-in. displacer rod used in a wear couple bearing, the stroke porting was weak, limiting the available stroke at which the engine could be operated. The dynamics were set at 2.0-cm instead of at 2.2-cm, as was done for the 0.002 and 0.0029-in.gap tests.

Area weighted mean head temperature, and displacer-to-piston phase and stroke ratio are plotted in Figure 8-1, showing very close agreement between tests. Upon completion of the 0.002-in. gap performance map, the engine was heated to a maximum head temperature of 600°C while holding the piston stroke at 2.2-cm.

The 1.1-mm shuttle gap displacer was reworked to accommodate a piston ring, and a performance map was run for a seal gap of 0.0015-in. with a piston ring installed. The engine was disassembled, the piston ring removed, and the performance test repeated after rebuilding and setting the dynamics similar to

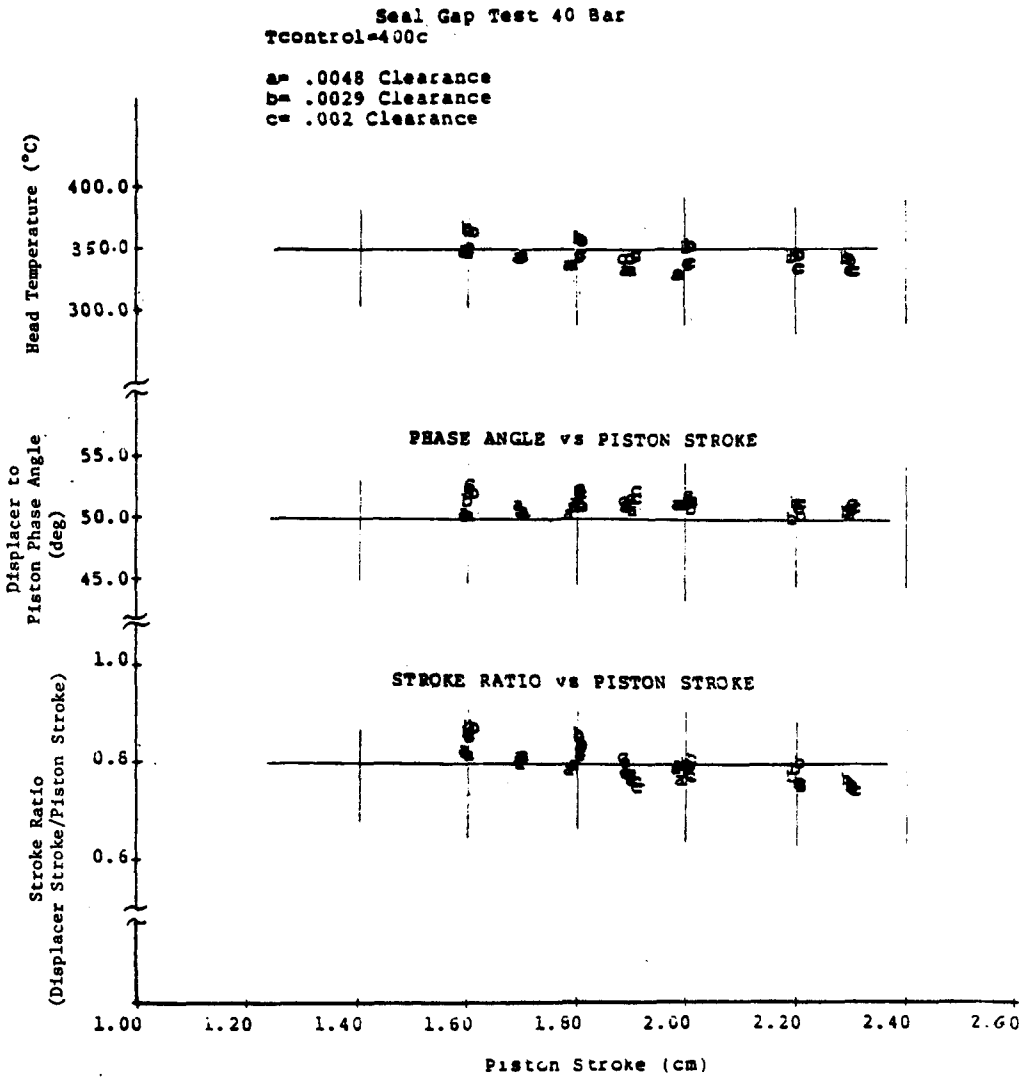

Fig. 8-1. Displacer Clearance Test: Average Head Temperature/Phase Angle/Stroke Ratio Measurements

those run with the piston ring at a piston stroke of 2.0-cm. The displacer was then removed and machined to a 0.0031-in. clearance, and the above performance maps were repeated both with and without the piston ring. The same procedure was repeated for a third point with a clearance gap of 0.005-in. Upon completion of the 0.005-in. clearance tests, the piston ring was reinstalled and backed with an O-ring to enhance the piston ring loading, completing the series of ten tests. Operating conditions for the piston ring tests are plotted in Figures 8-2 through 8-5.

8.3 EXPERIMENTAL RESULTS

The experimental results from the displacer seal tests are presented in two parts: tests results from the clearance test (Section 8.3.1), and test results from the piston ring tests (Section 8.3.2).

8.3.1 Displacer Clearance Seal Tests

Indicated power measurements are plotted in Figure 8-6 for clearance gaps of 0.002, 0.0029, and 0.0048 in. A significant change in power is shown with varying clearance seal gaps. The compression-space pressure amplitude is shown to be constant with clearance gap in Figure 8-7. Decline in power with increasing seal gap is shown to be due to the decline in pressure phase (Fig. 8-8). As cold gas from the cold space leaks past the seal clearance and is displaced to the engine hot end, the cold gas quenches down the expansion-space gas temperature. As the gas is displaced back to the cold space, gas that leaks past the clearance seal is, in part, cooled by the cooler before mixing with the cold space gas that passed through the heat exchangers. As a result, hot space temperature is lowered with increasing enthalpy transport from the cold space, reducing compression-space pressure phase/power. Engine heat rejection increases (Fig. 8-9) as seal clearance is increased, while hot gas leaks to the cooler. Cold space temperature increases slightly, as shown by the normalized plot of compression-space temperature (Fig. 8-10) to water-inlet temperature (Fig. 8-11). Reduced power due to hot space quenching effects, coupled with an increase in heat rejection as hot gas is shorted to the cooler, results in a significant reduction in efficiency as the clearance gap is increased (Fig. 8-12).

While the engine was assembled with the 0.002-in. displacer clearance gap, it was heated to a maximum head temperature of 595°C (mean head temperature 500°C) at a piston stroke of 2.2-cm. Figures 8-13 and 8-14 show the variation of indicated power and efficiency with head temperature at this stroke. Extrapolation of the efficiency data to a mean head temperature of 600°C suggests the potential for achieving an efficiency of 45%.

8.3.2 Piston Ring Tests

Indicated power results from the piston ring tests are plotted in Figure 8-15 for clearance gaps of 0.0015, 0.0031, and 0.0050 in., both with and without the piston ring. General trends that can be derived are:

- At small clearance gaps, use of a piston ring results in a degradation of power,

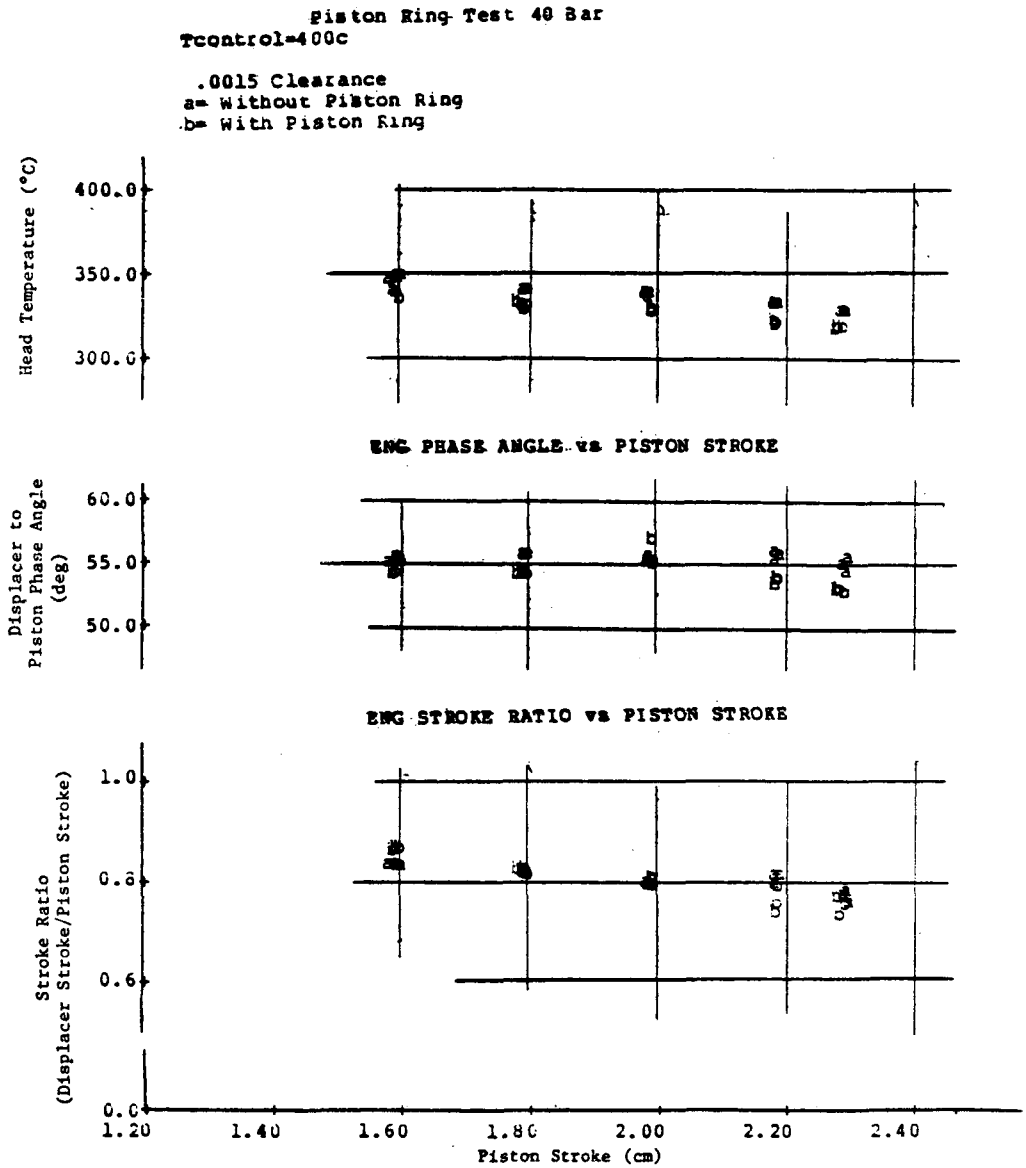

Fig. 8-2. Displacer Clearance Test: Mean Head Temperature/Phase Angle/Stroke Ratio Measurements at .0015-in. Clearance with and without Piston Ring

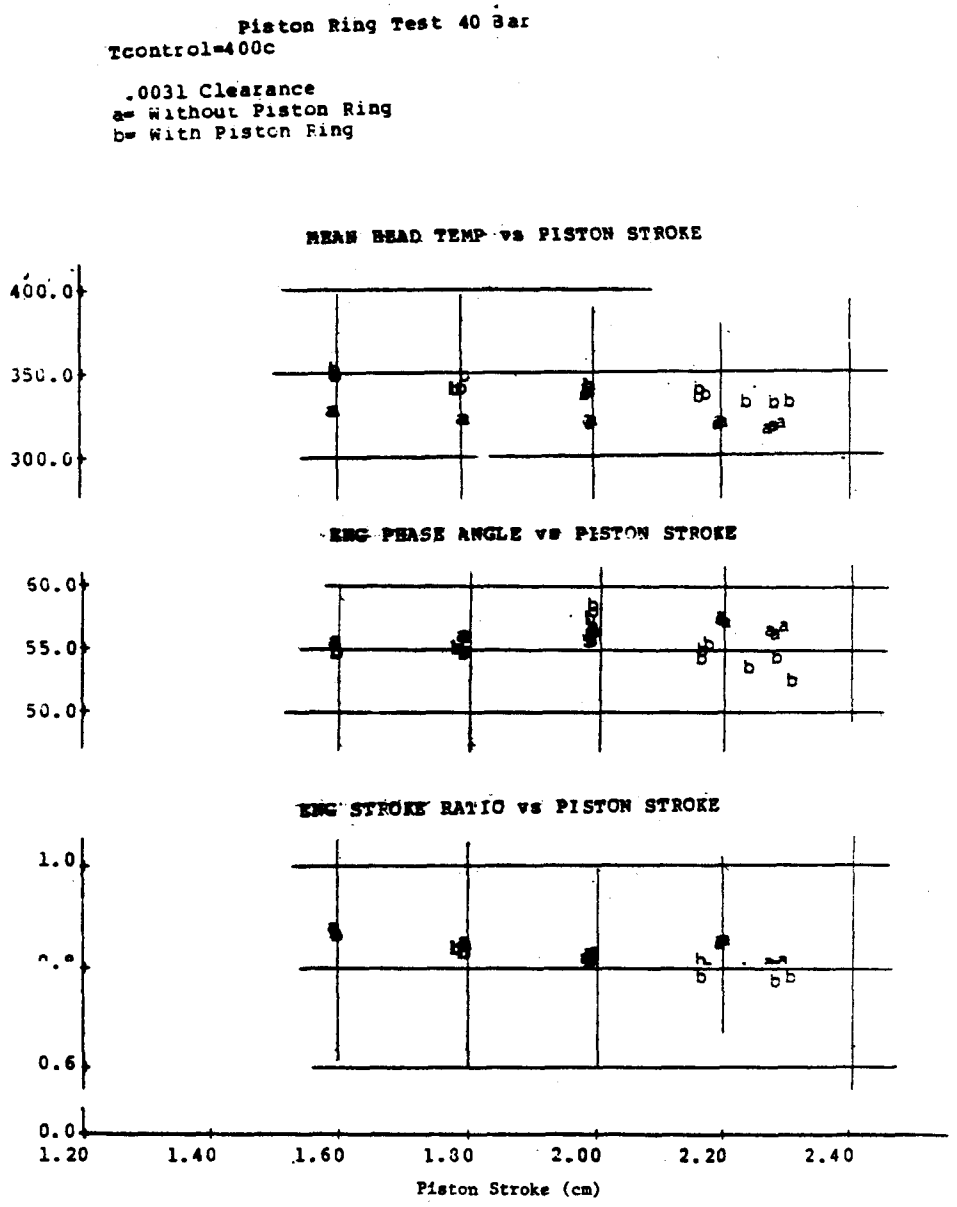

Fig. 8-3. Displacer Clearance Test: Mean Head Temperature/Phase Angle/Stroke Ratio Measurements at .0031-in. Clearance with and without Piston Ring

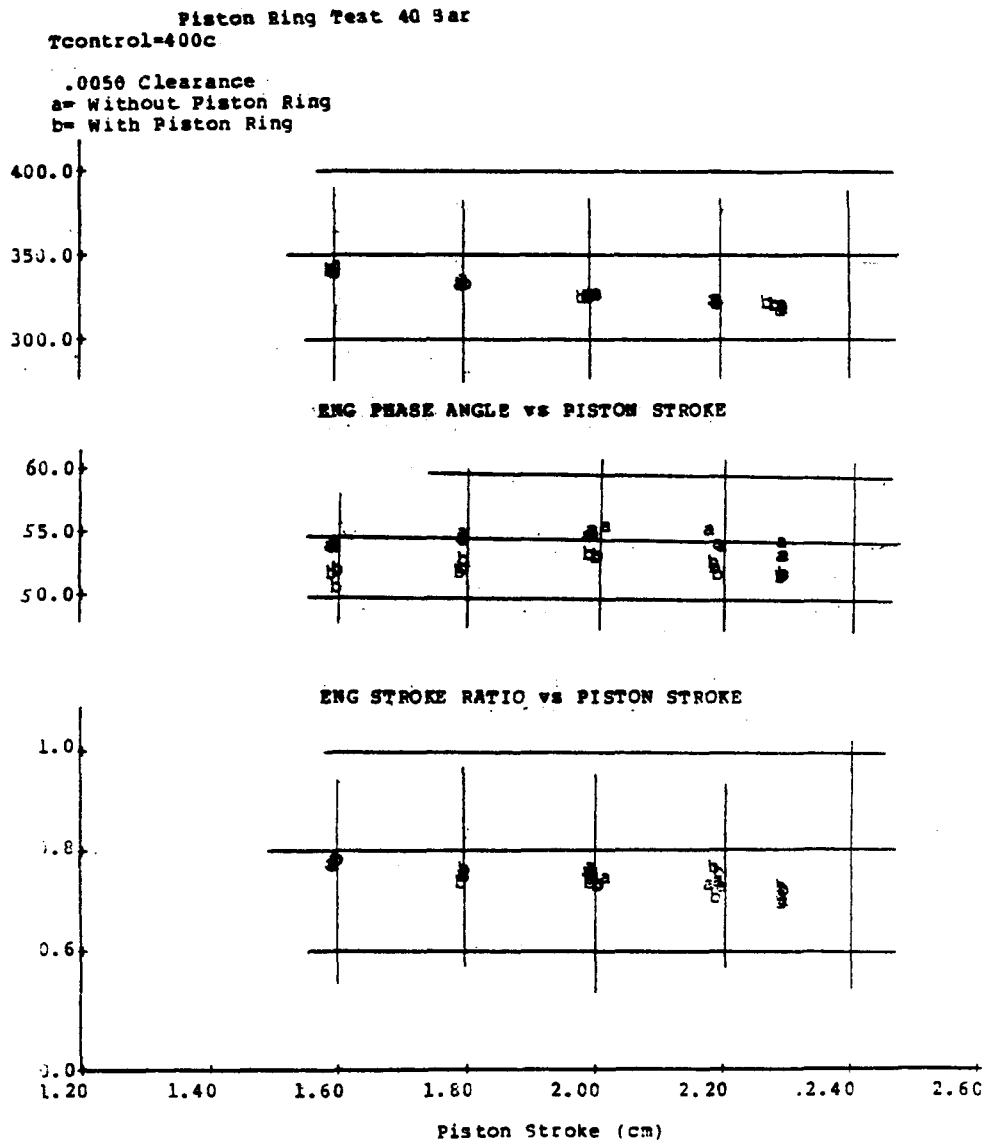

Fig. 8-4. Displacer Clearance Test: Mean Head Temperature/Phase Angle/Stroke Ratio Measurements at .0050-in. Clearance with and without Piston Ring

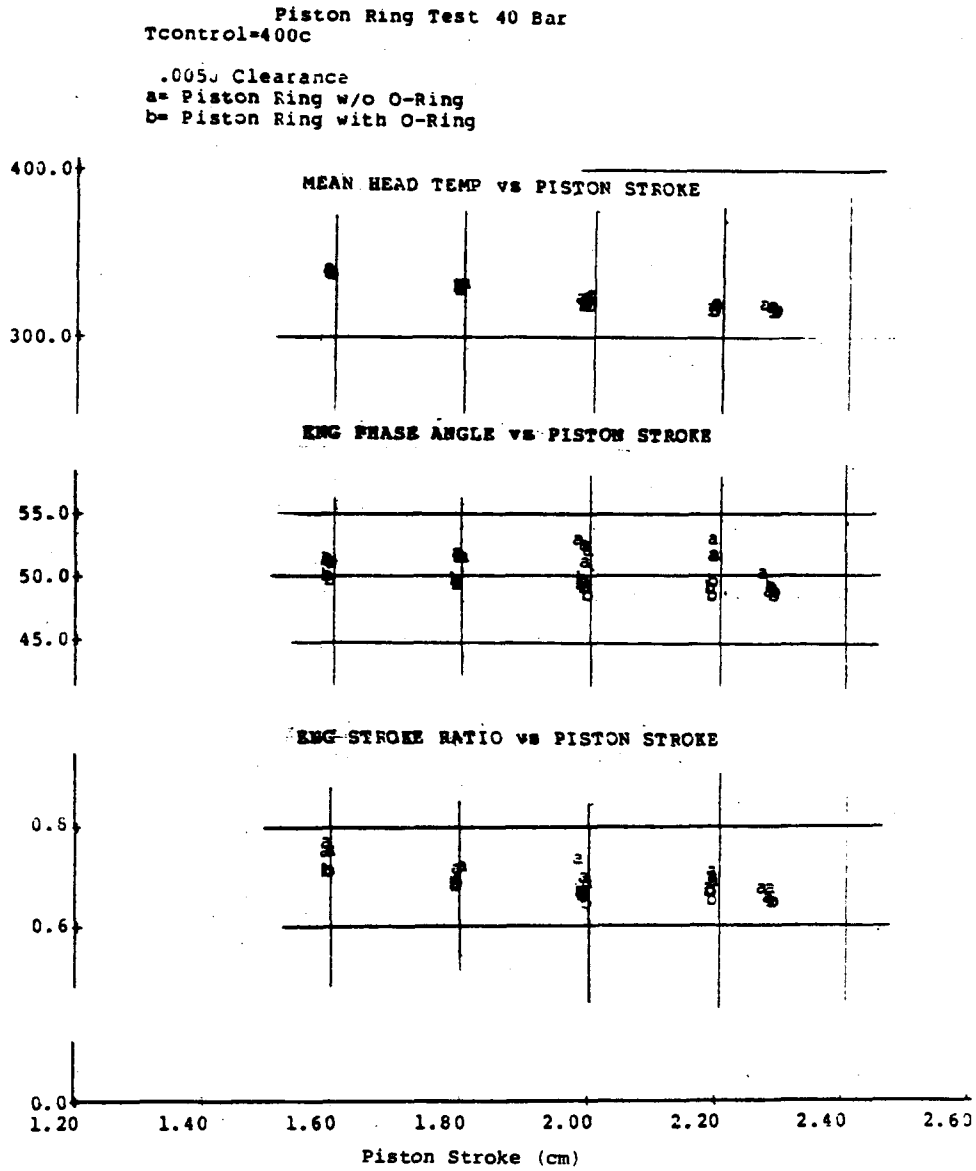

Fig. 8-5. Displacer Clearance Test: Mean Head Temperature/Phase Angle/Stroke Ratio Measurements at .0050-in. Clearance Using Piston Ring with O-Ring Backing

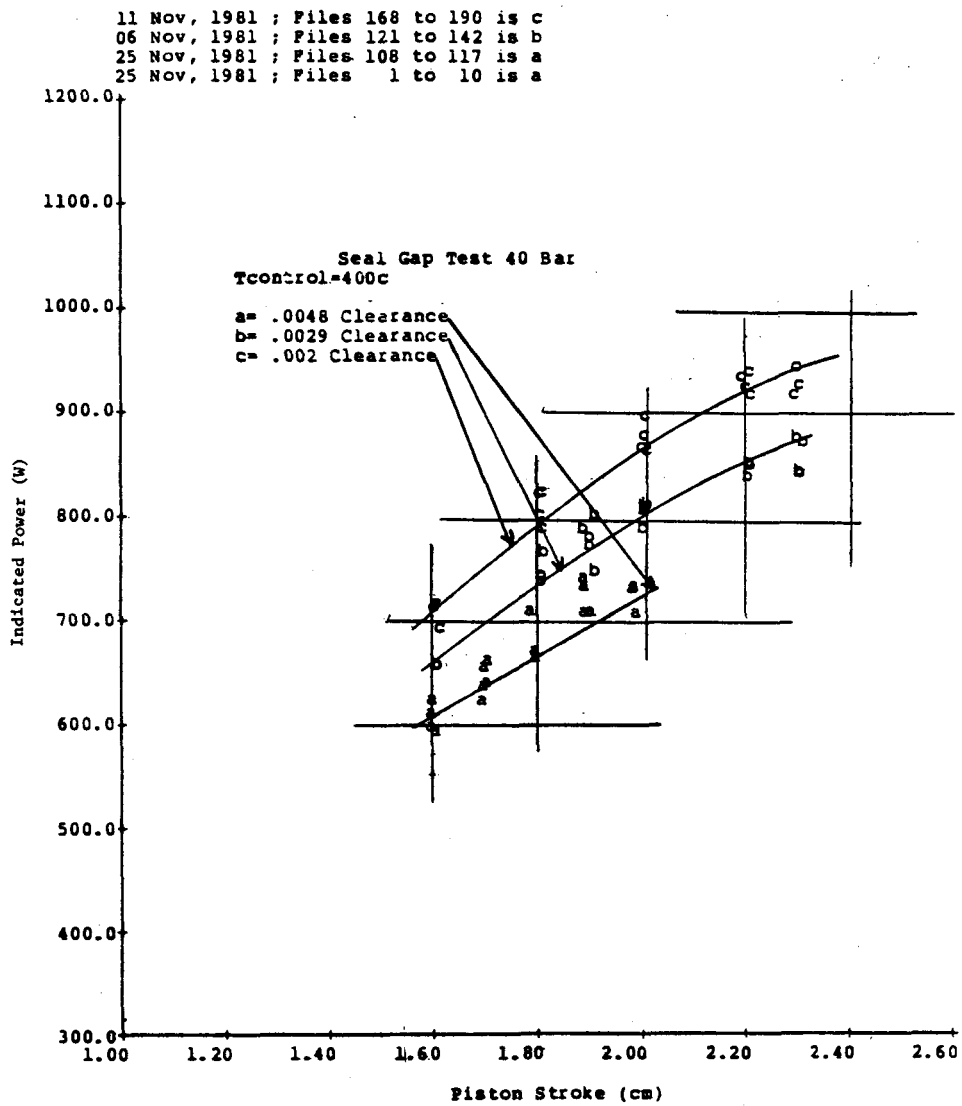

Fig. 8-6. Displacer Clearance Test: Indicated Power Measurements with Various Clearances

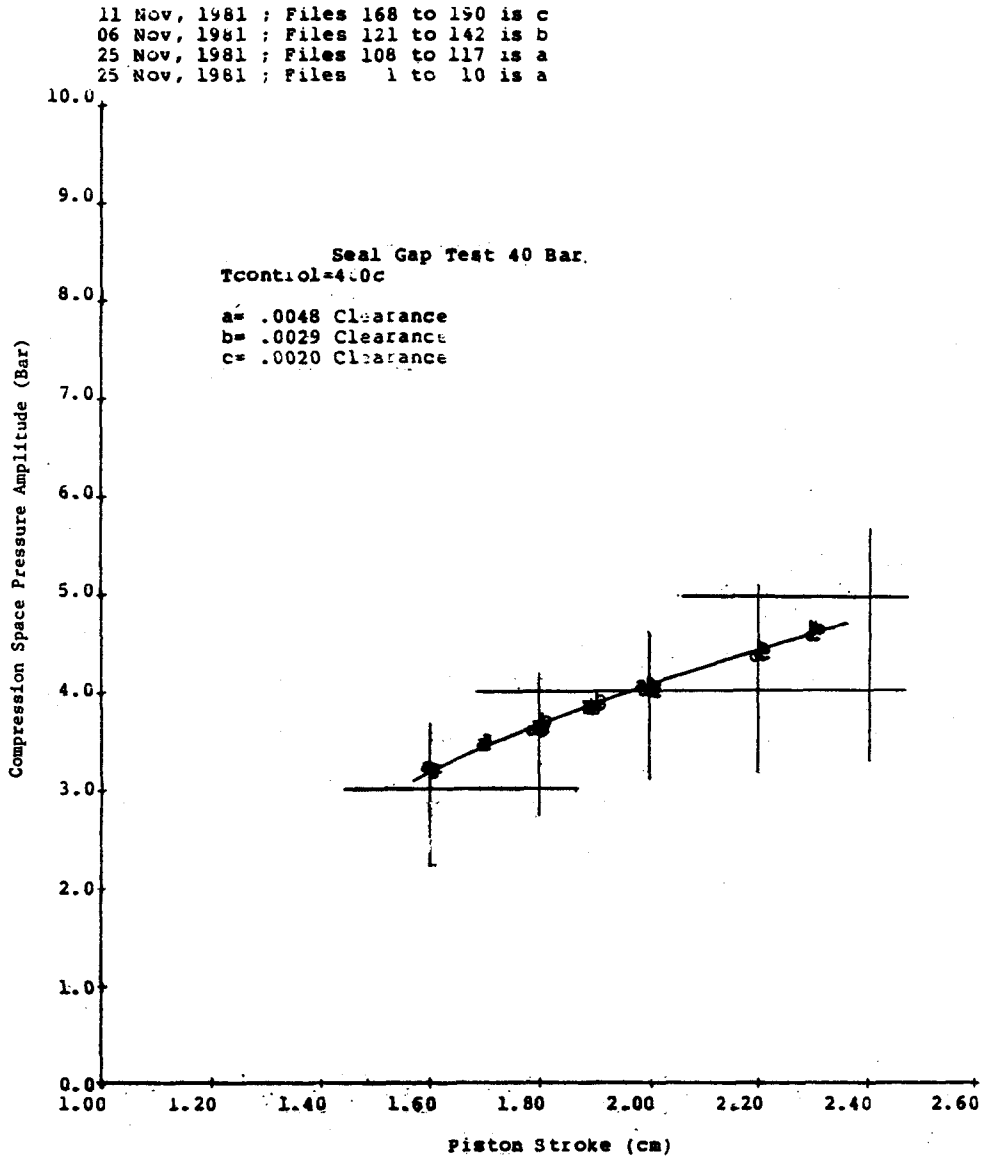

Fig. 8-7. Displacer Clearance Test: Engine Pressure Amplitude Measurements at Various Clearances

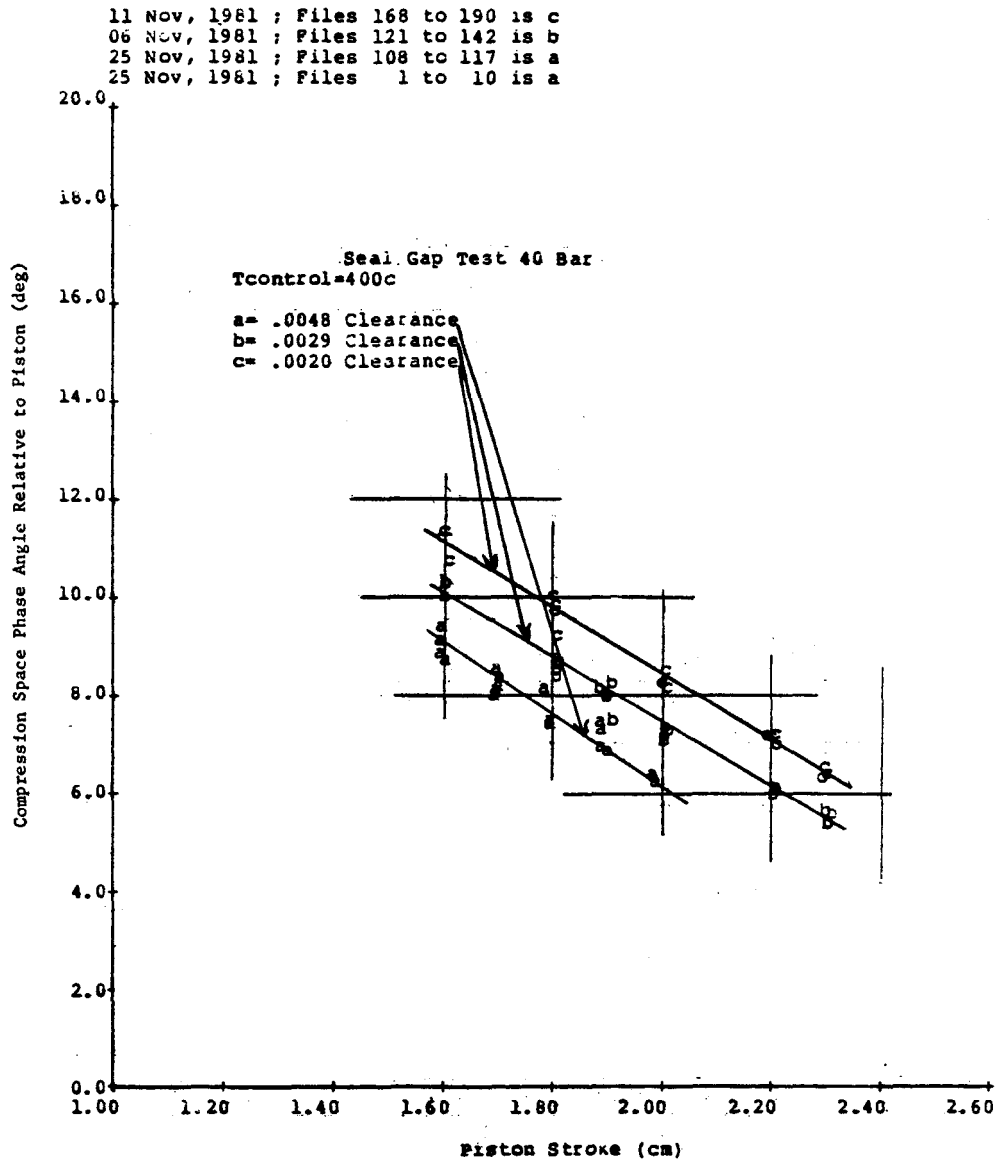

Fig. 8-8. Displacer Clearance Test: Engine Pressure Angle Measurements at Various Clearances

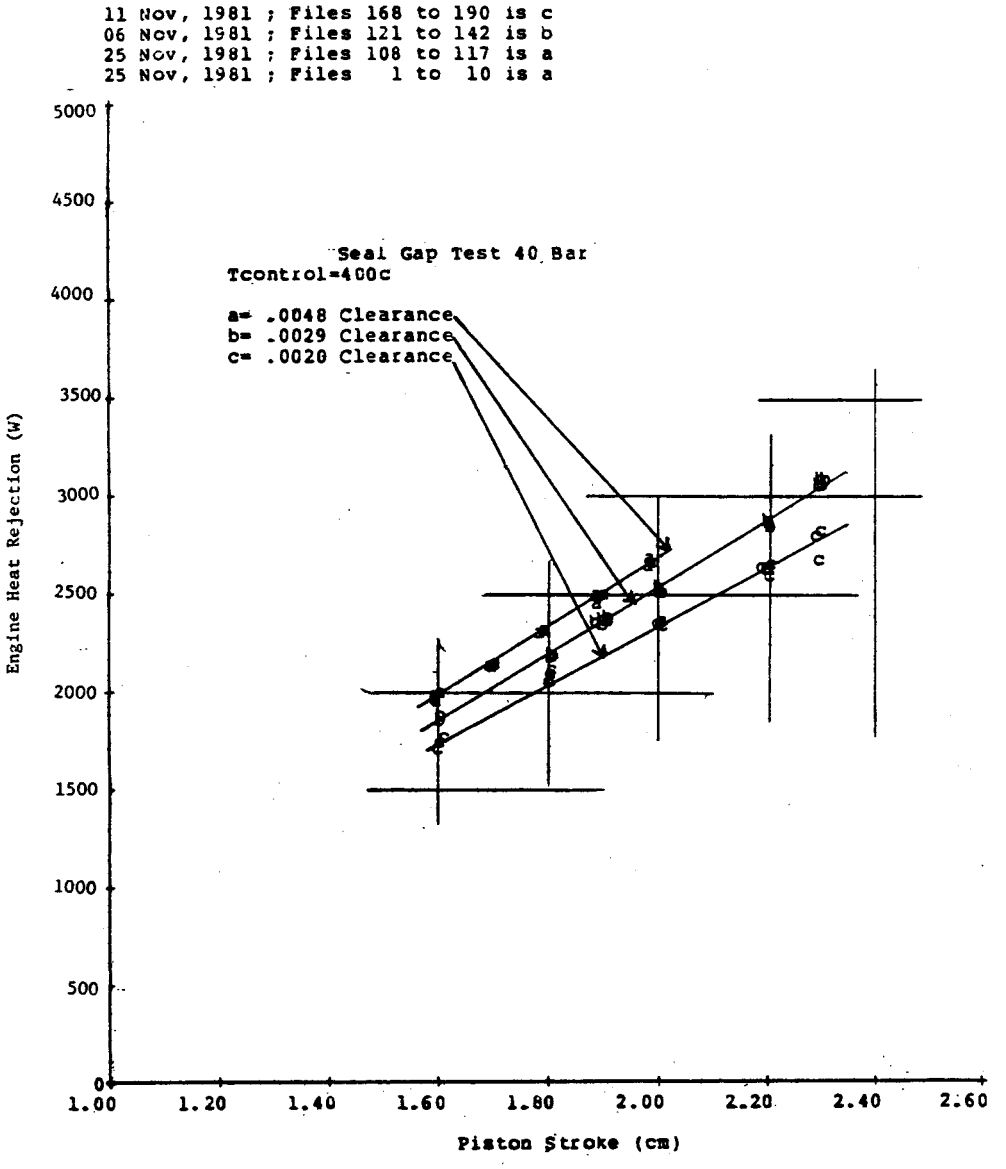

Fig. 8-9. Displacer Clearance Test: Engine Heat Rejection Measurements at Various Clearances

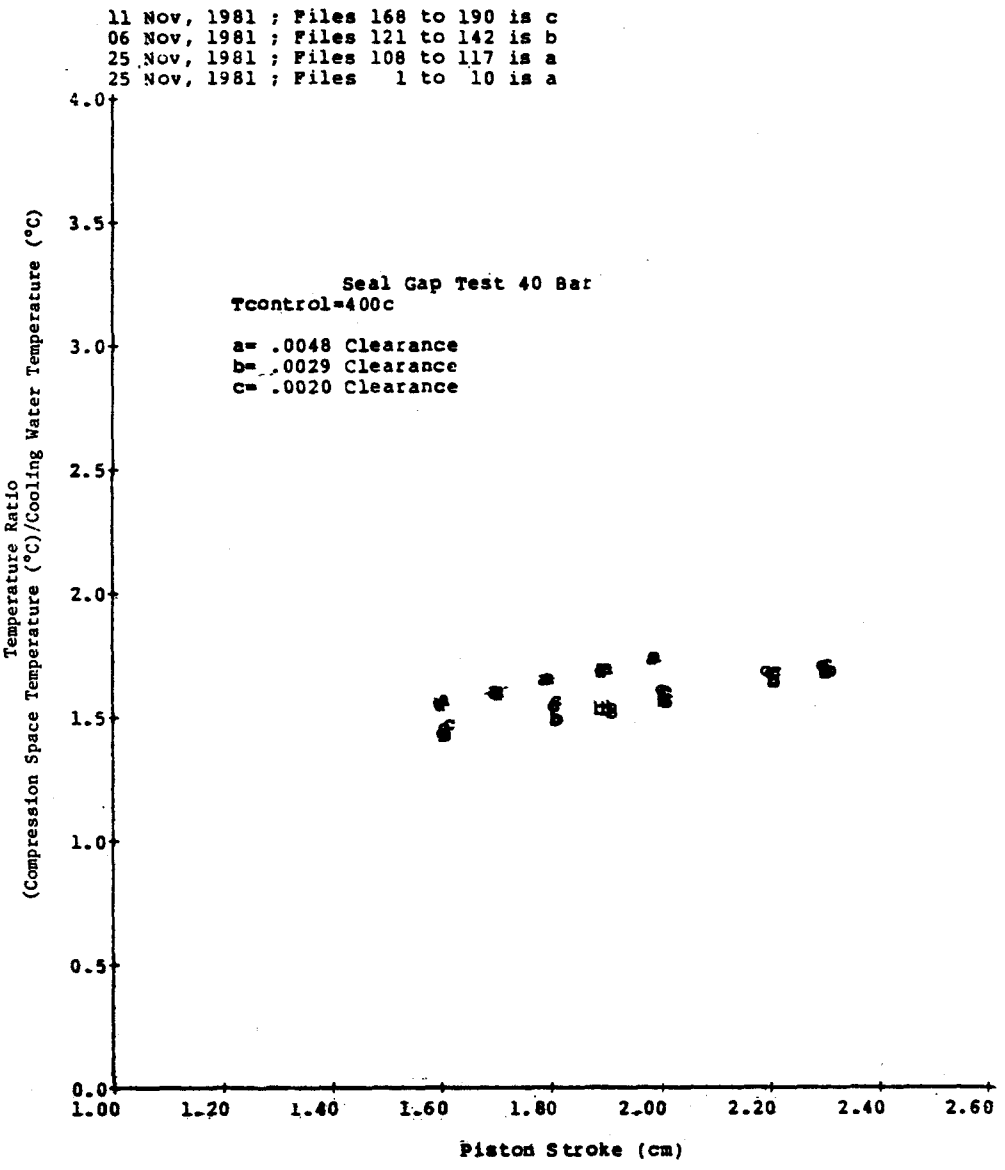

Fig. 8-10. Displacer Clearance Test: Compression Space Temperature Ratio Measurements

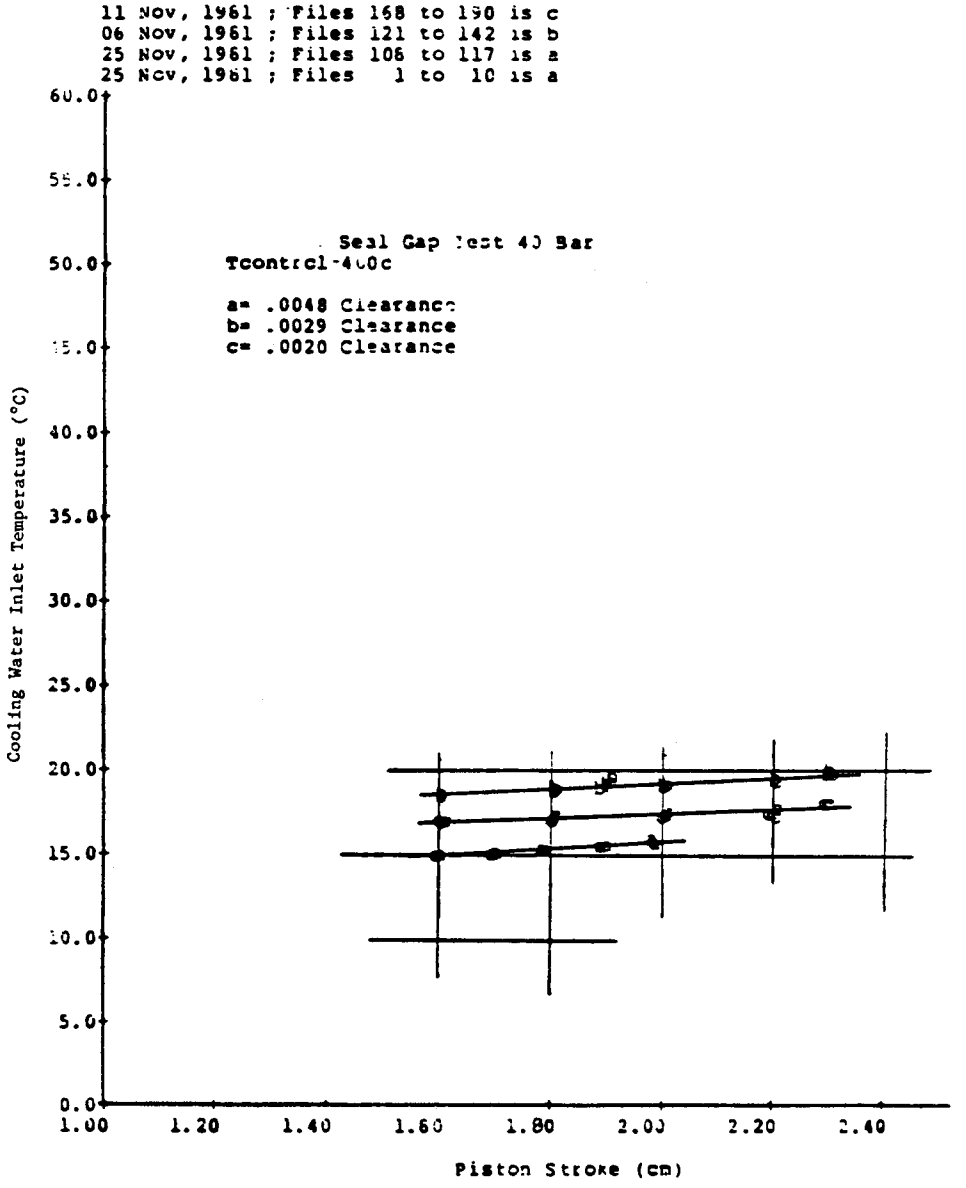

Fig. 8-11. Displacer Clearance Test: Water-In Temperature Measurements

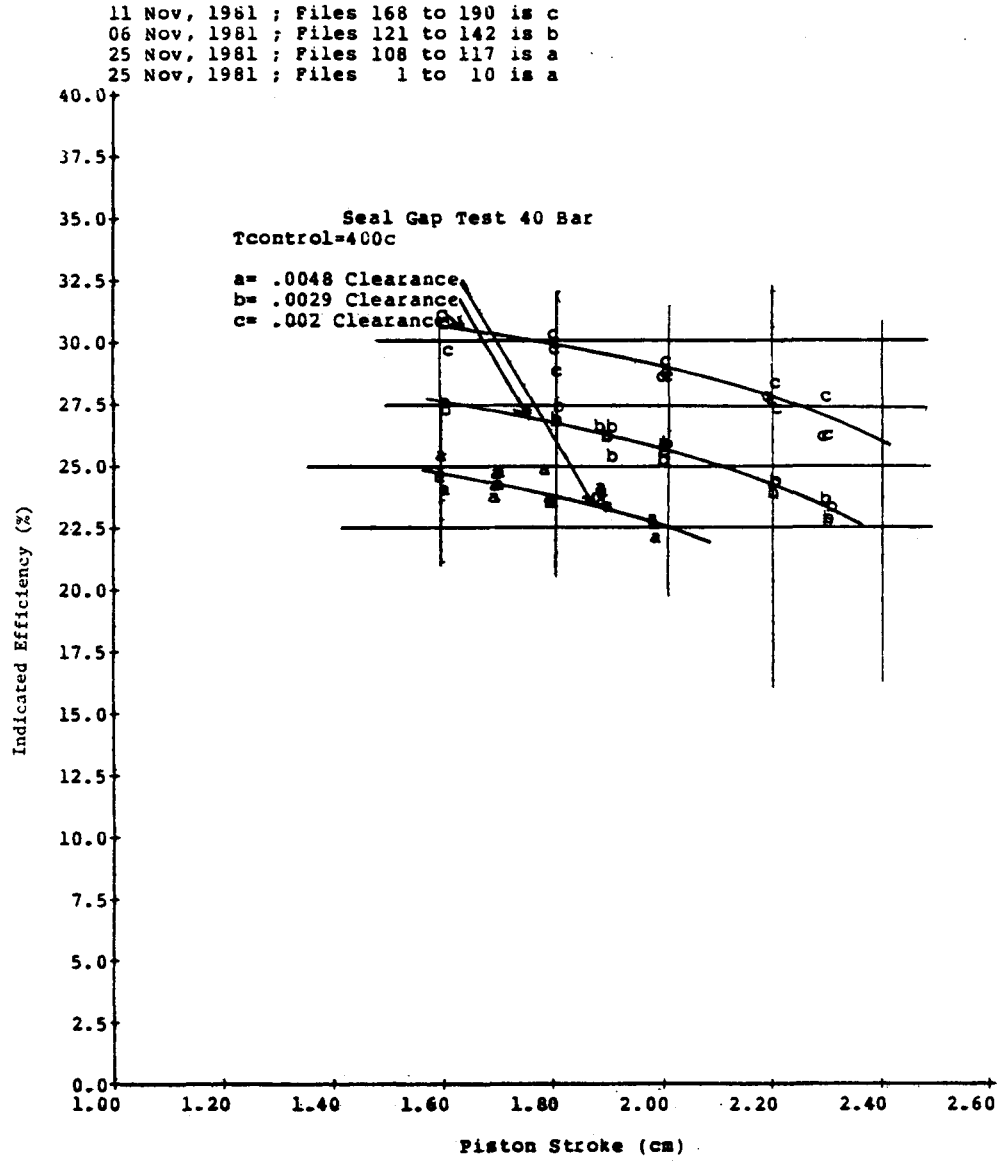

Fig. 8-12. Displacer Clearance Test: Indicated Efficiency Measurements at Various Clearances

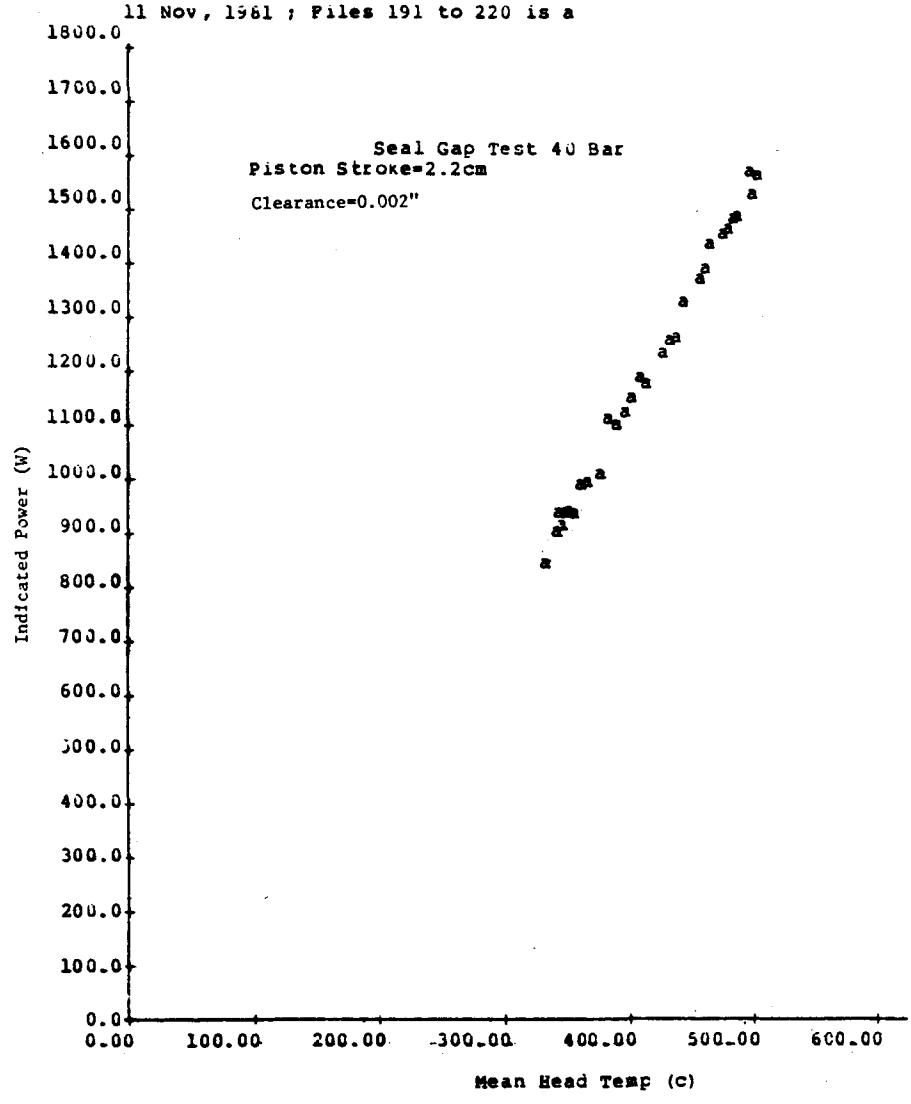

Fig. 8-13. Displacer Clearance Test: Indicated Power Measurements at 0.002-in. Clearance

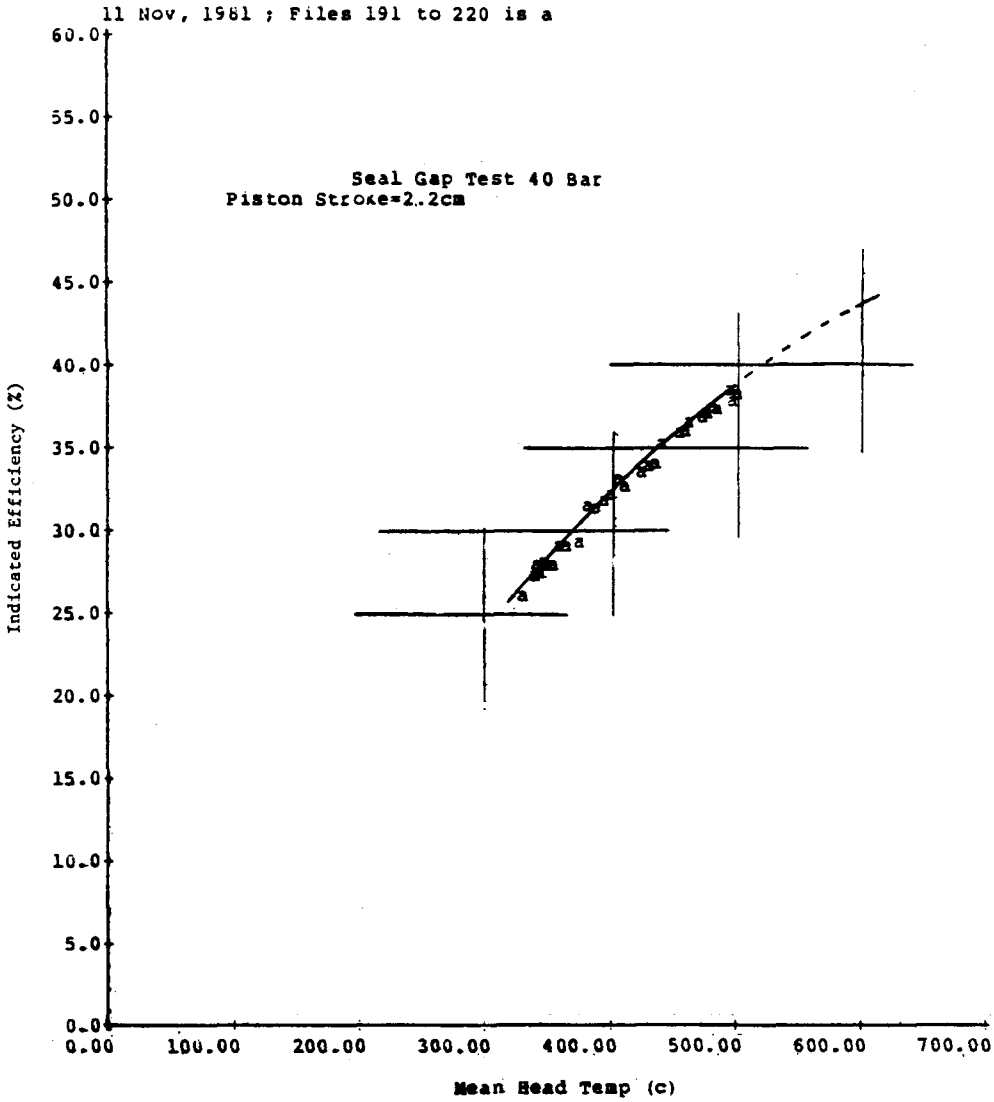

Fig. 8-14. Displacer Clearance Test: Indicated Efficiency Measurements at 0.002-in. Clearance

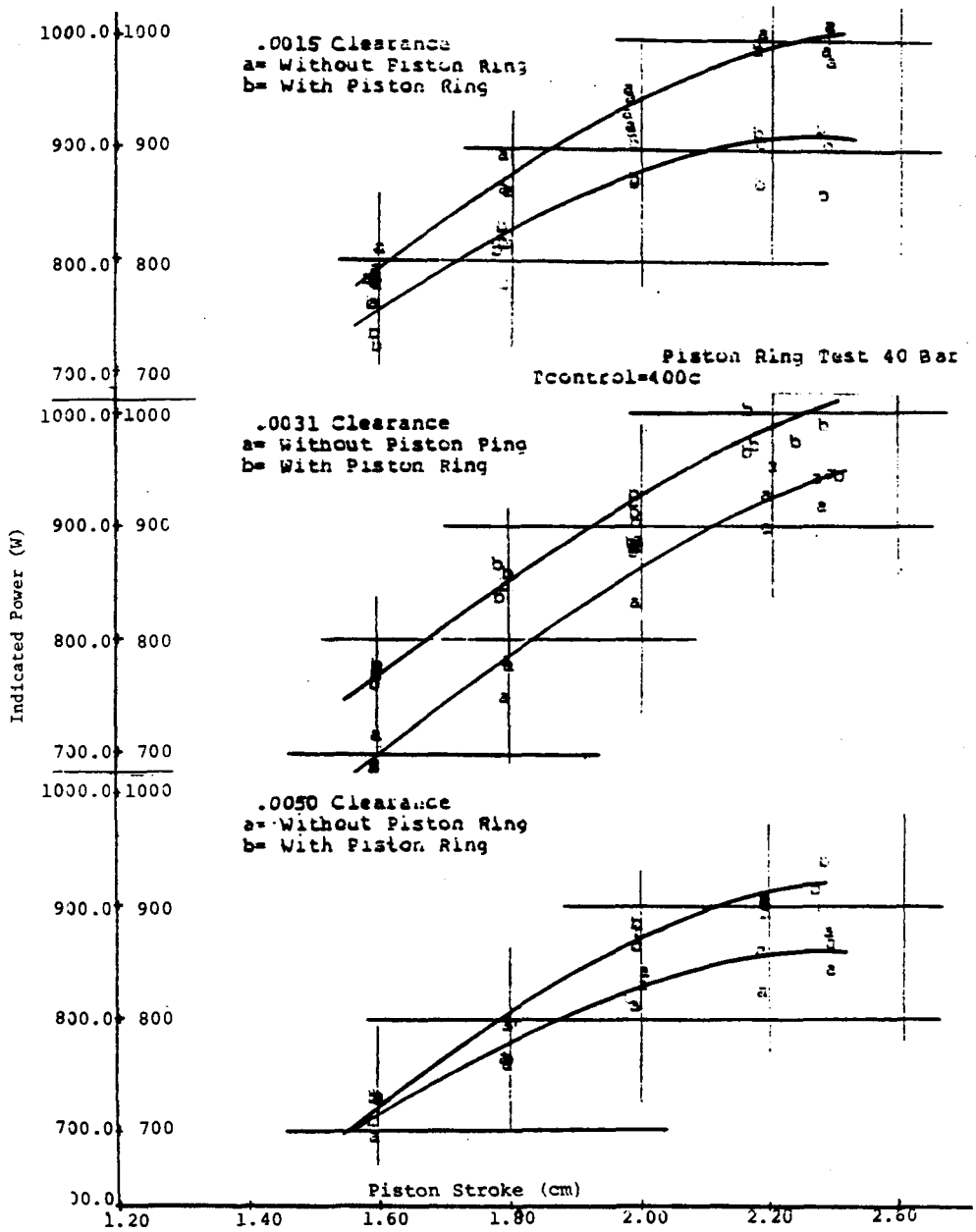

Fig. 8-15. Displcer Clearance Test: Indicated Power Measurements at Various Clearances with and without Piston Rings

- At larger clearances, use of a piston ring results in power improvement, and

- Power improvement with the piston ring at higher clearances is still less than the power achieved with a small clearance seal.

A comparison of indicated power results for the O-ring-backed piston ring tests and piston ring tests without O-ring backing (Fig. 8-16) indicates a reduction in power with the O-ring-backed piston ring, as well as a sensitivity of performance to seal friction.

The trends in Figures 8-15 and 8-16 are consistent; it is expected that power will remain constant for the piston ring tests. As expected, the results steadily decline for the tests without the piston ring. Power for the 0.0031-in. piston ring test was higher than for the 0.0015 and 0.0050 in. tests. Normalizing the power results by plotting the P-V power factor (Fig. 8-17) indicates that power actually improved as tests were run for each of the successive clearances. This power improvement may be due to ring wear-in or masking of displacer seal clearance effects by ring-to-groove wall friction force reduction. The normalized P-V power factors for the 0.0015, 0.0031, and 0.0050 in. tests are plotted in Figures 8-18 through 8-20 to compare the results from tests with and without the piston ring. The results indicate the same general trends, i.e., power improvement at higher clearances, and power degradation at lower clearances with the use of the piston ring.

Figure 8-21 compares the indicated efficiencies for each of the piston ring tests. The same general trends are evident for the efficiency results as was observed for the power results. Efficiency improved at the higher clearances with the piston ring installed, and was slightly lower for the small clearances. There was no preceptible difference in efficiency between the cases run with and without O-ring-backed piston rings (Fig. 8-22).

The uncertainty of piston ring seating and the possibility of the ring design's influence on displacer shuttle gap boundary conditions render data interpretation difficult. An attempt was made to quantify the magnitude of ring friction power by plotting the damping coefficient as a result of displacer pumping versus displacer stroke. From a displacer force balance, it would be expected that the damping coefficient (as a result of the difference between the displacer drive power and displacer gas spring power) would increase with additional friction loading on the displacer.

As the TDE is not instrumented to measure heat exchanger pressure drop, expansion-space pressure and phase are inferred from a displacer force balance of the dynamic forces, which assumes zero friction forces present. Figures 8-23 and 8-24 show an increase in δP amplitude and phase, suggesting the presence of friction force. Solving for the damping coefficient for the pumping power inferred from the force balance results in the plot of Figure 8-25. The Δ between the tests with and without the piston ring suggests a 15-W power dissipation due to piston ring friction for a displacer stroke of 1.5-cm.

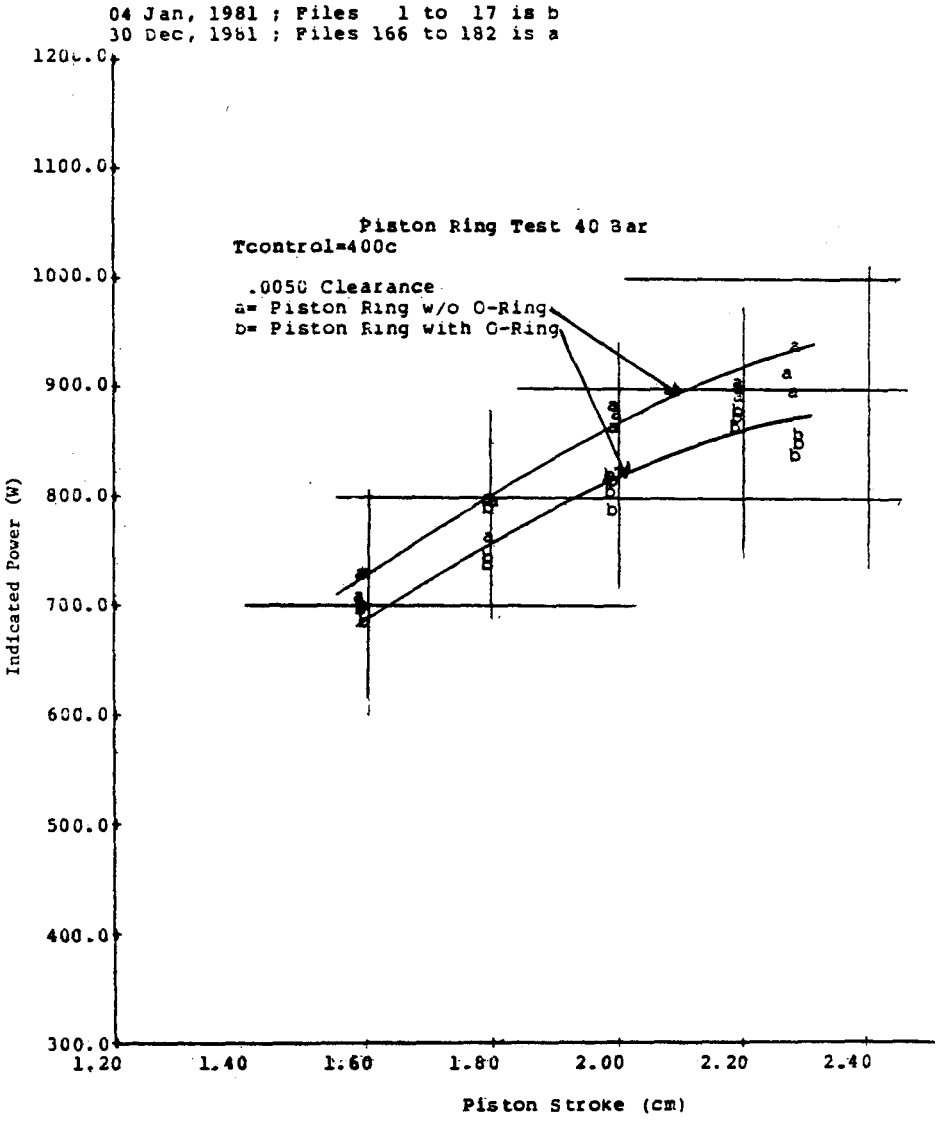

Fig. 8-16. Displacer Clearance Test: Indicated Power Measurements with Piston Ring at .0050-in. Clearance with and without O-Ring Backing

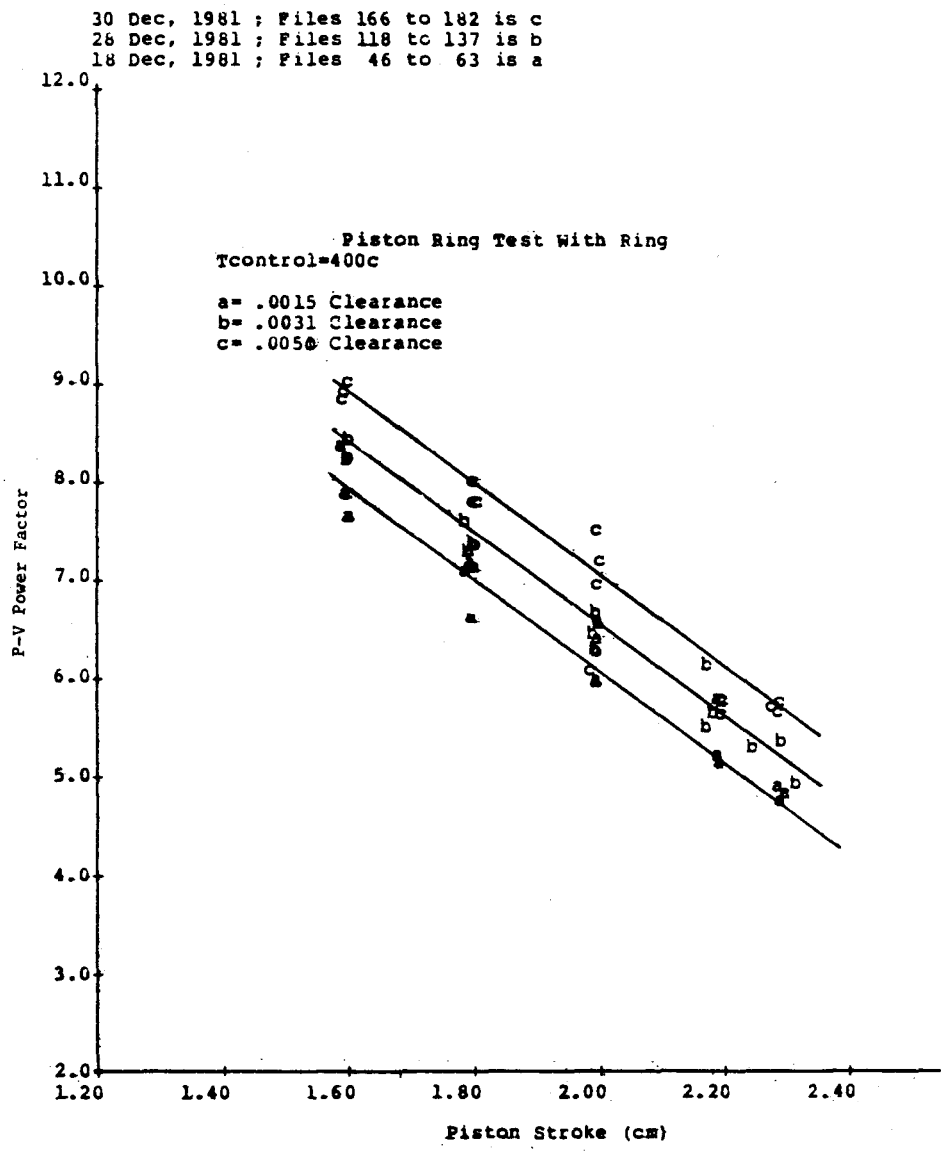

Fig. 8-17. Displacer Clearance Test: P-V Power Factor (Equation 5.1) for Various Clearances with Piston Ring

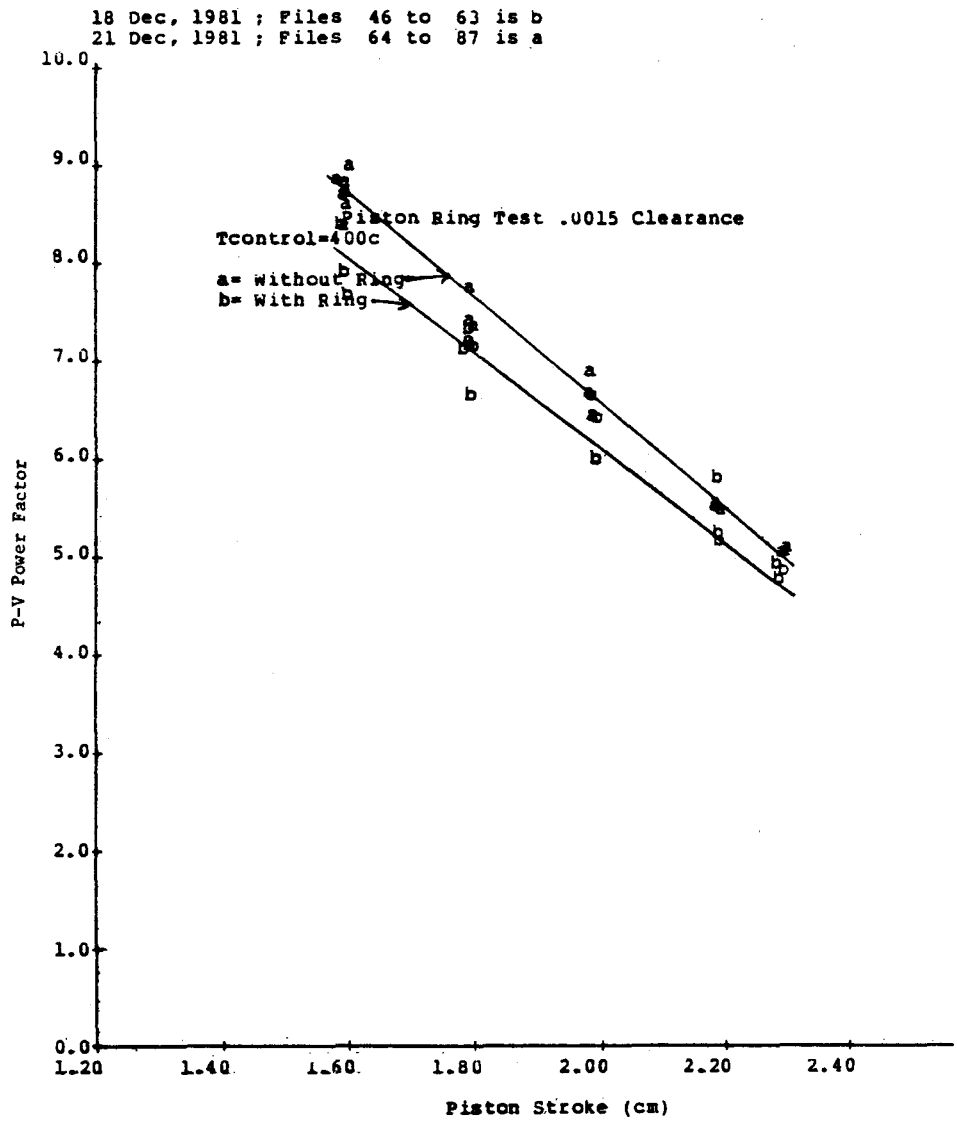

Fig. 8-18. Displacer Clearance Test: P-V Power Factor (Equation 5.1) at .0015-in. Clearance with and without Piston Ring

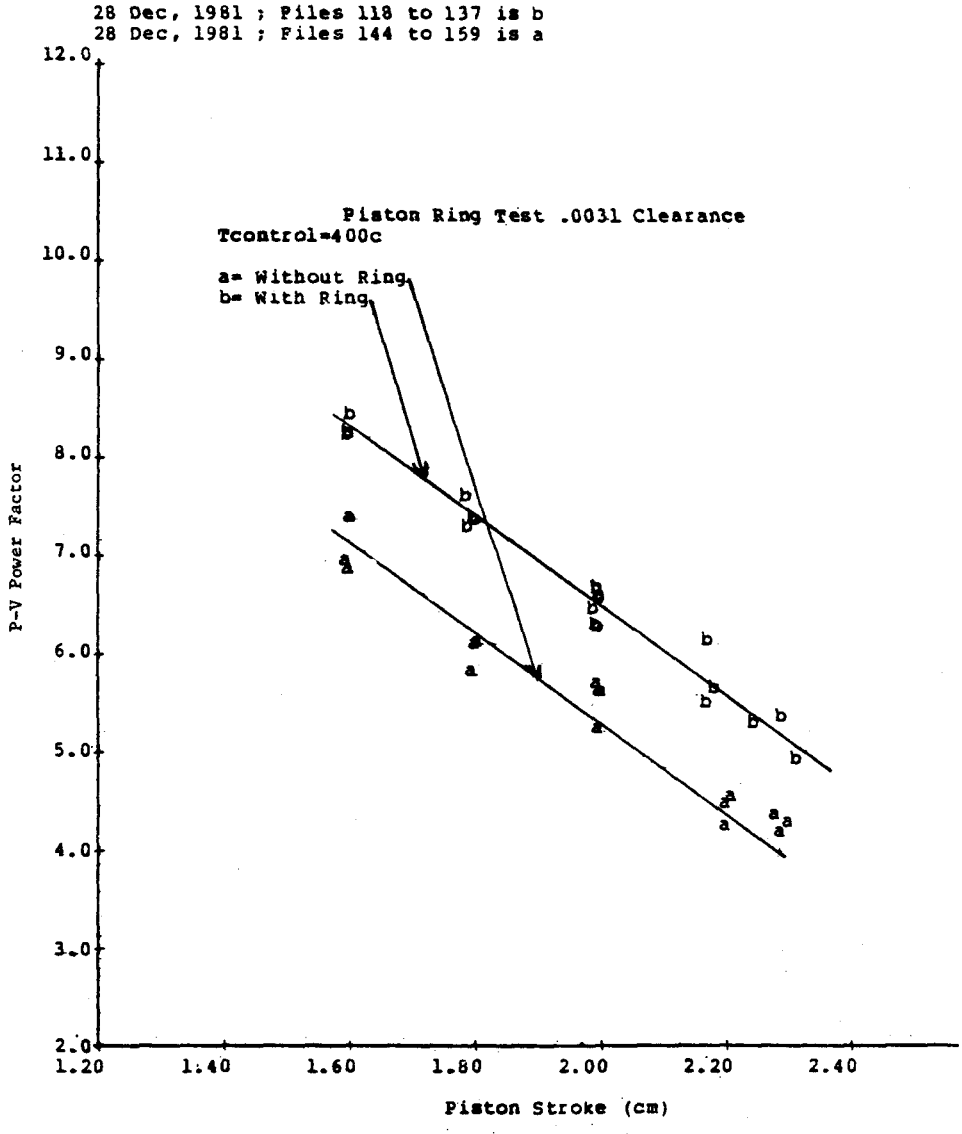

Fig. 8-19. Displacer Clearance Test: P-V Power Factor (Equation 5.1) at .0031-in. Clearance with and without Piston Ring

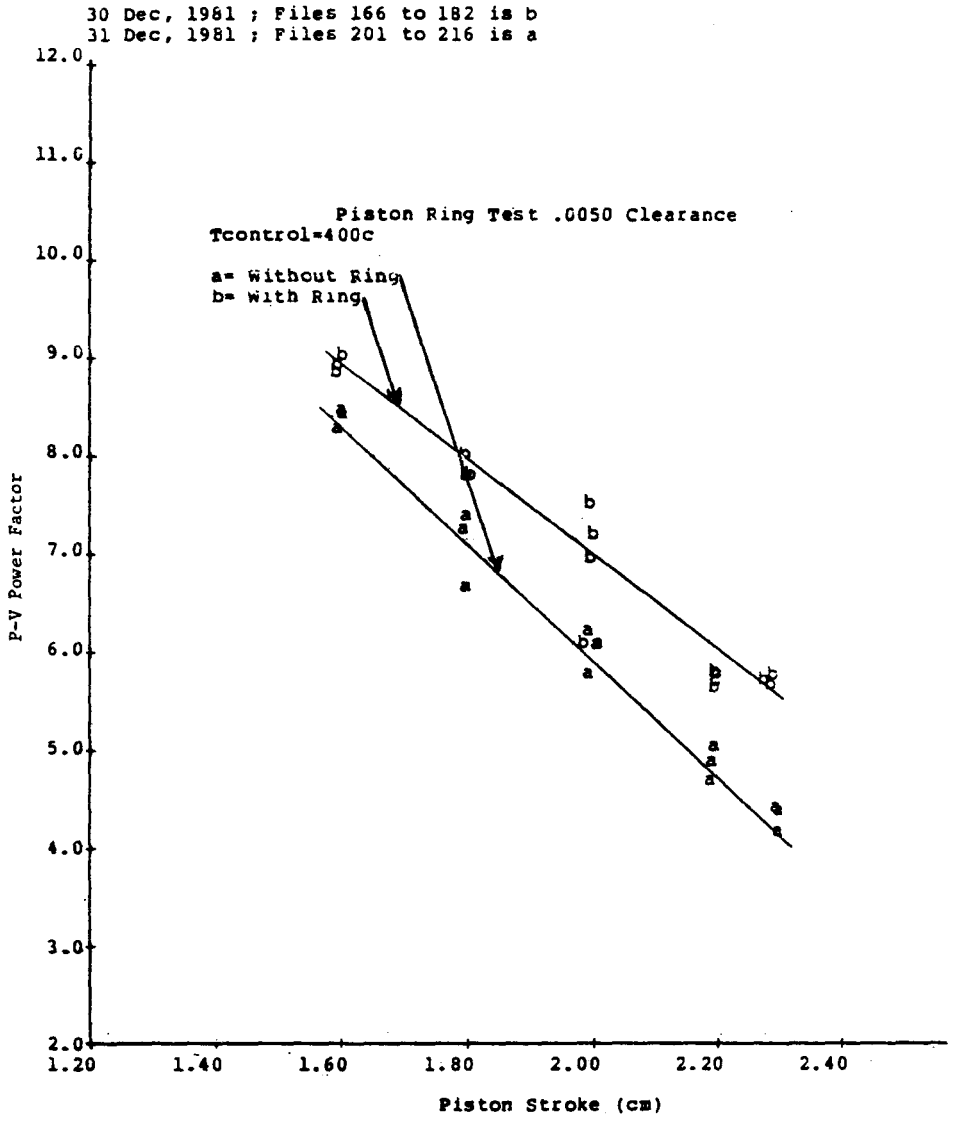

Fig. 8-20. Displacer Clearance Test: P-V Power Factor (Equation 5.1) at .0050-in. Clearance with and without Piston Ring

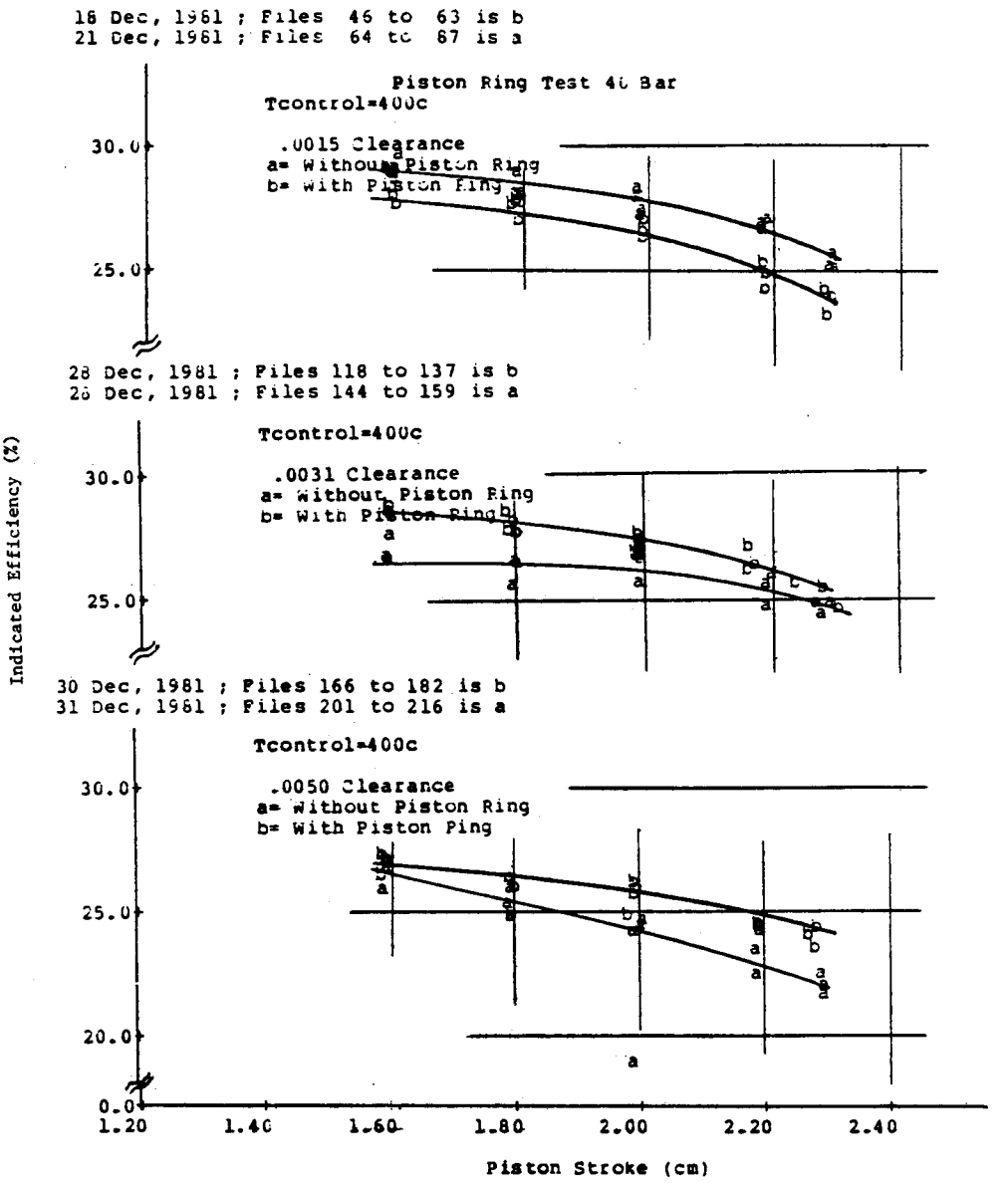

Fig. 8-21. Displacer Clearance Test: Indicated Efficiency Measurements at Various Clearances with and without Piston Ring

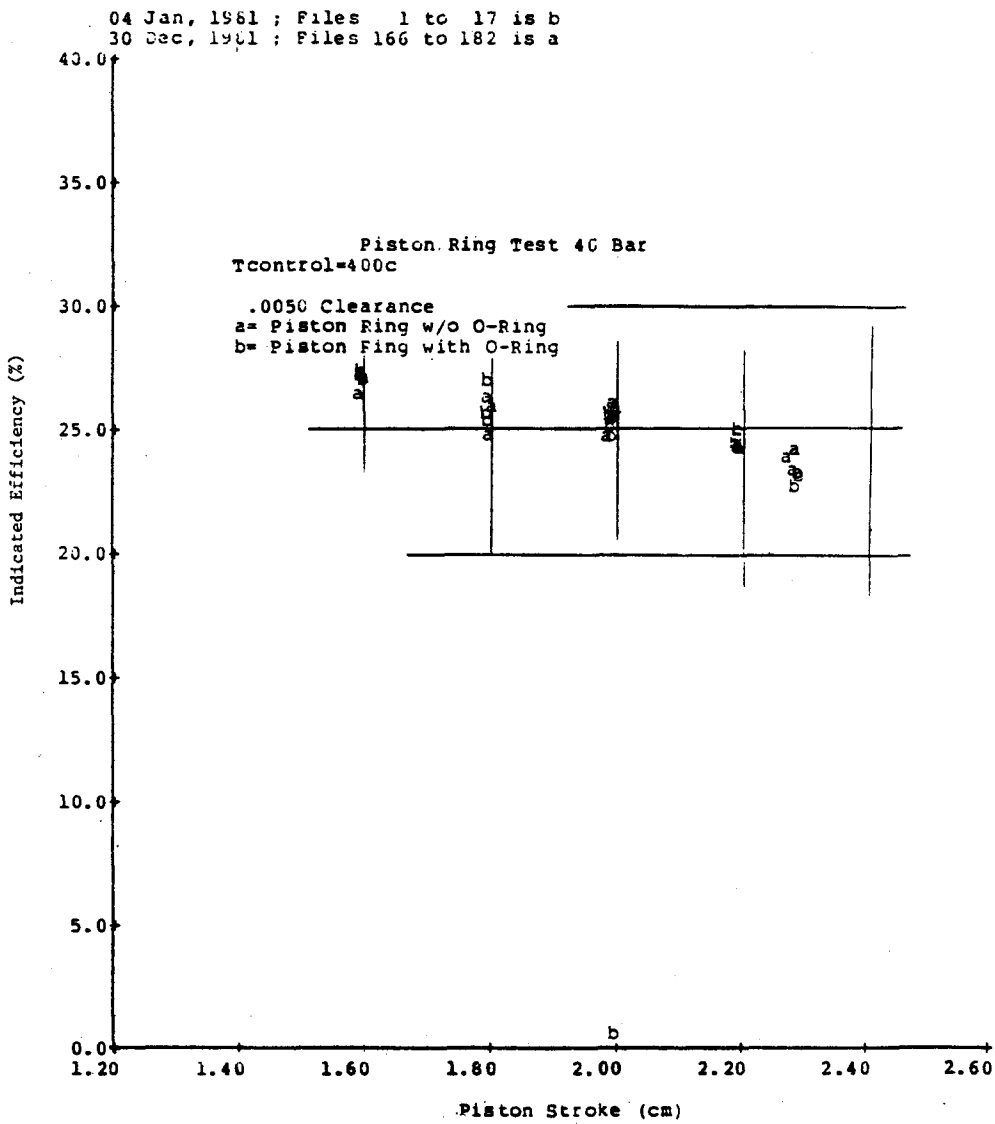

Fig. 8-22. Displacer Clearance Test: Indicated Efficiency Measurements with Piston Ring at .0050-in. Clearance with and without O-Ring Backing

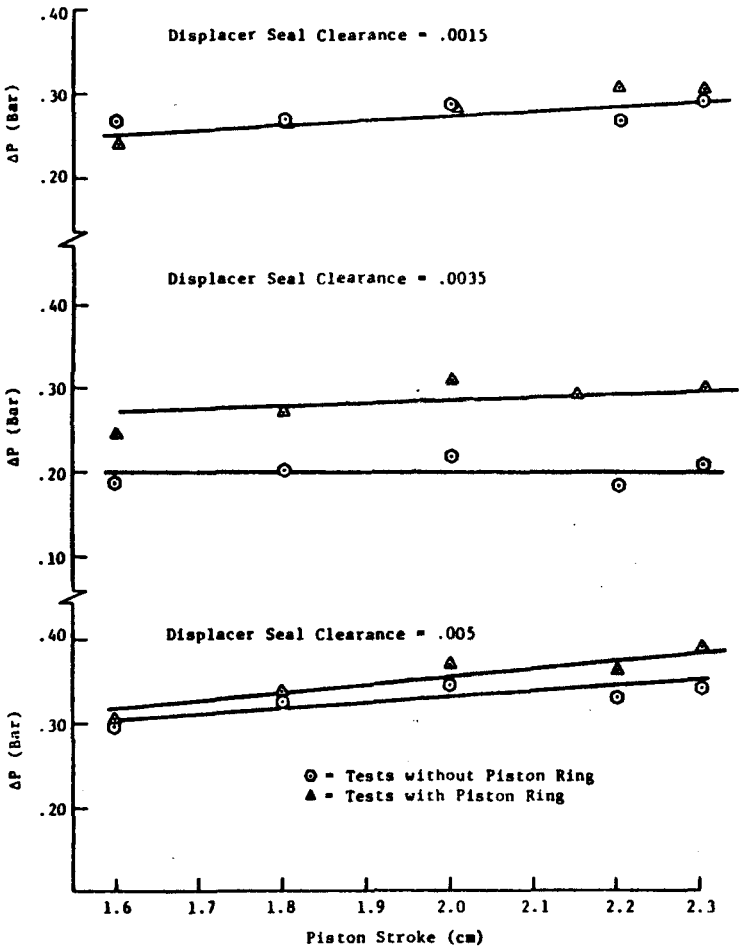

Fig. 8-23. Displacer Clearance Test: Heat Exchanger ΔP Amplitude at Various Clearances with and without Piston Ring

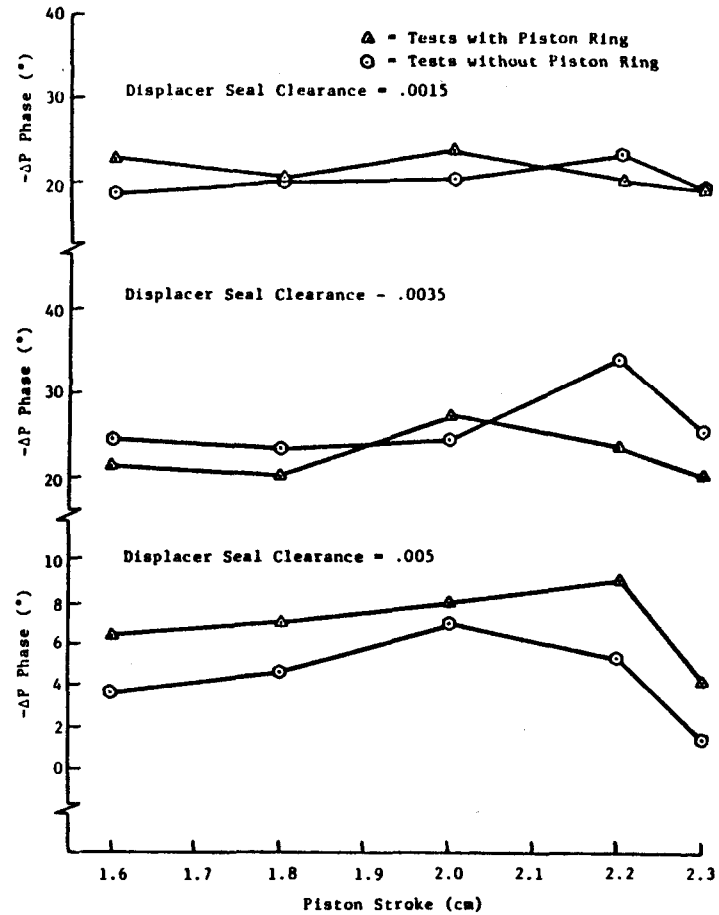

Fig. 8-24. Displacer Clearance Test: Heat Exchanger ΔP Phase Angle at Various Clearances with and without Piston Ring

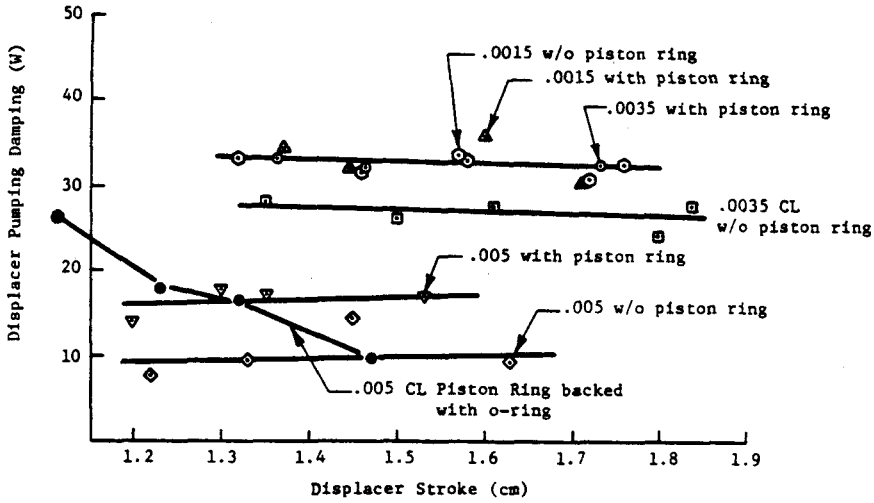

Fig. 8-25. Displacer Pumping Damping vs. Displacer Stroke

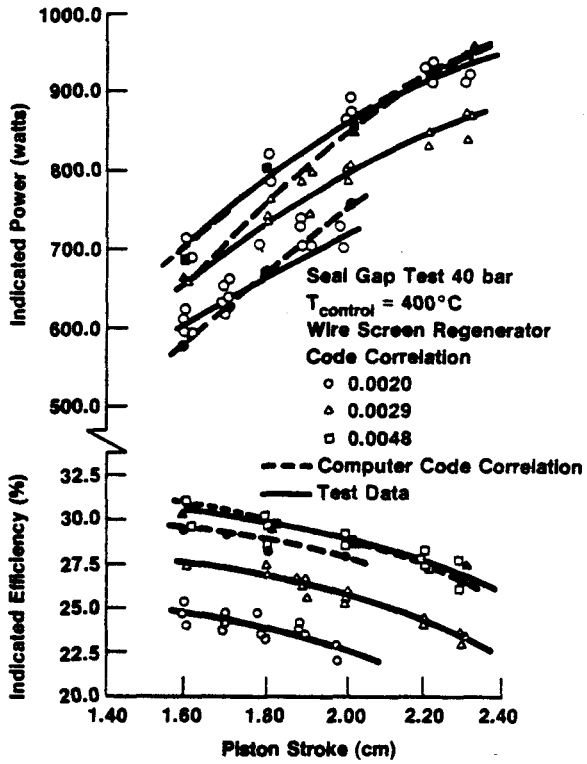

Fig. 8-26. Displacer Clearance Test: Comparison between Measured and Calculated Indicated Power and Efficiency for Various Clearances

8.4 ANALYTICAL COMPARISON

Figure 8-26 shows the analytical comparison for the 0.002, 0.0029, and 0.0048 in. clearance seal tests of calculated and measured power and efficiency. Because the code does not model enthalpy transport from the hot space to the cooler, the correlation in efficiency is seen to deviate significantly with increasing clearance. Correlation in power is seen to be almost exact for the small clearance, deviating slightly for the larger clearance at small strokes. As the stroke is increased, the deviation at larger clearances becomes stronger as the leakage effect becomes more dominant.

8.5 CONCLUSIONS AND RECOMMENDATIONS

8.5.1 Conclusions

- The TDE is shown to be sensitive to displacer seal gap clearances,
- At a small clearance, TDE performance is degraded with the installation of a displacer piston ring, and
- At larger seal clearances, TDE performance improves with the installation of the piston ring.

8.5.2 Recommendations

- Design engines with displacer seal clearances of 0.002-in. or less.
- Conduct a test to evaluate engine performance as a function of cold space temperature.
- Perform engine thermodynamic maps with a close clearance seal at different pressures.
- Study regenerator flow maldistribution.

REFERENCES

1. T. Moynihan and J. Rauch, "Technology Demonstrator Engine Period Test Report for August 1979-May 1981," MTI-11290-1 (DE83002272), prepared by Mechanical Technology Incorporated, Latham, New York, for U.S. Dept. of Energy (Final Report).

2. M. W. Spatz, "Regenerator Matrices for Stirling Engines," MTI Report 81ASE223PR16.

3. R. Berggren and T. Moynihan, "Free-Piston Stirling Engine Experimental Program: Part 1 - Baseline Test Summary," ANL-83-48 (in press).

4. D. M. Berchowitz, "Appendix Gap Losses in Reciprocating Machines," MTI Report 81ASE187ER16.

5. F. J. Zimmerman and R. C. Longsworth, "Shuttle Heat Transfer," Paper H-5, Cryogenic Engineering Conference, Boulder, Colorado (1970).

6. P. A. Rios, "An Appropriate Solution to the Shuttle Heat-Transfer Losses in a Reciprocating Machine," Paper 70-WA/Ener-3, ASME meeting, New York (1970); also J. Eng. Power, pp. 177-289 (April 1971).